Universitat Autònoma de Barcelona

Natural and Synthetic Hydrogels as Biomimetic Materials for Cancer Immunotherapies

Roberto Fabião Santos Abreu

Universitat Autònoma
de Barcelona

Natural and Synthetic Hydrogels as Biomimetic Materials for Cancer Immunotherapies

Roberto Fabião Santos Abreu

Doctor of Philosophy in Material Science by the Autonomous University of Barcelona

Directors: Dr. Judith Guasch and Dr. Imma Ratera

Tutor: Dr. Imma Ratera

February 2022

This Thesis is presented for the partial fulfillment of the degree of Doctor of Philosophy by:

Roberto Fabião Santos Abreu

Accepted by:

Judith Guasch

Imma Ratera

Dr. JUDITH GUASCH and **Dr. IMMA RATERA** scientific researchers of the Spanish National Research Council at the Institute of Materials Science of Barcelona (ICMAB-CSIC)

CERTIFY

that **Roberto Fabião Santos Abreu**, biochemist and Master in Chemistry and Biotechnology, has performed, under their supervision, the research entitled "Natural and Synthetic Hydrogels as Biomimetic Materials for Cancer Immunotherapies". This work has been performed under the framework of the Materials Science PhD program of the Autonomous University of Barcelona.

And in witness of this, below this is signed,

Directors:

Dr. Judith Guasch Dr. Imma Ratera

February, 2022

Acknowledgements

> ”
> Science knows no country, because knowledge belongs to humanity, and is the torch which illuminates the world.
>
> - *Louis Pasteur* -

Better our knowledge to better preserve people's life, has been from a very early age, one of my main priorities in life. With this clear sight and knowing about the great impact of cancer in our society, while the current treatments are still far from optimal, I felt the urge to contribute on this area.

It all started for me, during my first year in the degree of Biochemistry, at Madeira University (Portugal), when in the class of Biochemistry I, we spoke about the current treatments of cancer. I was amazed by how inefficient, unspecific, and harmful those treatments, such as chemotherapy and radiotherapy were. I could not believe that was the best we could do!

I also felt it was important to have an international experience, and connect with people, collaborate, learn, and grow to have a broader knowledge, a better understanding and different point of views. So after, my degree, and Master studies at the University of Tokyo (Japan) in the field of Material Science I found the perfect match for a PhD. The EU-Marie Curie Fellowship - DOCtoral training program in Functional Advanced Materials (DOC-FAM), to develop Natural and Synthetic Hydrogels as Biomimetic Materials for Cancer Immunotherapies, at Institut de Ciència de Materials de Barcelona (ICMAB-CSIC).

I am very happy with the opportunity I got to work and learn under the supervision of two amazing directors that always supported me! Dr. Judith Guasch and Dr. Imma Ratera, were always available and willing to help, which I consider quite unique and incredibly valuable to the success of a student. Not only their professionalism but also kindness and understanding allowed

me to present this thesis in a very challenging 3 years schedule, with a pandemic in between. I really feel lucky to have had, not one but two incredible directors, that allowed me to grow and find my way within the research group.

These acknowledgements should be also extended to Prof. Jaume Veciana, that always commented in a positive way and asked me thought-provoking questions, during my presentations, making me feel always encouraged to keep going.

Also, I am very grateful to all the NANOMOL group, with whom I was able to create many enjoyable moments. I always felt backed, and I always felt I wanted to support them the best way I could. This is a beautiful reciprocal culture within the group, based on respect and friendship. Specifically, I would like to mention the great companions Eduardo Pérez, Marc Martinez, Xavi Rodriguez, Miquel Castellote and the two amazing master students I had the opportunity to work within the scope of this thesis, Julia Valderas (Chapter 4) and Roberto Martinez (Chapter 5).

Likewise, I would like to acknowledge Prof. Ralf Kemkemer and his PhD student Karen Ende, for giving me such a great environment and opportunity to learn in their research group at Reutlingen University (Germany) during my international stay, about migration of T cells, but also for the possibility to enjoy a bit of the German culture.

I would like to further acknowledge, the collaborator Dr. Mar Alvarez, (Institute of Microelectronics of Barcelona (IMB-CNM) for the discussions and kind support on the development towards a Lymph node-on-a-chip.

Moreover, outside the professional environment, all the emotional support and help, from my girlfriend Núria, specially during this last year and half, in a world very different from the one we were born, was so valuable to me.

The unconditional love and support from my parents, Juan and Graziela who are without a doubt, my heroes, and my main source of will power to be a better person and to fight for what I believe to be right. Also, my little brother, João Marcos, already a man, but to me, he will be always my

beloved little brother, that cares and supports me like no other! I am so proud of them, and everything is so much easier when you are loved by the way I am by my family. Thank you so much!

Each of these people, helped me to arrive to this point today, and for that reason, I feel this doctoral thesis is not more mine, than theirs.

Abstract

Cancer immunotherapy is based on harnessing the immune system of patients, instead of directly targeting the tumour as the conventional treatments (e.g. surgery, radiotherapy, and chemotherapy) do. It is undoubtedly one of the most promising therapeutic approaches towards the final goal of defeating cancer, as already recognized in 2013 by the journal "Science" as a "Breakthrough of the Year".

One of the most promising branches of current immunotherapies is adoptive cell therapy (ACT). ACT is demonstrating great promise by achieving long-term remissions in late-stage and refractory cancers, especially in haematological cancers and melanoma.

However, these advanced personalized immunotherapies have to overcome several biomedical and technical limitations before they become a routine cancer treatment. One of the main limitations relies on the capacity to obtain adequate numbers of therapeutic T cells in the patients, which are persistent *in vivo*. Moreover, the time and elevated costs to produce these T cells should be reduced.

In this thesis, all efforts were aligned to tackle these limitations by developing and applying hydrogels (synthetic and natural) as artificial lymph nodes (LNs) to efficiently expand primary human T cells and control the obtained phenotypes.

Through a collaboration with the company Biogelx (United Kingdom), we studied commercial synthetic hydrogels capable to mimic extracellular matrix (ECM) properties, according to specifications. Several parameters were modified in order to optimize the conditions for T cell culture, i.e. the stiffness of the hydrogels, the cell density used in seeding, the hydrogel formation step and the cell recovery method. Despite many efforts in conjunction with the company, no proliferation of T cells was observed, and the material was found to be cytotoxic to human T cells.

In another industrial collaboration with Viscofan S.A. (Spain), 3D natural collagen hydrogels were used for the expansion of primary human T cells. After several optimizations, an important improvement in primary human T cell expansion was obtained in some of the collagen hydrogels used. Additionally, the phenotype obtained was not altered when compared with the state-of-the-art methodology, consisting of expanding these cells in suspension systems.

An inverse opal (IOPAL) strategy was employed to fabricate a second generation of our previously reported bulk hydrogels in order to increase the pore size and control their microstructure. These hydrogels were made of poly(ethylene) glycol (PEG) covalently combined with heparin (PEG-Hep) with the objective to mimic the ECM of the LNs. The PEG-Hep IOPAL hydrogels were fully characterized in terms of morphology and mechanical properties. Moreover, they resulted in an improvement in T cell proliferation when compared both to the state-of-the-art methodologies, and to its bulk form. Additionally, the phenotypes obtained with the IOPAL hydrogels were adequate to achieve T cell persistence *in vivo*.

To mimic the fluid flow of the LNs, we have initiated the creation of a LN-on-a-chip containing our artificial LNs, the IOPAL PEG-Hep hydrogels, in collaboration with the Institute of Microelectronics of Barcelona (IMB-CNM-CSIC). An extensive optimization of the set-up conditions has been performed in terms of the design of the microfluidic device, the volumetric flow, the sterilization process and the cell seeding conditions. This process has allowed us to gather the necessary information to successfully fabricate a LN-on-a-chip in a recent future.

In conclusion, this thesis has led to a better understanding on how to create a 3D hydrogel platform for T cell expansion, by taking inspiration from the human LN environment, to help improving current limitations of ACT.

Abbreviations

µCT	Micro-computed tomography
2D	Two dimensions
3D	Three dimensions
AcOH	Acetic acid
ACT	Adoptive cell therapy
AEM	N-(2-aminoethyl) maleimide trifluoroacetate salt
ALL	Acute lymphoblastic leukemia
AML	Acute myeloid leukemia
APCs	Antigen-presenting cells
CAR	Chimeric antigen receptor
CD	Cluster of differentiation
CFSE	Carboxyfluorescein succinimidyl ester
CH	Collagen hydrogel
CLL	Chronic lymphoblastic leukemia
CMPs	Collagen-mimetic peptides
ConA	Concanavalin A
CRI	Cancer Research Institute
CRS	Cytokine release syndrome
CTLA	Cytotoxic T lymphocyte antigen
cw	Continuous wave
DC	Dried collagen
DCM	Dichloromethane
DMF	Dimethylformamide
DMSO	Dimethyl sulfoxide
DOCT	Doppler optical coherence tomography
ECM	Extracellular matrix

EDC-HCl	1-Ethyl-3-(3-dimethylaminopropyl) carbodiimide
ELISA	Enzyme-linked immunosorbent assay
EMA	European Medicines Agency
EPR	Electron paramagnetic resonance
ESEM	Environmental scanning electron microscopy
FBS	Fetal bovine serum
FITC	Fluorescein isothiocyanate
Fmoc-F_2	Fmoc-diphenylalanine
Fmoc-S	Fmoc-serine
FRCs	Fibroblastic reticular cells
FSC	Forward scatter
G'	Storage modulus
G''	Loss modulus
GAB	Biomedical Applications Group
GMP	Good manufacture practices
HCl	Hydrochloric acid
HCQ	Hydroxychloroquine
Hep	Heparin
Hep-Mal	Maleimide-functionalized heparin
HLA	Human leukocyte antigen
HOBt	Hydroxybenzotriazole
ICP-MS	Inductively coupled plasma mass spectrometry
IL-2	Interleukin-2
IL	Interleukin
IMB-CNM	Institute of Microelectronics - National Microelectronics Center
IOPAL	Inverse opal
IS	Immunological synapse
LNs	Lymph nodes
LVE	Linear viscoelastic region

M	Millions
mAb	Monoclonal antibodies
MCs	Microfluidic chips
MHC	Major histocompatibility complex
MSCs	Mesenchymal stem cells
NK	Natural Killer
NMR	Nuclear magnetic resonance
PBMCs	Peripheral blood mononuclear cells
PBS	Phosphate saline buffer
PD-1	Programmed cell death protein 1
PDMS	Polydimethylsiloxane
PE	Phycoerythrin
PEG	Poly(ethylene glycol)
PEG-SH	Thiolated PEG
PET	Polyethylene terephthalate
PHA	Phytohemagglutinin
PI	Propidium iodine
PMA	Phorbol 12-myristate 13-acetate
PMMA	Polymethyl methacrylate
PPs	Peyer's patches
PS	Polystyrene
PTFE	Polytetrafluoroethylene
PVC	Polyvinyl chloride
PWM	Pokeweed mitogen
RBCs	Red blood cells
RPM	Rotations per minute
RPMI	Roswell Park Memorial Institute medium
RT	Room temperature
SAOS	Small-amplitude oscillatory shear

SAQ	Servei d'Anàlisi Química
SCS	Subcapsular sinus
SLO	Secondary lymphoid organs
SME	Small-medium enterprise
SSC	Side scatter
ST	Standard
TAAs	Tumor-associated antigens
T_{CM}	Central memory T cells
TCR	T cell receptor
T_{EFF}	Effector T cells
T_{EM}	Effector memory T cells
T_{EMRA}	Terminally differentiated effector memory T cells
THF	Tetrahydrofuran
TILs	Tumor infiltrating lymphocytes
T_N	Naïve T cells
UAB	Universitat Autònoma de Barcelona
VOI	Volume of interest
wt	Weight

Contents

Chapter 1

Introduction and objectives

1.1 Immunotherapy. Historical background

Late summer of 1890, in New York city, a fascinating step towards cancer treatment took place, thanks to a young surgeon who was willing to think outside the box, Dr. William B. Coley, known nowadays as the father of cancer immunotherapy.

On that summer, Elizabeth Dashiell who was only 17 years old, visited the recently graduated Dr. Coley, complaining about severe pain in her hand. At first Coley thought it would be an infection, but surprisingly he found it was a very advanced sarcoma. At these times, when very little was known about cancer, and before chemotherapy and radiotherapy, the young bone surgeon did the only think he could do, he amputated Dashiell's right arm. Sadly, it did not work, the cancer spread all over the body and shortly after Elizabeth died.[1,2]

Elizabeth Dashiell early death, one of his very first patients, made a huge impression on Coley, who decided at that moment, to study dozens and dozens of old records at New York Hospital looking for something that would help him understand this ruthless and aggressive disease.

Indeed, he found one case of a German immigrant, Fred Stein, that had been hospitalized in 1885 with an egg-sized tumor mass on his cheek. During the next three years, Fred Stein underwent five operations to remove the tumor from his left cheek. After each surgical resection, the mass grew again and bigger until it became the size of a man's fist. As it was common at the time among people undergoing surgery, Stein contracted a Streptococcus pyogenes infection. This bacterial infection causes very high fever, inflammation and, in many patients, death. But Fred Stein, survived to the infection and the high fever, and more than that, the tumor disappeared.[1,2]

For years, Dr. Coley tried to find this man. When he eventually did and examined the patient, he found out that Stein was free from cancer 8 years after the infection event.

After this case, Dr. Coley speculated the Streptococcus pyogenes infection had reversed the cancer. For the following 40 years, Coley injected over 1000 patients with bacteria or bacterial products in order to treat various cases of cancer. Very good results were obtained at that time, especially in bone and soft-tissue sarcomas. These products became known as Coley's Toxins.[3–6]

Despite these great results, the work of Dr. William Coley was dealt with great criticism by other doctors since those results did not have a well understood reason behind. All these doubts, together with the development of radiation and chemotherapy caused his approach to be largely abandoned during his lifetime.

However, in the 50s, several notable events took place that helped to improve the understanding of the immune system and its functions. For example, the clonal selection theory was introduced in 1957 by Frank Macfarlane Burnet (Nobel Prize in Physiology or Medicine – 1960).[7] In fact, he stated in his published work entitled "Cancer – A Biological Approach, III. Viruses Associated with Neoplastic Conditions. IV. Practical Applications", in the British Medical Journal: "The chemotherapeutic approach to date (…) suffers from one overwhelming intrinsic disadvantage, which may be put in oversimplified from – namely, that all anti-cancer drugs are also carcinogens." Macfarlane Burnet continues further on the same report "A slightly more hopeful approach, which, however, is so dependent on the body's own resources that it has never been seriously propounded, is the immunological one."[8]

Indeed, immunotherapy and the work carried on by Coley was not forgotten, and during this period, Coley's daughter, Helen Coley Nauts, with the help of a grant (2000 dollars) from John D. Rockefeller Jr.'s son Nelson, created the well-known Cancer Research Institute (CRI).[6] John D. Rockefeller Jr. was a close friend of Elizabeth Dashiell, the patient that motivated Dr. Coley's work.

The following years were fulfilled with important discoveries that helped uncover the mysteries of the immune system, and to finally explain why the bacterial products used by Dr. Coley were successful, in the treatment of cancer patients. Indeed, it is currently known that the bacterial products were not responsible to fight cancer cells, but to awake the patient immune system. Specifically, the bacterial infection activated the immune system, which would also find the cancer cells and destroy them.

Between 1958-1962 there were the discoveries of the human leukocyte antigen (HLA) by Jean Dausset[9] (Nobel Prize of Medicine). In 1973, the discovery and characterization of dendritic cells by Ralph Steinman (Nobel Prize in Physiology or Medicine),[10] and in 1974, the description of the major histocompatibility complex (MHC) restriction by Rolf Martin Zinkernagel and Peter Charles Doherty (shared Nobel Prize in Physiology or Medicine).[11] On the same year, Georges Jean Franz Köhler together with César Milstein and Niels Kaj Jerne, contributed to the generation of monoclonal antibodies (shared Nobel Prize in Physiology or Medicine).[12]

Around 1980 took place the important discovery and characterization of interleukins (ILs) such as IL-2, by Robert Gallo, Kendall A. Smith and Tadatsugu Taniguchi.[13–16] In 1983, Philippa Marrack and her husband, John Wayne Kappler, discovered the T cell receptor (TCR), together with Ellis Reinherz and James Allison.[17,18]

Around this time, a new branch of immunotherapy started to rise, the adoptive cell therapy (ACT), in which T cells are administered to patients in order to fight several diseases, such as cancer.[19] One of the most prominent types of T cells used in ACT are the tumor infiltrating lymphocytes (TILs), which are T cells that have the ability to invade tumor tissues. In 1986, Dr. Rosenberg, a pioneer in this field, demonstrated that human TILs harvested from resected melanomas, contained cells able to specifically recognize autologous tumors (individual's own tumor).[20] Just one year after, the same research group reported the first use of autologous TILs in ACT for patients with metastatic melanoma, leading to a regression of cancer.[21]

All these great discoveries in the last century, among others not mentioned in this introduction, brought us to the modern immunotherapies. In 2010 the first autologous cell-based cancer

vaccine, Sipuleucel-T (known as Provenge®), developed by Dendreon Pharmaceuticals, was approved by the Food and Drug Administration (FDA) for the treatment of metastatic, asymptomatic stage IV prostate cancer.[22] On the same year, Ipilimumab (Yervoy®), an anti-cytotoxic T-lymphocyte antigen (CTLA)-4 monoclonal antibody was also approved by the FDA, for the treatment of patients with malignant melanoma.[23]

In 2011, Carl H. June reports the first successful use of chimeric antigen receptor (CAR) T cells expressing the 4-1BB costimulatory signaling domain for the treatment of CD19+ malignancies.[24] Another great year for the field of cancer immunotherapy was 2017, with the first two CD19-target CAR T cell therapies approved by the FDA, the tisagenlecleucel-T (Kymriah®; Novartis) and axicabtagene ciloleucel (Yescarta®; Kite Pharma/Gilead Sciences).[25]

Ultimately, the area of cancer immunotherapies was awarded for its positive social impact once more when in 2018, James P. Allison and Tasuku Honjo shared the Nobel Prize in Physiology or Medicine for their contribution to the discovery of cancer therapy by the inhibition of negative immune regulation.[26,27]

These recent successes in the field have proved the important role of immunotherapy in the treatment of cancer, placing this strategy as one of the most promising. However, the response rates are still modest in many cases, especially in solid tumors. Moreover, the mechanisms underlying the therapy should be better understood and the not so unusual secondary effects related with the boost of the immune system such as the cytokine release syndrome (CRS) should be minimized. Last but not least, the capacity to obtain adequate numbers of therapeutic T cells in the patients remains a challenge, and the time and costs to produce these T cells should be reduced.[28]

1.2 Immune system

The immune system is responsible from protecting the body from harmful substances, germs and cell changes, and it is formed by various organs, cells and proteins. This system can be divided into two subsystems, the innate immune system (non-specific) and the adaptive immune system (specific). The innate immune system is the first line of defense against non-self-pathogens, with the main purpose of immediately prevent the spread of foreign pathogens throughout the body. On the other hand, the second line of defense is the adaptive immune system, which is specific to the pathogen. The hallmark of the adaptive immune system is the clonal expansion of lymphocytes (T and B cells) with an antigen receptor capable to fight a specific pathogen or cancer type.[29]

The coordination of these immune responses in mammals are made in the secondary lymphoid organs (SLOs), which include the spleen, Peyer's patches (PPs), tonsils, adenoids and lymph nodes (LNs). All SLOs include B and T cells, antigen presenting cells, stromal cells and a vascular supply.

Moreover, if the immune cells (B and T cells) do not encounter an antigen, they simply receive homeostatic survival signals and continue their passage through the SLOs. But, if either T or B cells do have an antigen recognition event, then the SLOs are critical in providing the needed environment for cellular activation, proliferation, differentiation and even selection for high affinity antibodies. Furthermore, such SLO development is closely related with a precise regulation of lymphoid chemokines and cytokines.[30]

1.2.1 Immune cells

Immune cells can also be divided into innate and adaptive cells. Innate immune cells include macrophages, polymorphonuclear granulocytes (neutrophils, basophils and eosinophils), mast cells, dendritic cells, natural killer cells and also platelets. Dendritic cells, take up foreign antigens and migrate to SLOs, such as LNs, where they present their antigens to adaptive immune cells.

Adaptive immune cells are T and B cells, which elaborate a response targeted to the foreign agent.

In ACT, the immune cells of interest are harvested from blood, through density gradient separation, where three different parts are obtained, the plasma components, the buffy coat containing leukocytes and platelets and a bottom layer of erythrocytes (red blood cells (RBCs)) with polymorphonuclear cells like neutrophils and eosinophils (**Figure 1.1**). In the buffy coat layer are the peripheral blood mononuclear cells (PBMCs), formed approximately by an 80% of T and B cells, 10% NK cells and 10% myeloid cells, mostly monocytes.[31]

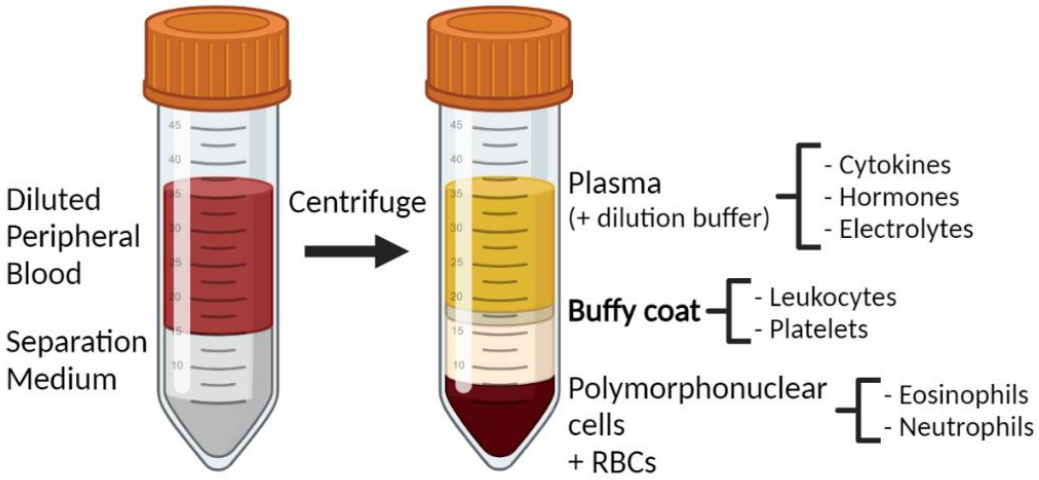

Figure 1.1 PBMC isolation by density gradient centrifugation.

T cells descendent from the lymphoid progenitor cells, emerge as naïve CD4+ or CD8+ T cells (T_N) (helper and cytotoxic types, respectively), until they detect an antigen through their interaction with antigen-presenting cells (APCs) such as dendritic cells. This encounter is mediated through a complex conjunction of signals including costimulatory receptors and secreted soluble cytokines, but mainly involving the interaction between the MHC/HLA of an APC and the TCR of a T cell.[32,33]

Then, T cells undergo proliferation and differentiation. T_N can differentiate into central memory T cells (T_{CM}), effector memory T cells (T_{EM}), and terminally differentiated (T_{EMRA})[34] (**Figure 1.2**) upon priming. T_{CM} has been reported to be a preferable phenotype for therapy, particularly due to their long-lasting responses.[35,36]

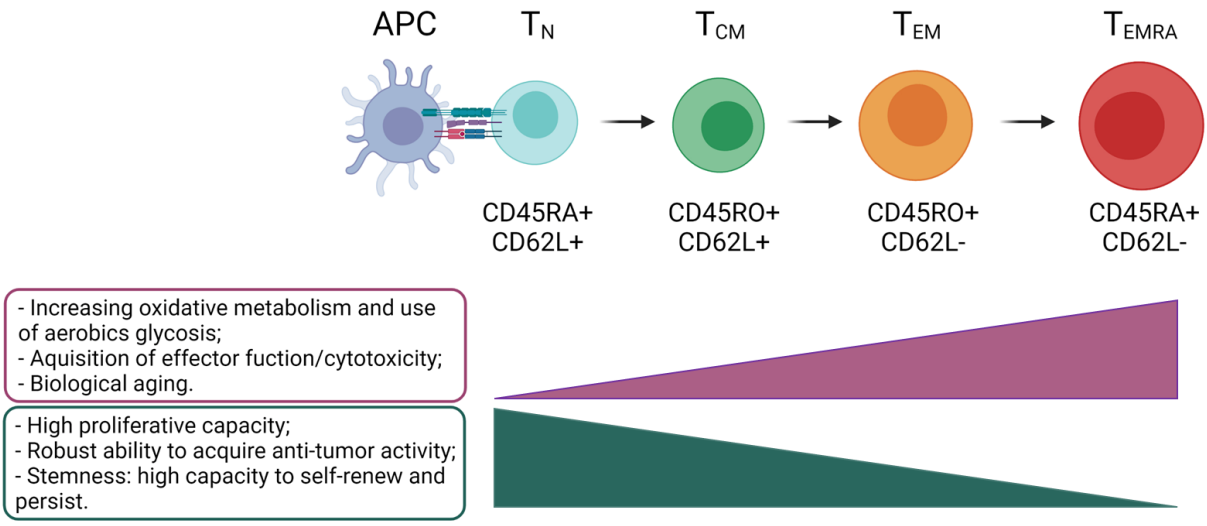

Figure 1.2 Differentiation of T cells from T_N to T_{CM}, T_{EM}, and T_{EMRA}. The diagram displays the metabolic alterations along the T cell differentiation.

1.2.2 Lymph nodes

There are hundreds of LNs (**Figure 1.3**) distributed throughout our bodies, all connected by the so called lymphatic system.[37] They promote cellular motility and T cell-APC interactions.[38,39] The LNs are divided in various micro compartments, such as the T and B cell zones, formed by connective tissue strands.[40] Specifically, the inner part of the LNs consists of reticular fibers forming a network of extracellular matrix (ECM) proteins. These proteins are mainly collagen but also fibronectin, laminin, entactin, or heparan sulfate,[41] responsible to form and support the LN compartments.[40,42] Furthermore, this network is highly covered by the non-hematopoietic stromal cells that exist in the LNs, forming a dense cellular environment.[38]

These stromal cells combined with circulating biomolecules (e.g. cytokines among others) provide an optimal environment for the survival, migration, activation, proliferation and differentiation of T cells.[43,44]

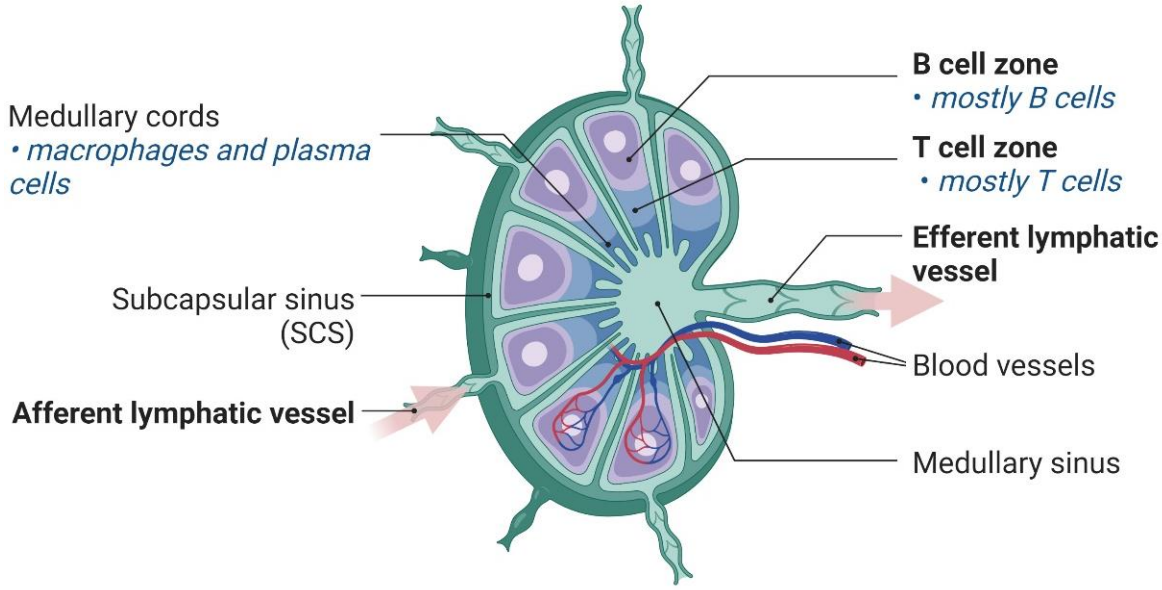

Figure 1.3 Representation of the LN structure, showing its complex microarchitecture. Lymph flow direction within the LN is depicted with arrows.

1.3 Main cancer immunotherapies

Immunotherapy is advancing towards the control of fundamental immune mechanisms to actively distinguish between healthy and cancerous tissues, and act specifically against malignant cells. Nowadays, there are two major strategies, the immune checkpoint therapy and ACT.[45]

The immune checkpoint therapy consists of targeting and controlling the regulatory immune pathways in order to enhance the T cell immune response. To counter act immunosuppression induced by tumors, the blockade of down-regulating molecules and inhibitory signaling pathways can be performed by the use of specific antibodies, also called immune checkpoint inhibitors, leading to the proper activation of T cells and response against the tumour.[46,47] Two of the most

relevant antibodies are the ones against CTLA-4 and the programmed cell death protein 1 (PD-1) or its ligand (PDL-1).

On the other hand, ACT involves the collection of (usually, autologous) T cells from peripheral blood or tumor excision, their *ex vivo* selection or engineering, their expansion *in vitro*, and their reinfusion into the patient to fight cancer cells (**Figure 1.4**).[48]

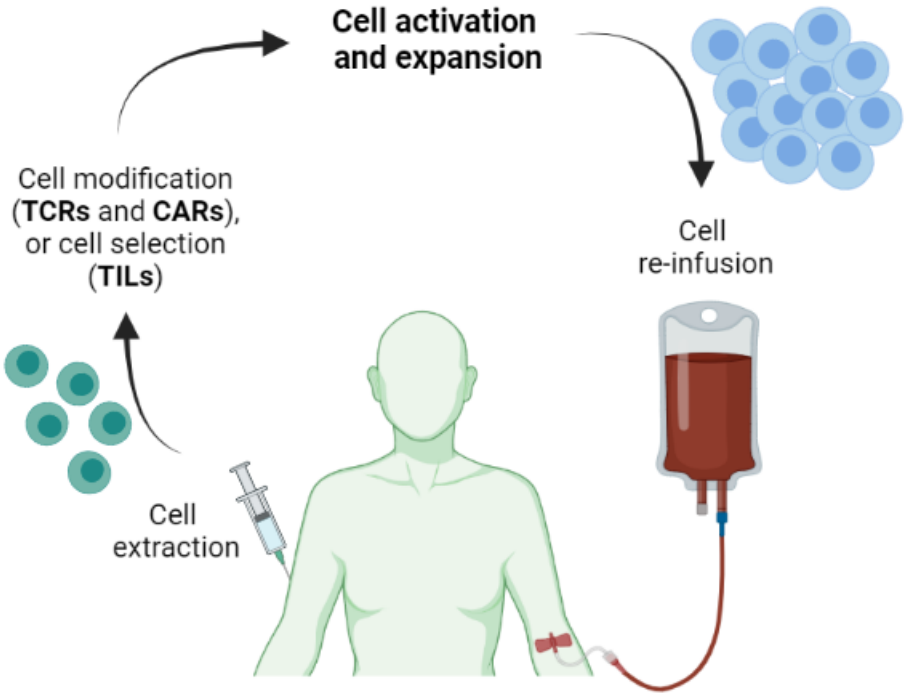

Figure 1.4 General diagram of the process of ACT for cancer treatment.

It is worth mentioning that, through memory subsets, durable antitumor therapeutic immunity was achieved in some cases of metastatic melanoma, lymphoma, lymphoid leukemias and other refractory tumors.[49–52] Thus, the potential of this cellular therapy is undoubtful. However, current ACTs have several challenges to overcome in order to become a commonly accessible anticancer therapy to the public.

There are different types of ACT depending of the T cell type employed. TIL-based techniques use autologous immune cells (generally mixtures of CD8+ and CD4+ T cells) extracted from cancer

tissues. TILs are specific against tumor cells, and thus can recognize tumor-associated antigens (TAAs).[53]

Although this strategy has been used in several solid cancers like renal, ovarian, breast and colon,[19] most of its success has been achieved with melanoma.[54] Nevertheless, this strategy has some limitations, like the difficulty of selecting and expanding pre-existing tumor-reacting T cells from patients with tumor types other than melanoma.

Recent advances have indicated that employing engineered T cells may be a better strategy to target cancer in some cases.[55] TCR-modified cells are T cells harvest from patients, that are further genetically modified (with genes obtained from a tumor-reactive T cell) to express its TCR, thus conferring the antigen-specificity of the transferred TCR to the T cells (**Figure 1.5**). The first reported cancer regression in melanoma patients with a TCR targeting MART-1 was successfully achieved in 2006.[56] However, this technique is still susceptible of causing severe adverse events, by destroying healthy tissues that express the target antigen in lower quantities, rising the importance of identifying target antigens that are highly selective only for tumor cells.

On the other hand, CAR T cells have tumor-reactivity because of their transduction with an artificial receptor, the CAR, consisting of an antibody variable domain fused to a TCR constant domain (**Figure 1.5**).

More specifically, CARs are synthetic constructs usually conformed by the tumor-reactive receptor, a CD3δ signaling domain and a costimulatory domain.[57] In another words, CAR T cells obtain the antigen recognition properties of an antibody, and thus, there is no need for dendritic cells.[58]

Several cases of medical successes have been reported with the use of CAR T cells targeting CD19 and CD20 to treat chronic lymphocytic leukemia (CLL), B-cell lymphoma and acute lymphoblastic leukemia (ALL).[24,59–62] Trials with CARs have also been performed to treat solid cancers, but the success rate is very limited, mostly due to the immunosuppressive capacity of the tumor microenvironment and the difficulty of identifying a suitable target antigen.[19]

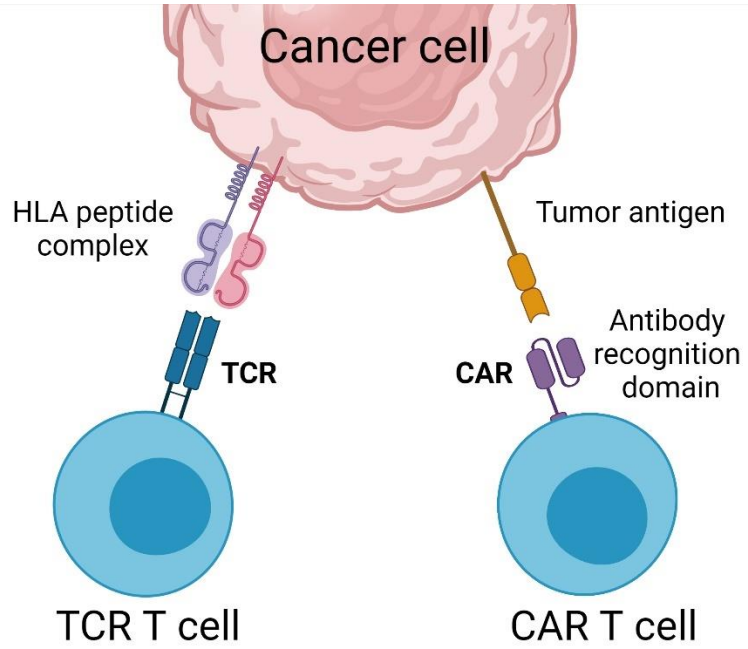

Figure 1.5 Scheme of the antigen-specificity of the transferred human TCR-T cells and CAR-T cells.

It is also worth noting in ACT strategies that different T cell subset plays different critical roles. The CD8+ subset is well known to display cytotoxic functions, while CD4+ T cells were thought to mostly help directing the immune response and activating cytotoxic subsets. However, there are indications that the combined effect of CD4+ and CD8+ T cell subsets results on the improvement of antitumor effectivity.[63–67] Furthermore, in some specific applications, CD4+ CAR T cells have recently proven to induce a higher antitumor responses when compared with CD8+ T cells alone, by ensuring a more persistent effect against some antigens in mice.[68] Indeed, CD4+ T cells are less inclined to exhaustion than CD8+ T cells.[69]

Furthermore, CAR T cells derived from T_N and T_{CM} subsets were reported to be more persistent than T_{EM} for a long-term immunity, while producing greater levels of cytokines. These findings highlight the importance in selecting adequate differentiated subsets to improve the efficacy of current cancer treatments.[63,68]

Finally, it is also worth mentioning that CD4+ T cells are an easy subset to purify given their natural abundance (up to 60% of total PBMCs), which makes them appealing for certain experimental procedures.

In summary, there are different advantages and disadvantages for each cell type used in the various ACTs, but all of them have a common step consisting of expanding the respective cell populations *ex vivo*. This step is currently one of the main limiting factors for the broad use of ACT in clinics, especially for TIL-based therapies.

Specifically, the time to produce these clinically relevant T cell types should be reduced, taking into consideration that patients with advanced cancers might worsen quickly. Also, the elevated costs derived from the bioengineering steps of T cells in the medical laboratories must be minimized. At present Kymriah® and Yescarta® (the two FDA-approved therapies) cost over 350 000 dollars per infusion, which points serious concerns over affordability.[70]

Thus, it is imperative to improve the performance of the state-of-the-art immune cell expansion systems to obtain clinically relevant doses in a short period of time and in a viable economic way.[71,72]

Another important challenge in immunotherapies relies on the development of adequate preclinical models capable to reduce the use of laboratory animals. The development of artificial models, such as organoids and organ-on a chip models, that could mimic to some extent the *in vivo* immune responses, would be very interesting for the field.

1.4 Current clinical expansion strategies for T cells

1.4.1 T cell activation and expansion agents

Current *ex vivo* T cell activation and proliferation systems are based on mimicking the APCs (**Figure 1.6 A**). Specifically, they use artificial APCs consisting of 3-5 µm-sized polymeric magnetic

covered with (co)stimulating antibodies, namely anti-CD3 and anti-CD28. (**Figure 1.6 B**).[38,73] Commercially, they are known as Dynabeads (Thermo Fisher Scientific) or MACS beads (Miltenyi Biotec GmbH). Nowadays, the majority of the clinical trials performed in the field of ACT to fight cancer use these beads.[65,74–76]

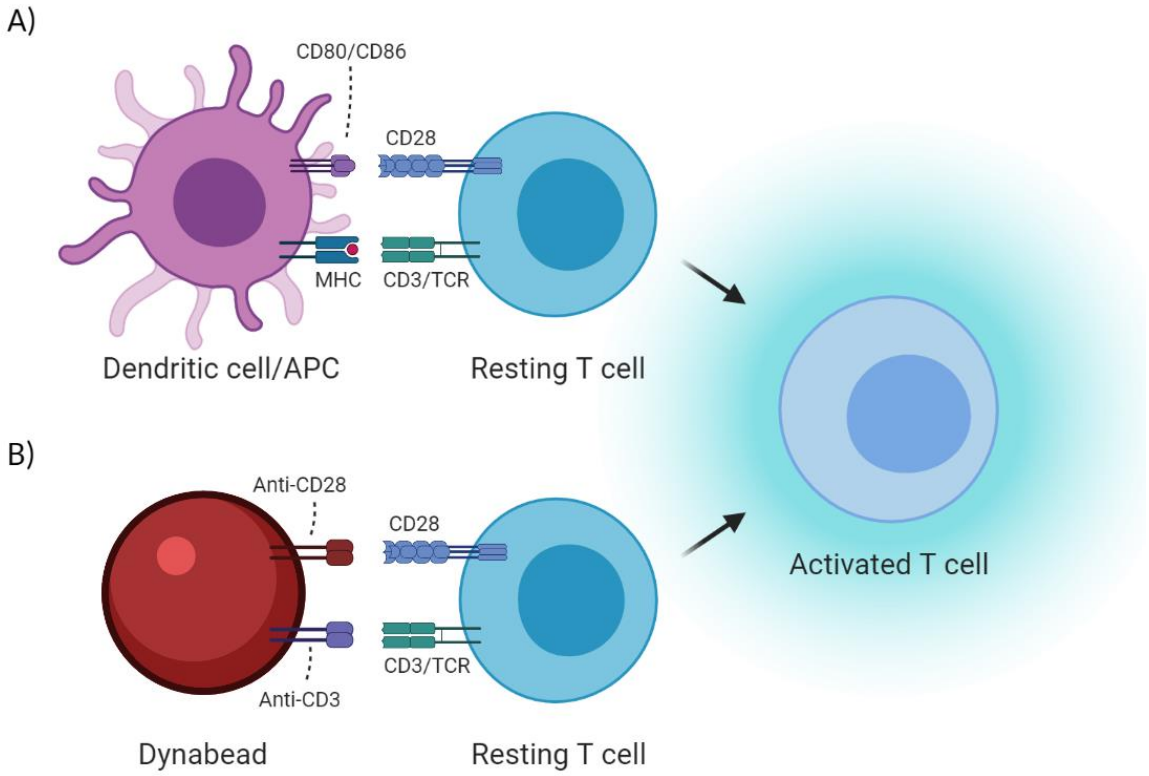

Figure 1.6 Representation of the IS. A) *In vivo* T cell activation process through its interaction with an APC (dendritic cell). B) *In vitro* activation of a T cell with a Dynabead.

Although they are simple to manipulate and remove through magnetic separation, they fail to provide the environmental signals naturally present in the human SLOs. The ECM of LNs is an important regulator of the T cell function, providing stimulatory biomechanical stimuli, that lead to adequate T cell communication, proliferation and differentiation.[44]

The alternatives to these artificial APCs (e.g. Dynabeads) are the use of mitogens[77–79], cell-based activation strategies[80–82] and antibody-based activations.[83,84]

Mitogens are soluble peptides or small proteins that induce cell division. Examples are the phytohemagglutinin (PHA), concanavalin A (ConA), pokeweed mitogen (PWM) or phorbol-12-myristate-13-acetate (PMA). Although some studies still use this strategy, as it was recently demonstrated in a clinical trial where PHA-expanded TILs were employed to treat patients with advanced melanoma[85] the implementation of these traditionally used mitogens has decreased, as it has been seen that with an antigen-specific stimulation a more physiologically relevant T cell activation occurs.[86]

With this objective, cell-based activation strategies that directly use APCs (e.g. dendritic cells and macrophages) to activate T cells have been described.[87] For example, they have been employed to activate TILs in ACT to treat melanoma patients.[80] Although these endogenous T cell activators provide a more *in vivo* like stimulation, their use has some general challenges such as the cost of generating good manufacture practices (GMP)-qualified APCs, risks of incomplete removal from the therapeutic cell population, potential donor-to-donor variation, and the limiting amount of these cells in the source material, especially if using autologous feeder cells from critically ill patients.[81] Furthermore dendritic cell-based expansions are time consuming, as they often require multiple cultures, large number of cytokines and long periods of time to get relevant numbers of T cells.[82]

Taking into account the challenges above mentioned, the use of more accessible approaches than cell-based methods, but more physiologically relevant than mitogens, has been popularized with antibody-based activations. These activation systems consist of the addition of antibodies, such as OKT3, an anti-CD3 monoclonal antibody (mAbs) that activates T cells by signal transduction through the TCR complex. For example, soluble anti-CD3 and recombinant IL-2 have been used to expand T cells with engineered TCRs for ACT. In a pilot trial, the expansion of T cells transduced with an NY-ESO-1-reactive TCR achieved durable tumor remissions in patients with metastatic synovial cell sarcoma and melanoma.[84]

However, the majority of the clinical trials performed in the field of immunotherapy to fight cancer uses the commercially available paramagnetic beads coated with anti-CD3 and anti-CD28,

whereas the use of soluble antibody strategies are usually limited to activations were large expansion of T cells are not required.

1.4.2 Bioreactors for T cell activation and expansion

Many of the available T cell bioreactors were inspired by a technology used to grow bacteria and yeast,[88] with the major objective of maximizing the numbers of T cells obtained, while reducing potential contaminations. The most common ones are those based on static, gas permeable culture bags, such as the G Rex bioreactors, WAVE bioreactors and the CliniMACS Miltenyi Prodigy system (**Figure 1.7**).[81]

The G Rex flasks consist of a common cell culture flask with a gas-permeable membrane on its base able to support large volumes of cell culture medium while allowing gas exchange. They provide a cell culture environment that should be linearly scalable and adaptable as a closed system, facilitating the translation of cell-based therapeutics from the laboratories to the clinics.[89] For example, it has been used to create in the clinics antigen-specific cytotoxic T cells for ACT.[90,91]

Figure 1.7 G Rex flask, (courtesy of ScaleReady); WAVE bioreactor, (courtesy of Cytiva); and CliniMACS Prodigy, (courtesy of CliniMACS Miltenyi Biotec).

However, in order to obtain a precise control on critical variables such as pH or media flow, other bioreactor systems have been developed such as the WAVE bioreactor or the Miltenyi Prodigy system.

The WAVE bioreactor also uses sterile culture bags that are transparent, disposable and allow cell culture media perfusion. This system allows high cell density, harvest, sampling and gas exchange.[92] They are also compatible with GMP conditions.[93] As an example, TILs from 4 melanoma patients were expanded in the WAVE bioreactor and compared with a traditional static culture method (gas-permeable bags). The WAVE bioreactor contributed for a rapid expansion of TILs, but no phenotypic or other differences between processes were identified.[92]

Finally, the CliniMACS Prodigy device is the first computer-controlled bioreactor in which each processing step can be automatized in a completely close system. This recent technology has been mainly employed in the optimization of T cell separation, selection and expansion protocols showing its robustness and reproducibility.[94–97] For example, the efficiency of the Prodigy has already been seen in the production of CAR-T cells (targeting CD19 and CD20), which did not require a clean-room facility.[98]

However, bioreactors mostly work with cells in suspension, but LNs are complex organs as explained above, and two-dimensional (2D) as well as suspension culture methods are not properly resembling the natural 3D environment of immune cells *in vivo*.[99]

1.5 Toward 3D cell culture

In order to mimic tissues and organs and/or recapitulate their key functions, the growing field of tissue engineering is developing and combining 3D scaffolds from natural or synthetic origin.[43] Among the most promising strategies, there are the hydrogels, which are (visco)elastic networks with interstitial spaces that can contain up to 99% w/w water.[100–102] This property confers the hydrogels their excellent capacity to mimic the ECM.

Natural hydrogels, which normally consist of natural ECM components and/or contain biologically recognizable moieties, are biocompatible and sometimes biodegradable.[103] The most prominent example is collagen, especially collagen type I, as it is the major structural component of many tissues.[104] Furthermore, collagen is a low-cost material easy to obtain and manipulate with great cytocompatibility. These collagen characteristics not only have called the attention of academic researchers, but also of companies like Viscofan SA. The first example in literature of fabricating an *in vivo* artificial SLO was done with collagen sponges as 3D scaffold for cell culture. TEL-2, a thymic stromal cell line, was used after being altered to express lymphotoxin-alfa, contributing to form a lymphoid tissue.[105] These collagen sponges once implanted into mice led to segregated B and T cells clusters as analyzed by immunohistochemical staining, and even high endothelial venule-like structures comparable to the ones found in the LNs. More interestingly, these artificial SLOs allowed B and T cell activation, which in immunodeficient mice enabled antigen specific immune responses.[106] More recently, the same research group, added gel beads on the collagen scaffolds, that could slowly release a cocktail of lymphorganogenic chemokines in the absence of lymphoid tissue organizer stromal cells.[107] Nevertheless, collagen 3D scaffolds have not yet been used for the activation and expansion of T cells for ACT applications.

Towards a drug screening application, agarose gels were used as scaffolds to create an artificial SLO model. In this study, human T cell clustering and proliferation was observed, after exposure with APCs.[108]

However, these natural hydrogels face some intrinsic disadvantages that challenge their translation to the clinics, such as the lack of reproducibility among samples, poor mechanical properties, low tuneability, and furthermore, they may trigger immune/inflammatory responses.[103]

Synthetic hydrogels usually offer the possibility to precisely control their chemical, structural and mechanical properties, although they do not have any inherent bioactivity.[103] Among the plethora of options, PEG is one of the most used synthetic polymers in tissue engineering, thanks to their interesting physicochemical properties. However, there are many more options, as

proven by the growing industry interest on the development of new synthetic hydrogels. For example, the small-medium enterprise (SME) Biogelx Limited is using aromatic peptide amphiphiles that can form self-supporting hydrogels with tunable mechanical properties and chemical compositions. These hydrogels can be applied in 2D and 3D cell cultures,[109–114] but up to date, no studies have been reported on the effect of such materials on lymphocyte expansion and differentiation.

With this objective, our research group performed a market study of the commercially available 3D scaffolds and studied two systems with very different physicochemical properties for T cell culture and expansion.[115] The synthetic 3D polystyrene scaffolds and Matrigel, a natural hydrogel prepared from a gelatinous protein mixture extract from the Engelbreth-Holm-Swarm mouse sarcoma. From this study we concluded that both 3D scaffolds improved human T cell proliferation, when compared with the state-of-the-art expansion method, i.e. Dynabeads in suspension, proving our hypothesis about the importance of adding 3D LN-like structures in T cell cultures.[115]

However, these commercial options are still far from the actual LN structural, mechanical and biochemical properties. For such reason there is a need to develop more realistic 3D scaffolds that better mimics the LN environment, with the potential to result in superior expansion rates of certain T cell phenotypes.

For that, we have recently reported 3D hydrogels with a design inspired by the LNs.[116] In these 3D scaffolds, we used cross-linked poly(ethylene)glycol (PEG) which provided the structural support, and heparin (Hep) that can bind to different proteins such as the cytokine CCL21, through its anionic character (**Figure 1.8**).[117,118]

The 3D PEG-Hep hydrogels developed can be tuned in terms of physicochemical properties by changing the concentration of PEG. We found the hydrogels produced with 3% weight (wt) PEG to have a fibrillar structure with a mean pore size of 55 µm and a storage modulus of 0.75 KPa.[116] These hydrogels were found to improve the proliferation of primary human CD4+ T cells when compared with the state-of-the-art T cell expansion systems in suspension. This improvement

was further enhanced by loading these scaffolds with CCL21 molecules, a known cytokine to promote T cell homing and proliferation.[44,119–121]

Besides, hydrogels with enlarged and homogeneous pore structures using the inverse opal (IOPAL) or inverted colloidal crystal technique, as a porogen method, have been reported.[122,123] They have been shown to increase T cell migration,[124] but no examples of IOPAL hydrogels for T cell expansion experiments have been reported up to now. The structuration method is reported to provide a porosity above 70%, being the reproducibility of the synthesis process one of the main advantages of the method. Moreover, the uniform interconnectivity achieved leads to a more homogeneous distribution of macromolecules and cells inside the 3D scaffold.[125,126]

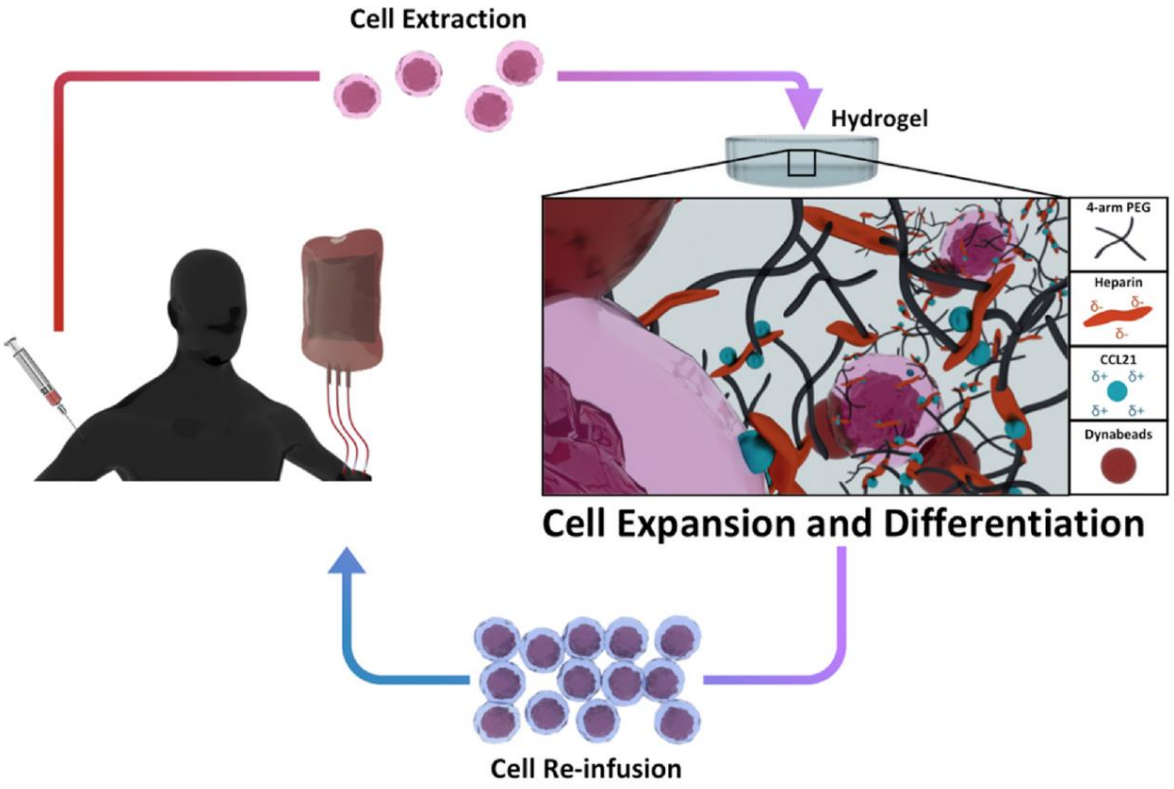

Figure 1.8 Simplified scheme of an ACT process with T cells cultured in the CCL21-loaded PEG-Hep hydrogels (not to scale). Human primary CD4+ T cells from adult healthy donors were activated with Dynabeads and used as a proof-of-concept prior to testing with patients. Thus, the expanded and differentiated T cells were not reinfused. (Adapted from ref. [116]).

1.6. Lymph Node-on-a-chip

Another main factor to be taken into consideration to recreate the natural LN conditions is the fluid flow, which can be studied and mimicked with microfluidic devices.[127] These devices allow the continuous circulation of cell culture medium, with a constant supply of nutrients while the cellular waste is removed. Additionally, the mechanical stimulus from the flow is expected to have an influence on cell morphology and behavior, as seen with the flow shear stress known to promote lymphocyte transmigration across inflamed endothelial barriers.[128] Moreover, shear stress variations affect naïve T cell interactions with APCs inside the LNs, thus influencing T cell activation and further development.[129]

As briefly discussed in the section 1.2.2, (**Figure 1.3**) the lymph flow enters the LNs through various afferent lymphatic vessels passing through the subcapsular sinus (SCS) and then flows into the trabecular sinuses within the cortex. Subsequently, the lymph passes through the medulla and gathers in the connected medullary sinus, draining into the efferent lymphatic vessels to leave the LNs.[130,131] This net unidirectional lymph flow, from afferent to efferent lymphatic vessels, found in the LNs is caused by intrinsic (such as phasic and fast vessel contractions) and extrinsic (such as muscle contraction and respiration) pumping processes.[132]

Emergent advanced techniques are allowing to obtain quantitative information about the lymph flow *in vivo*, despite the technical challenge, improving the knowledge of lymphatic mechanobiology.[130] Still, differences are observed in the results obtained for the lymph flow rates ranging from 0.3-14.0 µL/h, mainly due to the different animal models used, intrinsic variations of lymph flow and techniques employed.[133–135]

In recent years microfluidic devices submitted to a flow have been used to create LN-on-a-chip models. As an example, an *ex vivo* polydimethylsiloxane (PDMS) microfluidic device with flow rates ranging from 7.2 to 24 µL/h allowed a spatiotemporal control of induced stimuli on mice LN slices embedded in agarose gel, thus forming a LN slice-on-a-chip.[136]

Recently, a multi-compartment microfluidic chip was fabricated to mimic inter-organ communication *ex vivo* between tumor and LN mice tissues. Specifically, a microfluidic chip constructed by several layers of PDMS and polymethyl methacrylate (PMMA) was filled with tissue slices embedded in agarose. They were interconnected with continuous medium recirculating with volumetric flow values varying from 30 to 120 µL/h.[137]

Finally, HIRIS™ III and IG-Device™ are two devices that were developed to mimic the *in vivo* LN environment. Both have been operated for long periods of time (14-30 days) with a continuous flow rate of 45 µL/h by using a peristaltic pump. The HIRIS™ III is a polysulfone device which attempts to recreate the human LN environment *in vitro* with emphasis on T cell activation. Briefly, this device consisted of a stationary network of human mature dendritic cells in an agarose hydrogel matrix separated by microporous membranes from a compartment with a suspension of B and T cells. The IG-Device™ is the first 3D-organoid system of a human LN for *in vitro* testing of immune functions.[108] This device holds different individually perfused culture compartments assembled for multi-parallel exposure of different drugs to matrix-assisted co-cultures. These cell cultures consisted of organoids formed with dendritic cells, B cells, T cells and agarose hydrogels.

These systems are an encouraging proof-of-concept of the benefits of including flow to artificial 3D LNs to better recreate the natural conditions that T cells find in these SLOs. However, the examples described so far do not consider the complex 3D structure, mechanical properties and composition of the LN ECM. In addition, these studies have not assessed the effect of flow in T cell proliferation and differentiation in detail, nor its possible potential to improve ACT platforms for cell culture.

1.7 Objectives

The focus of this PhD thesis was the synthesis, preparation, and use of new 3D hydrogel platforms for lymphocyte (primary human CD4+ T cells) proliferation and differentiation to improve ACT.

Specifically, we aimed at mimicking the ECM of SLOs in order to create a more appropriate and realistic environment for immune cells.

Within this main goal, several specific objectives were proposed:

1. Study the potential of commercially available synthetic peptide-based supramolecular 3D hydrogels in collaboration with the SME Biogelx Ltd. **(Chapter 2)**.

2. Study the potential of in-development collagen matrices in collaboration with the publicly traded company Viscofan S.A. to mimic the LN composition **(Chapter 3)**.

3. Design and optimization of an artificial ECM inspired by the LNs, based on 3D PEG-Hep hydrogels with controlled pore sizes and interconnectivity, achieved through the inverse opal porogen strategy **(Chapter 4)**.

4. Design, fabrication and optimization of a microfluidic device to submit artificial LNs consisting of 3D PEG-Hep hydrogels and T cells to a flow to mimic the lymph **(Chapter 5)**.

1.8 References

1. Hoption Cann, S. A., van Netten, J. P. & van Netten, C. Dr William Coley and tumour regression: a place in history or in the future. *Postgrad. Med. J.* **79**, 672–680 (2003).

2. McCarthy, E. F. The toxins of William B. Coley and the treatment of bone and soft-tissue sarcomas. *Iowa Orthop. J.* **26**, 154–158 (2006).

3. Leech, P. N. Erysipelas and prodigiosus toxins (Coley). *J. Am. Med. Assoc* **103**, 1067–1069 (1934).

4. Coley, W. B. The treatment of inoperable sarcoma with the 'mixed toxins of erysipelas and bacillus prodigiosus.: immediate and final results in one hundred and forty cases. *J. Am. Med. Assoc.* **XXXI**, 456–465 (1898).

5. Coley, W. B. The treatment of malignant tumors by repeated inoculations of erysipelas: With a report of ten original cases. *Am. J. Med. Sci.* **105**, 487–516 (1893).

6. Fesnak, A. D., June, C. H. & Levine, B. L. Engineered T cells: the promise and challenges of cancer immunotherapy. *Nat. Rev. Cancer* **16**, 566–581 (2016).

7. Cohn, M. *et al.* Reflections on the clonal-selection theory. *Nat. Rev. Immunol.* **7**, 823–830 (2007).

8. Burnet, F. M. Cancer: a biological approach. III. Viruses associated with neoplastic conditions. IV. Practical applications. *Br. Med. J.* **1**, 841–847 (1957).

9. Dausset, J. Leucocytes, Platelets and Human Homografts. *Vox Sang.* **7**, 257–266 (1962).

10. Steinman, R. M. & Cohn, Z. A. Identification of a novel cell type in peripheral lymphoid organs of mice. I. Morphology, quantitation, tissue distribution. *J. Exp. Med.* **137**, 1142–1162 (1973).

11. Zinkernagel, R. M. & Doherty, P. C. Restriction of in vitro T cell-mediated cytotoxicity in lymphocytic choriomeningitis within a syngeneic or semiallogeneic system. *Nature* **248**, 701–702 (1974).

12. Köhler, G. & Milstein, C. Continuous cultures of fused cells secreting antibody of predefined specificity. *Nature* **256**, 495–497 (1975).

13. Taniguchi, T. *et al.* Structure and expression of a cloned cDNA for human interleukin-2. *Nature* **302**, 305–310 (1983).

14. Arya, S. K. & Gallo, R. C. Transcriptional modulation of human T-cell growth factor gene by phorbol ester and interleukin 1. *Biochemistry* **23**, 6685–6690 (1984).

15. Arya, S. K. & Gallo, R. C. Human T-cell growth factor (interleukin 2) and gamma-interferon genes: expression in human T-lymphotropic virus type III-and type I-infected cells. *Proc. Natl. Acad. Sci.* **82**, 8691–8695 (1985).

16. Cantrell, D. A. & Smith, K. A. The interleukin-2 T-cell system: a new cell growth model. *Science* **224**, 1312–1316 (1984).

17. Haskins, K. *et al.* The major histocompatibility complex-restricted antigen receptor on T cells. I. Isolation with a monoclonal antibody. *J. Exp. Med.* **157**, 1149–1169 (1983).

18. Kappler, J. *et al.* The major histocompatibility complex-restricted antigen receptor on T cells in mouse and man: Identification of constant and variable peptides. *Cell* **35**, 295–302 (1983).

19. Feldman, S. A., Assadipour, Y., Kriley, I., Goff, S. L. & Rosenberg, S. A. Adoptive Cell Therapy-

-Tumor-Infiltrating Lymphocytes, T-Cell Receptors, and Chimeric Antigen Receptors. *Semin. Oncol.* **42**, 626–639 (2015).

20. Muul, L. M., Spiess, P. J., Director, E. P. & Rosenberg, S. A. Identification of specific cytolytic immune responses against autologous tumor in humans bearing malignant melanoma. *J. Immunol.* **138**, 989–995 (1987).

21. Rosenberg, S. A. *et al.* Use of tumor-infiltrating lymphocytes and interleukin-2 in the immunotherapy of patients with metastatic melanoma. A preliminary report. *N. Engl. J. Med.* **319**, 1676–1680 (1988).

22. Plosker, G. L. Sipuleucel-T. *Drugs* **71**, 101–108 (2011).

23. Cameron, F., Whiteside, G. & Perry, C. Ipilimumab. *Drugs* **71**, 1093–1104 (2011).

24. Porter, D. L., Levine, B. L., Kalos, M., Bagg, A. & June, C. H. Chimeric antigen receptor-modified T cells in chronic lymphoid leukemia. *N. Engl. J. Med.* **365**, 725–733 (2011).

25. Yip, A. & Webster, R. M. The market for chimeric antigen receptor T cell therapies. *Nat. Rev. Drug Discov.* **17**, 161–162 (2018).

26. Terawaki, S. *et al.* IFN-α Directly Promotes Programmed Cell Death-1 Transcription and Limits the Duration of T Cell-Mediated Immunity. *J. Immunol.* **186**, 2772–2779 (2011).

27. Waitz, R. *et al.* Potent Induction of Tumor Immunity by Combining Tumor Cryoablation with Anti–CTLA-4 Therapy. *Cancer Res.* **72**, 430–439 (2012).

28. Velcheti, V. & Schalper, K. Basic Overview of Current Immunotherapy Approaches in Cancer. *Am. Soc. Clin. Oncol. Educ. book. Am. Soc. Clin. Oncol. Annu. Meet.* **35**, 298–308 (2016).

29. Hoebe, K., Janssen, E. & Beutler, B. The interface between innate and adaptive immunity. *Nat. Immunol.* **5**, 971–974 (2004).

30. Ruddle, N. H. & Akirav, E. M. Secondary lymphoid organs: responding to genetic and environmental cues in ontogeny and the immune response. *J. Immunol.* **183**, 2205–2212 (2009).

31. Acosta Davila, J. A. & Hernandez De Los Rios, A. An Overview of Peripheral Blood Mononuclear Cells as a Model for Immunological Research of Toxoplasma gondii and Other Apicomplexan Parasites. *Front. Cell. Infect. Microbiol.* **9**, 1–10 (2019).

32. Dustin, M. L. The immunological synapse. *Cancer Immunol. Res.* **2**, 1023–1033 (2014).

33. Harris, D. T. & Kranz, D. M. Adoptive T Cell Therapies: A Comparison of T Cell Receptors and Chimeric Antigen Receptors. *Trends Pharmacol. Sci.* **37**, 220–230 (2016).

34. Kishton, R. J., Sukumar, M. & Restifo, N. P. Metabolic Regulation of T Cell Longevity and Function in Tumor Immunotherapy. *Cell Metab.* **26**, 94–109 (2017).

35. Sadelain, M., Rivière, I. & Riddell, S. Therapeutic T cell engineering. *Nature* **545**, 423–431 (2017).

36. Ghassemi, S. *et al.* Reducing Ex Vivo Culture Improves the Antileukemic Activity of Chimeric Antigen Receptor (CAR) T Cells. *Cancer Immunol. Res.* **6**, 1100–1109 (2018).

37. Standring, S. *Gray's anatomy : the anatomical basis of clinical practice*. (Elsevier Health Sciences, 2015, 2008).

38. Cupedo, T., Stroock, A. & Coles, M. Application of tissue engineering to the immune system: Development of artificial lymph nodes. *Front. Immunol.* **3**, 1–6 (2012).

39. Purwada, A. *et al.* Ex vivo engineered immune organoids for controlled germinal center reactions. *Biomaterials* **63**, 24–34 (2015).

40. Mueller, S. N. & Germain, R. N. Stromal cell contributions to the homeostasis and functionality of the immune system. *Nat. Rev. Immunol.* **9**, 618–629 (2009).

41. Kramer, R. H., Rosen, S. D. & McDonald, K. A. Basement-membrane components associated with the extracellular matrix of the lymph node. *Cell Tissue Res.* **252**, 367–375 (1988).

42. van de Pavert, S. A. & Mebius, R. E. New insights into the development of lymphoid tissues. *Nat. Rev. Immunol.* **10**, 664–674 (2010).

43. Caliari, S. R. & Burdick, J. A. A practical guide to hydrogels for cell culture. *Nat. Methods* **13**, 405–414 (2016).

44. Saxena, V. *et al.* Role of lymph node stroma and microenvironment in T cell tolerance. *Immunol. Rev.* **292**, 9–23 (2019).

45. Galluzzi, L. *et al.* Classification of current anticancer immunotherapies. *Oncotarget* **5**, 12472–12508 (2014).

46. Sharma, P. & Allison, J. P. The future of immune checkpoint therapy. *Science* **348**, 56–61 (2015).

47. Munn, D. H. & Bronte, V. Immune suppressive mechanisms in the tumor microenvironment. *Curr. Opin. Immunol.* **39**, 1–6 (2016).

48. Restifo, N. P., Dudley, M. E. & Rosenberg, S. A. Adoptive immunotherapy for cancer: harnessing the T cell response. *Nat. Rev. Immunol.* **12**, 269–281 (2012).

49. Rosenberg, S. A. *et al.* Durable complete responses in heavily pretreated patients with metastatic melanoma using T-cell transfer immunotherapy. *Clin. Cancer Res.* **17**, 4550–4557 (2011).

50. Robbins, P. F. *et al.* Tumor regression in patients with metastatic synovial cell sarcoma and melanoma using genetically engineered lymphocytes reactive with NY-ESO-1. *J. Clin. Oncol.* **29**, 917–924 (2011).

51. Kochenderfer, J. N. *et al.* Eradication of B-lineage cells and regression of lymphoma in a patient treated with autologous T cells genetically engineered to recognize CD19. *Blood* **116**, 4099–4102 (2010).

52. Brentjens, R. J. *et al.* Safety and persistence of adoptively transferred autologous CD19-targeted T cells in patients with relapsed or chemotherapy refractory B-cell leukemias. *Blood* **118**, 4817–4828 (2011).

53. Radvanyi, L. G. *et al.* Specific lymphocyte subsets predict response to adoptive cell therapy using expanded autologous tumor-infiltrating lymphocytes in metastatic melanoma patients. *Clin. Cancer Res.* **18**, 6758–6770 (2012).

54. Goff, S. L. *et al.* Tumor infiltrating lymphocyte therapy for metastatic melanoma: analysis of tumors resected for TIL. *J. Immunother.* **33**, 840–847 (2010).

55. Zhang, S. *Progress in Cancer Immunotherapy. Advances in experimental medicine and biology* (2016).

56. Morgan, R. A. *et al.* Cancer regression in patients after transfer of genetically engineered lymphocytes. *Science* **314**, 126–129 (2006).

57. Inaguma, Y. *et al.* Construction and molecular characterization of a T-cell receptor-like antibody and CAR-T cells specific for minor histocompatibility antigen HA-1H. *Gene Ther.* **21**, 575–584 (2014).

58. Gross, G., Waks, T. & Eshhar, Z. Expression of immunoglobulin-T-cell receptor chimeric molecules as functional receptors with antibody-type specificity. *Proc. Natl. Acad. Sci. U. S. A.* **86**, 10024–10028 (1989).

59. Kalos, M. *et al.* T cells with chimeric antigen receptors have potent antitumor effects and can establish memory in patients with advanced leukemia. *Sci. Transl. Med.* **3**, 1–11 (2011).

60. Grupp, S. A. *et al.* Chimeric antigen receptor-modified T cells for acute lymphoid leukemia. *N. Engl. J. Med.* **368**, 1509–1518 (2013).

61. Davila, M. L. *et al.* Efficacy and toxicity management of 19-28z CAR T cell therapy in B cell acute lymphoblastic leukemia. *Sci. Transl. Med.* **6**, 1–23 (2014).

62. Maude, S. L. *et al.* Chimeric antigen receptor T cells for sustained remissions in leukemia. *N. Engl. J. Med.* **371**, 1507–1517 (2014).

63. Sommermeyer, D. *et al.* Chimeric antigen receptor-modified T cells derived from defined CD8+ and CD4+ subsets confer superior antitumor reactivity in vivo. *Leukemia* **30**, 492–500 (2016).

64. Borst, J., Ahrends, T., Bąbała, N., Melief, C. J. M. & Kastenmüller, W. CD4(+) T cell help in cancer immunology and immunotherapy. *Nat. Rev. Immunol.* **18**, 635–647 (2018).

65. Turtle, C. J. *et al.* CD19 CAR-T cells of defined CD4+:CD8+ composition in adult B cell ALL patients. *J. Clin. Invest.* **126**, 2123–2138 (2016).

66. Turtle, C. J. *et al.* Immunotherapy of non-Hodgkin's lymphoma with a defined ratio of CD8+ and CD4+ CD19-specific chimeric antigen receptor-modified T cells. *Sci. Transl. Med.* **8**, 1–24 (2016).

67. Brightman, S. E., Naradikian, M. S., Miller, A. M. & Schoenberger, S. P. Harnessing neoantigen specific CD4 T cells for cancer immunotherapy. *J. Leukoc. Biol.* **107**, 625–633 (2020).

68. Wang, D. *et al.* Glioblastoma-targeted CD4+ CAR T cells mediate superior antitumor activity. *JCI Insight* **3**, 1–18 (2018).

69. Wherry, E. J. T cell exhaustion. *Nat. Immunol.* **12**, 492–499 (2011).

70. Fiorenza, S., Ritchie, D. S., Ramsey, S. D., Turtle, C. J. & Roth, J. A. Value and affordability of CAR T-cell therapy in the United States. *Bone Marrow Transplant.* **55**, 1706–1715 (2020).

71. Zarour, H. M. & Ferrone, S. Cancer immunotherapy: Progress and challenges in the clinical setting. *Eur. J. Immunol.* **41**, 1510–1515 (2011).

72. Oiseth, S. J. & Aziz, M. S. Cancer immunotherapy: a brief review of the history, possibilities, and challenges ahead. *J. Cancer Metastasis Treat.* **3**, 250–261 (2017).

73. Hickey, J. W., Vicente, F. P., Howard, G. P., Mao, H.-Q. & Schneck, J. P. Biologically Inspired Design of Nanoparticle Artificial Antigen-Presenting Cells for Immunomodulation. *Nano Lett.* **17**, 7045–7054 (2017).

74. Park, J. H. *et al.* Long-Term Follow-up of CD19 CAR Therapy in Acute Lymphoblastic Leukemia. *N. Engl. J. Med.* **378**, 449–459 (2018).

75. Brentjens, R. J. *et al.* CD19-targeted T cells rapidly induce molecular remissions in adults with chemotherapy-refractory acute lymphoblastic leukemia. *Sci. Transl. Med.* **5**, 1–19 (2013).

76. Liu, H. *et al.* CD19-specific CAR T Cells that Express a PD-1/CD28 Chimeric Switch-Receptor are Effective in Patients with PD-L1–positive B-Cell Lymphoma. *Clin. Cancer Res.* **27**, 473–484 (2021).

77. Touraine, J. L. *et al.* Phorbol myristate acetate: a mitogen selective for a T-lymphocyte subpopulation. *J. Exp. Med.* **145**, 460–465 (1977).

78. Suzawa, T. *et al.* Comparison of phorbol myristate acetate and phytohaemagglutinin as stimulators of in vitro T lymphocyte colony formation of human peripheral blood lymphocytes. I. Surface markers of colony cells. *Immunology* **53**, 499–505 (1984).

79. Cai, G. *et al.* Decrease in immune function and the role of mitogen-activated protein kinase (MAPK) overactivation in apoptosis during T lymphocytes activation induced by zearalenone, deoxynivalenol, and their combinations. *Chemosphere* **255**, 1–11 (2020).

80. Dudley, M. E., Wunderlich, J. R., Shelton, T. E., Even, J. & Rosenberg, S. A. Generation of tumor-infiltrating lymphocyte cultures for use in adoptive transfer therapy for melanoma patients. *J. Immunother.* **26**, 332–342 (2003).

81. Iyer, R. K., Bowles, P. A., Kim, H. & Dulgar-Tulloch, A. Industrializing Autologous Adoptive Immunotherapies: Manufacturing Advances and Challenges. *Front. Med.* **5**, 1–9 (2018).

82. Neal, L. R. *et al.* The Basics of Artificial Antigen Presenting Cells in T Cell-Based Cancer Immunotherapies. *J. Immunol. Res. Ther.* **2**, 68–79 (2017).

83. Chandran, S. S. *et al.* Treatment of metastatic uveal melanoma with adoptive transfer of tumour-infiltrating lymphocytes: a single-centre, two-stage, single-arm, phase 2 study. *Lancet. Oncol.* **18**, 792–802 (2017).

84. Robbins, P. F. *et al.* A pilot trial using lymphocytes genetically engineered with an NY-ESO-1-reactive T-cell receptor: long-term follow-up and correlates with response. *Clin. Cancer Res.* **21**, 1019–1027 (2015).

85. Saint-Jean, M. *et al.* Adoptive Cell Therapy with Tumor-Infiltrating Lymphocytes in Advanced Melanoma Patients. *J. Immunol. Res.* **2018**, 1–10 (2018).

86. Trickett, A. & Kwan, Y. L. T cell stimulation and expansion using anti-CD3/CD28 beads. *J. Immunol. Methods* **275**, 251–255 (2003).

87. Gomes-Silva, D. & Ramos, C. A. Cancer Immunotherapy Using CAR-T Cells: From the Research Bench to the Assembly Line. *Biotechnol. J.* **13**, 1–16 (2018).

88. Garcia-Aponte, O. F., Herwig, C. & Kozma, B. Lymphocyte expansion in bioreactors: upgrading adoptive cell therapy. *J. Biol. Eng.* **15**, 1–34 (2021).

89. Bajgain, P. *et al.* Optimizing the production of suspension cells using the G-Rex 'M' series. *Mol. Ther. Methods Clin. Dev.* **1**, 1–9 (2014).

90. Vera, J. F. *et al.* Accelerated production of antigen-specific T cells for preclinical and clinical applications using gas-permeable rapid expansion cultureware (G-Rex). *J. Immunother.* **33**, 305–315 (2010).

91. Jin, J. *et al.* Simplified method of the growth of human tumor infiltrating lymphocytes in gas-permeable flasks to numbers needed for patient treatment. *J. Immunother.* **35**, 283–292 (2012).

92. Sadeghi, A. *et al.* Large-scale bioreactor expansion of tumor-infiltrating lymphocytes. *J. Immunol. Methods* **364**, 94–100 (2011).

93. Somerville, R. P. T., Devillier, L., Parkhurst, M. R., Rosenberg, S. A. & Dudley, M. E. Clinical scale rapid expansion of lymphocytes for adoptive cell transfer therapy in the WAVE® bioreactor. *J. Transl. Med.* **10**, 1–11 (2012).

94. Klöß, S. *et al.* Optimization of Human NK Cell Manufacturing: Fully Automated Separation, Improved Ex Vivo Expansion Using IL-21 with Autologous Feeder Cells, and Generation of Anti-CD123-CAR-Expressing Effector Cells. *Hum. Gene Ther.* **28**, 897–913 (2017).

95. Priesner, C. *et al.* Automated Enrichment, Transduction, and Expansion of Clinical-Scale CD62L(+) T Cells for Manufacturing of Gene Therapy Medicinal Products. *Hum. Gene Ther.* **27**, 860–869 (2016).

96. Mock, U. *et al.* Automated manufacturing of chimeric antigen receptor T cells for adoptive immunotherapy using CliniMACS prodigy. *Cytotherapy* **18**, 1002–1011 (2016).

97. Lock, D. *et al.* Automated Manufacturing of Potent CD20-Directed Chimeric Antigen Receptor T Cells for Clinical Use. *Hum. Gene Ther.* **28**, 914–925 (2017).

98. Zhu, F. *et al.* Closed-system manufacturing of CD19 and dual-targeted CD20/19 chimeric antigen receptor T cells using the CliniMACS Prodigy device at an academic medical center. *Cytotherapy* **20**, 394–406 (2018).

99. Tibbitt, M. W. & Anseth, K. S. Hydrogels as extracellular matrix mimics for 3D cell culture. *Biotechnol. Bioeng.* **103**, 655–663 (2009).

100. Wichterle, O. & Lim, D. Hydrophilic Gels for Biological Use. *Nature* **185**, 117–118 (1960).

101. Peppas, B. N. A., Hilt, J. Z., Khademhosseini, A. & Langer, R. Hydrogels in Biology and Medicine : From Molecular Principles to Bionanotechnology. *Adv. Mater.* **18**, 1345–1360 (2006).

102. Drury, J. L. & Mooney, D. J. Hydrogels for tissue engineering: Scaffold design variables and applications. *Biomaterials* **24**, 4337–4351 (2003).

103. Madduma-Bandarage, U. S. K. & Madihally, S. V. Synthetic hydrogels: Synthesis, novel trends, and applications. *J. Appl. Polym. Sci.* **138**, 1–23 (2021).

104. Shoulders, M. D. & Raines, R. T. Collagen Structure and Stability Ann Rev Biochemistry. *Annu Rev Biochem* **78**, 929–958 (2009).

105. Suematsu, S. & Watanabe, T. Generation of a synthetic lymphoid tissue-like organoid in mice. *Nat. Biotechnol.* **22**, 1539–1545 (2004).

106. Okamoto, N., Chihara, R., Shimizu, C., Nishimoto, S. & Watanabe, T. Artificial lymph nodes induce potent secondary immune responses in naive and immunodeficient mice. *J. Clin. Invest.* **117**, 997–1007 (2007).

107. Kobayashi, Y. & Watanabe, T. Gel-Trapped Lymphorganogenic Chemokines Trigger Artificial Tertiary Lymphoid Organs and Mount Adaptive Immune Responses In Vivo. *Front. Immunol.* **7**, 1–10 (2016).

108. Giese, C. *et al.* Immunological substance testing on human lymphatic micro-organoids in vitro. *J. Biotechnol.* **148**, 38–45 (2010).

109. Simunovic, M. *et al.* A 3D model of a human epiblast reveals BMP4-driven symmetry breaking. *Nat. Cell Biol.* **21**, 900–910 (2019).

110. Smith, A. M. *et al.* Fmoc-diphenylalanine self assembles to a hydrogel via a novel architecture based on π-π interlocked β-sheets. *Adv. Mater.* **20**, 37–41 (2008).

111. Alakpa, E. V. *et al.* Improving cartilage phenotype from differentiated pericytes in tunable

peptide hydrogels. *Sci. Rep.* **7**, 1–11 (2017).

112. Jayawarna, V. *et al.* Nanostructured hydrogels for three-dimensional cell culture through self-assembly of fluorenylmethoxycarbonyl-dipeptides. *Adv. Mater.* **18**, 611–614 (2006).

113. Zhou, M. *et al.* Self-assembled peptide-based hydrogels as scaffolds for anchorage-dependent cells. *Biomaterials* **30**, 2523–2530 (2009).

114. Jayawarna, V., Smith, A., Gough, J. E. & Ulijn, R. V. Three-dimensional cell culture of chondrocytes on modified di-phenylalanine scaffolds. *Biochem. Soc. Trans.* **35**, 535–537 (2007).

115. Pérez Del Río, E., Martinez Miguel, M., Veciana, J., Ratera, I. & Guasch, J. Artificial 3D Culture Systems for T Cell Expansion. *ACS omega* **3**, 5273–5280 (2018).

116. Pérez Del Río, E. *et al.* CCL21-loaded 3D hydrogels for T cell expansion and differentiation. *Biomaterials* **259**, 1–13 (2020).

117. Freudenberg, U., Liang, Y., Kiick, K. L. & Werner, C. Glycosaminoglycan-Based Biohybrid Hydrogels: A Sweet and Smart Choice for Multifunctional Biomaterials. *Adv. Mater.* **28**, 8861–8891 (2016).

118. Meneghetti, M. C. Z. *et al.* Heparan sulfate and heparin interactions with proteins. *J. R. Soc. Interface* **12**, 1–13 (2015).

119. Flanagan, K., Moroziewicz, D., Kwak, H., Hörig, H. & Kaufman, H. L. The lymphoid chemokine CCL21 costimulates naive T cell expansion and Th1 polarization of non-regulatory CD4+ T cells. *Cell. Immunol.* **231**, 75–84 (2004).

120. Adutler-Lieber, S. *et al.* Substrate-bound CCL21 and ICAM1 combined with soluble IL-6 collectively augment the expansion of antigen-specific murine CD4+ T cells. *Blood Adv.* **1**, 1016–1030 (2017).

121. Adutler-Lieber, S., Friedman, N. & Geiger, B. Expansion and Antitumor Cytotoxicity of T-Cells Are Augmented by Substrate-Bound CCL21 and Intercellular Adhesion Molecule 1. *Front. Immunol.* **9**, 1–14 (2018).

122. Peyton, S. R. *et al.* Marrow-derived stem cell motility in 3D synthetic scaffold is governed by geometry along with adhesivity and stiffness. *Biotechnol. Bioeng.* **108**, 1181–1193 (2011).

123. da Silva, J., Lautenschläger, F., Kuo, C.-H. R., Guck, J. & Sivaniah, E. 3D inverted colloidal crystals in realistic cell migration assays for drug screening applications. *Integr. Biol.* **3**,

1202–1206 (2011).

124. Stachowiak, A. N. & Irvine, D. J. Inverse opal hydrogel-collagen composite scaffolds as a supportive microenvironment for immune cell migration. *J. Biomed. Mater. Res. A* **85**, 815–828 (2008).

125. Shirahama, H. *et al.* Fabrication of Inverted Colloidal Crystal Poly(ethylene glycol) Scaffold: A Three-dimensional Cell Culture Platform for Liver Tissue Engineering. *J. Vis. Exp.* **114**, 1–12 (2016).

126. Zhang, Y. S., Zhu, C. & Xia, Y. Inverse Opal Scaffolds and Their Biomedical Applications. *Adv. Mater.* **29**, 1–29 (2017).

127. Adriani, G. *et al.* Microfluidic models for adoptive cell-mediated cancer immunotherapies. *Drug Discov. Today* **21**, 1472–1478 (2016).

128. Cinamon, G., Shinder, V. & Alon, R. Shear forces promote lymphocyte migration across vascular endothelium bearing apical chemokines. *Nat. Immunol.* **2**, 515–522 (2001).

129. Moura Rosa, P., Gopalakrishnan, N., Ibrahim, H., Haug, M. & Halaas, Ø. The intercell dynamics of T cells and dendritic cells in a lymph node-on-a-chip flow device. *Lab Chip* **16**, 3728–3740 (2016).

130. O'Melia, M. J., Lund, A. W. & Thomas, S. N. The Biophysics of Lymphatic Transport: Engineering Tools and Immunological Consequences. *iScience* **22**, 28–43 (2019).

131. Schmid-Schönbein, G. W. Microlymphatics and lymph flow. *Physiol. Rev.* **70**, 987–1028 (1990).

132. Gashev, A. A. Physiologic aspects of lymphatic contractile function: current perspectives. *Ann. N. Y. Acad. Sci.* **979**, 178–196 (2002).

133. Dixon, J. B. *et al.* Lymph flow, shear stress, and lymphocyte velocity in rat mesenteric prenodal lymphatics. *Microcirculation* **13**, 597–610 (2006).

134. Blatter, C. *et al.* In vivo label-free measurement of lymph flow velocity and volumetric flow rates using Doppler optical coherence tomography. *Sci. Rep.* **6**, 1–10 (2016).

135. Jafarnejad, M. *et al.* Quantification of the Whole Lymph Node Vasculature Based on Tomography of the Vessel Corrosion Casts. *Sci. Rep.* **9**, 1–11 (2019).

136. Ross, A. E., Belanger, M. C., Woodroof, J. F. & Pompano, R. R. Spatially resolved microfluidic stimulation of lymphoid tissue ex vivo. *Analyst* **142**, 649–659 (2017).

137. Shim, S., Belanger, M. C., Harris, A. R., Munson, J. M. & Pompano, R. R. Two-way communication between ex vivo tissues on a microfluidic chip: application to tumor-lymph node interaction. *Lab Chip* **19**, 1013–1026 (2019).

Chapter 2

3D commercial synthetic peptide hydrogels for T cell culture

2.1 Introduction

There is a continuously growing interest in the development of new biomaterials able to interact with biological tissues and cells for different applications.[1]. As introduced in the previous chapter, it is important to study the effect of different types of materials with distinct properties as a scaffold for immune cell culture for immunotherapy.

One of the most recurrent strategies nowadays is the use of hydrogels,[2–4] i.e. (visco)elastic networks with interstitial spaces that contain as much as 90-99% w/w water. As explained in Chapter 1, our group has evaluated the performance of Matrigel (Thermo Fisher Scientific, United States of America), a gold standard hydrogel in the field of 3D cell culture systems for T cell culture.[5] Nevertheless, Matrigel suffers from batch to batch variability and its composition is not well established, which limits its applicability. Alternatively, our group has developed a synthetic 3D PEG-Hep hydrogel that has been proven to be an effective scaffold for primary human CD4+ T cell expansion.[6] Indeed, synthetic polymers are an attractive option due to the possibility to control their chemical, structural and physical properties.

Recently, small amphiphilic molecules have emerged as a new class of hydrogelators, forming supramolecular or molecular hydrogels.[7–9] The Biogelx™ hydrogel technology (Biogelx, United Kingdom) is advertised to produce completely synthetic hydrogels by a simple peptide technology. According to the company, the commercialized supramolecular hydrogels can be independently adjusted in terms of both mechanical and chemical properties, to provide an optimal environment for the culture of a variety of cell types.

Chemically, the Biogelx™ hydrogels are based on a two-peptide system modified at the N-terminus with an aromatic structure. Specifically, there is a hydrophobic "gelator" peptide Fmoc-diphenylalanine (Fmoc-F_2) and a hydrophilic "surfactant" Fmoc-serine (Fmoc-S). Through a combination of H-bonding and π-stacking interactions, these peptide building blocks co-assemble to form nanoscale fibers in aqueous environments (**Figure 2.1**). In the presence of Ca^{2+} ions, these peptide nanofibers crosslink to form hydrogels and the so-called "standard hydrogel" from Biogelx (Biogelx™-S) is obtained. Furthermore, these peptide fibers present a hydrophilic functionality on the surface, being appropriate for cell adhesion.[10–15]

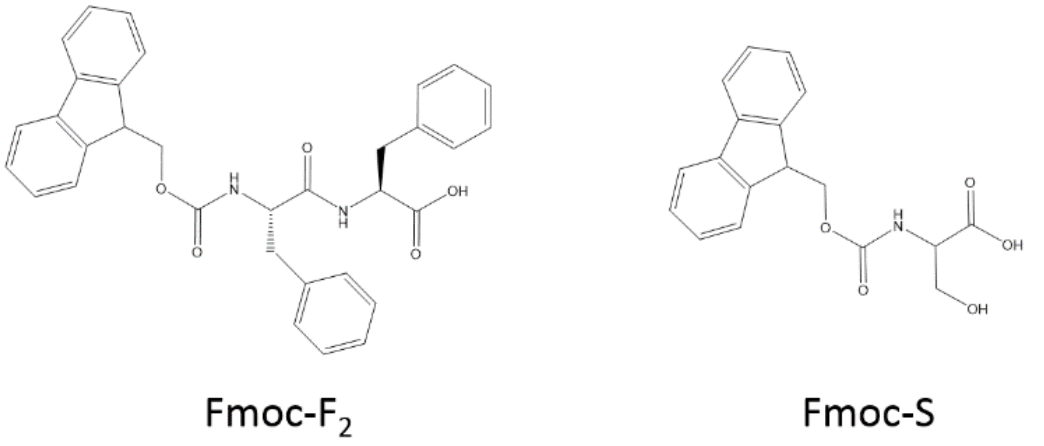

Figure 2.1 Molecular structures of the Biogelx™-S precursors: Fmoc-diphenylalanine (Fmoc-F_2) and Fmoc-serine (Fmoc-S).

In addition, the fiber density of the hydrogel controls its stiffness. More specifically, it is possible to tune the stiffness of the hydrogels from 0.5 kPa up to 100 kPa, matching a wide range of tissue types (**Figure 2.2**). This range of values contains the reported stiffness of a healthy LN which present a mean stiffness around 15 kPa, as found in several studies based on elastography, in contrast to metastatic LNs showing significantly higher values.[16–19]

Additionally, some Biogelx products also incorporate biomimetic peptide sequences of the ECM proteins like fibronectin, laminin, and collagen. The collagen-mimetic peptide sequence is

glycine-phenylalanine-hydroxyproline-glycine-glutamate-arginine (GFOGER). The Biogelx™-GFOGER hydrogels are particularly interesting for T cell culture, as collagen is the major structural component of the LNs.[20,21]

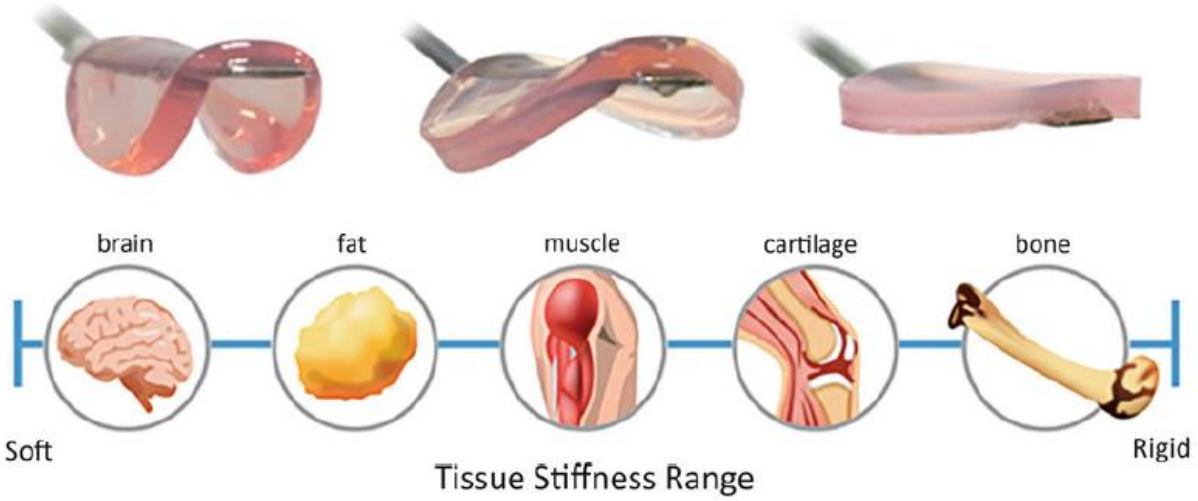

Figure 2.2 Scheme of Biogelx's 3D hydrogels with different stiffness, tuned to match different tissue environments. Adapted from: http://www.biogelx.com/.

These options provide a synthetic yet biologically-relevant alternative to animal-derived 3D matrices such as Matrigel and natural collagen.[22] Previous work with Biogelx samples consisted in culturing perivascular stem cells on the hydrogels of different stiffness, soft (1 kPa), stiff (13 kPa), and rigid (32 kPa), resulting in neuronal, chondrogenic and osteogenic differentiation, respectively.[23]

2.2 Objectives and strategy

The objective of this chapter is to study the commercial synthetic Biogelx hydrogels as artificial ECM to improve the current methodologies of expansion of T cells. In collaboration with the Biogelx company, two different hydrogels were studied, the Biogelx™-S and Biogelx™-GFOGER. Primary human CD4+ T cells from adult healthy donors were chosen between all the different

immune cell types, given their relevance for ACT in the clinics.[24–26] Moreover, they ensured reduced biological variability as compared with PBMCs. Finally, they were more appealing than CD8+ T cells due to their natural abundance as immune cell population.

The effect of each 3D matrix in comparison with the standard static suspension cultures were analyzed, but also the differences between the two studied samples. Furthermore, several parameters were studied in order to optimize the conditions for T cell culture with the Biogelx hydrogels, including the stiffness of the hydrogels, the cell density used for seeding, the pre-gel formation, the gelation step and the cell recovery method.

2.3 Preparation of Biogelx™-S and Biogelx™-GFOGER hydrogels

Biogelx products were supplied as lyophilized powder (Biogelx Powder). These powders are rehydrated with water to form a pre-gel solution at a desired concentration. The gelation of these products is triggered by divalent cations, such as Ca^{2+}, which cross-link the hydrogel fibers resulting in a hydrogel. For such reason, the gelation process is triggered instantly when the Biogelx pre-gel solution encounters cell culture medium containing divalent cations (**Figure 2.3**).

For the pre-gel formation the desired hydrogel stiffness is considered. According to the "Biogelx Powder – Preparation and Guidelines for Use" document (available at: http://www.biogelx.com/) the reference values are showed in **Table 2.1** for standard and collagen Biogelx powders.

With these reported values a "calibration curve" was created for each case, Biogelx™-S and Biogelx™-GFOGER. The "calibration curve" allowed to determine the amount of sample needed for a specific stiffness (**Figure 2.4**). These equations were also used to prepare hydrogels with stiffness values outside the range stated in the document "Biogelx Powder – Preparation and Guidelines for Use", were we assumed linearity of the calibration curve to be maintain as also suggested by Biogelx™ team.

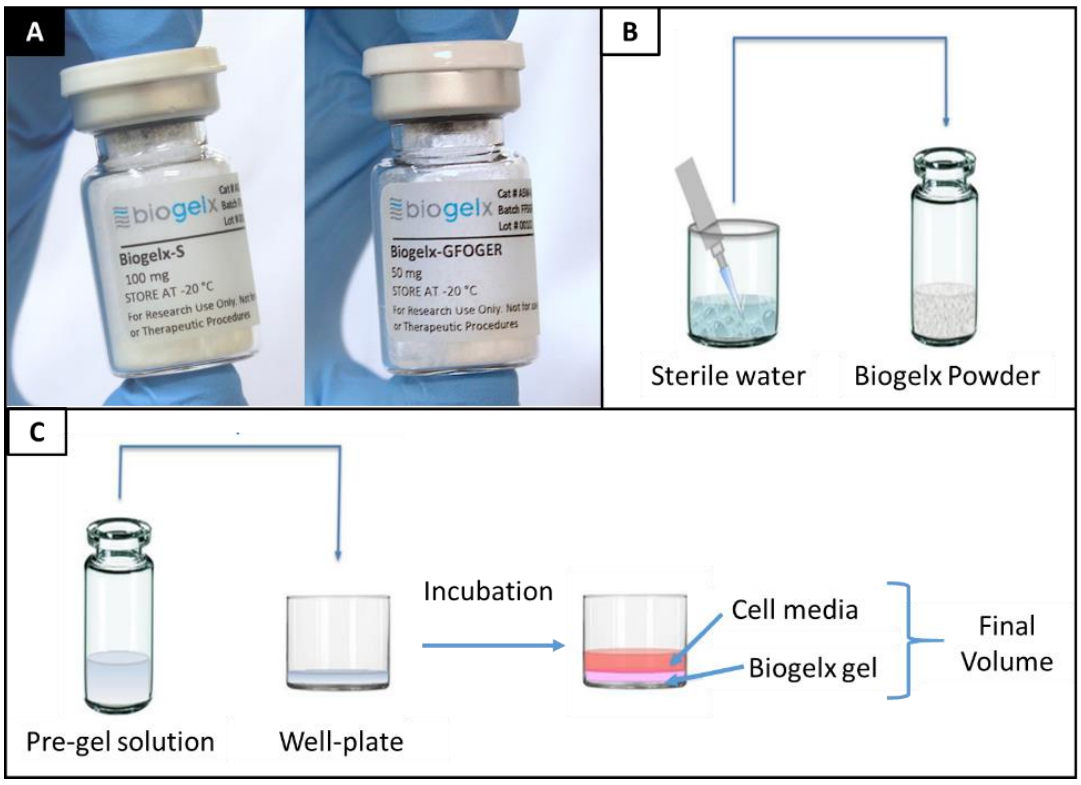

Figure 2.3 Schematic formation of the Biogelx hydrogels. A) Lyophilized Biogelx powders: the standard version Biogelx™-S (left side) and the collagen mimetic version Biogelx™-GFOGER (right side). B) Pre-gel formation step and C) hydrogel formation step. Adapted from: http://www.biogelx.com/.

Table 2.1 Weight of Biogelx Powder–S and Biogelx Powder–GFOGER needed to prepare hydrogels of a certain stiffness. Adapted from http://www.biogelx.com/.

Stiffness range of hydrogel required (kPa)	Weight of Biogelx Powder (milligrams) for 5 mL	Weight of Biogelx Powder – GFOGER (milligrams) for 5 mL
0.8 – 1.1	22 mg	26 mg
3.0 – 4.0	43 mg	52 mg
8.0 – 9.2	67 mg	78 mg

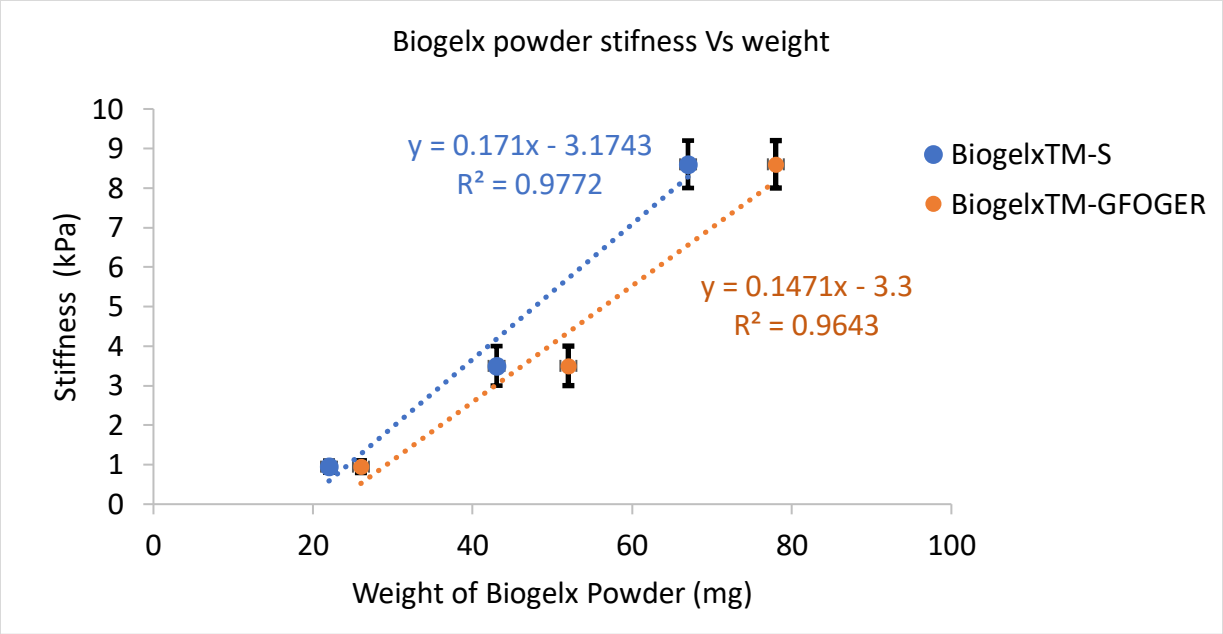

Figure 2.4 Calibration curves of Biogelx powder samples weight (mg) vs the corresponding stiffness (kPa) reported in the "Biogelx Powder – Preparation and Guidelines for Use" document, available at http://www.biogelx.com/.

In a typical experiment, hydrogels were prepared in a 96 well plate by adding 100 µL of pre-gel at the desired concentration, followed by a 15 min incubation at 37°C. During the pre-gel preparation air bubbles were formed but easily removed by centrifugation.

Then the cell culture media Roswell Park Memorial Institute (RPMI) containing calcium ions was added to the pre-gel slowly and another incubation for at least 2 h at 37°C was performed to obtain the hydrogels. After removing the remaining media on top of the hydrogels the cells were added in a 2D seeding fashion (see Chapter 6 for further details).

As an example, **Figure 2.5** shows two hydrogels obtained with Biogelx^{TM}-S at different stiffness: 5 kPa (**Figure 2.5 A**) and 25 kPa (**Figure 2.5 B**). Worth noticing is the challenge of working with these hydrogels at higher stiffness, such as 25 kPa, because they were very brittle, as explained in the flowing sections.

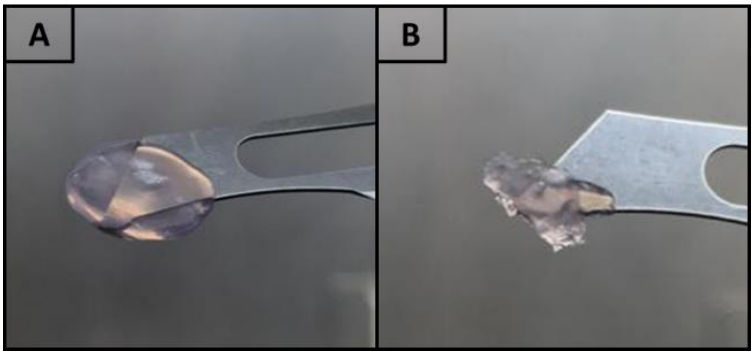

Figure 2.5 Example of the hydrogels obtained with Biogelx™-S powder at different stiffness: (A) 5 kPa and (B) 25 kPa.

2.4 CD4+ T cell proliferation study

Primary human CD4+ T cells were obtained from a purification process of buffy coats of healthy adult donors, previously reported[6] (see Chapter 6 for details). Then, the cells were cultured in suspension without Dynabeads (negative control), with Dynabeads (positive control) and with Dynabeads on the hydrogels under study (**Figure 2.6**).

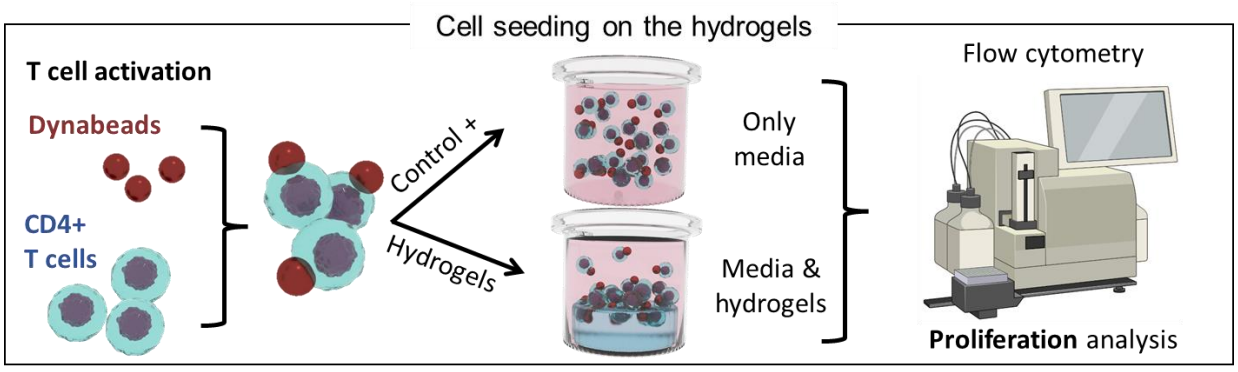

Figure 2.6 Scheme of the cell seeding in suspension (control +) and on hydrogels.

CD4+ T cells were seeded and activated with Dynabeads on the 3D structure of the Biogelx hydrogels (Biogelx™-S and Biogelx™-GFOGER). After 6 days of culture, we analyzed CD4+ T cell proliferation through a carboxyfluorescein succinimidyl ester (CFSE) cell proliferation kit (see

Chapter 6 for details). CSFE is a cell permeable fluorescent molecule, used as a staining dye that covalently couples to intracellular molecules, via its succinimidyl group, such as lysine residues. Due to the covalent binding, this fluorescent dye can stay inside cells for long periods of time and is not transferred to adjacent cells. Furthermore the use of CFSE to monitor lymphocyte proliferation was found very useful, due to the gradual halving of CFSE fluorescence with each cell division[27] (**Figure 2.7**). Nowadays, CFSE staining is a common procedure in immunology to study lymphocyte proliferation by flow cytometry allowing to quantify the proliferation of labelled cells up to 10 divisions.[28]

For this analysis, the initial population is stained before cell seeding, therefore determining the maximum fluorescence, represented in **Figure 2.7** as the "peak 0" (red line). Then, the stained cell population proliferates over time producing in the CFSE graph, as many peaks as cell generations. On **Figure 2.7**, it is also represented 5 generations, and in each generation, the fluorescence inside the cells is halved compared to their precursors.

The resulting graph is analyzed to assess T cell proliferation by evaluating the proliferation, expansion and replication indexes.

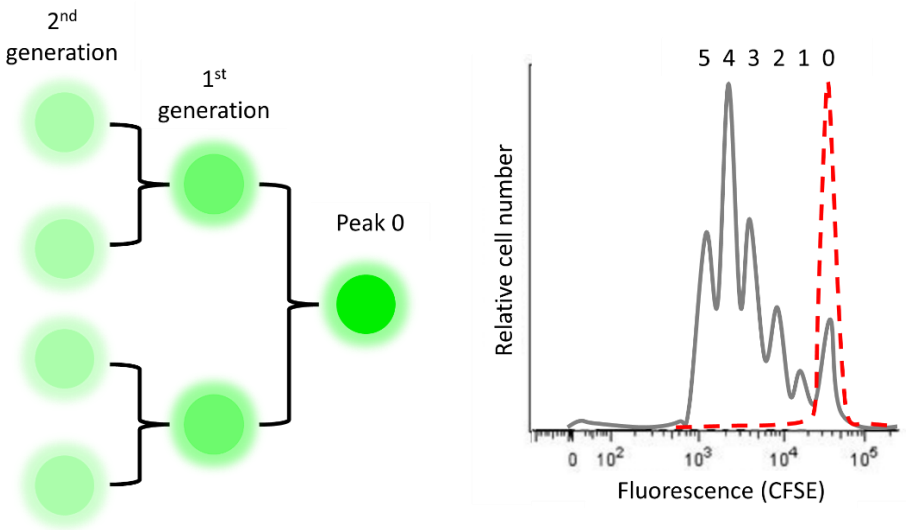

Figure 2.7 Representation of a typical CSFE analysis. On the left side the progressive halving of fluorescence within daughter cells after cell division, until generation 2. On the right, the peaks obtained by flow cytometry indicating 5 generations.

The proliferation index is the number of divisions suffered by the cells from the original population divided by the number of divided cells. The expansion index establishes the fold-expansion of the whole population while the replication index determines the fold-expansion of the responding cells. The higher these values are, the higher quantity of cells after the proliferative process are obtained. These three indexes are relevant for cell therapy, especially when dealing with immune cell expansions by showing how responsive are cells after the proliferative stimulus, and how much they divide after such stimulus. Quantitatively, it is also possible to know how many cells are achieved after a proliferation event.[29]

After 6 days of culture, the stained CSFE cells (and the Dynabeads, if present) are removed from the well plates after several re-suspensions. Dynabeads are removed through a magnetic separation. The cells are centrifuged to replace the RPMI growth media by a phosphate-buffered saline (PBS) solution to be then analyzed by flow cytometry (see Chapter 6 for details).

2.4.1 CD4+ T cell proliferation using Biogelx™-S hydrogels

Taking into consideration the reported work with Biogelx hydrogels with stiffness ranging from 1-32 kPa[23] and the information provided by the company, Biogelx™-S hydrogels were prepared and studied at two different stiffness, 25 kPa and 5 kPa. These values are 10 kPa lower and higher than the reported healthy LN stiffness of 15 kPa.[16–19] Furthermore, with the soft hydrogel (5 kPa), we expected to compare the obtained results with the Matrigel system[5] and the synthetic PEG-Hep hydrogels,[6] as briefly introduced in Chapter 1.

The parameters used in the cell seeding protocol with the Biogelx samples consisted in 100 000 cells per well (96 well plates) at a cell concentration of 2 million (M) cells/mL in RPMI (supplemented with 10% FBS, 1% PS, 100 mg/L $CaCl_2$, denominated in this thesis as complete RPMI medium). The pre-gel was prepared with 100 µL of sterile water. The gelation was performed with the same RPMI, at 37°C for at least 2 h, and the standard cell recovery step was performed mechanically, with several resuspensions with a micropipette (see Chapter 6 for

further details). Any change on these parameters is highlighted in red colour on the specifications section of each corresponding figure.

Figure 2.8 shows the proliferation graphs obtained by flow cytometry measurements, where side versus forward scatter (SSC vs FSC) gating was used to identify cell populations of interest based on granularity (complexity) and size, respectively. In the case of the negative control, the alive cell population can be clearly seen. A larger alive population have been also obtained for the positive control. However, no clear population of alive cells was observed for the cells cultured on the Biogelx hydrogels. In the case of hydrogels of 25 kPa, more events were recorded within the "alive cells" gate than when using 5 kPa hydrogels. Nevertheless, the typical alive cell population was not observed. Additionally, the hydrogels at 25 kPa were more brittle as commented before (**Figure 2.5**) and disrupted when trying to collect the cells for flow cytometry measurements. This situation raised the possibility that all the events recorded in the SSC vs FSC gate were little pieces of the hydrogel material. In conclusion, it was not possible to assess T cell proliferation through the expansion, replication and proliferation indexes.

To improve the results obtained, we focused on the 25 kPa hydrogels, as higher number of events were obtained on the SSC vs FSC graphs. To avoid disrupting the hydrogels into little pieces, the cells were collected by using trypsin, since it is an agent commonly used in cell biology to help detaching the cells from surfaces or scaffolds. Additionally, we reduced the hydrogel amount to half to increase the ratio of cells/hydrogel with the objective to increase the chances to see the cell population during flow cytometry analysis (**Figure 2.9**). However, it was not possible to observe a clear population of alive cells when using the hydrogels.

Then, we analyzed hydrogels of lower stiffness with the previous conditions to better mimic the LN stiffness values found on the literature.[16–19] Despite being also challenging to handle due to their softness, we avoided working with brittle material as the Biogelx^{TM}-S hydrogel at 25 kPa. **Figure 2.10** shows the flow cytometry measurements obtained when using hydrogels at 9 and 2 kPa.

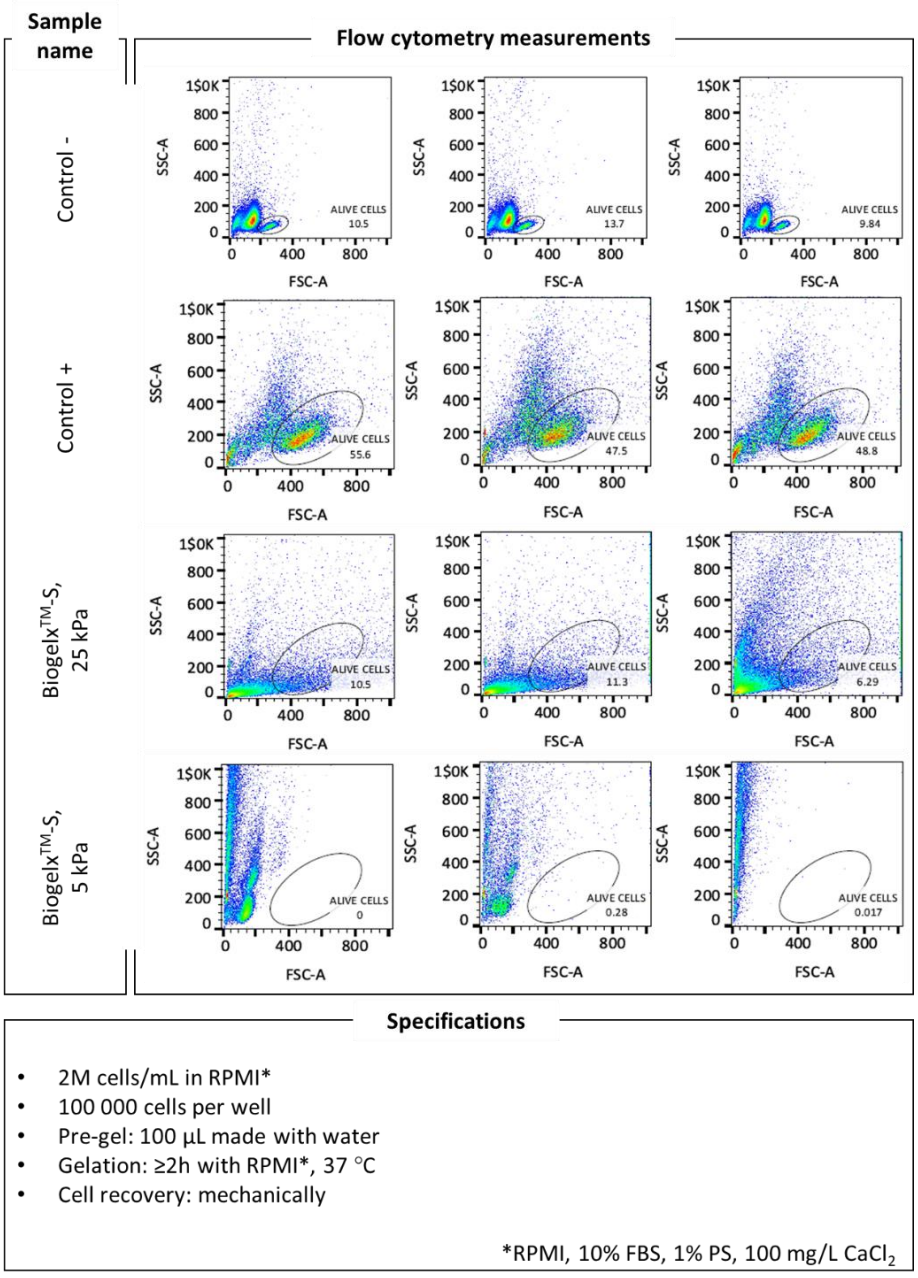

Figure 2.8 Flow cytometry measurements presenting SSC vs FSC gating for the Biogelx™-S, 25 kPa and Biogelx™-S, 5 kPa hydrogels in the presence of Dynabeads, according to the stated specifications. Control - are cells in suspension without Dynabeads, whereas the control + are cells in suspension with Dynabeads.

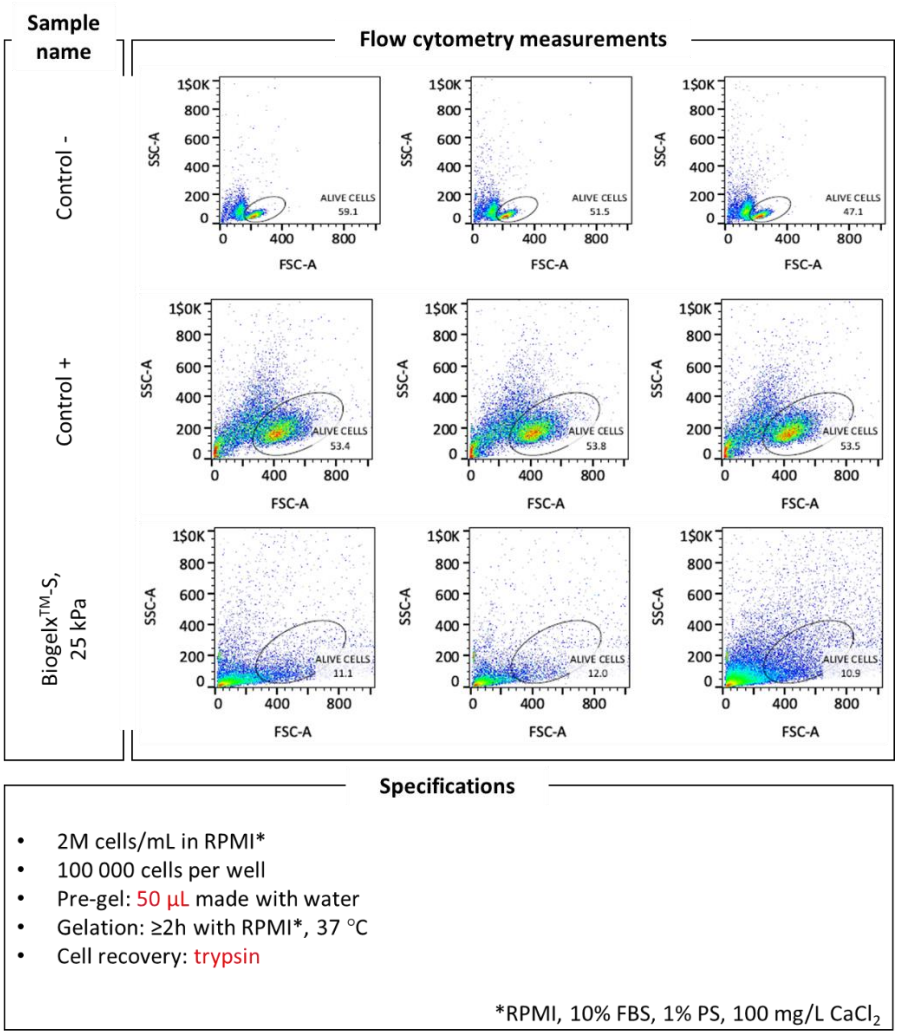

Figure 2.9 Flow cytometry measurements presenting SSC vs FSC gating for the BiogelX™-S, 25 kPa hydrogels in the presence of Dynabeads, according to the stated specifications. Control - are cells in suspension without Dynabeads, whereas the control + are cells in suspension with Dynabeads.

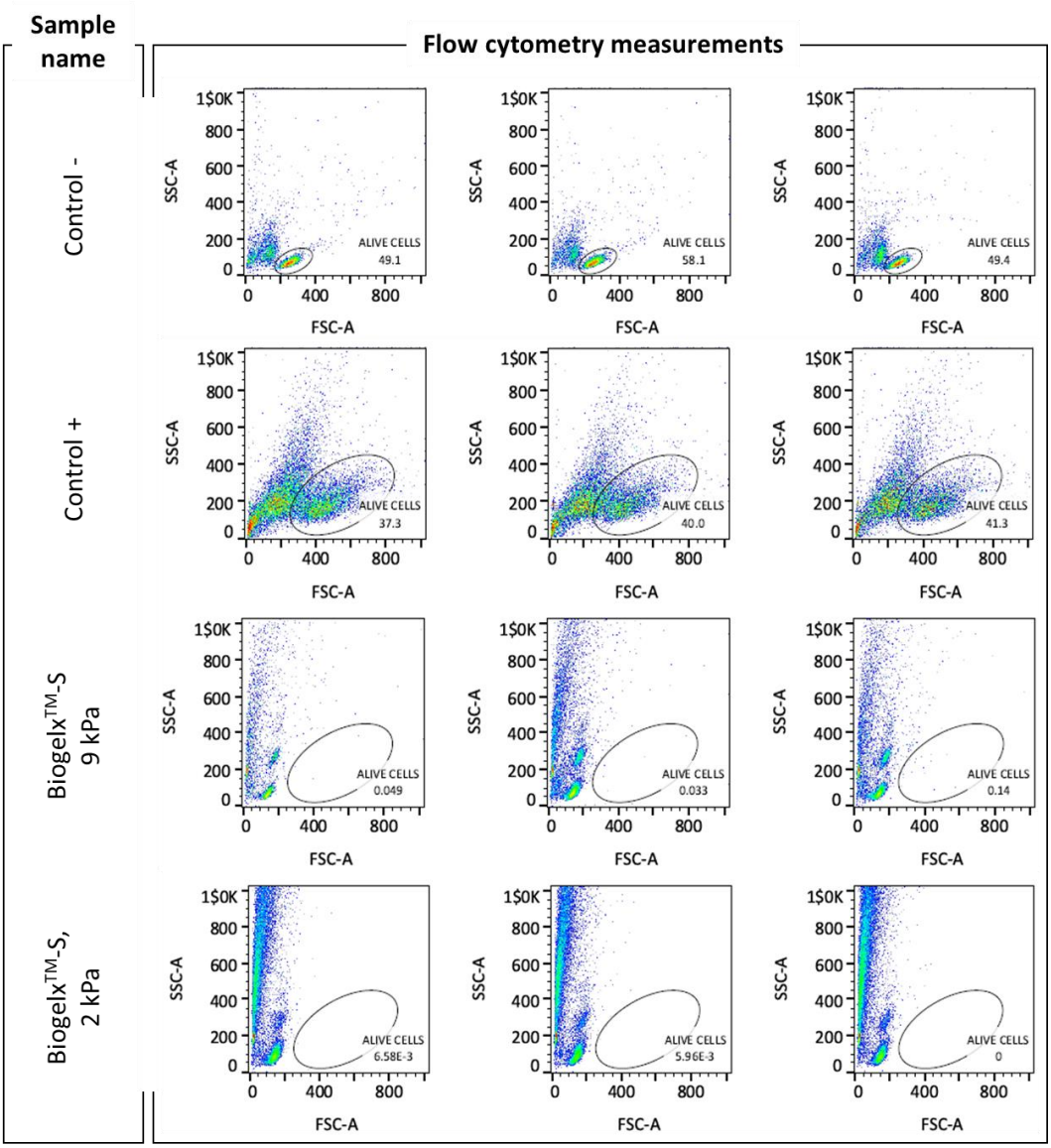

Figure 2.10 Flow cytometry measurements presenting SSC vs FSC gating for the BiogelX™-S, 2 kPa and BiogelX™-S, 9 kPa hydrogels in the presence of Dynabeads, according to the stated specifications. Control - are cells in suspension without Dynabeads, whereas the control + are cells in suspension with Dynabeads.

Again, we could not observe a population of alive cells for the samples, unlike the negative and positive controls. Furthermore, as seen before, lower stiffness hydrogels contributed to lower events detected on the flow cytometry measurements.

To improve cell proliferation using the hydrogels, we evaluated the possibility of substituting the water used to form the pre-gel by more cell-friendly alternatives. As the Biogelx hydrogel formation is highly dependent on calcium ions, we also considered using complete RPMI supplemented with a higher concentration of $CaCl_2$.

Consequently, we checked the proliferation of the CD4+ T cells in suspension by using different solutions. We added 50 uL of: a) RPMI, 10% FBS, 1% PS, 100 mg/L $CaCl_2$, b) RPMI, 10% FBS, 1% PS, 200 mg/L $CaCl_2$, c) PBS or d) H_2O to a 50 uL of cell suspension (at $2x10^6$ cells/mL) in RPMI, 10% FBS, 1% PS, 100 mg/L $CaCl_2$ (**Figure 2.11**). All cases presented a characteristic alive population of cells (**Figure 2.11 A**), and further investigation of the proliferation parameters was possible (**Figure 2.11 B**).

From this data, it was possible to investigate the proliferation, expansion and replication indexes of the cells in the different suspension environments (**Figure 2.12**).

Adding RPMI, 10% FBS, 1% PS, 100 mg/L $CaCl_2$, which is the cell culture media commonly used for CD4+ T cell cultures, resulted into the highest values in all three proliferation parameters. Specifically, the median values were 2.40, 6.55 and 8.88 for the proliferation, expansion and replication indexes, respectively.

When adding H_2O, the median values were 1.98, 3.84 and 4.83 for the proliferation, expansion and replication indexes, respectively, being the lowest among all conditions. When adding PBS, the median values were 2.00, 4.69 and 5.84, whereas when adding RPMI, 10% FBS, 1% PS, 200 mg/L $CaCl_2$ the median values were 2.17, 5.39 and 7.04 for the proliferation, expansion and replication indexes, respectively.

Taking these results into consideration and knowing that the gelation of these hydrogels is triggered by divalent cations, we used complete RPMI with a higher content of calcium ions. Thus, we compared the typical experiments with RPMI supplemented with 100 mg/L of $CaCl_2$ to samples where the RPMI was supplemented with 200 mg/L of $CaCl_2$.

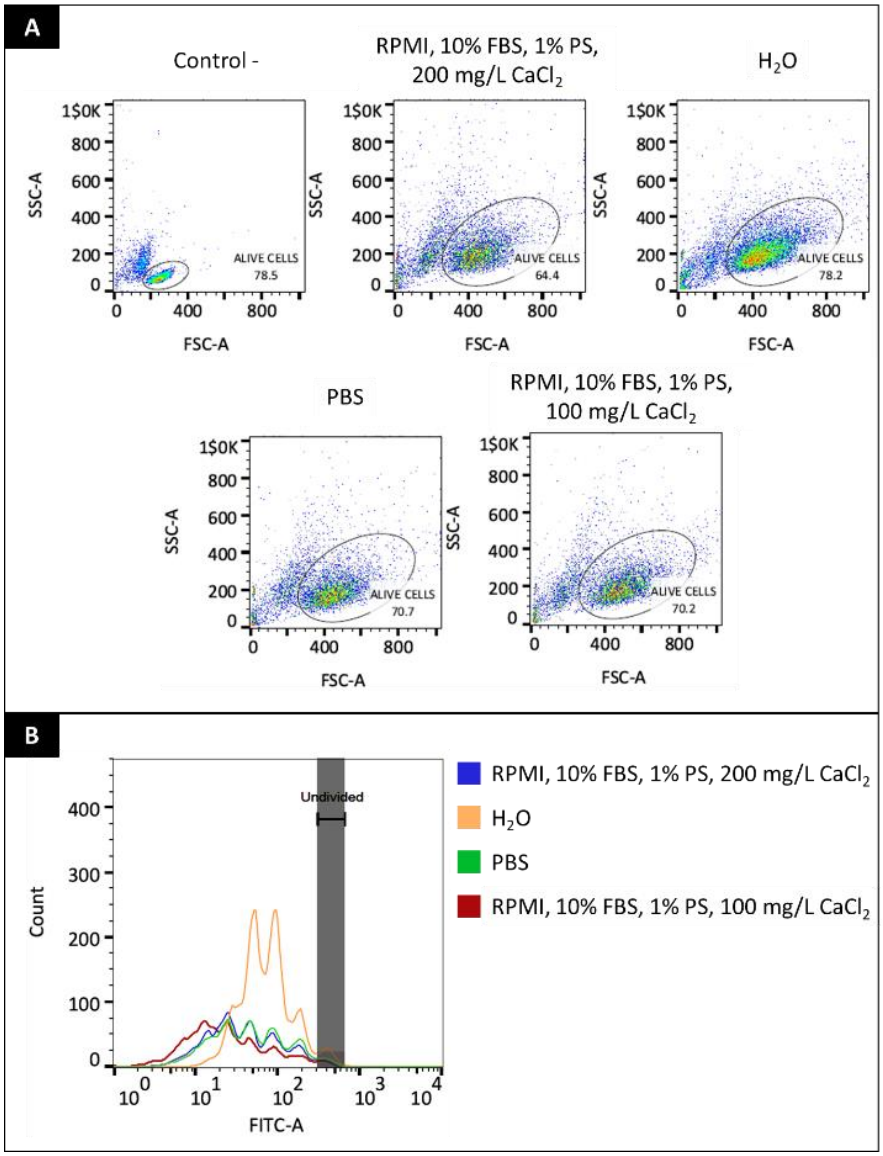

Figure 2.11 Flow cytometry measurements A) presenting SSC vs FSC gating for the cell suspensions in the presence of Dynabeads, in RPMI, 10% FBS, 1% PS, 200 mg/L $CaCl_2$; H_2O; PBS and RPMI, 10% FBS, 1% PS, 100 mg/L $CaCl_2$. Control - are cells in suspension without Dynabeads. B) Diagrams of the resulting CFSE fluorescence peaks of a representative data point.

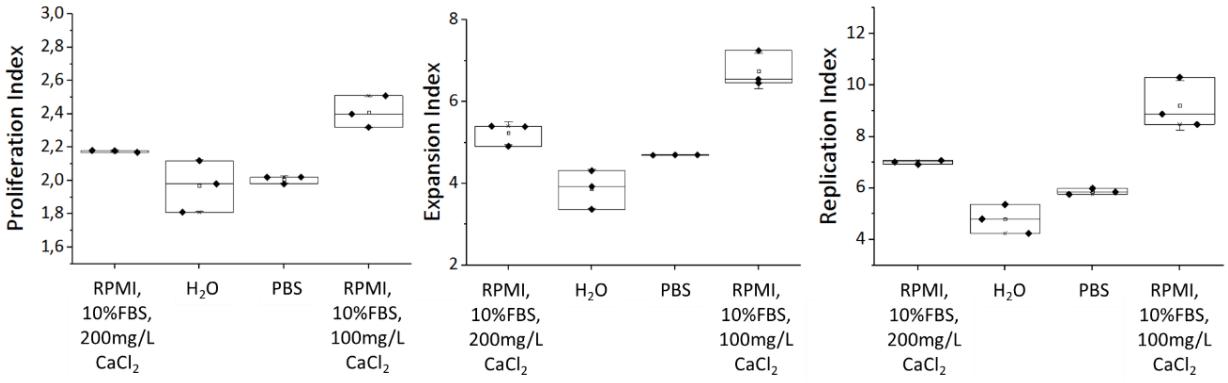

Figure 2.12 Raw data of the proliferation, expansion and replication indexes obtained for CD4+ T cells 6 days after culture in different solutions: RPMI, 10% FBS, 1% PS, 200 mg/L $CaCl_2$; H_2O; PBS and RPMI, 10% FBS, 1% PS, 200 mg/L $CaCl_2$ with Dynabeads, (N_{donors} = 1).

The lower proliferation values obtained on **Figure 2.12** are the ones in water and thus, to decrease the amount of water, the pre-gel solution was prepared in water/complete RPMI in the ratio 85/25. For these experiments we used a stiffness not as high as 25 kPa where the hydrogels are brittle, and not as low as 5 kPa where the hydrogels are more difficult to handle due their softness. We chose an intermediate stiffness of 15 kPa, the one of the healthy LNs.

On **Figure 2.13**, it is shown the proliferation results obtained when using 100 µL hydrogels at 15 kPa and two different cell recovery methods, mechanical or with trypsin. But, once again, no specific population of alive cells was observed on the SSC vs FSC graphs, despite of the good controls obtained.

Then, we tried the same experiment, but the cells seeded were also in a solution of RPMI with 200 mg/L $CaCl_2$. Nevertheless, the results shown on **Figure 2.14** are very similar to the ones obtained previously, since no alive population was found when using the hydrogels as scaffolds for T cell expansion.

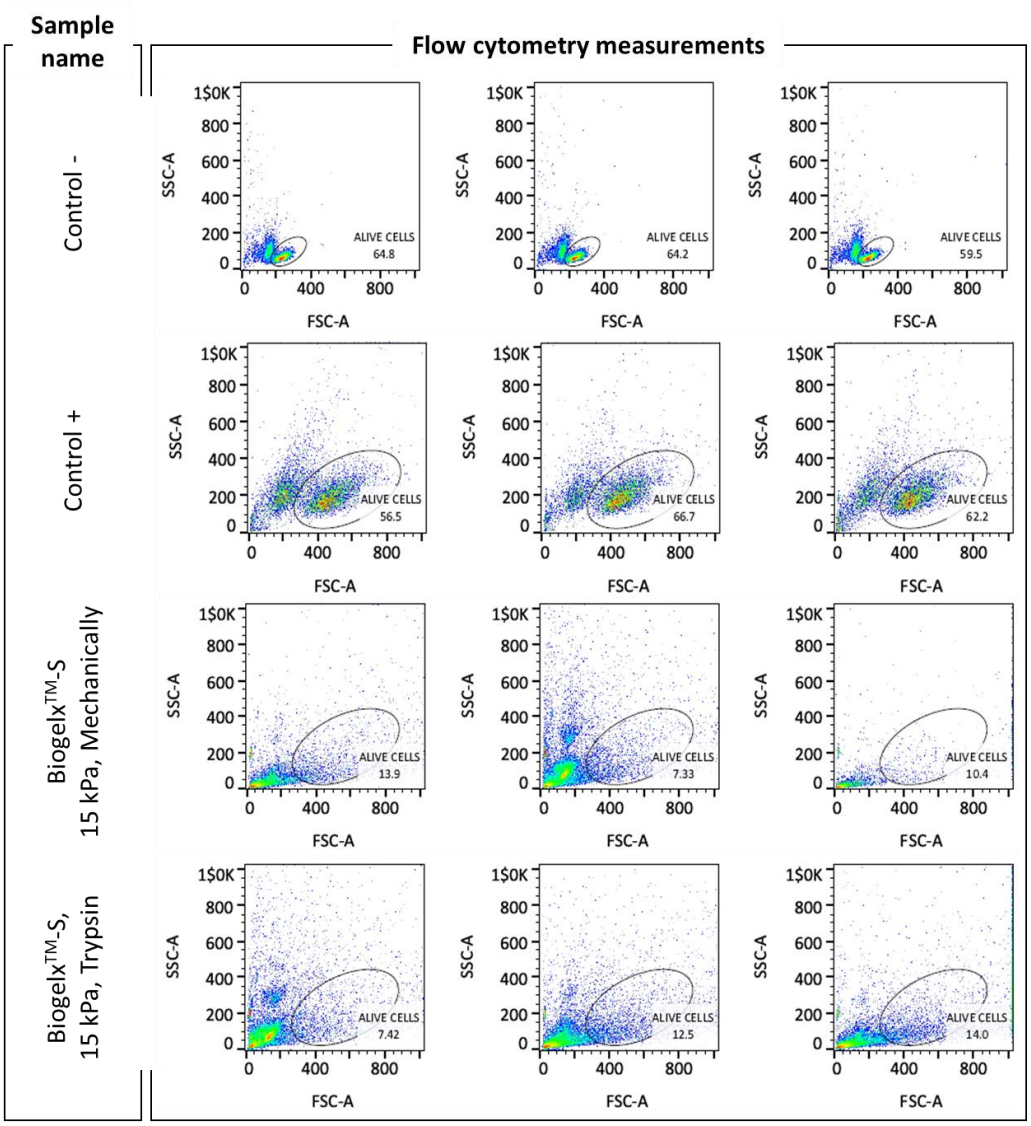

Figure 2.13 Flow cytometry measurements presenting SSC vs FSC gating for the Biogelx™-S, 15 kPa hydrogels with a mechanically or chemically (trypsin) cell recovery step, in the presence of Dynabeads, according to the stated specifications. Control - are cells in suspension without Dynabeads, whereas the control + are cells in suspension with Dynabeads.

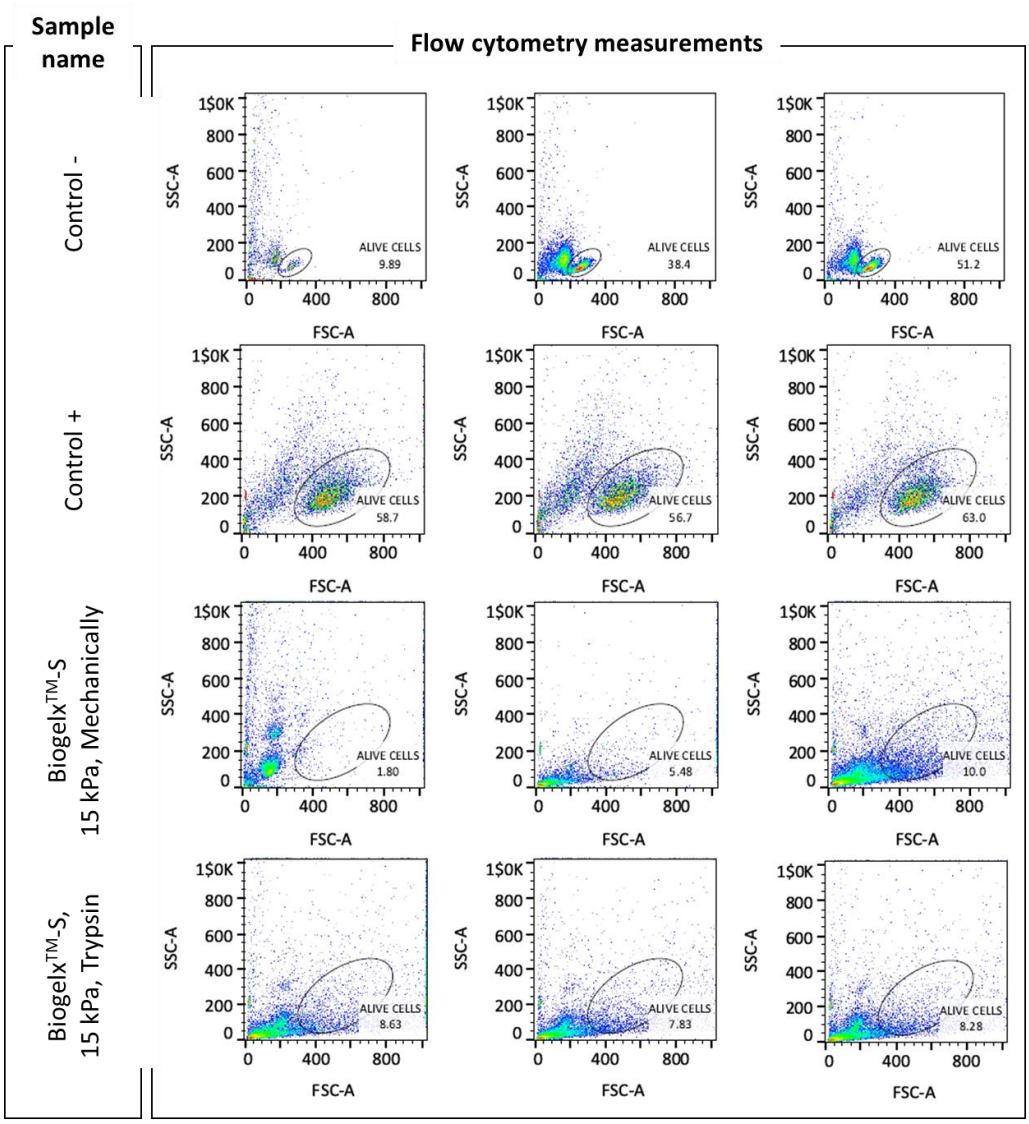

Figure 2.14 Flow cytometry measurements presenting SSC vs FSC gating for the Biogelx™-S, 15 kPa hydrogels with a mechanically or chemically (trypsin) cell recovery step, in the presence of Dynabeads, according to the stated specifications. Control - are cells in suspension without Dynabeads, whereas the control + are cells in suspension with Dynabeads.

In the next step, we seeded high cell densities in low stiffness hydrogels, inspired by a scientific paper entitle "Injectable Biomimetic Hydrogels as Tools for Efficient T Cell Expansion and Delivery".[30] Specifically, we seeded 2.5 times more cells than usual on top (2D seeding) and inside (3D seeding) of 1 kPa hydrogels (**Figure 2.15**). For the 3D seeding, the pre-gel solution was mixed with the cell suspension to obtain a final concentration of 5 M cells/mL. A volume of 100 µL of the mixture pre-gel/cell suspension was used (see Chapter 6 for further details). Again, RPMI with 200 mg/L of $CaCl_2$ was used for the gelation step. Unfortunately, no alive cells were observed even when using a high cell density (5 M cells/mL) in contrast to the positive control (**Figure 2.15**).

After all these trials, we decided to evaluate the possibility that the small number of events appearing on the SSC vs FSC graphs could indeed be little pieces of hydrogel instead of cells. To confirm this hypothesis, we used the following conditions: hydrogel with cells and Dynabeads, hydrogel with no cells but with Dynabeads, and hydrogels with no cells and no Dynabeads. For this experiment, a $2x10^6$ cells/mL cell suspension in the commonly used RPMI, 10% FBS, 1% PS, 100 mg/L $CaCl_2$ was used to seed the cells on top of 25 kPa hydrogels (**Figure 2.16**).

In this experiment, we only observed alive cell populations for the negative and positive controls. All the SSC vs FSC graphs obtained when using hydrogels were similar and did not present a clear alive cell population. These results indicated that even when not using cells or Dynabeads, several events were recorded on the flow cytometry measurements, which were then clearly attributed to little pieces of hydrogel.

With these experiments, we could conclude that the Biogelx™-S hydrogels seem to be cytotoxic to primary human CD4+ T cells. Furthermore, the fact that they are so brittle at high stiffness, made the cell recovery step very challenging, resulting in little pieces of hydrogel.

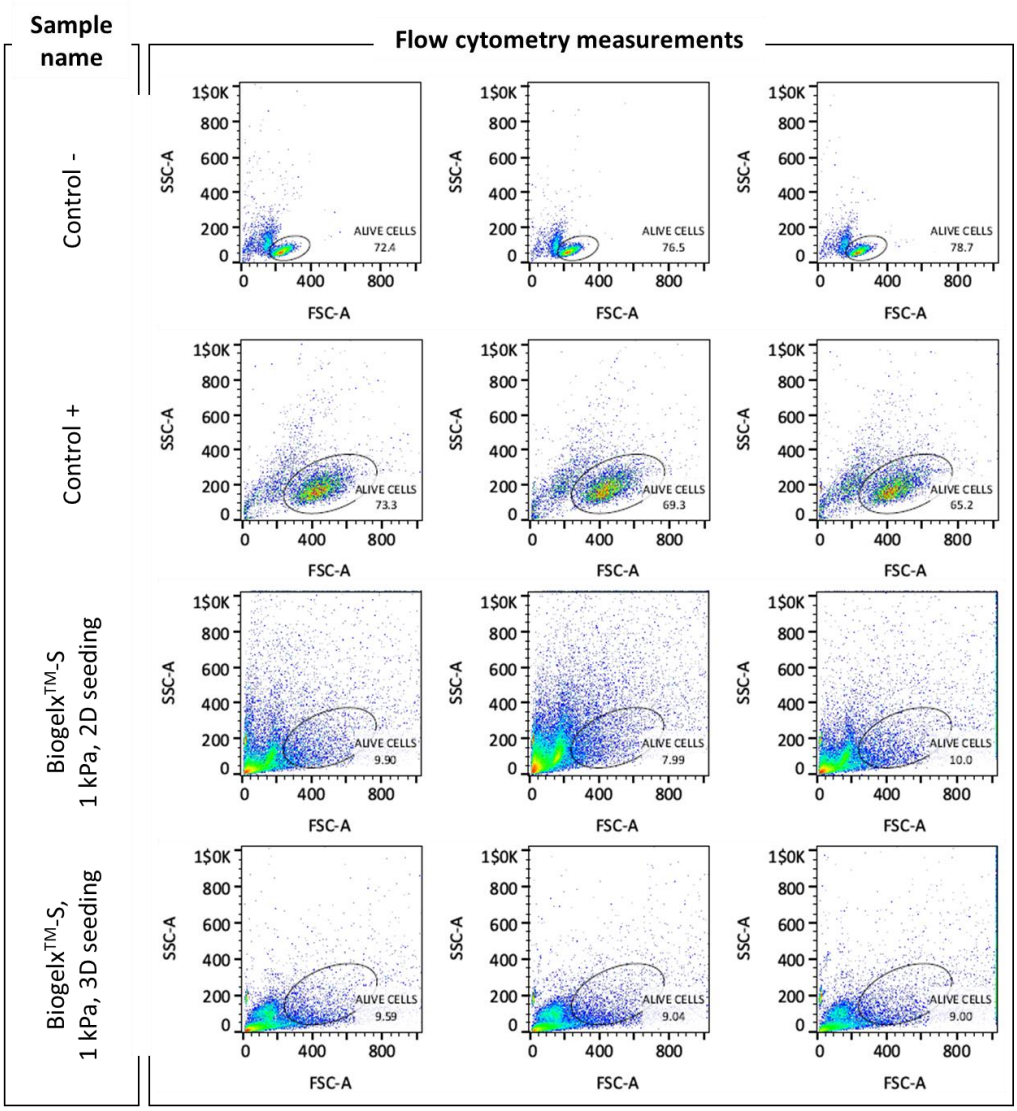

Figure 2.15 Flow cytometry measurements presenting SSC vs FSC gating for the BiogelX™-S, 1 kPa hydrogels with a 2D or 3D seeding, in the presence of Dynabeads, according to the stated specifications. Control - are cells in suspension without Dynabeads, whereas the control + are cells in suspension with Dynabeads.

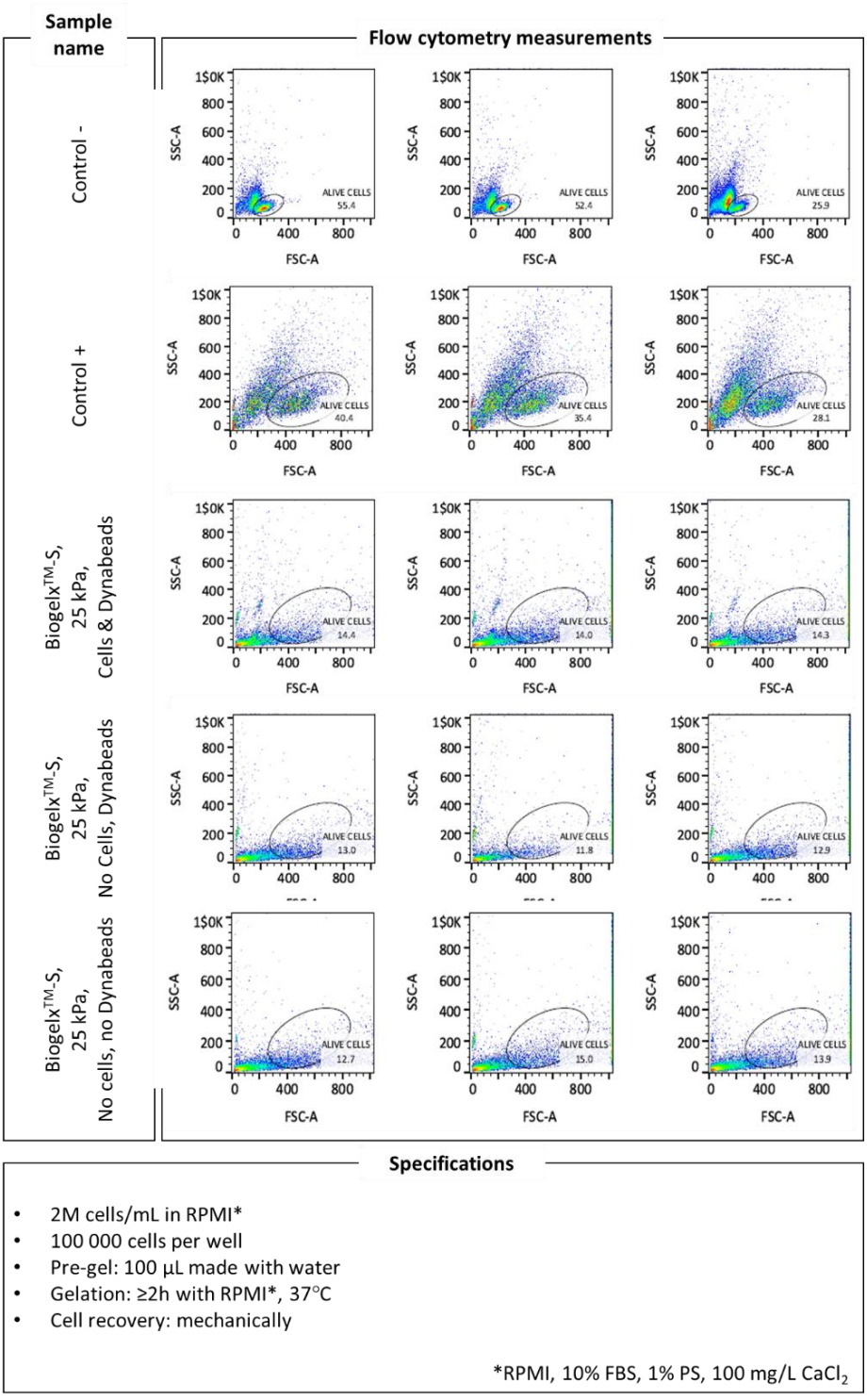

Figure 2.16 Flow cytometry measurements presenting SSC vs FSC gating for the Biogelx^{TM}-S, 25 kPa hydrogels with cells & Dynabeads; with no cells, but with Dynabeads; and with no cells and no Dynabeads, according to the stated specifications. Control - are cells in suspension without Dynabeads, whereas the control + are cells in suspension with Dynabeads.

2.4.2 CD4+ T cell proliferation using Biogelx^{TM}-GFOGER hydrogels

Primary human CD4+ T cells were seeded on top of 9 kPa Biogelx^{TM}-GFOGER hydrogels at a concentration of 2x10^6 cells/mL. Two different pre-gel volumes, one of 100 µL and the another of 50 µL were used. For cell recovery, we used a mechanical approach with several resuspensions and the action of trypsin for 2 min. Thus, we also intended to better recover cells from the possible attachment to the scaffold (**Figure 2.17**). As observed before, alive cells were only present in the cases of positive and negatives controls. For the Biogelx^{TM}-GFOGER hydrogels, no alive cell population was obtained.

Figure 2.18 depicts the results obtained when using the previously used conditions but reducing the cell suspension concentration from 2x10^6 cells/mL to 0.5 x10^6 cells/mL. The main motivation to decrease the number of cells by 75% was to explore the possibility that an excess of cells and their segregation products, such as interleukin-2 (IL-2), could influence the proliferation outcome.[31–33]

Some results showed that mice engineered to lack the IL-2 or IL-2 receptors genes are not markedly immunocompromised, but instead develop autoimmune diseases, such as inflammatory bowel disease, due to a high number of activated T and B cells, elevated immunoglobin secretion and anti-colon antibodies. This means that IL-2, which drives T cell proliferation *in vitro*, is also being somehow required to limit T cell responses.[34,35]

The samples where cells were seeded on top of the hydrogels showed no alive cell population. On the other hand, the controls presented the typical alive cell population, except for one replicate of the positive control. This result is attributed to a potential technical error during seeding or in the cell recovery step, as the other two positive controls showed a typical alive cell population.

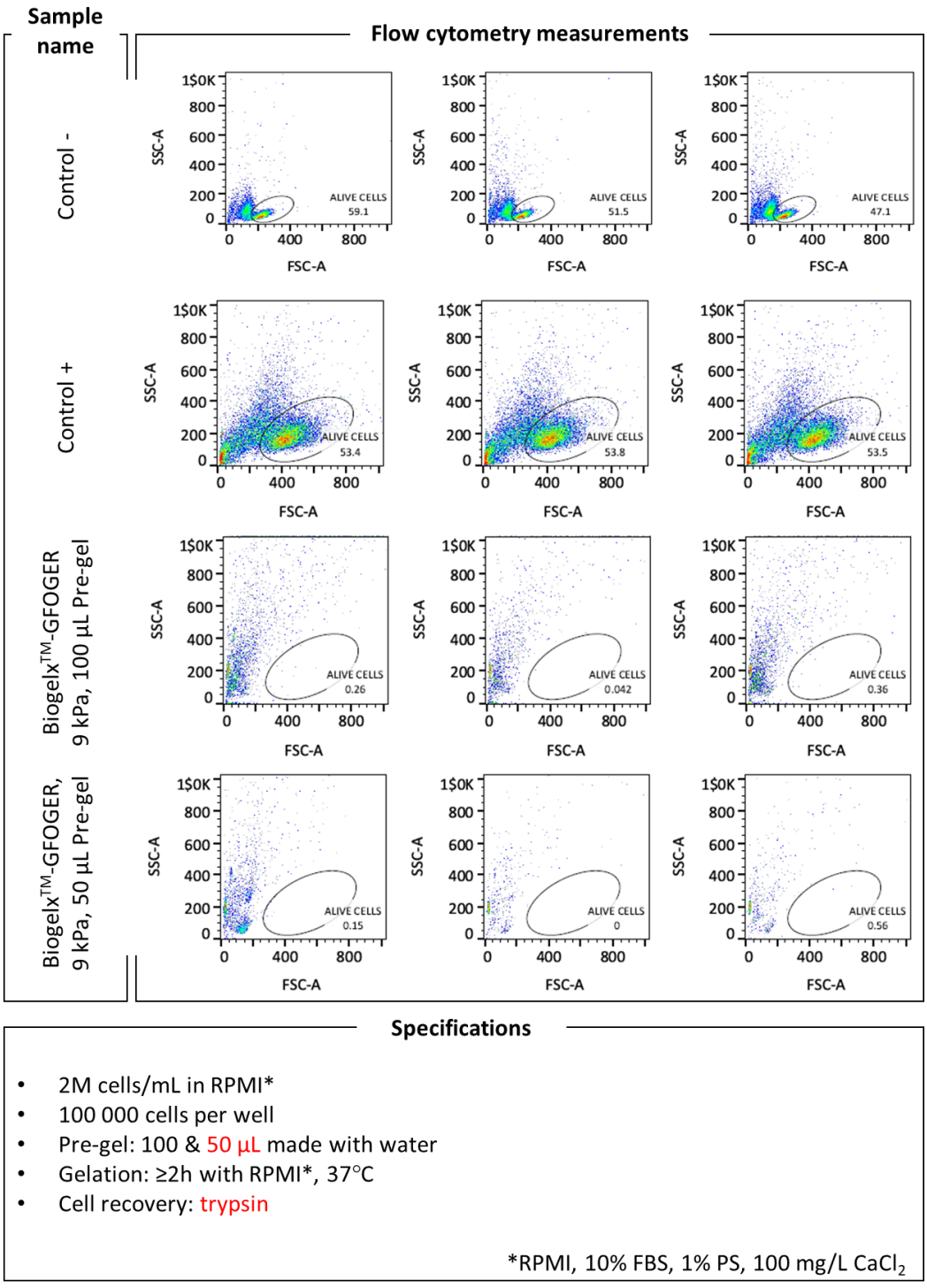

Figure 2.17 Flow cytometry measurements presenting SSC vs FSC gating for the Biogelx™-GFOGER, 9 kPa hydrogels with 50 or 100 µL of pre-gel with Dynabeads, according to the stated specifications. Control - are cells in suspension without Dynabeads, whereas the control + are cells in suspension with Dynabeads.

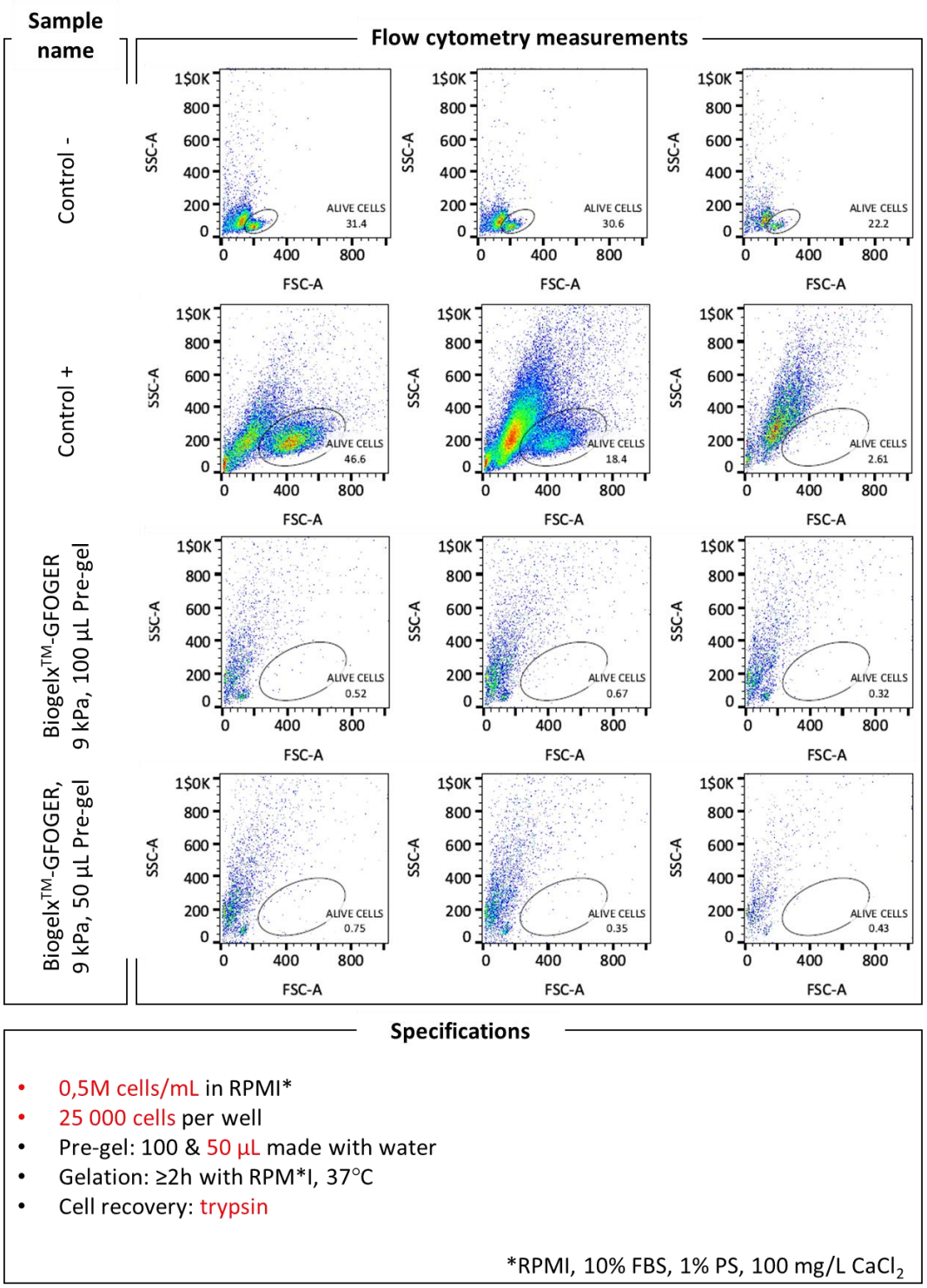

Figure 2.18 Flow cytometry measurements presenting SSC vs FSC gating for the Biogelx™-GFOGER, 9 kPa hydrogels with 50 or 100 µL of pre-gel with Dynabeads, according to the stated specifications. Control - are cells in suspension without Dynabeads, whereas the control + are cells in suspension with Dynabeads.

In the next experiment, the effect of the stiffness was also evaluated, which was reduced from 9kPA to 2kPa. Thus, we used 100 and 50 µL of pre-gel to form hydrogels at a stiffness of 2 kPa (**Figure 2.19**). Once again, cells only survived for the control conditions, showing a typical alive cell population.

To check if the hydrogels were cytotoxic, we exposed cells to only one drop of this hydrogel formulation (**Figure 2.20**). Additionally, we tried again the condition of using 100 µL of pre-gel to form a hydrogel of 9 kPa to ensure reproducibility. Once more, alive cell populations were only observed for the control conditions. Moreover, the cells did not survive with the presence of only one drop of hydrogel confirming a high toxicity of the Biogelx^{TM}-GFOGER hydrogels towards T cells, as shown before for the Biogelx^{TM}-S.

Finally, we evaluated the potential disaggregation of the Biogelx^{TM}-GFOGER hydrogels. For that, we tested the following conditions: hydrogel with cells and Dynabeads, hydrogel with no cells but with Dynabeads, and hydrogel with no cells and no Dynabeads. In this experiment a concentration of $2x10^6$ cells/mL was used with RPMI, 10% FBS, 1% PS, and 100mg/L $CaCl_2$. Cells were seeded on top of 25 kPa hydrogels (**Figure 2.21**). Similar to the results obtained with Biogelx^{TM}-S, all the SSC vs FSC graphs obtained when using Biogelx^{TM}-GFOGER hydrogels did not present alive cells. The results indicated that the events recorded by flow cytometry measurements could most probably be attributed to little pieces of the hydrogel.

In conclusion, both Biogelx^{TM}-S and Biogelx^{TM}-GFOGER hydrogels break into little pieces during the cell recovery step, making the cell analysis by flow cytometry complicated. More important, the cells cultured on these hydrogels are not viable and thus, these materials are not suitable for T cell culture.

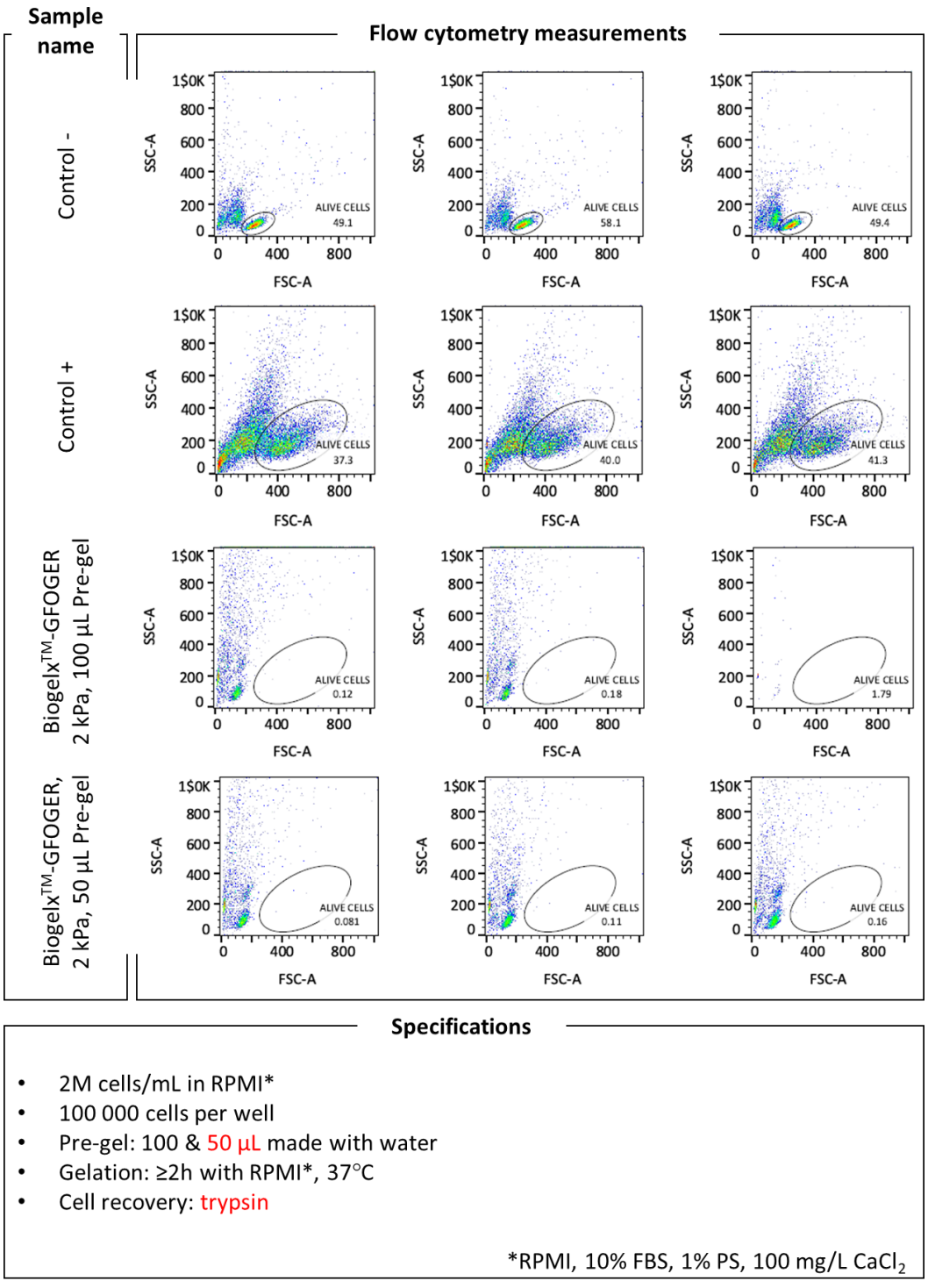

Figure 2.19 Flow cytometry measurements presenting SSC vs FSC gating for the Biogelx™-GFOGER, 2 kPa hydrogels with 50 or 100 µL of pre-gel with Dynabeads, according to the stated specifications. Control - are cells in suspension without Dynabeads, whereas the control + are cells in suspension with Dynabeads.

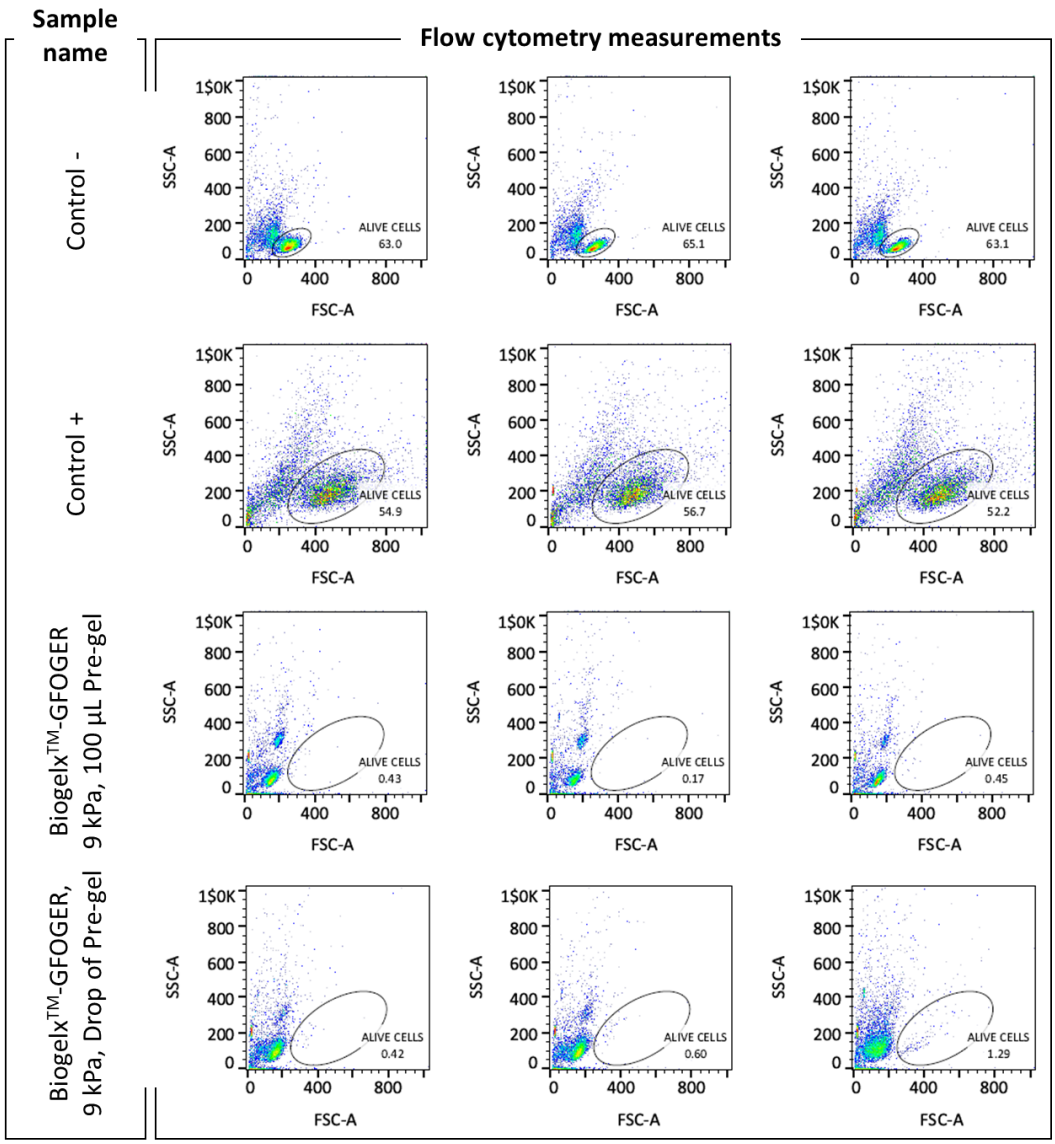

Figure 2.20 Flow cytometry measurements presenting SSC vs FSC gating for the Biogelx™-GFOGER, 9 kPa hydrogels with a drop or 100 µL of pre-gel with Dynabeads, according to the stated specifications. Control - are cells in suspension without Dynabeads, whereas the control + are cells in suspension with Dynabeads.

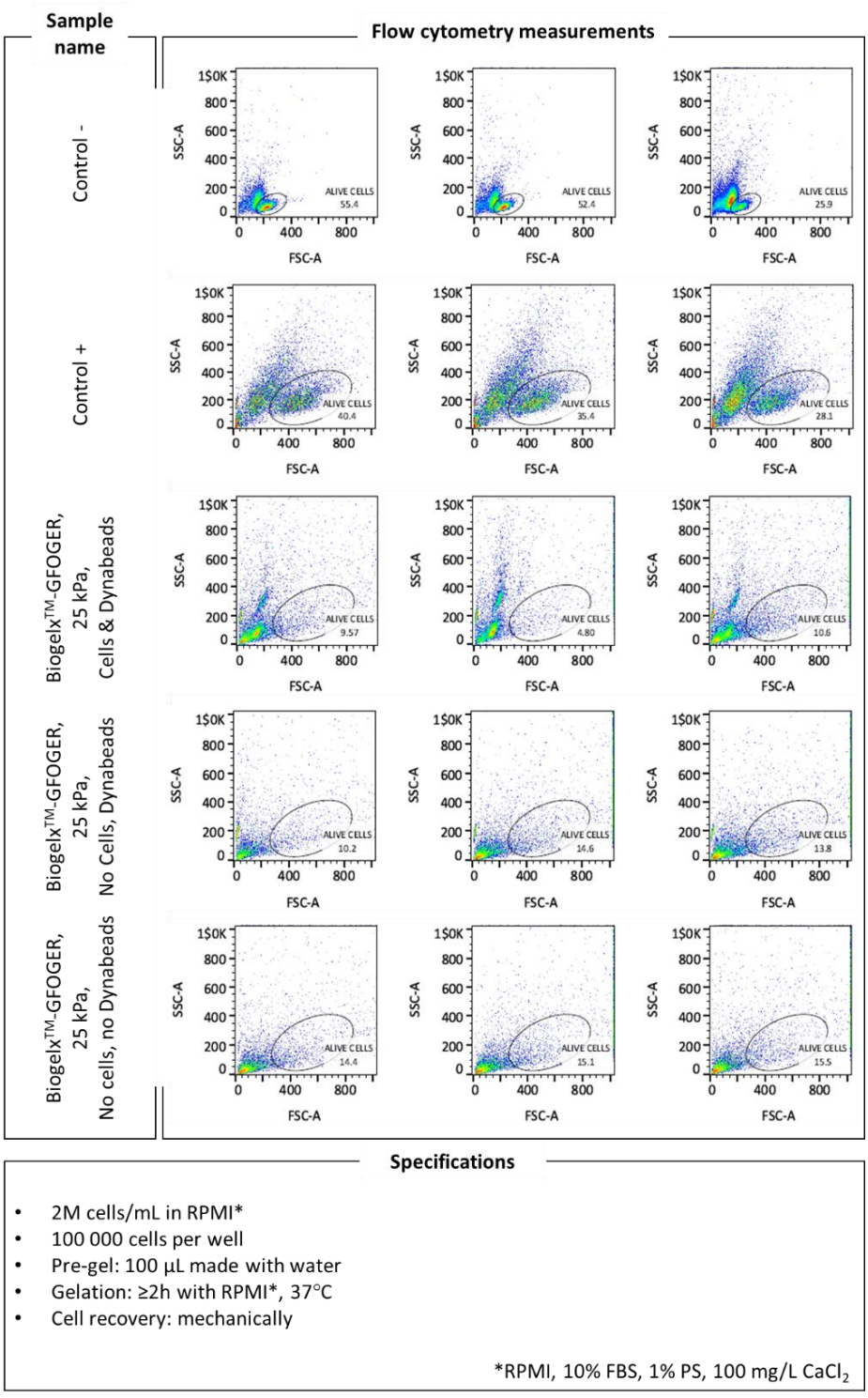

Figure 2.21 Flow cytometry measurements presenting SSC vs FSC gating for the BiogelX™-GFOGER, 25 kPa hydrogels with cells & Dynabeads; with no cells, but with Dynabeads; and with no cells and no Dynabeads, according to the stated specifications. Control - are cells in suspension without Dynabeads, whereas the control + are cells in suspension with Dynabeads.

2.5 Fluorescence analysis

The fluorescence analyses were carried out with the objective to evaluate how the CD4+ T cells interacted with these hydrogels after activation and during proliferation. The experiments were performed on the same 96 well plate where the cells were normally seeded. Furthermore, since the cells were stained with CSFE, as previously mentioned, it was possible to directly observe them under the fluorescent microscope (**Figure 2.22**).

In these experiments, cells, at the concentration of 10^6 cells/mL, were cultured in suspension without Dynabeads in the case of the negative control, and with Dynabeads in the case of the positive control. Both Biogelx™-S and Biogelx™-GFOGER hydrogels were prepared at 25 kPa, and the respective pre-gels were made from 100 µL in water. After seeding the cells, 50 µL of RPMI, 10% FBS, 1% PS, 100 mg/L $CaCl_2$ were added to the wells (see Chapter 6 for further details). The microscopy images of the fluorescent cells were taken at different time points after seeding, i.e., with 1 h, 2 days and 5 days of incubation.

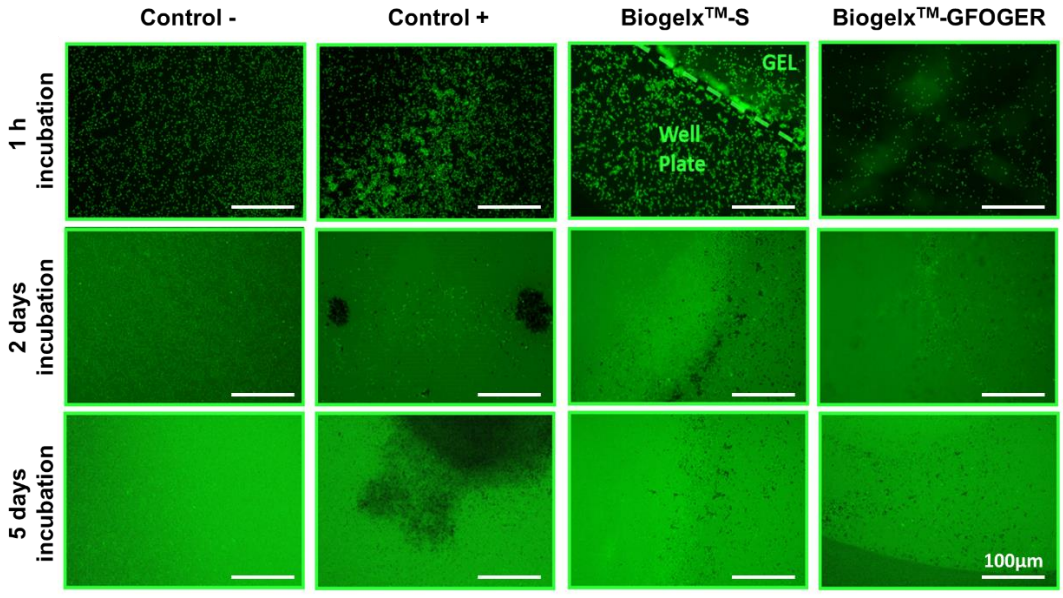

Figure 2.22 Fluorescence microscopy images obtained from primary human CD4+ T cells seeded on the Biogelx™-S, 25 kPa and Biogelx™-GFOGER, 25 kPa hydrogels at different times of incubation (1 h, 2 days and 5 days). Cells in suspension without Dynabeads was control -, whereas cells in suspension with Dynabeads were control +. Scale bar: 100 µm

From these results, it was seen an increase of unspecific fluorescence with the pass of time, probably, due to the presence of free dye. Furthermore, the fluorescence of the cells as well as the contrast of the images decreased with time, because of the halving of the fluorescence happening in each division as mentioned before.

The images show small black dots on the control + and on the Biogelx™-S and Biogelx™-GFOGER samples, which are the Dynabeads. However, the typical aggregation of cells together with the Dynabeads characteristic of cell proliferation was only seen in the control +. This behavior was not found for the cells seeded on the hydrogels.

Additionally, on day 5, very few cells could be distinguished in accordance with the flow cytometry results discussed in the previous section. Furthermore, the images represent the bottom of the well plate with the cells under the hydrogels, since obtaining images of the possible cells inside the hydrogels was not possible.

2.6 Stability of the hydrogels over time

At this point, the stability of the Biogelx™-S and Biogelx™-GFOGER hydrogels was measured over time (up to 30 days) at two different stiffness (5 and 25 kPa).

For this purpose, 100 mg of each hydrogel was prepared in triplicate, and its weight was verified at different times. For every weight check, the cell culture media (100 µL) was removed, the hydrogel's weight was measured, fresh media was added again on top of the hydrogels and the samples were placed inside the incubator at 37°C, until the next weight check. The results obtained are shown in **Figure 2.23**.

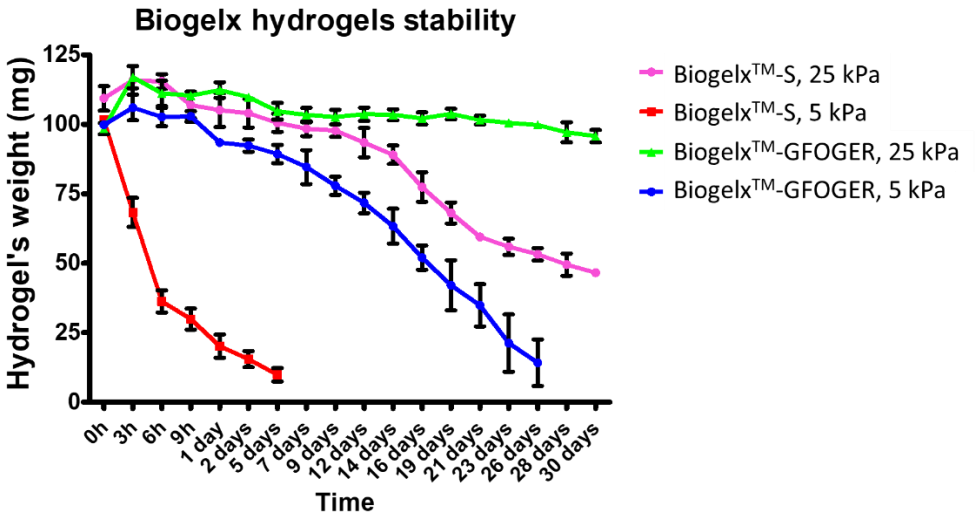

Figure 2.23 Stability of Biogelx-S and -GFOER hydrogels at 5kPa and 25kPa over time, up to 30 days ($N_{hydrogels}$ = 3).

With this basic experiment, which was not performed before as our industrial collaborators never stated the possibility of degradation issues, it was observed that the hydrogels with low stiffness (5 kPa) were totally degraded in a short time. On the other hand, samples with higher stiffness (25 kPa) showed higher stability. Interestingly, these hydrogels were stable during a week, which is the time we use to perform our cell culture experiments. The Biogelx™-GFOGER hydrogels showed a better stability overtime than the standard ones. It is probably, the presence of the GFOGER sequence in the hydrogel which contributes to a higher number of H-bonding and π-stacking interactions, leading to a more stable hydrogel.

2.7 Hydrogel morphology characterization

The scanning electron microscopy (SEM) technique is usually used to analyze dry samples at high vacuum. However, images of the surface of the hydrated hydrogels could be obtained by slowly decreasing the pressure and temperature of the vacuum chamber, i.e. using the so-called environmental SEM (ESEM) operational mode.

Morphological characterization of the Biogelx™-S and Biogelx™-GFOGER hydrogels with a stiffness of 9 kPa was performed by ESEM. Biogelx hydrogels with a stiffness of 25 kPa were not considered despite their high stability in cell culture media, because they are brittle, and therefore challenging to handle. On the other hand, the hydrogels of 5 kPa were too soft, and less stable overtime in comparison with stiffer hydrogels. For these reasons, we decided to measure hydrogels with intermediate stiffness of 9 kPa by ESEM. Representative images of the surface of each hydrogel are shown in **Figure 2.24**.

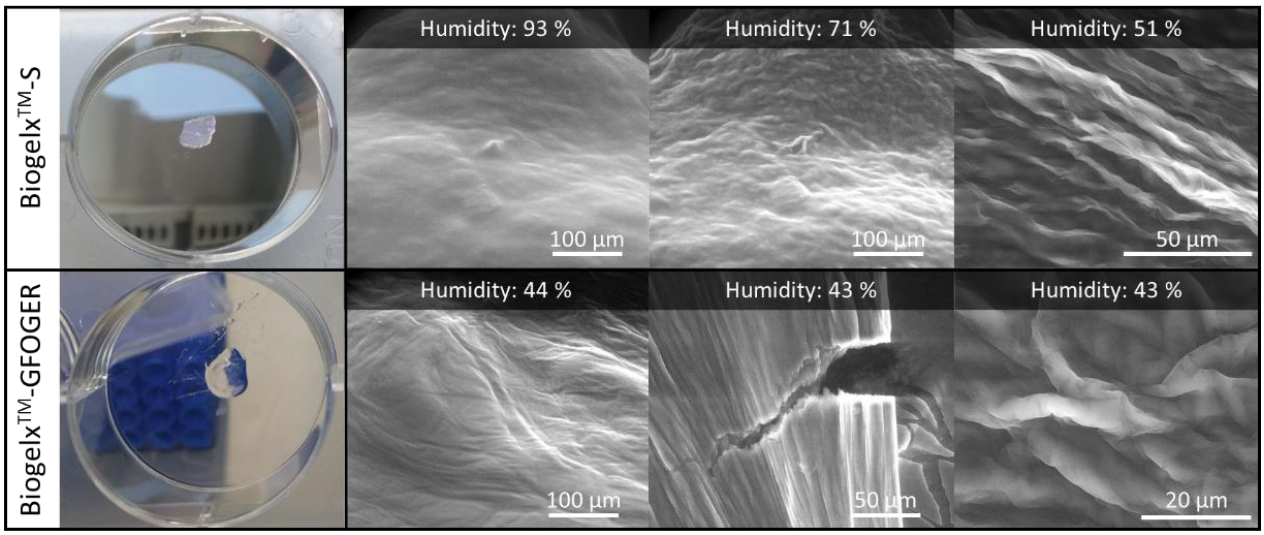

Figure 2.24 Left: Photographs of the hydrogels analyzed by environmental SEM. Right: Environmental SEM images of the Biogelx™-S and Biogelx™-GFOGER hydrogels (9 kPa).

These images show the roughness of the surface of the hydrogels, which is an important factor for cell adhesion, regardless of cell type and matrix materials.[36] However, no pores were observed even at lower humidity levels. This fact may be one of the reasons of the low cell viability found for theses hydrogels, which may prevent cells to penetrate and move freely within the Biogelx hydrogels, which is one of the desired characteristics to mimic the LN environment.

2.8 Summary and conclusions

In this chapter the potential of two different 3D scaffolds from the SME Biogelx Ltd., the Biogelx^{TM}-S and Biogelx^{TM}-GFOGER hydrogels were studied as 3D scaffolds for CD4+ T cell proliferation, as an alternative to the standard suspension systems.

However, none of the flow cytometry experiments performed with the hydrogels resulted in an alive population of cells, despite the good results obtained with the controls. The fluorescent experiment results also supported these findings. No alive cells were clearly identified on the hydrogels unlike the positive controls, which showed the aggregation of cells together with Dynabeads that is typical of activated and proliferative T cell cultures.

Furthermore, these hydrogels were found to be very challenging to handle, especially on the cell recovery step, because they tend to desegregate into small pieces. This situation led to several undesired events recorded in the flow cytometry as shown on the SSC vs FSC graphs.

As a conclusion, we can affirm that despite the interesting physicochemical characteristics of these hydrogels, they were found to be not suitable for T cell proliferation in the conditions used in this study.

2.9 References

1. Ulijn, R. V. *et al.* Bioresponsive hydrogels. *Mater. Today* **10**, 40–48 (2007).

2. Wichterle, O. & Lim, D. Hydrophilic Gels for Biological Use. *Nature* **185**, 117–118 (1960).

3. Peppas, B. N. A., Hilt, J. Z., Khademhosseini, A. & Langer, R. Hydrogels in Biology and Medicine : From Molecular Principles to Bionanotechnology. *Adv. Mater.* **18**, 1345–1360 (2006).

4. Drury, J. L. & Mooney, D. J. Hydrogels for tissue engineering: Scaffold design variables and applications. *Biomaterials* **24**, 4337–4351 (2003).

5. Pérez Del Río, E., Martinez Miguel, M., Veciana, J., Ratera, I. & Guasch, J. Artificial 3D Culture Systems for T Cell Expansion. *ACS omega* **3**, 5273–5280 (2018).

6. Pérez Del Río, E. *et al.* CCL21-loaded 3D hydrogels for T cell expansion and differentiation. *Biomaterials* **259**, 1–13 (2020).

7. De Loos, M., Feringa, B. L. & Van Esch, J. H. Design and application of self-assembled low molecular weight hydrogels. *European J. Org. Chem.* **2005**, 3615–3631 (2005).

8. Yang, Z., Liang, G. & Xu, B. Enzymatic control of the self-assembly of small molecules: A new way to generate supramolecular hydrogels. *Soft Matter* **3**, 515–520 (2007).

9. Estroff, L. A. & Hamilton, A. D. Water gelation by small organic molecules. *Chem. Rev.* **104**, 1201–1217 (2004).

10. Jayawarna, V. *et al.* Nanostructured hydrogels for three-dimensional cell culture through self-assembly of fluorenylmethoxycarbonyl-dipeptides. *Adv. Mater.* **18**, 611–614 (2006).

11. Jayawarna, V., Smith, A., Gough, J. E. & Ulijn, R. V. Three-dimensional cell culture of chondrocytes on modified di-phenylalanine scaffolds. *Biochem. Soc. Trans.* **35**, 535–537 (2007).

12. Smith, A. M. *et al.* Fmoc-diphenylalanine self assembles to a hydrogel via a novel architecture based on π-π interlocked β-sheets. *Adv. Mater.* **20**, 37–41 (2008).

13. Zhou, M. *et al.* Self-assembled peptide-based hydrogels as scaffolds for anchorage-dependent cells. *Biomaterials* **30**, 2523–2530 (2009).

14. Alakpa, E. V. *et al.* Improving cartilage phenotype from differentiated pericytes in tunable peptide hydrogels. *Sci. Rep.* **7**, 1–11 (2017).

15. Simunovic, M. *et al.* A 3D model of a human epiblast reveals BMP4-driven symmetry breaking. *Nat. Cell Biol.* **21**, 900–910 (2019).

16. Tourasse, C. *et al.* Elastography in the assessment of sentinel lymph nodes prior to dissection. *Eur. J. Radiol.* **81**, 3154–3159 (2012).

17. Kilic, F. *et al.* Ex Vivo Assessment of Sentinel Lymph Nodes in Breast Cancer Using Shear Wave Elastography. *J. Ultrasound Med.* **35**, 271–277 (2016).

18. Bae, S. J. *et al.* Ex Vivo Shear-Wave Elastography of Axillary Lymph Nodes to Predict Nodal Metastasis in Patients with Primary Breast Cancer. *J. Breast Cancer* **21**, 190–196 (2018).

19. You, J. *et al.* The value of quantitative shear wave elastography in differentiating the cervical lymph nodes in patients with thyroid nodules. *J. Med. Ultrason.* **45**, 251–259 (2018).

20. Kim HD. *et al.* Epidermal growth factor-induced enhancement of glioblastoma cell migration in 3D arises from an intrinsic increase in speed but an extrinsic matrix- and proteolysis-dependent increase in persistence. *Mol. Biol. cellell* **19**, 4249–4259 (2008).

21. Doyle, A. D., Carvajal, N., Jin, A., Matsumoto, K. & Yamada, K. M. Local 3D matrix microenvironment regulates cell migration through spatiotemporal dynamics of contractility-dependent adhesions. *Nat. Commun.* **6**, 1–15 (2015).

22. Marx, V. How some labs put more bio into biomaterials. *Nat. Methods* **16**, 365–368 (2019).

23. Alakpa, E. V. *et al.* Tunable Supramolecular Hydrogels for Selection of Lineage-Guiding Metabolites in Stem Cell Cultures. *Chem* **1**, 298–319 (2016).

24. Borst, J., Ahrends, T., Bąbała, N., Melief, C. J. M. & Kastenmüller, W. CD4(+) T cell help in cancer immunology and immunotherapy. *Nat. Rev. Immunol.* **18**, 635–647 (2018).

25. Brightman, S. E., Naradikian, M. S., Miller, A. M. & Schoenberger, S. P. Harnessing neoantigen specific CD4 T cells for cancer immunotherapy. *J. Leukoc. Biol.* **107**, 625–633 (2020).

26. Saillard, M., Cenerenti, M., Romero, P. & Jandus, C. Impact of Immunotherapy on CD4 T Cell Phenotypes and Function in Cancer. *Vaccines* **9**, 1–21 (2021).

27. Lyons, A. B. & Parish, C. R. Determination of lymphocyte division by flow cytometry. *J. Immunol. Methods* **171**, 131–137 (1994).

28. Luzyanina, T. *et al.* Computational analysis of CFSE proliferation assay. *J. Math. Biol.* **54**, 57–89 (2007).

29. Roederer, M. Interpretation of cellular proliferation data: Avoid the panglossian. *Cytom. Part A* **79**, 95–101 (2011).

30. Weiden, J. *et al.* Injectable biomimetic hydrogels as tools for efficient T Cell expansion and delivery. *Front. Immunol.* **9**, 1–15 (2018).

31. Sojka, D. K., Bruniquel, D., Schwartz, R. H. & Singh, N. J. IL-2 secretion by CD4+ T cells in vivo is rapid, transient, and influenced by TCR-specific competition. *J. Immunol.* **172**, 6136–6143 (2004).

32. Malek, T. R. The main function of IL-2 is to promote the development of T regulatory cells. *J. Leukoc. Biol.* **74**, 961–965 (2003).

33. Villarino, A. V *et al.* Helper T cell IL-2 production is limited by negative feedback and STAT-dependent cytokine signals. *J. Exp. Med.* **204**, 65–71 (2007).

34. Nelson, B. H. IL-2, Regulatory T Cells, and Tolerance. *J. Immunol.* **172**, 3983–3988 (2004).

35. Waters, R. S., Perry, J. S. A., Han, S., Bielekova, B. & Gedeon, T. The effects of interleukin-2 on immune response regulation. *Math. Med. Biol. A J. IMA* **35**, 79–119 (2018).

36. Cai, S. *et al.* Recent advance in surface modification for regulating cell adhesion and behaviors. *Nanotechnol. Rev.* **9**, 971–989 (2020).

Chapter 3

Collagen scaffolds for T cell expansion

3.1 Introduction

Collagen is 1/3 of the total protein content in humans and it is crucial in maintaining the biological and structural integrity of the ECM providing physical support to tissues, such as in the LNs.[1,2] Collagen features a structural motif composed of three parallel polypeptide strands forming a right-handed triple helix (**Figure 3.1 A**). These individual triple helices know as tropocollagen, further assemble in a hierarchical manner forming macroscopic fibers observed in tissues, bones and basement membranes.[3]

LNs are filled with a reticular meshwork of porous, sponge-like tissue comprised of fibroblastic reticular cells (FRCs) and reticular fibers. These fibers are composed of a core of collagen fibrils enveloped in a layer of ECM proteins and other components of basement membranes.

Collagen scaffolds for cell culture have been widely explored in tissue engineering due do its traits such as low immunogenicity, biocompatibility, biodegradability, good permeability and for its porous structure.[4] As an example, a recent study reported 3D cultures of T cells using collagen hydrogels with high and low density.[5] The effect of the different collagen densities on CD4+ and CD8+ T cell proliferation was evaluated. In this work it was concluded that T cell proliferation was significantly reduced in a high-density matrix compared to a low-density matrix. It was also reported a reduction in proliferation when cells were cultured in 3D compared to 2D.[5] Such experiments are very relevant, since it is known that tumor progression is accompanied by the formation of a tumor-specific ECM, which is often rich in collagen, that leads to an increased stiffness.[5,6]

With the objective of exploring new potentialities of collagen and further improving the current state of cellular immunotherapies, in this Thesis various collagen samples were evaluated as a 3D scaffold for T cell proliferation and differentiation. Collagen samples were provided by the publicly-traded company Viscofan S.A., whose collagen products have been used for different biomedical applications. These applications include skin regeneration,[7] urethra structure repair,[8] dentistry[9] and cardiology,[10–12] but it has never been used for lymphocyte proliferation and differentiation purposes. Among the available products, we worked with different collagen samples made from a collagen type I suspension. This collagen was produced from bovine skin and processed with different industrial treatments. The materials should retain the *in vivo* like structure of insoluble collagen fibers and as such, its biocompatibility and biodegradability (**Figure 3.1 B**).

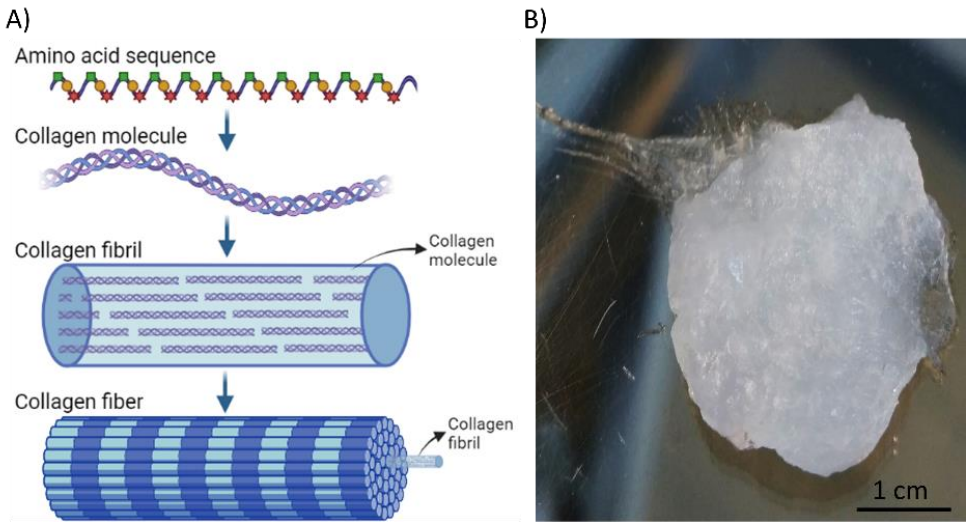

Figure 3.1 A) Scheme of the collagen fiber structure made of several collagen fibrils, that are made of triple helix collagen chains and B) a collagen mass photograph.

3.2 Objectives and strategy

To improve the existing approaches of culture and expansion of T cells with therapeutic phenotypes by using artificial ECMs consisting of 3D collagen hydrogels, a collaboration with

Viscofan S.A. was established. In this chapter we evaluate the performance of the Viscofan products for T cell proliferation and differentiation of adult donors. The samples studied, with 4% and 5% collagen, have been processed by different mechanical treatments. Due to industrial secrecy, the exact conditions applied on the different collagen samples used in this study were not shared with us.

3.3 Pre-treatment of collagen masses for T cell culture

3.3.1 Neutralization of collagen masses

The collagen samples presented a jellylike consistency and were delivered in cooled and non-sterile conditions. They were suspended in hydrochloric acid (HCl) at two different collagen concentrations, 4% and 5%. Furthermore, the samples received different processing approaches, resulting in 4 different collagen masses, the "Col1" and "Col2" (both at 4% of collagen), and "Col3" and "Col4" (both at 5% collagen).

To perform cell experiments, the collagen masses needed to be firstly neutralized, since they were found to be at pH 3-4 with a pH indicator paper. Thus, we initially developed a neutralization protocol following recommendations of Viscofan. The first step consisted in soaking a portion of the masses in ammonium hydroxide (0.28-0.30%) for 20 min. After washing with PBS, the masses were cut and placed inside a 96 well plate template. The gels were left in the incubator for 3 days to ensure the complete evaporation of all the acidic solution. Finally, they were soaked in fresh PBS to obtain collagen masses at pH 6-7. Although the neutralization step was successful, ammonium hydroxide is potentially harmful for CD4+ T cell viability.[13] For that reason, we developed an alternative protocol with sodium hydroxide (NaOH) at 0.05 M (**Figure 3.2**). This time, the hydration step was performed with complete RPMI medium instead of PBS. The reason behind this change was to present a more adequate environment to the cells at the seeding stage.

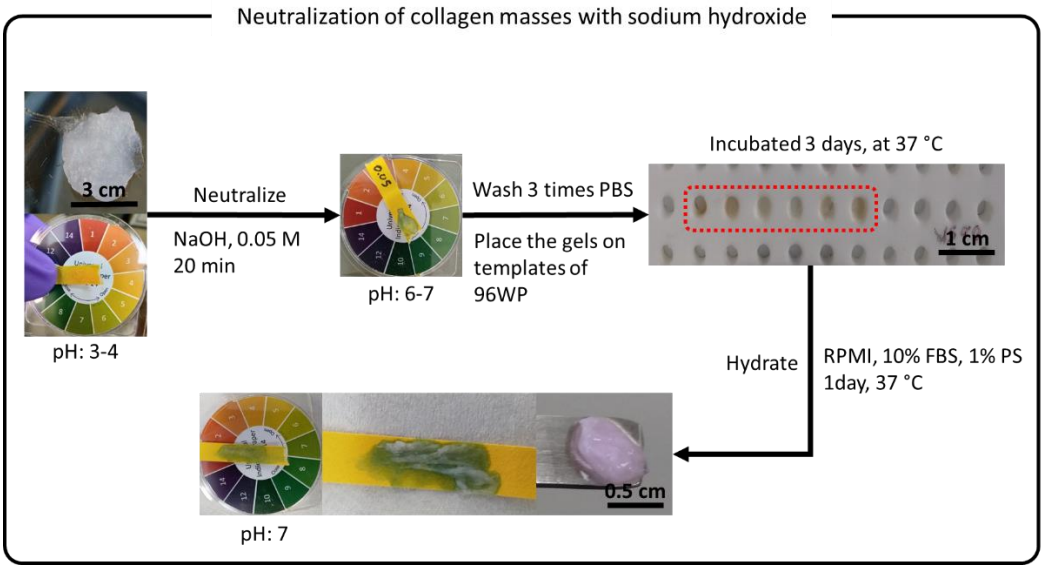

Figure 3.2 Neutralization protocol of collagen masses with sodium hydroxide.

Once the neutralization of the masses was successfully achieved, the physical characterization of the material was performed by different techniques, as described in the following sections.

3.3.2 Environmental SEM characterization

The porosity of the different scaffolds hydrated in water was studied by ESEM. As mentioned in the previous chapter, the images of the inner structure could be obtained by slowly decreasing the pressure and temperature of the SEM vacuum chamber. Representative images for the different samples are shown in **Figure 3.3**.

All samples showed the desired collagen fibres for T cell culture. Nevertheless, as it can be seen in the images, the Col2, Col3 and Col4 samples were contaminated with bacteria. These results pointed out the special attention that these collagen masses require in terms of sterilization.

For this reason, the development of a sterilization protocol was considered to be incorporated into the pre-treatment step together with the neutralization process.

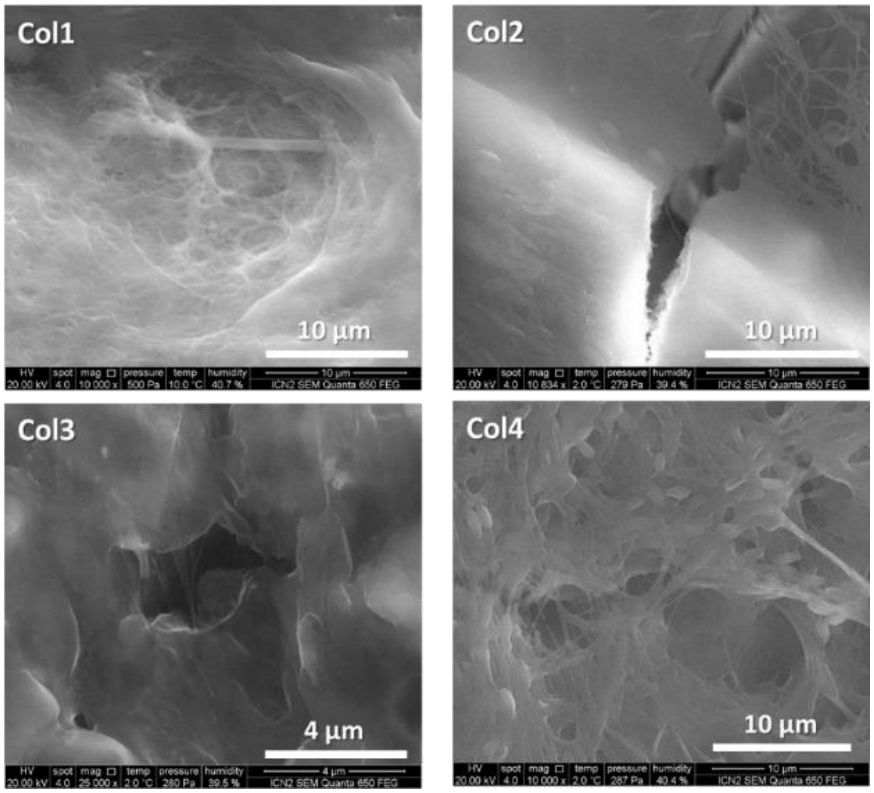

Figure 3.3 ESEM images of the different collagen masses Col1, Col2, Col3 and Col4.

3.3.3 Neutralization and sterilization of collagen masses

Upon reception, a sterilization step was performed by placing the samples under UV light for 1 h. Then the masses were frozen (-20˚C) until use. In this case, the collagen masses were thawed and the neutralization process was performed with NaOH (0.05 M) for 30 min. After this, the masses were re-treated with UV irradiation for 1 h, before being cut and placed inside the 96 well plates. After, the collagen masses were hydrated in cell culture medium (200 µL complete RPMI) for at least one day. Finally, their pH was measured concluding that the collagen masses were successfully neutralized (**Figure 3.4**).

A)

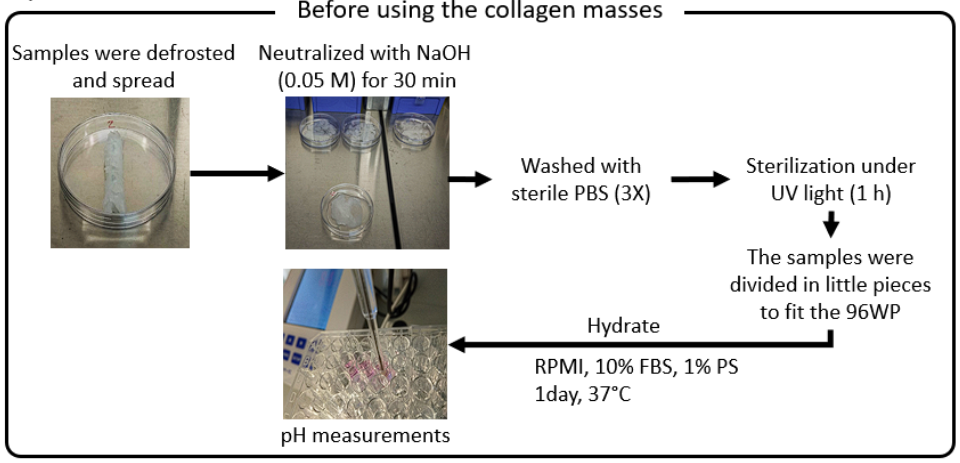

B)

Samples	pH
Control	7.7 ± 0.1
Col1	7.9 ± 0.0
Col2	7.8 ± 0.1
Col3	7.8 ± 0.1
Col4	7.9 ± 0.0

Figure 3.4 A) Process of neutralization and sterilization steps performed before using the collagen masses for T cell culture. B) pH measurements of the medium after the collagen masses (Col1, Col2, Col3 and Col4) sterilization and neutralization. The control sample is cell culture medium alone.

3.4 T cell activation and expansion on collagen masses

For these experiments, primary human CD4+ T cells were seeded on top of the collagen masses (Col2, Col3 and Col4) at the concentration of $1x10^6$ cells/mL using complete RPMI (RMPI with 10% FBS and 1% PS) with Dynabeads in 96 well-plates. The positive control, which corresponds to the state-of-the-art culture method, consisted of cells in suspension at the same concentration with Dynabeads. For further details see Chapter 6.

3.4.1 Fluorescence microscopy analyses

Fluorescence analyses were carried out with CFSE-stained CD4+ T cells. CSFE is a cell permeable fluorescent staining dye commonly used in proliferation studies, as explained in Chapter 2. Thus, it was possible to directly observe the fluorescent cells under the optical microscope at different

time points after seeding, namely 2 h, 2 days and 6 days. Samples of Col2, Col3 and Col4 were analysed (**Figure 3.5**).

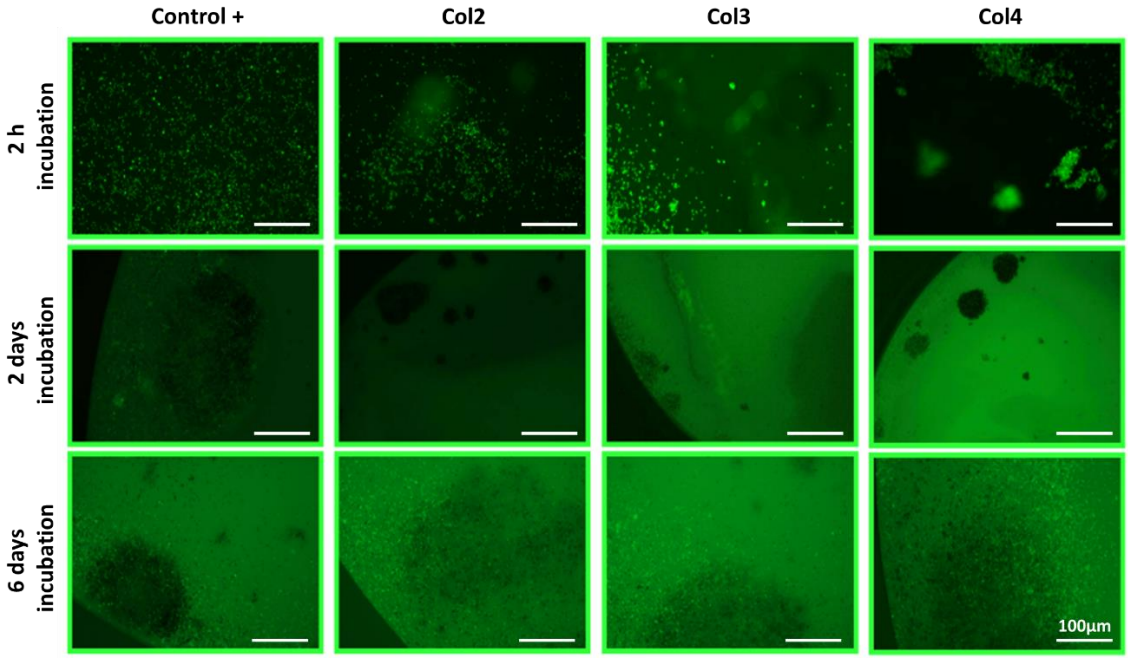

Figure 3.5 Fluorescence microscopy images obtained from cells in suspension (control +) and seeded on different collagen masses (Col2, Col3 and Col4) at different times (2 h, 2 days and 6 days). Scale bar: 100 µm.

It was possible to see that the cell number increased over time together with a decrease on the fluorescence intensity of the cells, which indicates that cell proliferation occurred not only in suspension (control +), but also in the presence of the collagen samples.

We observed more cells on superior layers than on the bottom of the well plate indicating that cells were mainly supported by the hydrogels. However, the characteristic opaque color of the collagen made difficult to analyze the existence of cells inside the collagen hydrogels by this technique. A significant number of cells was also observed on the edges of the wells because the cell suspension was added on top of the hydrogels and some cells slipped to the sides.

3.4.2 CD4+ T cell proliferation analyses

T cell expansion was studied using the different collagen samples (Col1, Col2, Col3 and Col4) as 3D scaffolds by flow cytometry. A static suspension of cells with Dynabeads was used as a positive control. After 6 days of culture, the stained CSFE T cells were removed from the well plate after several mechanical re-suspensions with the micropipette. Then, Dynabeads were removed through magnetic separation. The cells were centrifuged to replace the complete RPMI medium by a PBS solution to be then analyzed by flow cytometry (see Chapter 6 for details).

T cell proliferation was assessed through the proliferation, expansion and replication indexes (**Figure 3.6**). In summary, the proliferation index represents the average number of divisions among the responding cells, the expansion index the fold-expansion of the whole population and the replication index is the fold-expansion of the responding cells.[14] These three parameters are relevant for cell therapy, as discussed in Chapter 2. Results are normalized to the positive control to reduce the influence of the intrinsic donor variability (**Figure 3.6**).

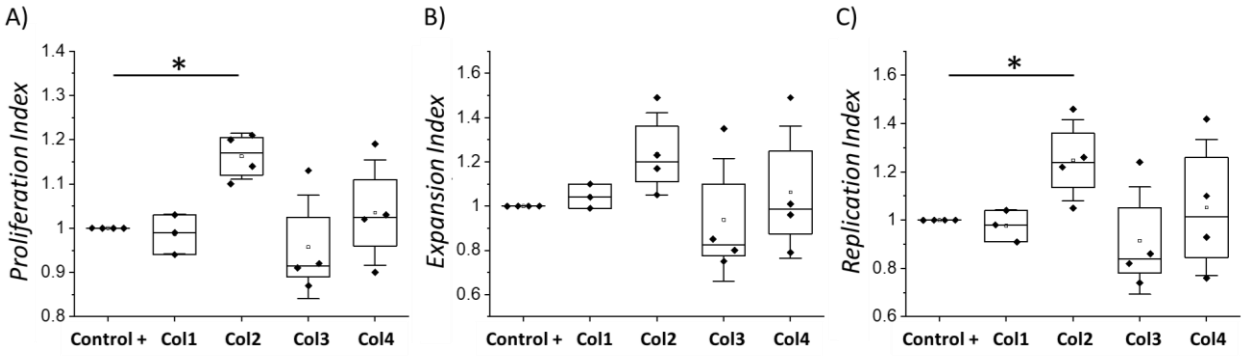

Figure 3.6 Normalized proliferation analyses of primary human CD4+ T cells 6 days after seeding on collagen scaffolds (N_{donors} = 4 for Col2, Col3, Col4 and N_{donors} = 3 for Col1). A) Proliferation index, B) expansion index and C) replication index. Statistical significance was determined by the Mann−Whitney U test (*$p < 0.05$).

The normalized proliferation index presented median values of 0.99, 1.17, 0.92 and 1.02, for the Col1, Col2, Col3 and Col4 samples, respectively. For the normalized expansion index, the Col1, Col2, Col3 and Col4 samples exhibited median values of 1.04, 1.20, 0.83 and 0.99, respectively, whereas for the normalized replication index, the values were of 0.98, 1.24, 0.84 and 1.01, respectively. As it can be observed, the collagen sample Col2, with 4% of collagen, significantly improved the results of the positive control by 17% and 24% in the proliferation and replication index, respectively.

In summary higher proliferation results than the positive control (commercial standard methodologies used in some of the clinical trials reported in Chapter 1) were obtained. Nevertheless, we had to develop a sterilization protocol to avoid bacterial contamination, which is a common problem of hydrogels that have a natural origin like collagen.

Finally, as the results for the 4% collagen were the most promising ones, especially the sample Col2, we decided together with the Viscofan S.A. team to continue the work only with samples with this percentage of collagen.

3.5 Effect of the mechanical treatment and morphology of collagen samples

We analyzed the effect of different mechanical treatments as well as sample morphology of 4% collagen samples on primary human CD4+ T cell proliferation. Specifically, we were provided with 4 cooled and non-sterile collagen masses (Col2, Col5, Col6 and Col7) that received different mechanical treatments, including Col2 which resulted in the best proliferation results. Moreover, we received 3 more collagen formulations with different industrial treatments, all at 4% of collagen. These last samples were named dried collagen (DC), collagen hydrogel (CH) and sponge, and they were already sterilized by the company Viscofan S.A (**Figure 3.7**). Consequently, the DC, CH and sponge samples were simply thawed one day before seeding, washed with sterile PBS and conditioned overnight in complete RPMI medium at 37˚C and 5% CO_2 (see Chapter 6 for

further details). The rest of samples (Col2, Col5, Col6 and Col7) needed to be neutralized and sterilized, as described before. This process was done without further problems.

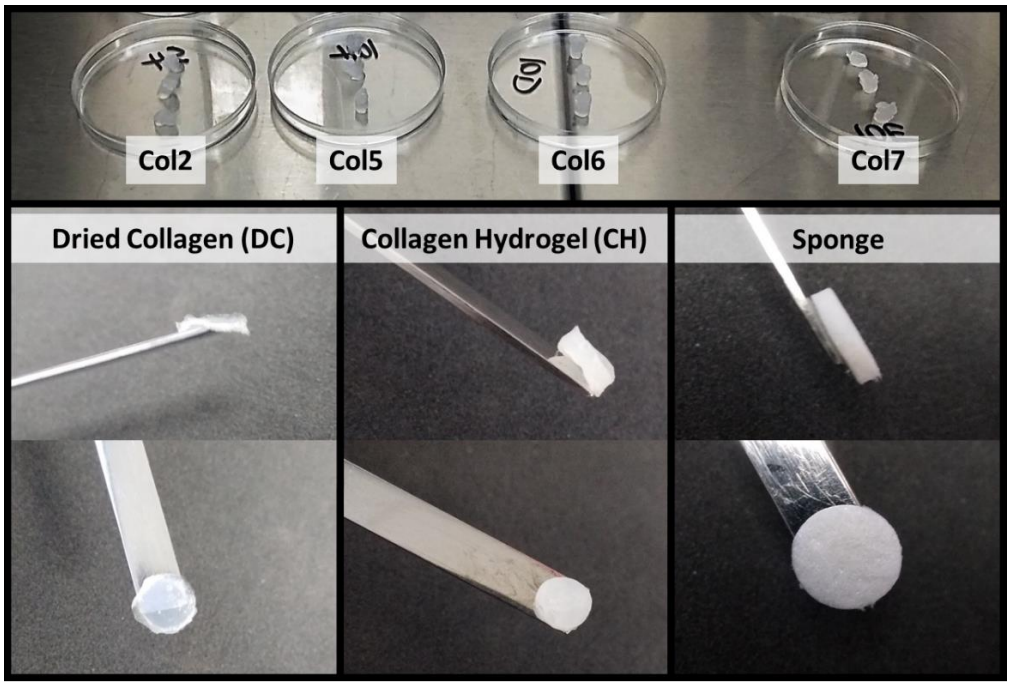

Figure 3.7 Photographs of the collagen masses after the sterilization and neutralization steps (Col2, Col5, Col6 and Col7) and DC, CH and sponge samples.

3.5.1 ESEM characterization of the collagen masses and DC, CH and the collagen sponge

The new collagen masses as well as the DC, CH and the sponge samples, all hydrated in Milli-Q water, were characterized by ESEM (**Figure 3.8**). All samples showed the desired collagen fibers for T cell culture, with the exception of the sponge. Interestingly, the sample CH presented large empty pores; some of them even larger than 100 µm. Even though the other samples also showed high porosity, they had several thin fibers, creating secondary smaller pores inside the larger ones. Such pore structure may be an impediment, to some extent, for the infiltration and movement of T cells in these materials. Furthermore, larger pores are expected to allow the formation of clusters of T cells with Dynabeads during the needed activation phase before proliferation.

3.5.2 CD4+ T cell proliferation analysis

After confirming the neutralization protocol was successful, the preparation of collagen masses for cell seeding experiments was performed, as explained before and in Chapter 6. Then, primary human CD4+ T cells were cultured on the different collagen masses (Col2, Col5, Col6, Col7) and on DC, CH and sponge collagen samples, as stated in section 3.4.2 (see Chapter 6 for further details). **Figure 3.9** shows the proliferation, expansion and replication indexes after normalization to the positive control, as before.

The normalized proliferation index (median) values obtained for the Col2, Col5, Col6, Col7, DC, CH and sponge samples were of 1.24, 1.23, 1.17, 1.17, 1.20, 1.60 and 1.09, respectively. For the normalized expansion and replication indexes, the (median) values achieved were of 1.15, 1.16, 1.16, 1.18, 1.20, 1.95, 0.96, as well as 1.38, 1.37, 1.25, 1.28, 1.32, 2.09, 1.14, for the Col2, Col5, Col6, Col7, DC, CH and sponge samples, respectively.

Thus, all samples significantly improved the state-of-the-art commercial systems. However, the sponge sample showed the lower results, which might be related to its structural stability and lack of pores as discussed previously on this chapter (**Figure 3.8**). On the other hand, the CH samples constantly provided outstanding results in terms of proliferation, improving more than 2 times the positive control. Specifically, the expansion index obtained for the positive control was in average 2.71 while the CH sample value was 5.49 before normalization, indicating that for each 1 million cells seeded on the CH samples, 5.49 million cells could be obtained after 6 days.

Consequently, we focused on the corroboration of the proliferation results obtained with the CH sample.

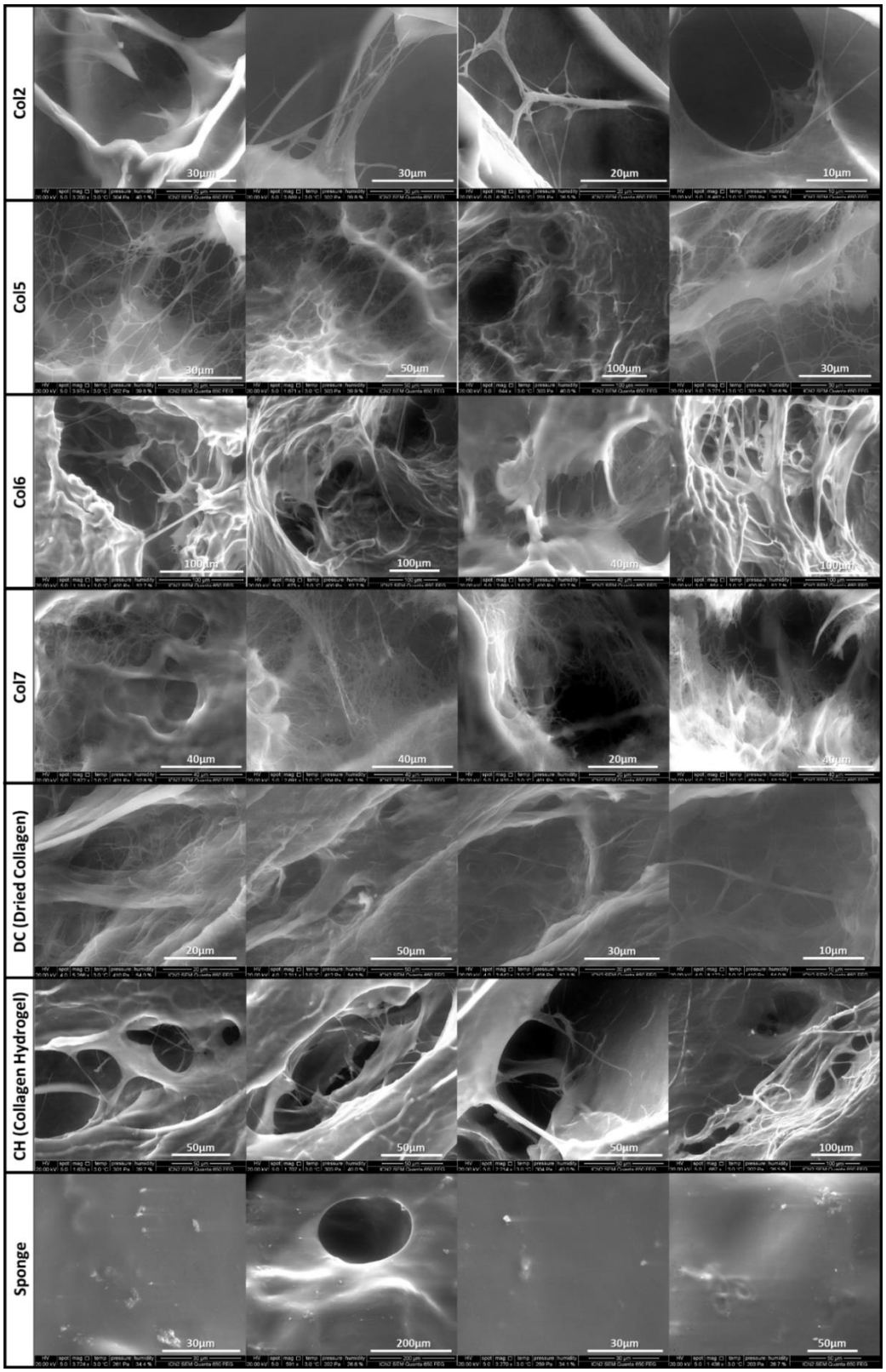

Figure 3.8 ESEM images of the different masses (Col2, Col5, Col6 and Col7) and the DC, CH and sponge samples.

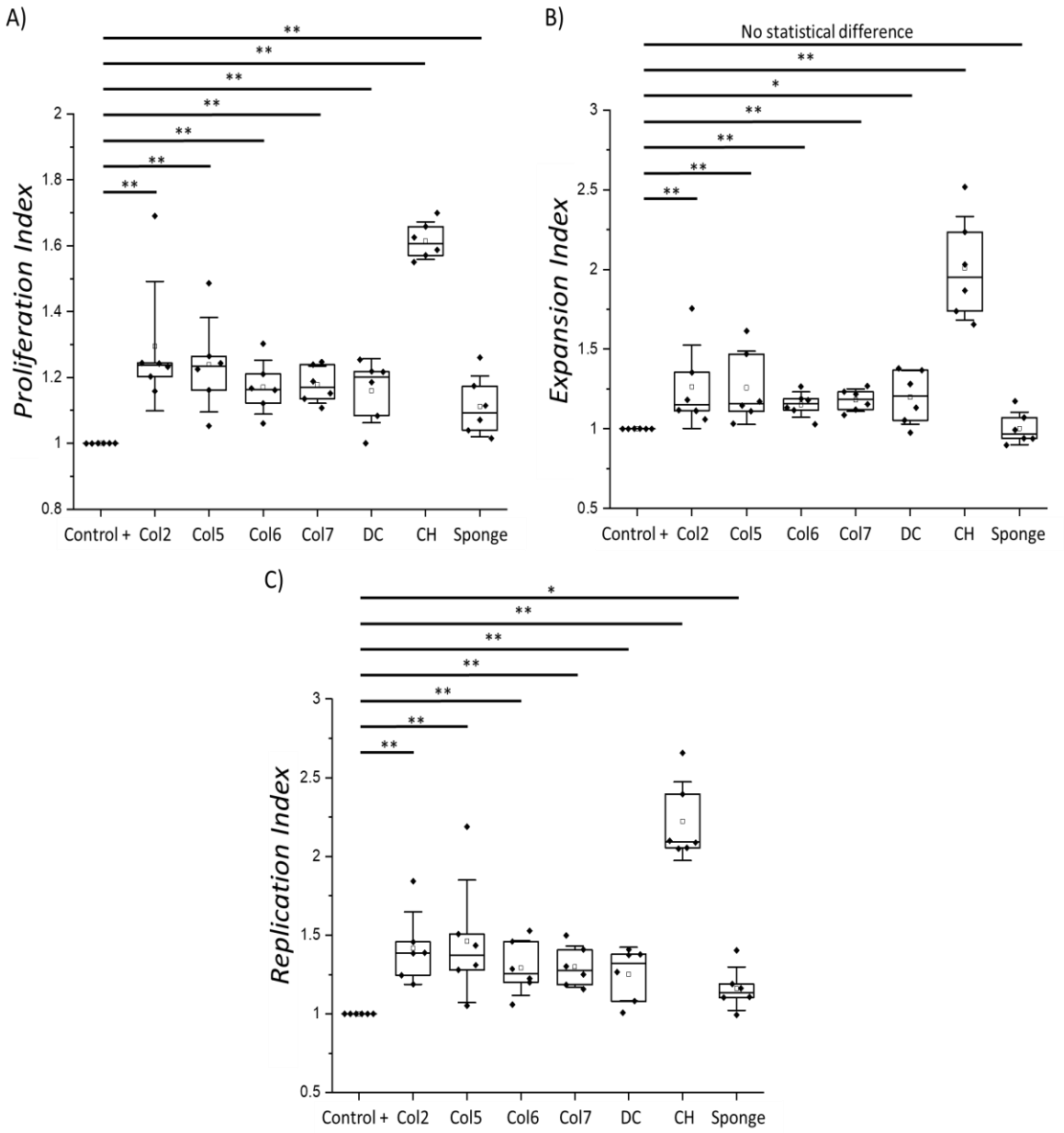

Figure 3.9 Normalized proliferation analyses of primary human CD4+ T cells 6 days after seeding on collagen masses (Col2, Col5, Col6 and Col7) and collagen DC, CH and sponge. Control +: cells in suspension with Dynabeads (N_{donors} = 6). A) proliferation, B) expansion and C) replication indexes. Statistical significance was determined by the Mann−Whitney U test (*p < 0.05 and **p < 0.01).

3.6 T cell proliferation analysis on the CH sample – three trials

Even though the same protocol was performed, the primary human CD4+ T cells seeded on the new batch of CH samples provided by Viscofan S.A. were found to be dead for all 4 different human donors tested after 6 days of culture. Thus, no proliferation results could be obtained by flow cytometry measurements as seen on the side versus forward scatter (SSC vs FSC) graphs. Nevertheless, a typical proliferated and alive population (60-70% alive) was obtained for the positive control with CD4+ T cells seeded in suspension with Dynabeads. These results suggested a potential fabrication issue in obtaining the CH sample or a possible contamination during transportation.

In a second trial, new CH samples were provided by Viscofan S.A. and treated as explained before (**Figure 3.10**). In this experiment, it was possible to observe CD4 + T cell proliferation in 6 different human donors, but only 7 out of 29 CH samples contributed to this effect (**Figure 3.10**; highlighted in red). **Figure 3.11** shows the normalized proliferation, expansion and replication indexes obtained for these populations. In the cases where more than one replicate was used per donor, the average value of the indexes was used.

Even though only 7 CH samples contributed to the T cell expansion results, the median values obtained this time for the normalized proliferation index (1.45) and expansion index (1.82) were comparable with the values initially obtained, being the normalized proliferation and expansion indexes at that time 1.60 and 1.95, respectively.

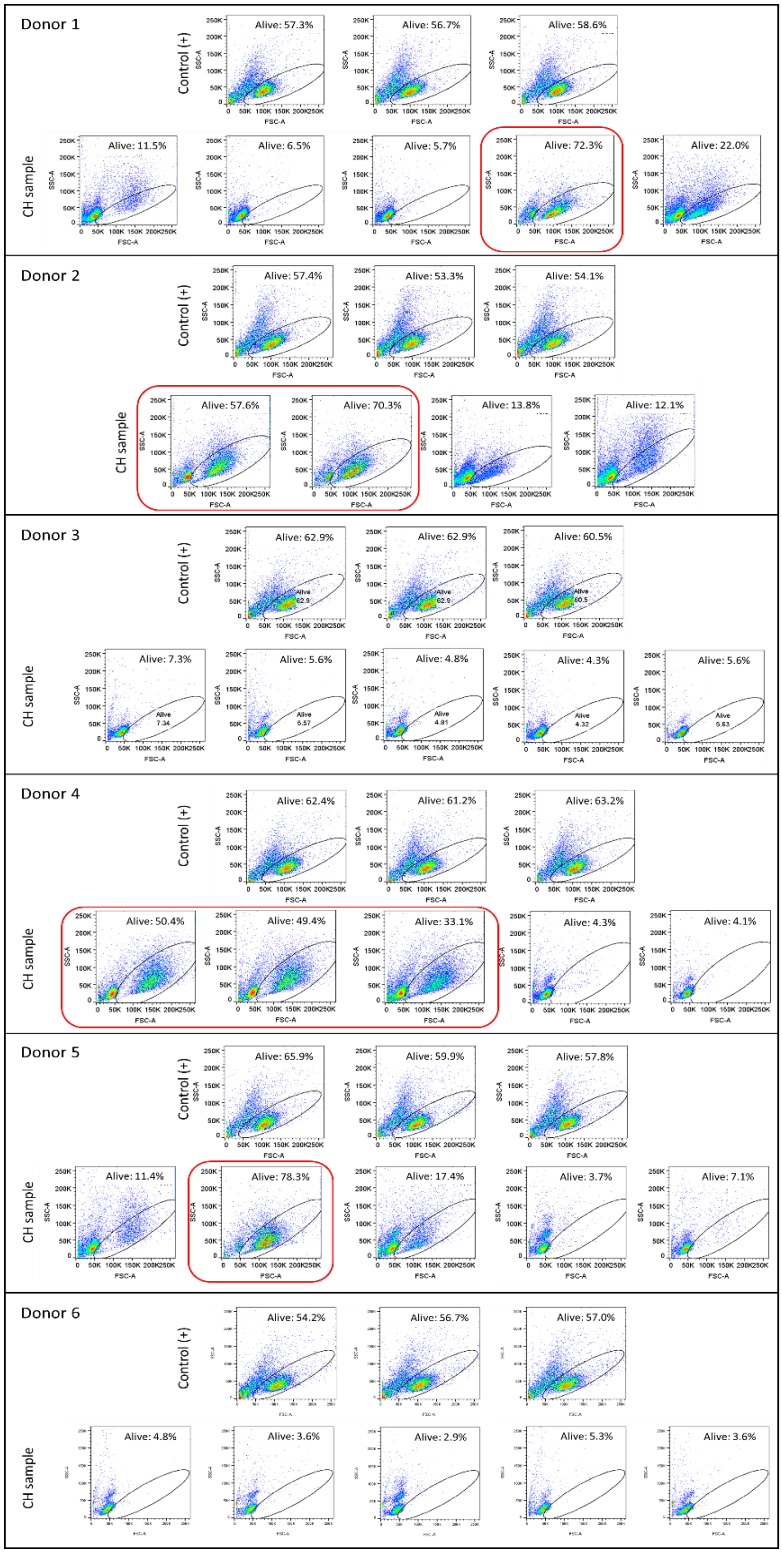

Figure 3.10 Flow cytometry measurements showing the SSC vs FSC graphs of primary human CD4+ T cells seeded on the CH sample in the presence of Dynabeads. Control +: cells in suspension with Dynabeads (N_{donors} = 6). With red, it is marked the populations used for proliferation analysis.

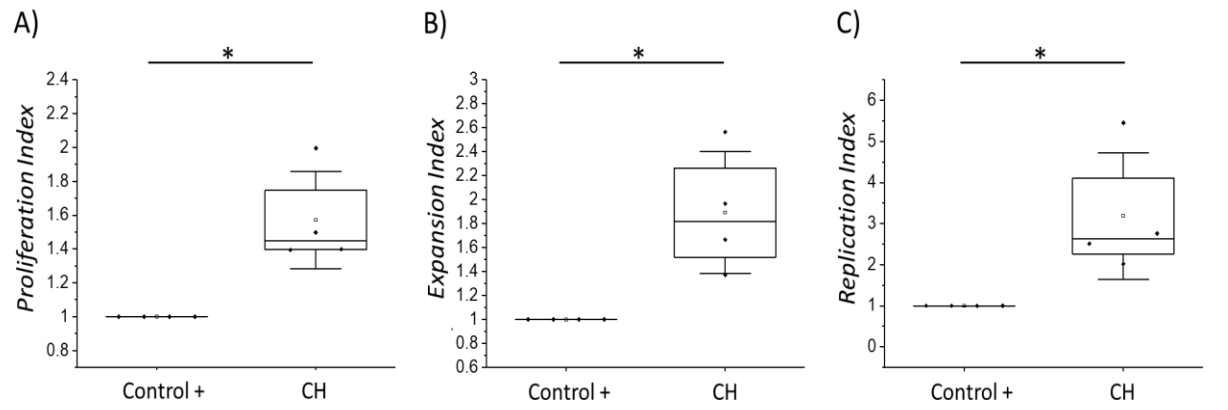

Figure 3.11 Normalized proliferation analyses of primary human CD4+ T cells seeded on the CH sample in the presence of Dynabeads. Control +: cells in suspension with Dynabeads (N_{donors} = 4). A) Proliferation, B) expansion and C) replication indexes. Statistical significance was determined by the Mann−Whitney U test (*$p < 0.05$).

For the normalized replication index, we obtained a median value of 2.63, which is even higher than the value initially achieved of 2.09. However, it should be considered the wide standard deviation of these CH samples (**Figure 3.11 C**) and the lack of homogeneity between CH samples on this batch.

Despite the fact that most samples showed cytotoxicity, the good results obtained for some samples were indicative of the potential of the CH samples, and thus a new batch of CH samples was analyzed.

For this new trial, Viscofan S.A. prepared 4 different CH samples (CH1, CH2, CH3 and CH4) of 4% collagen. These samples were differently processed with the objective to eliminate the possible cytotoxicity problem observed with the two previous batches. Nevertheless, the Viscofan S.A. team could not share with us the processes performed due to industrial secrecy.

3.6.1 Cell viability test

We analyzed cell viability with propidium iodide (PI) after 2 days of culture in the presence of the different CH samples for 2 different donors (**Figure 3.12**). PI acts as a nucleic acid dye that distinguishes dead cells from alive ones (see Chapter 6 for further details).[15,16]

As clearly shown in the cell viability graphs, all the CH samples contributed to cell death. In contrast, cells in suspension with Dynabeads (control +), and cells in suspension without Dynabeads (control -) remained mostly alive.

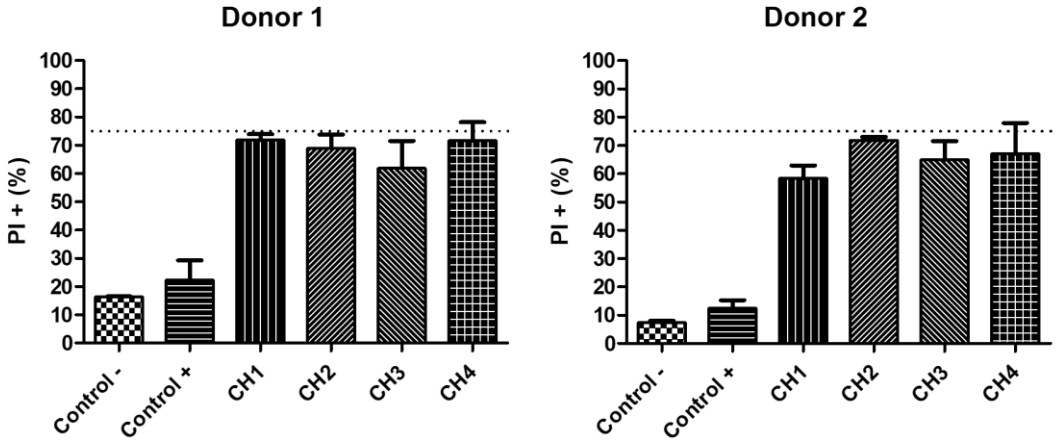

Figure 3.12 Cell viability assay using PI as a staining agent for dead cells, after 2 days of cell culture with cells seeded on the collagen hydrogels (CH1, 2, 3 and 4) with Dynabeads, in suspension without Dynabeads (control -) or in suspension with Dynabeads (control +), (N_{donors} = 2).

3.6.2 Optical microscopy analyses

To further investigate the reason for the observed cytotoxicity on these collagen hydrogels, an analysis under the optical microscope was performed to investigate the presence of possible contaminations (**Figure 3.13**).

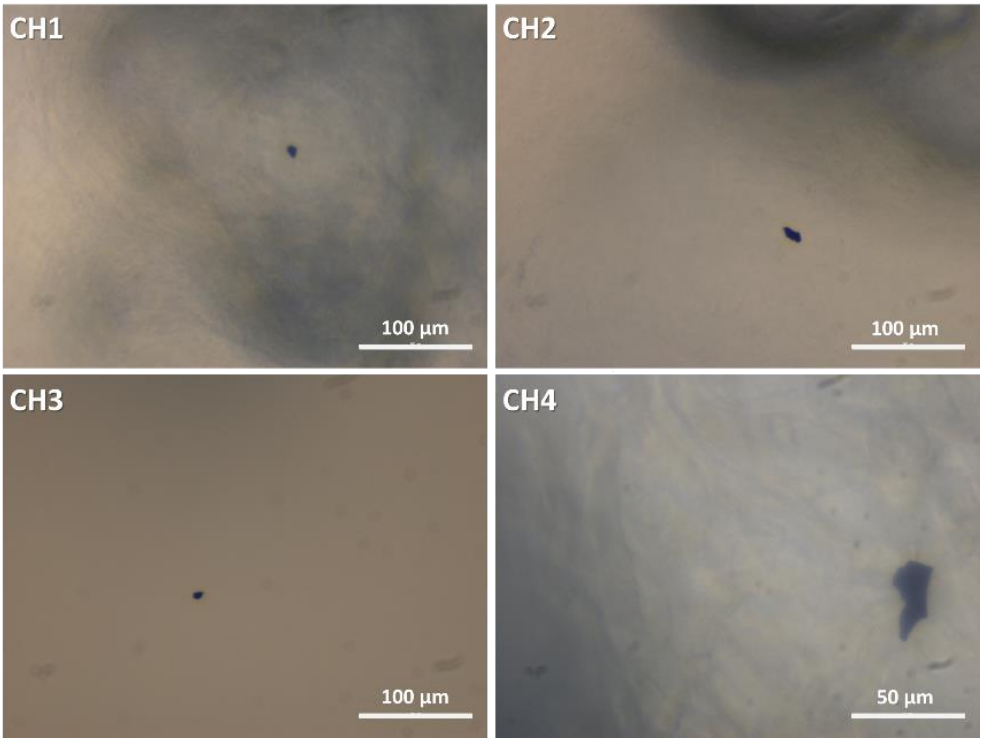

Figure 3.13 Optical microscope images obtained from the CH samples (CH1, CH2, CH3 and CH4).

In all the CH samples little "blue" fragments were observed, although in very low amounts and high dispersion throughout each CH sample. However, even after discussing with the Viscofan S.A. team, these fragments could not be identified.

3.6.3 Inductively coupled plasma mass spectrometry measurements

To further investigate the possible contamination, the 4 collagen hydrogels were analyzed by inductively coupled plasma mass spectrometry (ICP-MS) by the "Servei d'Anàlisi Química" (SAQ) of the "Universitat Autònoma de Barcelona" (UAB, Spain).

This type of mass spectrometry uses an inductively coupled plasma to ionize the sample, creating atomic and small polyatomic ions, which are then detected. This technique is known for its ability

to detect metals and several non-metals in liquid samples at very low concentrations. Furthermore, it allows multiple elements to be measured simultaneously in a single analysis.[17] The results obtained by ICP-MS for the 4 CH samples can be seen in **Figure 3.14**.

We only detected sodium (Na), potassium (K) and phosphorus (P) which was already expected taking into consideration the main components of PBS: monopotassium phosphate (KH_2PO_4), disodium phosphate (Na_2HPO_4), potassium chloride (KCl) and sodium chloride (NaCl). Thus, no clear contamination was identified, despite the small blue fragments observed by optical microscopy.

Sample	CH1	CH2	CH3	CH4
Li (ug/g)	< 5	< 5	< 5	< 5
Be (ug/g)	< 5	< 5	< 5	< 5
B (ug/g)	< 50	< 50	< 50	63
Na (ug/g)	4289	4646	5052	5859
Mg (ug/g)	< 250	< 250	< 250	< 250
Al (ug/g)	< 250	< 250	< 250	< 250
Si (ug/g)	< 2500	< 2500	< 2500	< 2500
P (ug/g)	4475	4713	5601	6112
S (ug/g)	< 10000	< 10000	< 10000	< 10000
K (ug/g)	3993	4519	4850	5630
Ca (ug/g)	< 10000	< 10000	< 10000	< 10000
Sc (ug/g)	< 5	< 5	< 5	< 5
Ti (ug/g)	< 5	< 5	< 5	< 5
V (ug/g)	< 5	< 5	< 5	< 5
Cr (ug/g)	< 5	< 5	< 5	< 5
Mn (ug/g)	< 5	< 5	< 5	< 5
Fe (ug/g)	< 50	< 50	< 50	< 50
Co (ug/g)	< 5	< 5	< 5	< 5
Ni (ug/g)	< 5	< 5	< 5	< 5
Cu (ug/g)	< 5	< 5	< 5	< 5
Zn (ug/g)	< 50	< 50	< 50	< 50
Ga (ug/g)	< 5	< 5	< 5	< 5
Ge (ug/g)	< 5	< 5	< 5	< 5
As (ug/g)	< 5	< 5	< 5	< 5
Se (ug/g)	< 5	< 5	< 5	< 5
Rb (ug/g)	< 5	< 5	< 5	< 5
Sr (ug/g)	< 5	< 5	< 5	< 5
Y (ug/g)	< 5	< 5	< 5	< 5
Zr (ug/g)	< 5	< 5	< 5	< 5
Nb (ug/g)	< 5	< 5	< 5	< 5
Mo (ug/g)	< 5	< 5	< 5	< 5
Ru (ug/g)	< 5	< 5	< 5	< 5
Rh (ug/g)	< 5	< 5	< 5	< 5
Pd (ug/g)	< 5	< 5	< 5	< 5
Ag (ug/g)	< 5	< 5	< 5	< 5
Cd (ug/g)	< 5	< 5	< 5	< 5
In (ug/g)	< 5	< 5	< 5	< 5
Sn (ug/g)	< 5	< 5	< 5	< 5
Sn (ug/g)	< 5	< 5	< 5	< 5
Te (ug/g)	< 5	< 5	< 5	< 5

Sample	CH1	CH2	CH3	CH4
I (ug/g)	< 5	< 5	< 5	< 5
Cs (ug/g)	< 5	< 5	< 5	< 5
Ba (ug/g)	< 5	< 5	< 5	< 5
La (ug/g)	< 5	< 5	< 5	< 5
Ce (ug/g)	< 5	< 5	< 5	< 5
Pr (ug/g)	< 5	< 5	< 5	< 5
Nd (ug/g)	< 5	< 5	< 5	< 5
Sm (ug/g)	< 5	< 5	< 5	< 5
Eu (ug/g)	< 5	< 5	< 5	< 5
Gd (ug/g)	< 5	< 5	< 5	< 5
Tb (ug/g)	< 5	< 5	< 5	< 5
Dy (ug/g)	< 5	< 5	< 5	< 5
Ho (ug/g)	< 5	< 5	< 5	< 5
Er (ug/g)	< 5	< 5	< 5	< 5
Tm (ug/g)	< 5	< 5	< 5	< 5
Yb (ug/g)	< 5	< 5	< 5	< 5
Lu (ug/g)	< 5	< 5	< 5	< 5
Hf (ug/g)	< 5	< 5	< 5	< 5
Ta (ug/g)	< 5	< 5	< 5	< 5
W (ug/g)	< 5	< 5	< 5	< 5
Te (ug/g)	< 5	< 5	< 5	< 5
Os (ug/g)	< 5	< 5	< 5	< 5
Ir (ug/g)	< 5	< 5	< 5	< 5
Pt (ug/g)	< 5	< 5	< 5	< 5
Au (ug/g)	< 5	< 5	< 5	< 5
Hg (ug/g)	< 5	< 5	< 5	< 5
Tl (ug/g)	< 5	< 5	< 5	< 5
Pb (ug/g)	< 5	< 5	< 5	< 5
Bi (ug/g)	< 5	< 5	< 5	< 5
Th (ug/g)	< 5	< 5	< 5	< 5
U (ug/g)	< 5	< 5	< 5	< 5

Figure 3.14 ICP-MS results of the collagen hydrogels CH1, CH2, CH3 and CH4.

3.6.4 Continuous wave electron paramagnetic resonance measurements

Finally, we evaluated the possibility that the sterilization process employed by Viscofan S.A. consisting of β-irradiation could partially damage the CH samples by creating free organic radicals.[18,19] Consequently, we performed continuous wave electron paramagnetic resonance (cw-EPR) measurements at the X-band (~9 GHz frequency) and at room temperature (**Figure 3.15**).

EPR is a spectroscopy method used in the study of materials with unpaired electrons, especially useful for the detection of organic radicals. The cw-EPR is designed to optimize the weak magnetic resonance signal. However, it was not possible to detect the existence of any impurity related with the presence of radical species.

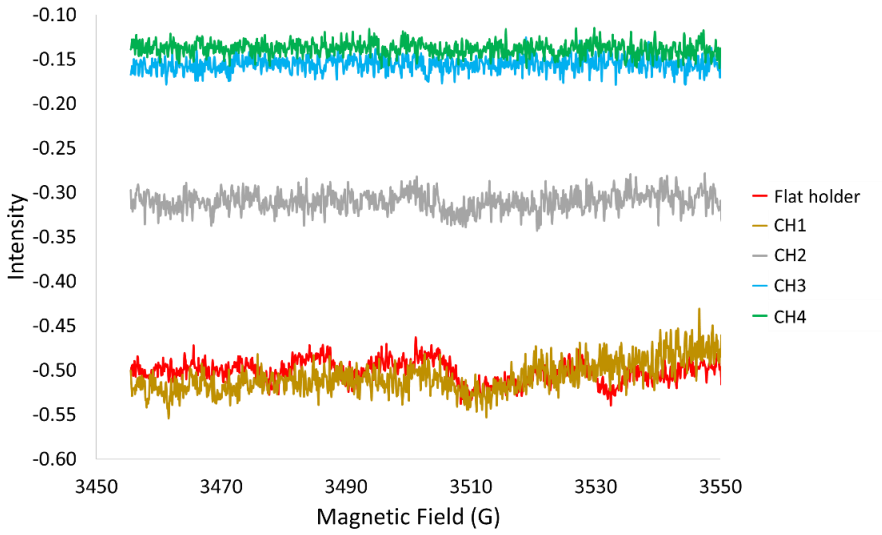

Figure 3.15 cw-EPR measurements at the X-band (~9 GHz frequency) and at room temperature of the collagen hydrogels (CH1, CH2, CH3 and CH4) and of the flat holder, where the CH samples were placed for the measurement.

Taking all these results into consideration, the Viscofan S.A. team suggested to move forward with a different material. The selection was their sponge, which was optimized to be more stable once in cell culture media.

3.7 CD4+ T cell proliferation and differentiation analysis using the optimized collagen sponges

An optimized formulation of the collagen sponges with improved stability was finally investigated for T cell proliferation and differentiation. The received collagen sponges were already sterile and cut in a circular shape that perfectly covered the bottom of a 96 well plate. These sponges were stored at 4˚C until use. Before seeding, the samples were hydrated in complete RPMI medium for 24 h. Given that the optimized sponges had a high porosity, some bubbles observed. To overcome this issue, the cell seeding protocol was slightly varied. Specifically, 50 µL of the cell suspension were added on top of the hydrogels followed by an incubation of 30 min (37˚C, 5% CO_2). Then, Dynabeads and the remaining 50 µL of complete RPMI were added, to have a total cell concentration of $1x10^6$ cells/mL (see Chapter 6 for details).

The normalized proliferation, expansion and replication indexes for the primary human CD4+ T cells seeded in suspension and on the optimized collagen sponges, both activated with Dynabeads, can be seen in **Figure 3.16**. The values obtained for the normalized proliferation index (1.10), expansion index (1.09) and replication index (1.43) were higher than the values initially obtained with the unmodified sponges, with the exception of the expansion index. Previously, we obtained (median) values of 0.97, 1.09 and 1.13 for the normalized proliferation, expansion and replication indexes.

After 5 days of culture the resulting phenotypes were analyzed by cell staining with two antibodies, the CD62L and CD45RO (**Figure 3.17**).

The CD45RO is a surface protein expressed by human leukocytes and used as a marker of memory T cells.[20] CD62L, also named L-selectin is a transmembrane cell adhesion molecule expressed on most circulating leukocytes.[21] The cells can be divided in subpopulations, which are called naïve (T_N: CD45RO−/CD62L+), central memory (T_{CM}; CD45RO+/CD62L+), effector memory (T_{EM}; CD45RO+/CD62L−) and effector (T_{EFF}; CD45RO−/CD62L−) cells.

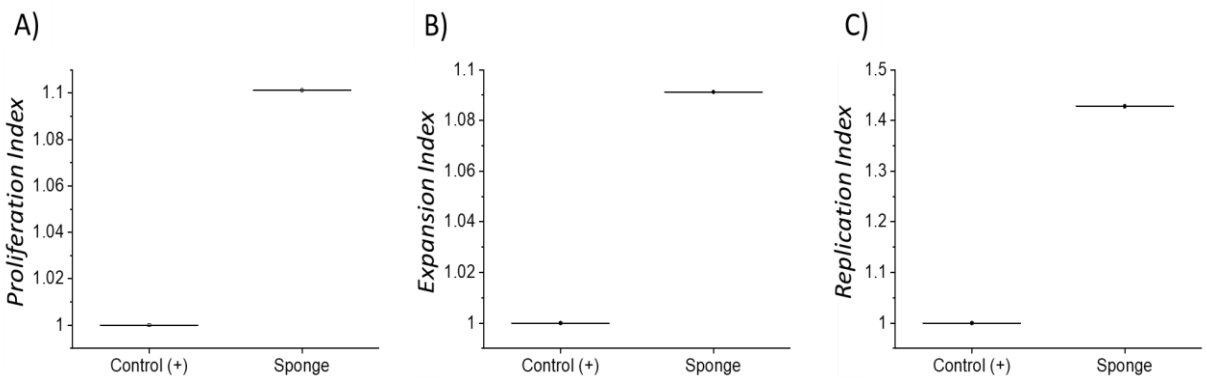

Figure 3.16 Normalized proliferation analyses of primary human CD4+ T cells 6 days after seeding on collagen sponge samples (N_{donors} = 1). A) Proliferation, B) expansion and C) replication indexes of cells seeded on the sponge sample in the presence of Dynabeads. Control +: cells in suspension with Dynabeads.

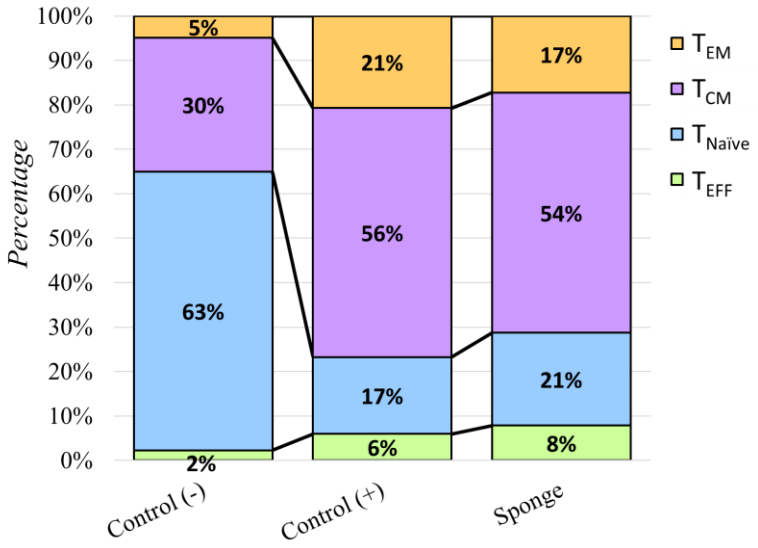

Figure 3.17 Differentiation analyses of primary human CD4+ T cells 5 days after seeding on the collagen sponge samples with Dynabeads (N_{donors} = 1), where T_{EM}: effector memory phenotype, T_{CM}: central memory phenotype, T_N: naïve phenotype, T_{EFF}: effector phenotype. Control -: cells in suspension without Dynabeads, control +: cells in suspension with Dynabeads.

A large naïve population (63%) was observed in the negative control, where cells were seeded with no Dynabeads. For both the control + and the sponge samples, in which cells had been seeded together with Dynabeads, a lower naïve population of 17% and 21%, respectively, was obtained. The T_{CM} population, a clinically relevant phenotype, was of 56% and 54% for the control + and the sponge samples, respectively, while the negative control only presented a 30%. Regarding the T_{EM} phenotype, the cells stimulated with Dynabeads also presented a higher percentage of 21% and 17%, for the control + and the sponge, respectively, compared to the negative control, which showed a 5%. For T_{EFF} phenotype we obtained for negative control, positive control and sponge samples values of 2%, 6% and 8%, respectively.

As it has been shown, the optimized sponge samples were robust, and facilitated the cell recovery step, allowing to properly perform the proliferation and differentiation experiments. Due to time limitation, no further experiments were performed, but these last results are encouraging enough to further characterize the new sponges and better analyze their performance as scaffolds for 3D T cell culture.

3.8 Summary and conclusions

In this chapter, collagen, the main structural protein in the body, was chosen and analyzed as a 3D scaffold to increase T cell proliferation in order to improve the performance of cellular immunotherapies such as ACT. With this objective, a collaboration with the Viscofan S.A. company was established.

The collagen masses received from Viscofan S.A. were in non-sterile and acidic conditions and thus, a neutralization and sterilization protocol was successfully developed and optimized. Due to the importance of the morphology of the scaffolds for T cell proliferation, we also analyzed three different samples in addition to the collagen masses, namely DC, CH and collagen sponge with different structures. These samples were received already sterilized. All samples were

analyzed by ESEM, and except for the initial sponge, all samples presented the characteristic collagen fibers and high porosity.

Preliminary T cell proliferation experiments were performed using fluorescence microscopy for the collagen masses Col2, Col3 and Col4. A good T cell proliferation was qualitatively observed over time in the presence of these collagen samples. To obtain quantitative results, T cell proliferation analysis were done through CFSE staining and flow cytometry. After 6 days of culture with collagen masses (Col2, Col5, Col6 and Col7) and the collagen samples DC, CH and sponge, interesting results were obtained. Importantly, the CH samples showed a median value 2.1 times higher than the positive control, which is based on the state-of-the-art commercial systems, on the normalized replication index. However, the reproducibility of this sample remains a challenge to be overcome. Different techniques (optical microscopy, cw-EPR and ICP-MS measurements) were used to understand this issue, but no unequivocal answer has yet been obtained.

Considering the promising characteristics of using natural collagen type I fibers, an optimized formulation of the collagen sponges with improved stability was finally investigated. Proliferation analysis and differentiation analyses, both by flow cytometry, indicated a remarkable improvement in CD4+ T cell expansion, while not altering the phenotype obtained when compared with the positive control.

In general, we can conclude that the collagen samples are promising materials for T cell proliferation. Nevertheless, further optimization procedures regarding material morphology and reproducibility should be obtained.

3.9 References

1. Gelse, K., Pöschl, E. & Aigner, T. Collagens - Structure, function, and biosynthesis. *Adv. Drug Deliv. Rev.* **55**, 1531–1546 (2003).

2. Konomi, H., Sano, J. & Nagai, Y. Immunohistochemical localization of types I, III and IV (basement membrane) collagens in the lymph node: Co-distribution of types I and III collagens in the reticular fibers. *Biomed. Res.* **2**, 536–545 (1981).

3. Shoulders, M. D. & Raines, R. T. Collagen structure and stability. *Annu. Rev. Biochem.* **78**, 929–958 (2009).

4. Dong, C. & Lv, Y. Application of Collagen Scaffold in Tissue Engineering: Recent Advances and New Perspectives. *Polymers.* **8**, 1–20 (2016).

5. Kuczek, D. E. *et al.* Collagen density regulates the activity of tumor-infiltrating T cells. *J. Immunother. cancer* **7**, 1–15 (2019).

6. Cox, T. R. & Erler, J. T. Molecular pathways: connecting fibrosis and solid tumor metastasis. *Clin. Cancer Res.* **20**, 3637–3643 (2014).

7. Rahmanian-Schwarz, A. *et al.* Improvement of skin quality using a new collagen scaffold in acute burns and reconstructive surgery: An in vivo evaluation of split skin graft transplantation in a rat model. *Dermatologic Surg.* **38**, 1338–1345 (2012).

8. Aufderklamm, S. *et al.* Collagen cell carriers seeded with human urothelial cells for urethral reconstructive surgery: first results in a xenograft minipig model. *World J. Urol.* **35**, 1125–1132 (2017).

9. Núñez-Toldrà, R. *et al.* Dental pulp pluripotent-like stem cells (DPPSC), a new stem cell population with chromosomal stability and osteogenic capacity for biomaterials evaluation. *BMC Cell Biol.* **18**, 1–15 (2017).

10. Araña, M. *et al.* Preparation and characterization of collagen-based ADSC-carrier sheets for cardiovascular application. *Acta Biomater.* **9**, 6075–6083 (2013).

11. Araña, M. *et al.* Epicardial delivery of collagen patches with adipose-derived stem cells in rat and minipig models of chronic myocardial infarction. *Biomaterials* **35**, 143–151 (2014).

12. Valarmathi, M. T., Fuseler, J. W., Potts, J. D., Davis, J. M. & Price, R. L. Functional Tissue Engineering: A Prevascularized Cardiac Muscle Construct for Validating Human Mesenchymal Stem Cells Engraftment Potential in Vitro. *Tissue Eng. - Part A* **24**, 157–185 (2018).

13. Schneider, M., Marison, I. W. & von Stockar, U. The importance of ammonia in mammalian cell culture. *J. Biotechnol.* **46**, 161–185 (1996).

14. Roederer, M. Interpretation of cellular proliferation data: Avoid the panglossian. *Cytom.*

Part A **79**, 95–101 (2011).

15. Lecoeur, H. Nuclear apoptosis detection by flow cytometry: Influence of endogenous endonucleases. *Exp. Cell Res.* **277**, 1–14 (2002).

16. Crowley, L. C. *et al.* Measuring Cell Death by Propidium Iodide Uptake and Flow Cytometry. *Cold Spring Harb. Protoc.* **2016**, 647–651 (2016).

17. Wilschefski, S. C. & Baxter, M. R. Inductively Coupled Plasma Mass Spectrometry: Introduction to Analytical Aspects. *Clin. Biochem. Rev.* **40**, 115–133 (2019).

18. Zapp, C. *et al.* Mechanoradicals in tensed tendon collagen as a source of oxidative stress. *Nat. Commun.* **11**, 1–8 (2020).

19. Faraj, K. A. *et al.* The effect of ethylene oxide sterilisation, beta irradiation and gamma irradiation on collagen fibril-based scaffolds. *Tissue Eng. Regen. Med.* **8**, 460–470 (2011).

20. Valentine, M. *et al.* Expression of the Memory Marker CD45RO on Helper T Cells in Macaques. *PLoS One* **8**, 1–16 (2013).

21. Ivetic, A. A head-to-tail view of L-selectin and its impact on neutrophil behaviour. *Cell Tissue Res.* **371**, 437–453 (2018).

Chapter 4

Inverse opal hydrogels for T cell expansion and differentiation

4.1 Introduction

To further improve the current T cell expansion methodology, 3D hybrid structures can be used to recreate the natural environment that T cells find in the LNs.

In general, depending on the nature of their composition, hydrogels can be classified as natural or synthetic. Synthetic hydrogels, as mentioned in Chapter 2, are formed by artificial polymers such as polyethylene glycol (PEG), polyvinyl alcohol or acrylamide. As 3D cell culture platforms, they usually exhibit high reproducibility, easy manufacturing and processing, and the possibility to control their physicochemical properties. However, they present some limitations, due to the lack of endogenous factors that promote and allow cell function.[1]

Natural derived hydrogels, as discussed in Chapter 3, are formed by proteins and ECM components such as collagen, fibrin or hyaluronic acid. Despite their inherent biocompatibility, they also tend to present certain limitations such as high risk of contamination, batch-to-batch variability and poor mechanical properties due in part to its quick degradation. This is why hybrid hydrogels combining the benefits of both natural and synthetic hydrogels are becoming more appealing.[2]

PEG is one of the most studied synthetic materials for the creation of hydrogels for cell culture purposes because of its characteristics. It is a biocompatible, transparent, hydrophilic, and a biologically inert polymer, which prevents unspecific protein attachment.[2,3] Its physicochemical properties can easily be adjusted, such as its elasticity that can be directly modified by the monomer length and PEG concentration during the synthesis.[4] PEG hydrogels can be

manufactured with high reproducibility under cytocompatibility conditions, and can further be functionalized with biomolecules of interest, such as cell adhesive motifs.[5–9]

Heparin (Hep) is a sulphated glycosaminoglycan naturally present in the ECM, with a high number of negative charges provided by carboxyl and sulphonyl groups.[10] Although this molecule is commonly known as an anticoagulant and widely used in drug and growth factor delivery systems, it allows the interaction with cationic molecules and basic peptides through its negative charge, leading to the mediation of many biological processes.[11–13]

Hydrogels consisting of PEG and Hep have been previously reported, more precisely low molecular weight heparin functionalized with maleimide (Mal-Hep) was crosslinked with 4-arm thiolated PEG (PEG-SH).[14,15] But, these previous works have not evaluated these hydrogels as platforms for T cell culture and expansion. Recently, our group has reported that PEG-Hep hydrogels with a 3% wt of PEG that maintain the 1:1.5 molar ratio of PEG-SH and Mal-Hep provides good structural and mechanical properties (porosity, interconnectivity, loading capacity and stiffness) for T cell culture. Specifically, we obtained an improvement of primary human CD4+ T cell proliferation and the capacity to influence on the phenotype, being an appealing option to mimic an adequate environment for ACT, as briefly described in previous chapters.[16]

Furthermore, it has been shown that hydrogels with enlarged and homogeneous pore structures can be prepared using the inverse opal (IOPAL) or inverted colloidal crystal strategy, as a porogen method.[17,18] An IOPAL structure is the negative replica of its opal. The opal structure is commonly prepared with mono-sized spheres that form 3D packed arrays. Then the space between spheres is filled with a new material, such as a hydrogel solution. After gelification, the spheres are removed, obtaining only the IOPAL structure. The obtained material presents high internal order, uniform interconnectivity, improved porosity (above 70%) and high reproducibility among samples.[19] The uniform interconnectivity achieved, leads to a more homogeneous distribution of macromolecules and cells inside the matrix.[20,21]

In a very recent scientific publication, a 3D co-culture system of endothelial-cell-encapsulated hepatocytes was used in an inverse opal scaffold to ensure the sufficient nutrient supply during cell proliferation, allowing to achieve a large volume of cell culture.[22] Moreover, it has been shown that such kind of hydrogels with larger pores increase T cell migration.[23]

Taking this information into consideration and our previously reported work using PEG-Hep hydrogels,[16] we proposed to develop a protocol using the IOPAL strategy to control the pore size and interconnectivity with respect to the previously reported material, named here as bulk hydrogel (**Figure 4.1**). The larger pores were expected to facilitate the interaction between Dynabeads and T cells, which commonly results in clusters during the activation phase.[24–26] Furthermore, the increase in connectivity provided by the IOPAL structure was foreseen to promote T cell migration and a better nutrient, gas and waste circulation, leading ultimately to an enhancement of T cell proliferation of desired phenotypes.

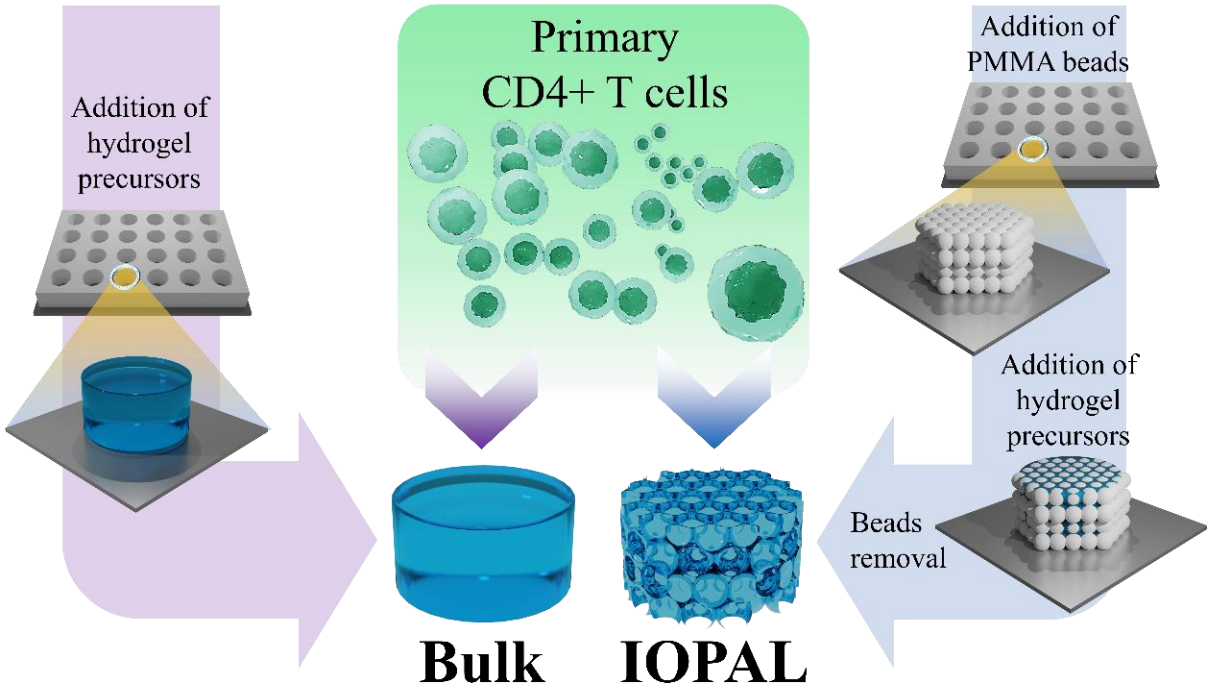

Figure 4.1 LN-inspired 3D PEG-heparin hydrogels on its bulk and IOPAL forms.

4.2 Objectives and strategy

To improve the current methodologies of expansion of human T cells to facilitate the introduction of ACT in the clinics, we proposed to use an IOPAL strategy to increase the pore size and interconnectivity of our previously reported PEG-Hep hydrogels. The synthesized 3D IOPAL PEG-Hep hydrogels were characterized in terms of morphology and mechanical properties. Moreover, the ability of such hydrogels to improve T cell culture was evaluated and compared with the bulk analogue.

4.3 Synthesis and characterization of PEG-Hep IOPAL hydrogels

For the creation of an opal, poly(methyl methacrylate) (PMMA) microbeads were selected, based on a previous work.[23] They are available in a wide size range, and the polymer is well described to be soluble in several organic solvents.[23,27,28] In an initial trial Spheromers® (Microbeads AS, Norway) with 60 ± 6 μm of diameter were used. This particle size was very similar to the pore sizes previously reported for our bulk PEG-Hep hydrogels.[16] To dissolve these beads, we used acetone, chloroform, acetic acid (AcOH), dichloromethane (DCM), tetrahydrofuran (THF) and potassium hydroxide (KOH) at 5 and 10%, all at room temperature (RT). After 8 days, no signs of degradation were observed. To promote degradation, we considered heating and agitation by using DCM, dimethylformamide (DMF), toluene, dimethyl sulfoxide (DMSO) and AcOH as solvents. Though, after 8 days at 40˚C with magnetic agitation, the partial breaking of the PMMA beads was only noticeable for DMF, AcOH and DMSO (**Figure 4.2**). However, we suspected that the breaking of the beads was mostly associated to the mechanical impact of the magnet to them. To corroborate this hypothesis, DMSO and AcOH degradation was studied with no magnetic agitation at 40˚C using an orbital shaker (260 rpm) for 8 days. After this time the beads were still intact.

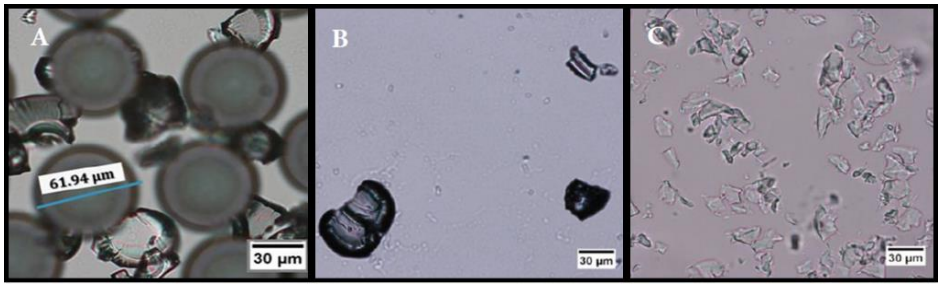

Figure 4.2 Images of PMMA beads (Spheromers®) degradation observed by optical microscopy. Degradation was analyzed after 8 days at 40˚C in (A) DMF, (B) AcOH, (C) DMSO with magnetic agitation.

Thus, these PMMA beads were found to be only degraded after heavy mechanical forces exposure, which is a practice not compatible with the formation of an IOPAL hydrogel. After a discussion with the provider of Spheromers®, we realized that the PMMA beads were crosslinked to increase solvent resistance.

Taking this information into consideration, non-crosslinked PMMA beads were purchased from a new provider (microParticles GmbH, Germany). In this case, a 10% aqueous suspension of PMMA beads with a diameter of 78.3 ± 1.7 µm were added in a Teflon template, and the opal was formed due to the Brownian interactions occurring during gradual solvent evaporation.[20,27] The diameter size of such PMMA beads was chosen, taking into consideration that pore sizes of 80 µm resulted in unconstrained migration.[23] Afterwards, a PEG-Hep hydrogel mixture, which is the one used for the bulk PEG-Hep hydrogels (**Figure 4.3**), was added on top of the PMMA opal in the template and left to infiltrate and solidify. Briefly, the mixture consisted of commercially available 4-arm thiolated PEG (PEG-SH) that undergoes a Michael-type reaction with maleimide-functionalize heparin (Mal-Hep) in PBS, resulting in an hydrogel with both components consslinked.[15]

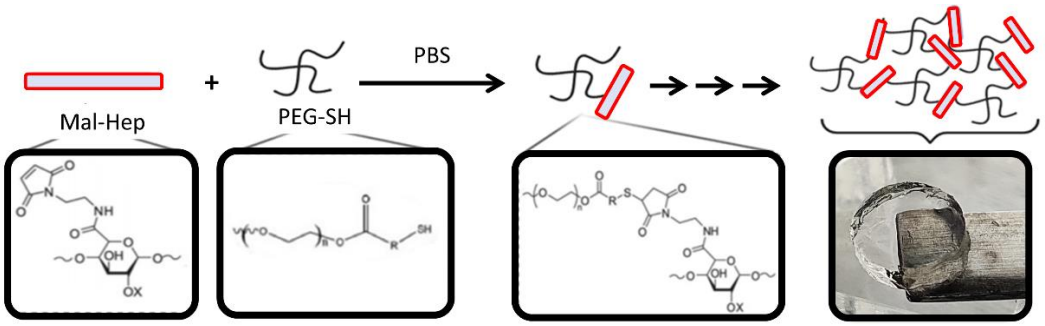

Figure 4.3 PEG-Hep bulk hydrogel synthesis. Mal-Hep mixed with 4-arm PEG-SH in PBS forms a hydrogel under a Michael-type reaction.

To form the IOPAL PEG-Hep hydrogels, the PMMA opal was dissolved in glacial AcOH, thus obtaining completely transparent hydrogels, indicating the successful removal of the PMMA beads (**Figure 4.4**). Finally, the resulting IOPAL PEG-Hep hydrogels were washed, sterilized and incubated at 37˚C until cell seeding.

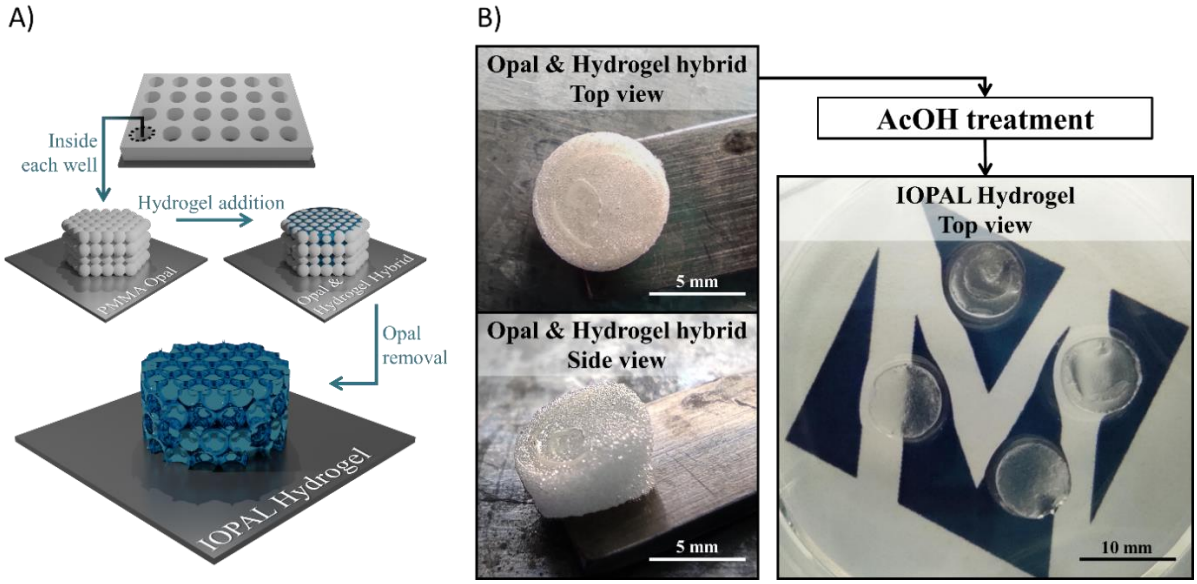

Figure 4.4 Formation of the IOPAL PEG-Hep hydrogel. A) Simplified scheme of the formation of an IOPAL PEG-Hep hydrogel. B) Photographs of the opal & hydrogel hybrid before the AcOH treatment, where they are white and opaque. After AcOH treatment, they result in transparent hydrogels, indicating the complete removal of the PMMA.

4.4 Structural properties of the IOPAL PEG-Hep hydrogels

The structural properties of IOPAL PEG-Hep hydrogels were studied and compared with bulk PEG-Hep hydrogels by different characterization techniques, namely: ESEM, X-ray tomography and confocal microscopy.

4.4.1 ESEM characterization

Both types of hydrogels, the bulk and the IOPAL, were studied by ESEM and their pore size ranges were calculated (**Figure 4.5**). From the ESEM images we calculated the average pore size (300 pores were analyzed) present in the bulk hydrogels. It was found to be 47 µm with a range of 9–204 µm, being these results consistent with the ones previously obtained.[16] The average pore size of the IOPAL hydrogels (300 pores analyzed) was 77 µm with a range of 24–165 µm, in accordance with the size of the PMMA beads used (78.7 µm ± 1.7 µm).

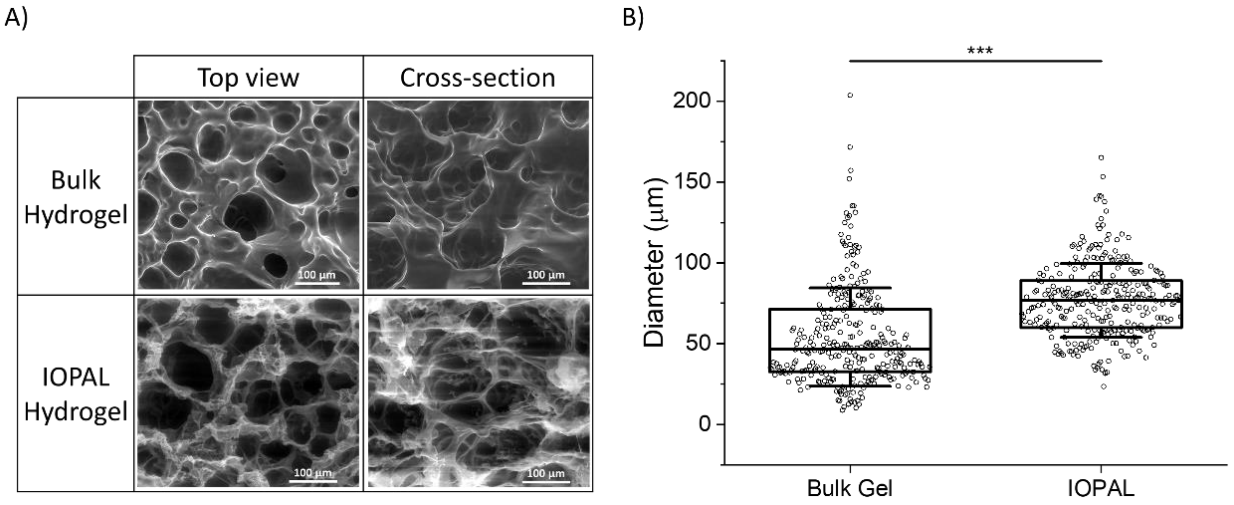

Figure 4.5 A) ESEM images and B) pore size evaluation of bulk and IOPAL PEG-Hep hydrogels. The statistical significance was determined by the Kruskal Wallis ANOVA test (***$p < 0.001$).

4.4.2 X-ray microtomography

Further physical characterization was performed by X-ray microtomography. The connectivity density for the IOPAL system was found to be four times superior when compared with the bulk hydrogel (**Figure 4.6**). This result is in accordance with the expected nature of an IOPAL structure, i.e. it presents interconnected pores.[21] The connectivity density was calculated, as explained in Chapter 6, and the values obtained are represented in the table of **Figure 4.6 C**.

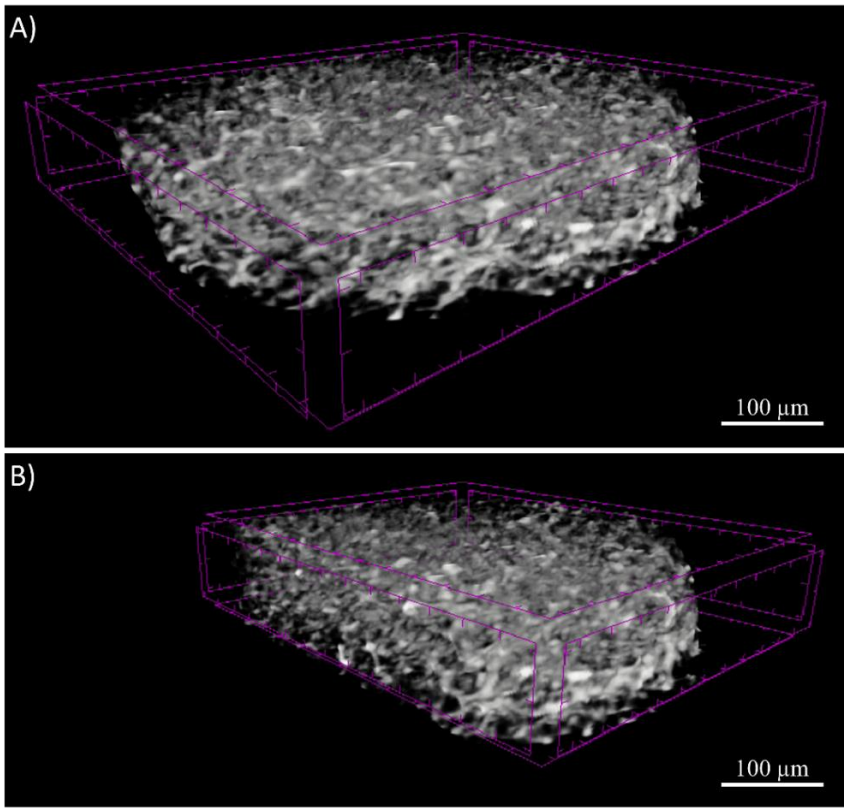

C)

	Bulk 1		Bulk 2		IOPAL 1		IOPAL 2	
Volume of interest	9.7	mm^3	4.7	mm^3	12.0	mm^3	12.1	mm^3
Connectivity	51077		24546		252234		228569	
Connectivity density	5265.7	mm^{-3}	5222.6	mm^{-3}	21019.5	mm^{-3}	18890.0	mm^{-3}

Figure 4.6 X-ray microtomography analysis of 3D PEG-Hep hydrogels. A) X-ray microtomographs of a representative volume of interest and its B) cross-section of an IOPAL PEG-Hep hydrogel of 1 cm of diameter. C) Connectivity density obtained (connectivity/volume of interest) for 3D PEG-Hep bulk and IOPAL hydrogels ($N_{hydrogels}$ = 2).

4.4.3 Confocal microscopy

Additionally, we assessed cell infiltration in our IOPAL hydrogels by confocal microscopy. Specifically, primary human CD4+ T cells from adult donors were stained with CFSE, an intracellular dye that is only fluorescent in viable cells, as previously explained (see Chapter 6 for details).

The volume represented in **Figure 4.7** is 1.5 cm x 1.5 cm x 0.4 cm, consisting of approximately 35% of the total volume of the IOPAL PEG-Hep hydrogel. These results indicate that the CD4+ T cells that have been seeded in a 2D fashion have penetrated quite homogenously through the IOPAL PEG-Hep hydrogel.

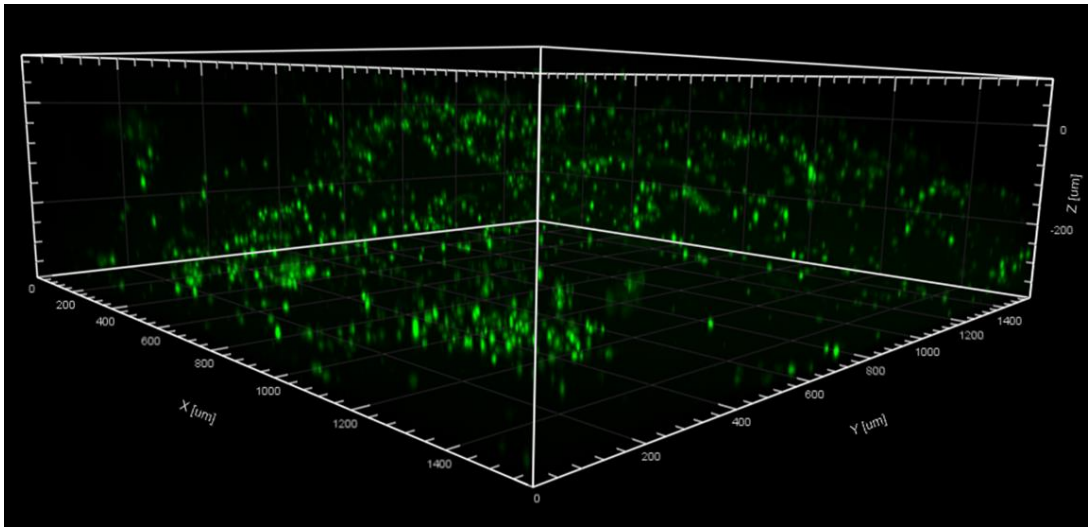

Figure 4.7 3D confocal microscopy projection showing CFSE-stained primary human CD4+ T cells in a representative IOPAL PEG-Hep hydrogel after 5 days of incubation (area = 1.5 cm x 1.5 cm x 0.4 cm).

According to the information obtained from all these structural characterizations, we found our IOPAL PEG-Hep hydrogels to have a median pore size of 77 µm, which is a size expected to be large enough to allow T cell-Dynabead clusters during the activation phase. Furthermore, these pores sizes allowed the human CD4+ T cells used in this study to penetrate through the hydrogel

and a higher connectivity was achieved with the IOPAL strategy when compared with the bulk hydrogel that we previously reported.[16]

4.5 Mechanical properties of IOPAL PEG-Hep hydrogels

The stiffness is also a very important parameter to be taken into consideration, since it is known that LNs with metastasis or in lymphoma cases, harder tissues are observed compared to the healthy ones.[29,30] Such histopathologic features may influence the T cell proliferation and differentiation outcomes and for such reason a mechanical study was performed. The mechanical properties of IOPAL PEG-Hep hydrogels were characterized by small-amplitude oscillatory shear (SAOS) rheology, in the linear-viscoelastic region (LVE). The protocol followed was a cycle of sweeps, namely strain and frequency sweeps.[31] For the strain sweeps (**Figure 4.8 A**) we employed a constant frequency of 1.0 Hz and the shear stress was swept from 1 Pa to 50 Pa. For the frequency sweeps (**Figure 4.8 B**), we used a constant shear stress of 50 Pa and the frequency was ranged from 0.01 Hz to 1.0 Hz.

The storage modulus (G') obtained for the IOPAL hydrogels was of 0.46 ± 0.01 KPa, which is lower than the one of the bulk hydrogel (0.75 ± 0.08 KPa),[16] as expected. This difference can be explained by the homogeneously larger and more interconnected pores of the IOPAL structure compared to the bulk. Furthermore, these values are in the same order of magnitude than Matrigel (Thermo Fisher Scientific, United States of America) with a stiffness of <5 KPa, being this material as explained in previous chapters, the gold standard in the growing field of 3D cell culture systems.[32–34] Nevertheless, these IOPAL gels are softer than the reported LN stiffness, which are around 10 KPa as measured by *in vivo* shear-wave elastography for healthy tissues.[35–38]

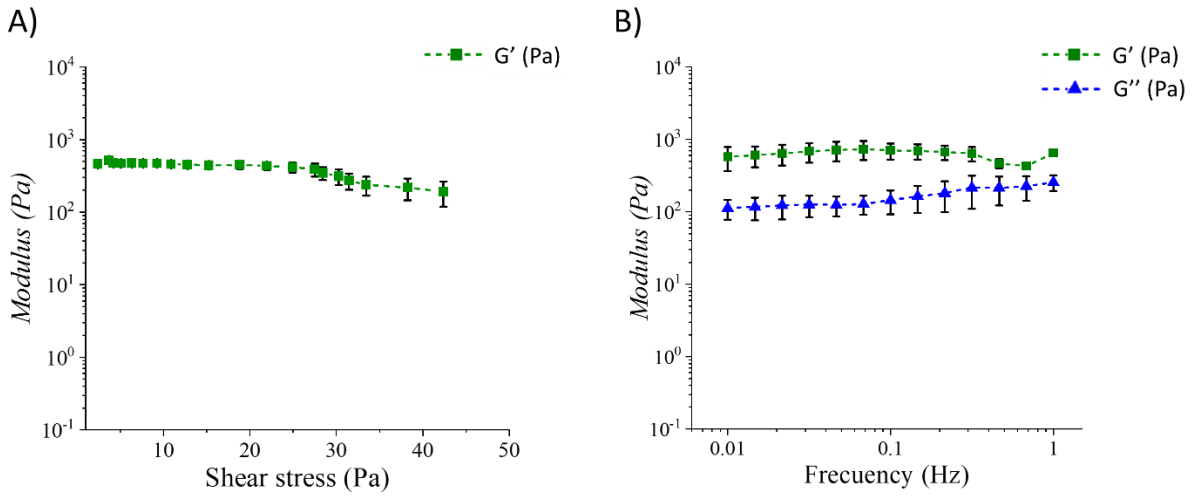

Figure 4.8 SAOS rheology of IOPAL PEG-Hep hydrogels. A) Strain sweeps ($N_{Hydrogels}$ = 2) and B) frequency sweeps ($N_{Hydrogels}$ = 2).

Furthermore, the IOPAL hydrogels (as seen previously also for the 3D PEG-Hep bulk hydrogels) have viscoelastic properties as G' is higher than loss modulus (G''), and therefore, they are more elastic than viscous.[39]

4.6 CD4+ T cell viability, expansion and differentiation using IOPAL PEG-Hep hydrogels

For the cell culture experiments, primary human CD4+ T cells from healthy adult donors were used. This is an interesting population not only due to their high natural abundance in comparison with other relevant T cell types such as CD8+ T cells or regulatory T cells, but also due to its usefulness and the growing interest they are attracting in the clinics.[40–44] Bulk and IOPAL PEG-Hep hydrogels were selected to culture CD4+ T with Dynabeads. As mentioned previously, Dynabeads are magnetic beads coated with anti-CD3 and anti-CD28 that are employed to polyclonally activate T cells. Both hydrogels were used as biomimetic LNs, as they were capable of providing a 3D culture environment, as confirmed by confocal microscopy. To determine the influence of the increased porosity and interconnectivity given by the IOPAL hydrogels compared

to the bulk hydrogels, T cell viability, differentiation and proliferation were measured by flow cytometry at days 5 or 6, as a standard time points.[31,45] Before each flow cytometry measurement, the cells were carefully removed through vigorous pipetting in order to collect as many cells as possible from the hydrogels (see Chapter 6 for details).

For T cell viability studies, a propidium iodide (PI) viability test with flow cytometry was performed after 5 days of culture (**Figure 4.9**). Less non-viable PI+ cells were obtained for bulk (31.8%) and IOPAL (26.1%) hydrogels than for suspension cultures activated with Dynabeads (control +; 39.9%). Cells in suspension without Dynabeads activation were only 15.5% PI+.

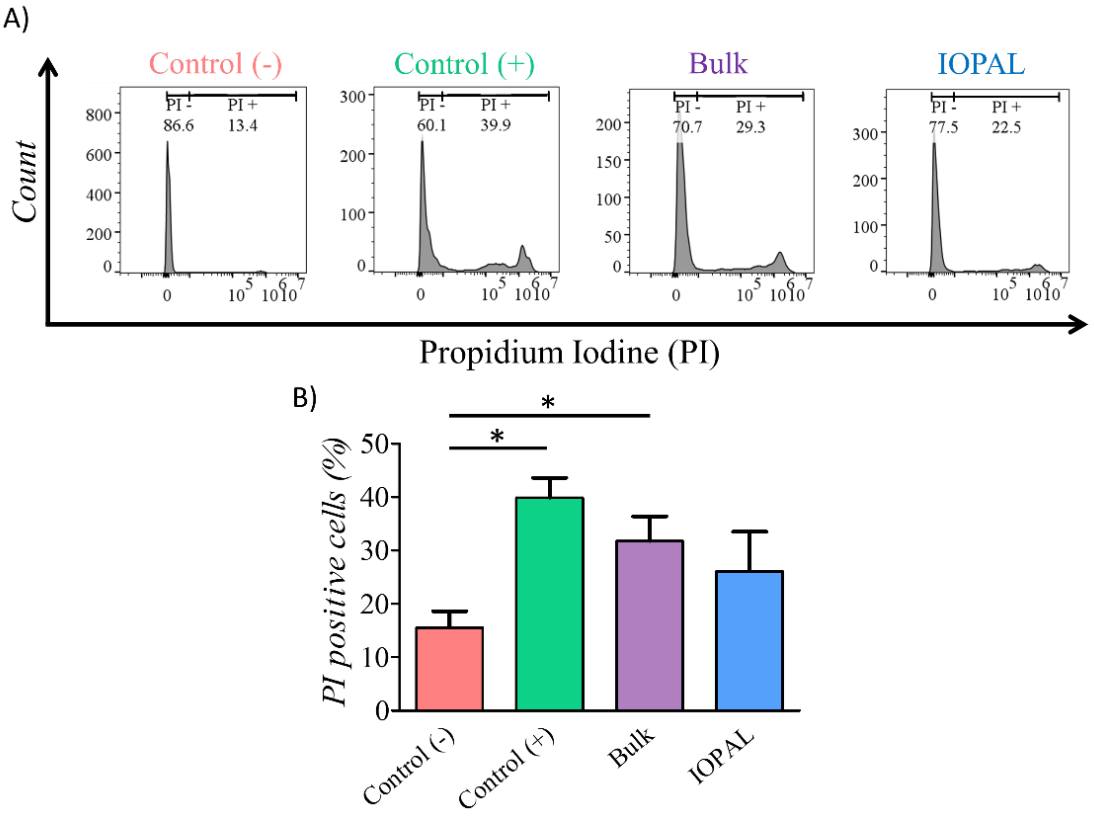

Figure 4.9 Effect of IOPAL and bulk PEG-Hep hydrogels on CD4+ T cell viability. A) Representative flow cytometry histograms of the B) PI viability test performed with CD4+ T cells seeded with IOPAL and bulk PEG-Hep hydrogels, or in suspension (control +) with Dynabeads for 5 days. Control - represents cells in suspension with no Dynabeads. Bars are mean + standard deviation, (N_{donors} = 4). Significance was determined by the Mann-Whitney U test (*$p < 0.05$).

As it can be observed in **Figure 4.9**, our 3D PEG-Hep hydrogels (bulk and IOPAL) show a tendency to increase, or at least maintain, cell viability compared to the current expansion systems.

The proliferation assay was performed using CFSE-stained cells analyzed by flow cytometry after 6 days of culture, as explained previously and in detail in Chapter 6. Specifically, we analyzed the expansion index which gives information about the growth of the whole culture, as a ratio between the final and the starting number of cells; the replication index, defined by the fold-expansion of the culture, but only taking into account the activated cells; and the proliferation index related with the average number of divisions that stimulated cells have undergone.[40] Given the donor-to-donor variability, the proliferation results (**Figure 4.10**) were normalized in each experiment to the positive control, consisting of CD4+ T cells with Dynabeads in suspension. For that reason, all the positive controls index values are 1.

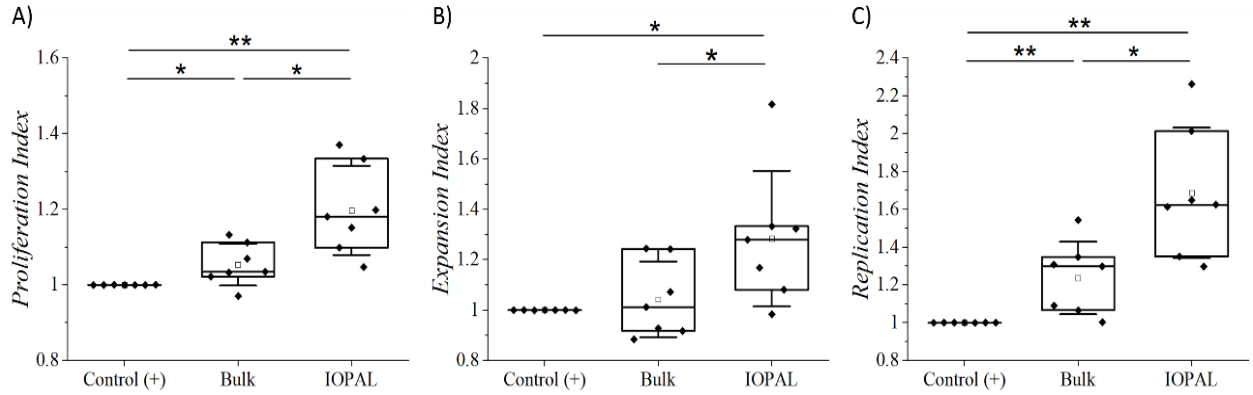

Figure 4.10 Effect of 3D PEG-Hep hydrogels on its bulk and IOPAL forms on CD4+ T cell proliferation. Normalized A) expansion, B) replication, and C) proliferation indexes of CD4+ T cells stimulated with Dynabeads 6 days after seeding on bulk and IOPAL PEG-Hep hydrogels. The control + consists of cells seeded in suspension with Dynabeads, (N_{donors} = 7).

The median normalized proliferation, expansion and replication indexes for the bulk hydrogels were 1.03, 1.01 and 1.29, respectively, in accordance with our previous results.[16] The normalized

proliferation, expansion and replication indexes were significantly higher for the IOPAL hydrogels, being 1.18, 1.28 and 1.63, respectively.

Both hydrogels showed statistically significant increases compared to the positive controls, except for the expansion index in the bulk hydrogel, even though a slight increase of 1% was observed. In another words, for each 0.1 million CD4+ T cells seeded on each replicate after 6 days of culture, 0.77, 0.79 and 1.08 million cells were obtained for the positive controls, bulk and IOPAL conditions, respectively.

Still, the major improvement was observed on the replication index with the IOPAL hydrogels. Specifically, these hydrogels resulted in an improvement of 63% compared to the cells activated in suspension (positive control), and an increase of 34% in comparison with the bulk hydrogels. This indicates that the responding cells that get activated in the hydrogels proliferate more than the activated cells in suspension.

In summary, we can confirm that the increase in pore size, homogeneity and interconnectivity introduced by the inverse opal strategy, contributed to a better overall cell growth than the standard bulk hydrogels, which provided in turn, better results than the state-of-the-art suspension systems.

Regarding the differentiation studies, the CD4+ T cell phenotypes were analyzed by flow cytometry on day 5 after seeding to obtain information about the subpopulations of naïve (T_N: CD45RO−/CD62L+), central memory (T_{CM}; CD45RO+/CD62L+), effector memory (T_{EM}; CD45RO+/CD62L−) and effector (T_{EFF}; CD45RO−/CD62L−) given their clinical importance in ACT.[46–48] In **Figure 4.11** we represent the results obtained for one representative donor.

As mentioned above, there is a donor-to-donor variability that should be taken into account. For this reason, we also analyzed the percentages of CD4+ T cells that express CD45RO and CD62L prior to stimulation with Dynabeads (negative control).

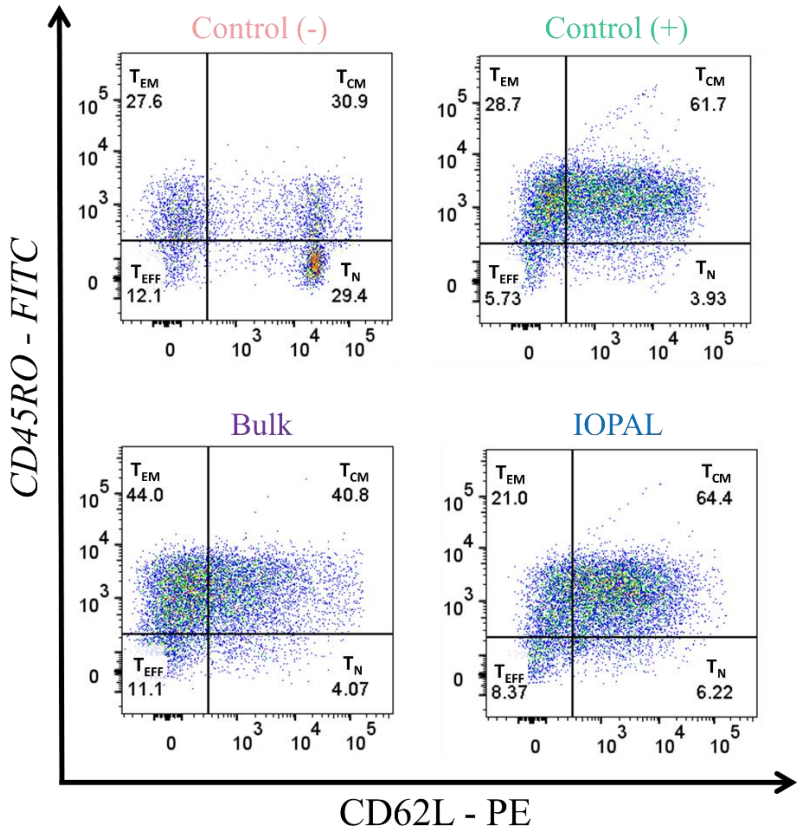

Figure 4.11 CD45RO-FITC vs CD62L-PE graphs for CD4+ T cells in bulk and IOPAL PEG-Hep hydrogels. Percentage of T_N, T_{CM}, T_{EM} and T_{EFF}. CD4+ T cells seeded on bulk and IOPAL PEG-Hep hydrogels (and their controls) on day 5, represented in a CD45RO-FITC vs CD62L-PE graph. The negative control consists of cells seeded in suspension without Dynabeads, whereas in the positive control, cells are seeded with Dynabeads. When cells are seeded in the hydrogels, they are always stimulated with Dynabeads. This figure shows representative data obtained from 1 donor.

The differentiation percentage results with the statistical treatment of the different subpopulations studied for 6 different donors are shown in detail in **Figures 4.12 A-D**. In **Figure 4.12 E** the differentiation results obtained are summarized in a column type graph, to simplify the comparison between the phenotypes when using the different seeding conditions above stated.

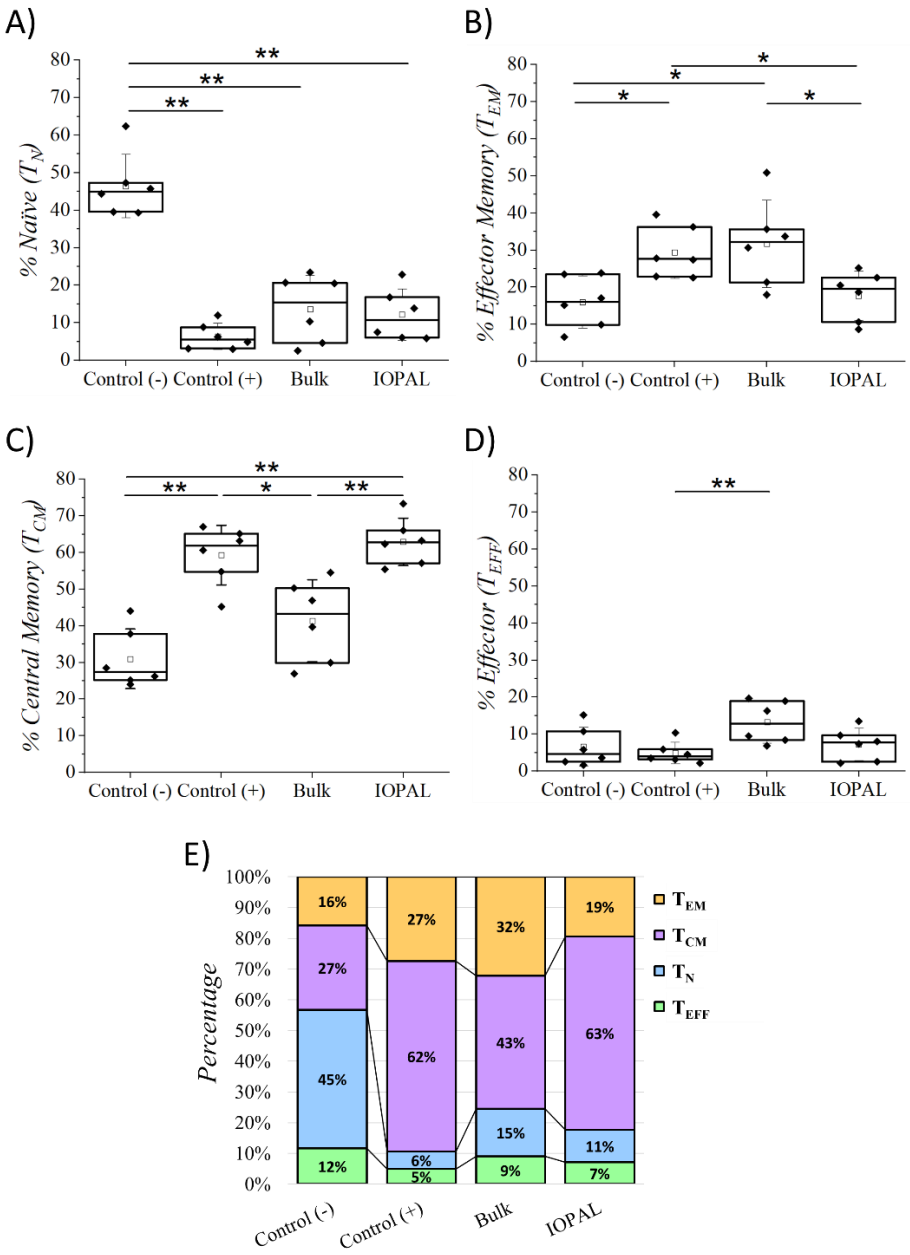

Figure 4.12 Differentiation of CD4+ T cells in bulk and IOPAL PEG-Hep hydrogels. A) Percentage of T_N, B) T_{EM} and C) T_{CM} D) T_{EFF} CD4+ T cells on day 5, (N_{donors} = 6). E) Percentage of T_N, T_{EM}, T_{CM} and T_{EFF} CD4+ T cells summarized in a column type graph. The negative control (control -) consists of cells seeded in suspension without Dynabeads, whereas in the positive control (control +) cells are seeded with Dynabeads. When cells are seeded in the hydrogels, they are always stimulated with Dynabeads. Statistical significance was determined by the Mann-Whitney U test (*$p < 0.05$, **$p < 0.01$).

The main phenotype obtained in the negative control was T_N with a median value of 45%. As expected, this subpopulation was found to be less preponderant when cells were activated. Specifically, the positive control, bulk and IOPAL hydrogels showed T_N percentages of 6, 15, and 11%, respectively. For the T_{EM} phenotype, median values rose to 27% for T cells in suspension, 32% for bulk hydrogels and 19% for IOPAL. Thus, the IOPAL hydrogels did not promote the T_{EM} phenotype compared to suspension and the bulk hydrogels. In contrast, the T_{EFF} phenotype resulted in lower percentages when cells were activated with values of 5, 9, and 7% for the positive control, bulk and IOPAL hydrogels, whereas the negative control showed a 12% of the total cell population. Remarkably, the median value for the T_{CM} phenotype obtained in CD4+ T cells cultured in the IOPAL hydrogels was of 63%. This percentage is higher than the 43% obtained with the bulk hydrogels and comparable with the 62% obtained in suspension. It is worth mentioning that the T_{CM} phenotype is of great importance for the clinics due its capacity to mediate an effective and sustained response. In contrast, effector cells present an immediate, but not a sustained defense response.[49–53] In conclusion, these results indicate that PEG-Hep hydrogels can be used to tune the resulting phenotype of T cells only by adding a morphological change to their structure, such as the higher pore size, homogeneity and interconnectivity achieved with the IOPAL strategy.

4.7 Summary and conclusions

In conclusion, IOPAL 3D PEG-Hep hydrogels were synthesized, characterized and used for primary human CD4+ T cell culture. They resulted in an improvement in cell proliferation when compared to the state-of-the-art methodologies, and to its bulk form. This fact indicates the importance of pore size and interconnectivity on T cell activation and proliferation. Indeed, the obtained IOPAL PEG-Hep hydrogels presented higher pore sizes and interconnectivity than the bulk and allowed cell infiltration, which are requirements to improve T cell proliferation. Moreover, we demonstrated the capacity of such hydrogels to influence the phenotype obtained, which is closely related with the clinical outcomes.[47,54]

Thus, these hydrogels have the potential to help surpassing the current limitation of ACT of producing large amounts of cells with therapeutic phenotypes.[55] This limitation is especially important in ACT based on TILs, i.e. in therapies with non-engineered T cells. Moreover, the IOPAL strategy could be applied to other hydrogels used in the growing field of 3D cell cultures for regenerative medicine and organoid engineering.

4.8 References

1. Madduma-Bandarage, U. S. K. & Madihally, S. V. Synthetic hydrogels: Synthesis, novel trends, and applications. *J. Appl. Polym. Sci.* **138**, 1–23 (2021).

2. Tibbitt, M. W. & Anseth, K. S. Hydrogels as extracellular matrix mimics for 3D cell culture. *Biotechnol. Bioeng.* **103**, 655–663 (2009).

3. Bryant, S. J. & Anseth, K. S. Hydrogel properties influence ECM production by chondrocytes photoencapsulated in poly(ethylene glycol) hydrogels. *J. Biomed. Mater. Res.* **59**, 63–72 (2002).

4. Aydin, D. *et al.* Polymeric substrates with tunable elasticity and nanoscopically controlled biomolecule presentation. *Langmuir* **26**, 15472–15480 (2010).

5. Guasch, J. *et al.* Synthesis of Binary Nanopatterns on Hydrogels for Initiating Cellular Responses. *Chem. Mater.* **28**, 1806–1815 (2016).

6. Zhu, J. Bioactive modification of poly(ethylene glycol) hydrogels for tissue engineering. *Biomaterials* **31**, 4639–4656 (2010).

7. Wang, H., Cai, L., Paul, A., Enejder, A. & Heilshorn, S. C. Hybrid elastin-like polypeptide-polyethylene glycol (ELP-PEG) hydrogels with improved transparency and independent control of matrix mechanics and cell ligand density. *Biomacromolecules* **15**, 3421–3428 (2014).

8. Cushing, M. C. & Anseth, K. S. Materials science. Hydrogel cell cultures. *Science* **316**, 1133–1134 (2007).

9. Huynh, C. T., Liu, F., Cheng, Y., Coughlin, K. A. & Alsberg, E. Thiol-Epoxy 'Click' Chemistry to Engineer Cytocompatible PEG-Based Hydrogel for siRNA-Mediated Osteogenesis of hMSCs. *ACS Appl. Mater. Interfaces* **10**, 25936–25942 (2018).

10. Li, J., Wu, C., Chu, P. K. & Gelinsky, M. 3D printing of hydrogels: Rational design strategies and emerging biomedical applications. *Mater. Sci. Eng. R* **140**, 1–76 (2020).

11. Nie, T., Baldwin, A., Yamaguchi, N. & Kiick, K. L. Production of heparin-functionalized hydrogels for the development of responsive and controlled growth factor delivery systems. *J. Control. Release* **122**, 287–296 (2007).

12. Schultz, K. M., Baldwin, A. D., Kiick, K. L. & Furst, E. M. Gelation of Covalently Cross-Linked PEG-Heparin Hydrogels. *Macromolecules* **42**, 5310–5316 (2009).

13. Meneghetti, M. C. Z. *et al.* Heparan sulfate and heparin interactions with proteins. *J. R. Soc. Interface* **12**, 1–13 (2015).

14. Baldwin, A. D. *et al.* In situ crosslinkable heparin-containing poly(ethylene glycol) hydrogels for sustained anticoagulant release. *J. Biomed. Mater. Res. A* **100**, 2106–2118 (2012).

15. Baldwin, A. D. & Kiick, K. L. Reversible maleimide-thiol adducts yield glutathione-sensitive poly(ethylene glycol)-heparin hydrogels. *Polym. Chem.* **4**, 133–143 (2013).

16. Pérez Del Río, E. *et al.* CCL21-loaded 3D hydrogels for T cell expansion and differentiation. *Biomaterials* **259**, 1–13 (2020).

17. Peyton, S. R. *et al.* Marrow-derived stem cell motility in 3D synthetic scaffold is governed by geometry along with adhesivity and stiffness. *Biotechnol. Bioeng.* **108**, 1181–1193 (2011).

18. da Silva, J., Lautenschläger, F., Kuo, C.-H. R., Guck, J. & Sivaniah, E. 3D inverted colloidal crystals in realistic cell migration assays for drug screening applications. *Integr. Biol.* **3**, 1202–1206 (2011).

19. Kotov, N. A. *et al.* Inverted colloidal crystals as three-dimensional cell scaffolds. *Langmuir* **20**, 7887–7892 (2004).

20. Shirahama, H. *et al.* Fabrication of Inverted Colloidal Crystal Poly(ethylene glycol) Scaffold: A Three-dimensional Cell Culture Platform for Liver Tissue Engineering. *J. Vis. Exp.* **114**, 1–12 (2016).

21. Zhang, Y. S., Zhu, C. & Xia, Y. Inverse Opal Scaffolds and Their Biomedical Applications. *Adv. Mater.* **29**, 1–29 (2017).

22. Shao, C., Liu, Y., Chi, J., Ye, F. & Zhao, Y. Hierarchically Inverse Opal Porous Scaffolds from Droplet Microfluidics for Biomimetic 3D Cell Co-Culture. *Engineering* **7**, 1778–1785 (2021).

23. Stachowiak, A. N. & Irvine, D. J. Inverse opal hydrogel-collagen composite scaffolds as a supportive microenvironment for immune cell migration. *J. Biomed. Mater. Res. A* **85**, 815–828 (2008).

24. Guasch, J., Muth, C. A., Diemer, J., Riahinezhad, H. & Spatz, J. P. Integrin-Assisted T-Cell Activation on Nanostructured Hydrogels. *Nano Lett.* **17**, 6110–6116 (2017).

25. Miller, M. J., Wei, S. H., Parker, I. & Cahalan, M. D. Two-Photon Imaging of Lymphocyte Motility and Antigen Response in Intact Lymph Node. *Science* **296**, 1869–1873 (2002).

26. Adutler-Lieber, S. *et al.* Substrate-bound CCL21 and ICAM1 combined with soluble IL-6 collectively augment the expansion of antigen-specific murine CD4+ T cells. *Blood Adv.* **1**, 1016–1030 (2017).

27. Stachowiak, A. N., Bershteyn, A., Tzatzalos, E. & Irvine, D. J. Bioactive Hydrogels with an Ordered Cellular Structure Combine Interconnected Macroporosity and Robust Mechanical Properties. *Adv. Mater.* **17**, 399–403 (2005).

28. Pei, Y., Molley, T. G. & Kilian, K. A. Enzyme Responsive Inverse Opal Hydrogels. *Macromol. Rapid Commun.* **41**, 1–6 (2020).

29. Miyaji, K. *et al.* The stiffness of lymph nodes containing lung carcinoma metastases. *Cancer* **80**, 1920–1925 (1997).

30. Wang, B. *et al.* Ultrasound Elastography for the Evaluation of Lymph Nodes. *Front. Oncol.* **11**, 1–12 (2021).

31. Zuidema, J. M., Rivet, C. J., Gilbert, R. J. & Morrison, F. A. A protocol for rheological characterization of hydrogels for tissue engineering strategies. *J. Biomed. Mater. Res. B. Appl. Biomater.* **102**, 1063–1073 (2014).

32. Xia, M. *et al.* Stimulus specificity of matrix metalloproteinase dependence of human T cell migration through a model basement membrane. *J. Immunol.* **156**, 160–167 (1996).

33. Cougoule, C. *et al.* Blood leukocytes and macrophages of various phenotypes have distinct abilities to form podosomes and to migrate in 3D environments. *Eur. J. Cell Biol.* **91**, 938–949 (2012).

34. Cross, V. L. *et al.* Dense type I collagen matrices that support cellular remodeling and microfabrication for studies of tumor angiogenesis and vasculogenesis in vitro. *Biomaterials* **31**, 8596–8607 (2010).

35. Tourasse, C. *et al.* Elastography in the assessment of sentinel lymph nodes prior to

dissection. *Eur. J. Radiol.* **81**, 3154–3159 (2012).

36. Kilic, F. *et al.* Ex Vivo Assessment of Sentinel Lymph Nodes in Breast Cancer Using Shear Wave Elastography. *J. Ultrasound Med.* **35**, 271–277 (2016).

37. Bae, S. J. *et al.* Ex Vivo Shear-Wave Elastography of Axillary Lymph Nodes to Predict Nodal Metastasis in Patients with Primary Breast Cancer. *J. Breast Cancer* **21**, 190–196 (2018).

38. You, J. *et al.* The value of quantitative shear wave elastography in differentiating the cervical lymph nodes in patients with thyroid nodules. *J. Med. Ultrason.* **45**, 251–259 (2018).

39. Chaudhuri, O. *et al.* Substrate stress relaxation regulates cell spreading. *Nat. Commun.* **6**, 1–7 (2015).

40. Roederer, M. Interpretation of cellular proliferation data: Avoid the panglossian. *Cytom. Part A* **79**, 95–101 (2011).

41. Turtle, C. J. *et al.* Immunotherapy of non-Hodgkin's lymphoma with a defined ratio of CD8+ and CD4+ CD19-specific chimeric antigen receptor-modified T cells. *Sci. Transl. Med.* **8**, 1–24 (2016).

42. Turtle, C. J. *et al.* CD19 CAR-T cells of defined CD4+:CD8+ composition in adult B cell ALL patients. *J. Clin. Invest.* **126**, 2123–2138 (2016).

43. Tran, E. *et al.* Cancer immunotherapy based on mutation-specific CD4+ T cells in a patient with epithelial cancer. *Science* **344**, 641–645 (2014).

44. Inderberg, E. M. & Wälchli, S. Long-term surviving cancer patients as a source of therapeutic TCR. *Cancer Immunol. Immunother.* **69**, 859–865 (2020).

45. Lyons, A. B. & Parish, C. R. Determination of lymphocyte division by flow cytometry. *J. Immunol. Methods* **171**, 131–137 (1994).

46. Zhang, S. Fabrication of novel biomaterials through molecular self-assembly. *Nat. Biotechnol.* **21**, 1171–1178 (2003).

47. Garfall, A. L. *et al.* T-cell phenotypes associated with effective CAR T-cell therapy in postinduction vs relapsed multiple myeloma. *Blood Adv.* **3**, 2812–2815 (2019).

48. Sommermeyer, D. *et al.* Chimeric antigen receptor-modified T cells derived from defined CD8+ and CD4+ subsets confer superior antitumor reactivity in vivo. *Leukemia* **30**, 492–500 (2016).

49. Roberts, A. D., Ely, K. H. & Woodland, D. L. Differential contributions of central and effector memory T cells to recall responses. *J. Exp. Med.* **202**, 123–133 (2005).

50. Dutton, R. W., Bradley, L. M. & Swain, S. L. T cell memory. *Annu. Rev. Immunol.* **16**, 201–223 (1998).

51. Harris, N. L., Watt, V., Ronchese, F. & Le Gros, G. Differential T cell function and fate in lymph node and nonlymphoid tissues. *J. Exp. Med.* **195**, 317–326 (2002).

52. Hengel, R. L. *et al.* Cutting edge: L-selectin (CD62L) expression distinguishes small resting memory CD4+ T cells that preferentially respond to recall antigen. *J. Immunol.* **170**, 28–32 (2003).

53. Berenzon, D. *et al.* Protracted protection to Plasmodium berghei malaria is linked to functionally and phenotypically heterogeneous liver memory CD8+ T cells. *J. Immunol.* **171**, 2024–2034 (2003).

54. Singh, N., Perazzelli, J., Grupp, S. A. & Barrett, D. M. Early memory phenotypes drive T cell proliferation in patients with pediatric malignancies. *Sci. Transl. Med.* **8**, 1–9 (2016).

55. Isser, A., Livingston, N. K. & Schneck, J. P. Biomaterials to enhance antigen-specific T cell expansion for cancer immunotherapy. *Biomaterials* **268**, 1–44 (2021).

Chapter 5

Lymph node-on-a-chip to improve adoptive cell therapy

5.1 Introduction

Microfluidic chip (MC) technology can nowadays provide a platform for cell culturing that is closer to the physiological environment than standard static cultures. In general terms, MCs can be described as devices with internal channels at the micro scale where the flow can be precisely controlled. These devices can be used for organ-on-a-chip applications.[1]

The technology holds the potential to overcome some limitations of the static cell cultures as well as those related to the use of laboratory animals. Static cell cultures are simple and, as discussed in previous chapters, do not recreate well tissue or organ complex microenvironments. On the other hand, the use of animals does provide a platform to study cell cultures at the organ and system levels, but this approach is expensive, time-consuming and in most cases do not reflect the human physiology, not to mention the associated ethical burden.[2,3]

Up to now, most of cell culture studies in MCs only involved cells. This approach can be a relevant option for some cell types, such as endothelial cells, but it does not recreate the 3D microenvironment found in the ECM.[1] To improve this situation, efforts are being devoted to introduce ECM-like materials into MCs for 3D cell cultures. One of the main candidates as a scaffold for 3D cultures for microfluidic systems are hydrogels.[4–6] In **Figure 5.1**, a scheme of a MC with a hydrogel suitable for cell culture is shown.

For the creation of a LN-on-a-chip, the lymph flow should also be carefully established to mimic T cell natural microenvironment.[7–10]

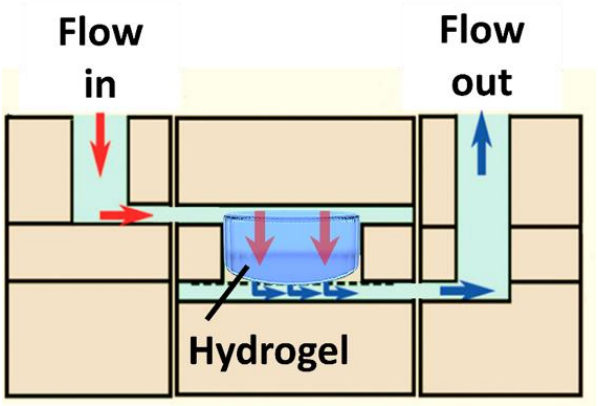

Figure 5.1 Schematic representation of a MC with a hydrogel. The microfluidic device represented allows the flow to enter from the top (Flow in), pass through the hydrogel and leave through the opposite side, to be finally collected from the top of the MC (Flow out).

In vivo, the unidirectional lymph flow is generated through the integration of extrinsic and intrinsic pumping processes,[10,11] as already mentioned in the introduction. However, obtaining quantitative information about the lymph flow rates *in vivo* remains a technical challenge. Still, some trials have been reported like the injection of radioactive or fluorescent tracers into the lymphatic system. These experiments allowed the imaging of the lymphatic network morphology, while providing an indirect measurement of flow through quantification of the tracer transport.[12] These labelled techniques have some technical drawbacks, such as the low spatial resolution and alteration of the interstitial fluid flow due to the injection step. Despite these difficulties, by using a high-speed video system, injected microparticles tagged with near-infrared dyes, permitted to measure the volumetric flow in rat mesenteric prenodal lymphatics with a value of 13.95µL/h.[12]

In a different approach, a continuous *in vivo* quantification of the lymph flow at high temporal resolution showed a volumetric flow value of 0.3 µL/h in mice lymphatic vessels by using a direct label-free measurement with a doppler optical coherence tomography (DOCT) technique.[13] Also, the combination of phase-contrast synchrotron micro-computed tomography (µCT) and a corrosion casting technique indicated a transmural flow throughout mouse LNs of 0.6 µL/h.[14]

In addition to the information provided by *in vivo* experimental models, there are also some examples of LN-on-a-chip described in the literature,[15–18] with volumetric flows ranging from 7.2 to 120 µL/h, as briefly discussed in the introduction section. However, these examples used animal LN slices[17,18] or a mixture of different cells types such as dendritic cells to activate T cells.[16] These approaches to not take into consideration the possible potential to improve ACT platforms for cell culture. In one side, the use of animal tissues to expand human T cells would rise several issues as explained previously in this introduction, on the other side the use of different cells contributes to a more complex culture system requiring further steps to isolate the clinically relevant T cells.

Finally, it is worth pointing out a very recent publication where a LN-on-a-chip design allowed the study of the effect of hydroxychloroquine (HCQ) delivered to cells in a dynamic 3D setting, enabling real-time monitoring of two immune cells at the same time (Jurkat T and Raji B cells).[19] This multi-compartment chip enabled measurements of immune cell motility in response to drugs, where HCQ added to the cells through a constant and continuous flow was found to induce a reduction in T cell velocity while promoting persistent rotational motion. These findings highlight the importance and further potential of these LN-on-a-chip devices for drug screening and cellular dynamic studies in general.[19]

In summary, there are no reported examples of a LN-on-a-chip including a 3D scaffold to imitate the ECM of the LNs, while considering the effect of flow on T cell proliferation and differentiation towards a better expansion strategy for ACT.

5.2 Objectives and strategy

In this thesis we focused on the design and fabrication of a LN-on-a-chip (**Figure 5.2**) with a net unidirectional pulsatile fluid flow that passes through a 3D hybrid hydrogel at a volumetric flow of 0.3 – 50 µL/h. This system was studied as a strategy to improve T cell expansion of specific

phenotypes, as well as to fabricate an animal-free system capable of performing some preclinical tests reliably.

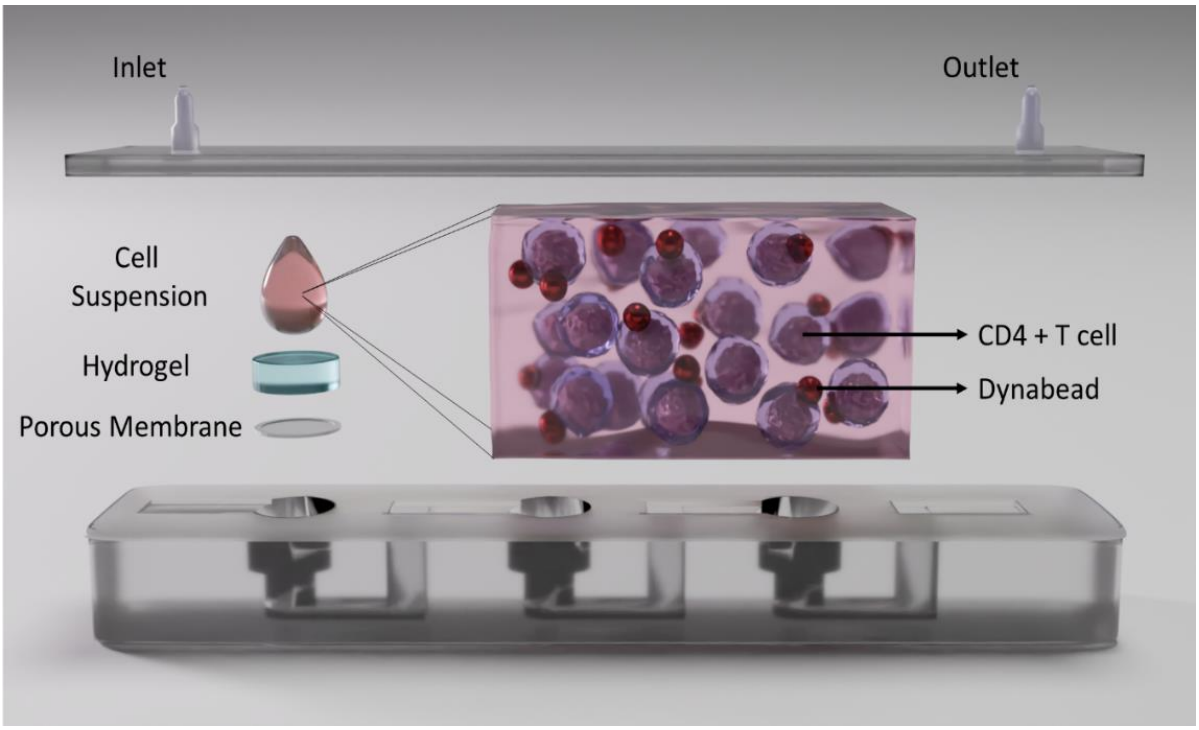

Figure 5.2 Schematic representation of the different components of a LN-on-a-chip. Primary human CD4+ T cell suspension with Dynabeads seeded in a PEG-Hep hydrogel, which resides on top of a porous membrane deposited at the bottom of the culture wells of the MC. This chip representation shows 3 connected wells. Once closed, tubes are connected to the inlet and outlet ports and a peristaltic pump is used to allow the complete RPMI cell medium flow. Scheme not to scale.

The tasks to achieve the main objective mentioned above involved the optimization of the design and material of the chip; optimization of the bulk and IOPAL PEG-Hep hydrogels; setup the peristaltic pump to obtain the desired flow; optimization of the cell seeding conditions; study the need of cytokine supplementation and sterilization procedures; and finally, analysis of primary human CD4+ T cell proliferation in the microfluidic device using both bulk and IOPAL PEG-Hep hydrogels in comparison with the standard suspension culture method.

5.3 Design and fabrication of the microfluidic device towards a LN-on-a-chip

In collaboration with the Biomedical Applications Group (GAB) at the Barcelona Institute of Microelectronics - National Microelectronics Center (IMB-CNM-CSIC), we designed and fabricated different MCs. The MC prototypes used in this thesis were a result of several rounds of redesign, containing all of them culture wells of 8 mm in depth and 6.58 mm in diameter. These values were chosen taking into consideration the diameter value of the common 96 well plates used in our laboratory (Greiner Bio-One, ref: 655180). In general terms all MCs fabricated consisted in a base, built of 4 layers of PMMA with a thickness of 2 mm in the three bottom layers and 8 mm for the upper one; and a cover with a 1 mm-thickness adhesive silicone layer and a 3 mm thickness layer of PMMA on top. Further details can be found in Chapter 6.

Once designed, the PMMA and silicone layers were cut in a laser machine. For the assemble of all the layers, a thermal press (at 20 kN, 80˚C, 45 min) was employed with isopropanol to improve the bonding. To be able to connect the tubes responsible for the circulation of cell culture medium, an inlet and outlet ports were glued on the top layer. Finally, the MCs could be properly closed with screws.

Furthermore, to hold the hydrogels, T cells and Dynabeads inside the culture wells, while allowing the passage of cell culture medium, porous membranes were used. They were cut with the same diameter as the culture wells in the laser machine, and then they were glued to the bottom of the well with a double tape o-ring as schematized in **Figure 5.2**.

5.3.1 Design and fabrication of the microfluidic chip 1

The initial prototype named microfluidic chip 1 (MC1) consisted of four independent wells, with 1 inlet and 1 outlet per well (**Figure 5.3 A**). However, the wells could also be connected externally with tubes, by connecting the outlet of one well with the inlet of the next well (**Figure 5.3 B**).

MC1 was designed to contain our PEG-Hep 3D hydrogels (bulk or IOPAL), both discussed in the previous chapter, for 5-6 days to mimic the lymph node in the body (**Figure 5.3 C**). The use of porous membranes (pore size: 0.45 µm) was needed, as mentioned before. After a simple flow experiment with only RPMI cell culture medium, it was possible to collect the hydrogels in very good shape and with a pink color, confirming the homogeneous circulation of the RPMI pink medium through the hydrogels (**Figure 5.3 D**).

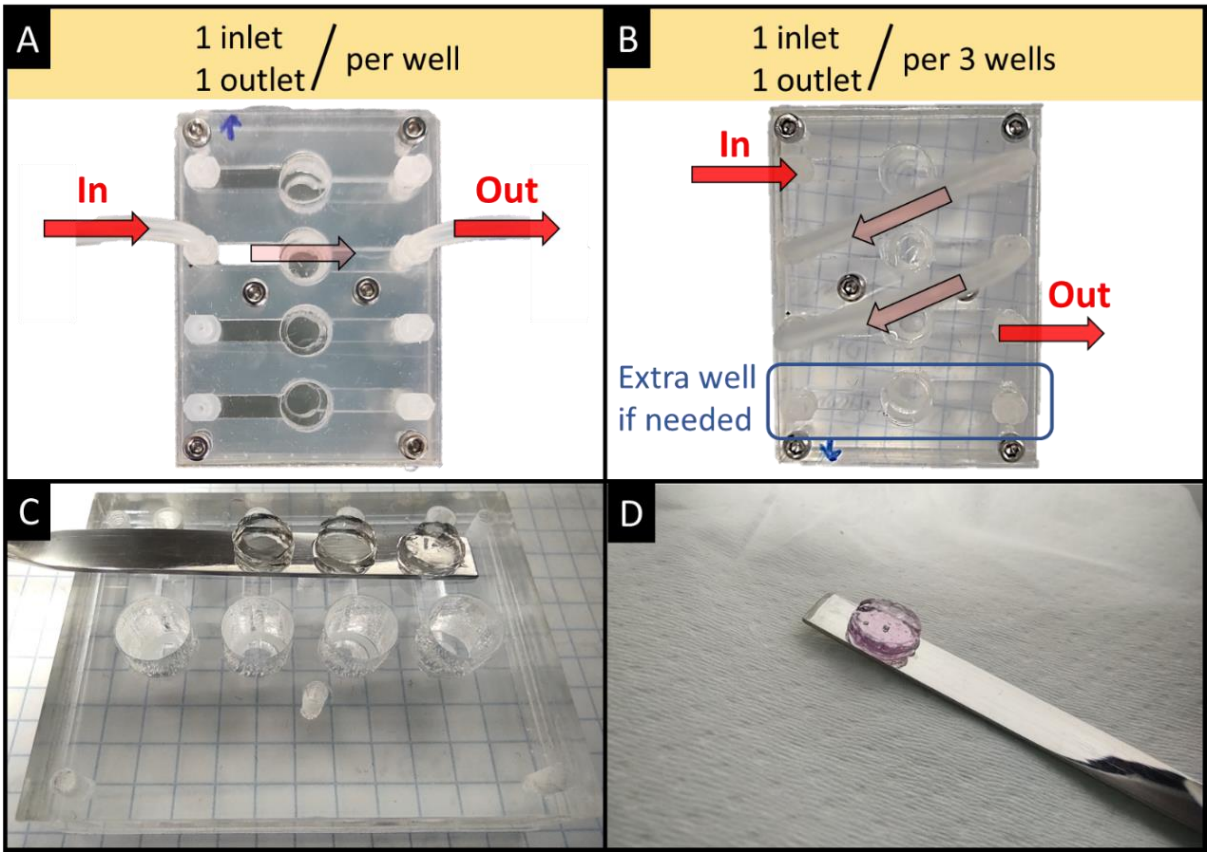

Figure 5.3 MC1 with four independent wells with (A) 1 inlet and 1 outlet per well or (B) 3 wells connected with 2 external tubes assuring the same flow in the 3 triplicates with 1 inlet and 1 outlet. (C) PEG-Hep bulk hydrogels before placing them inside the MC1. (D) PEG-Hep bulk hydrogels removed for the MC1 after RPMI flow.

5.3.2 Optimization of the flow rate

First, we calculated the minimum flow rate needed in our MC for the optimal culture of primary human CD4+ T cells, by taking into consideration the following equation:

$$F(C_{in} - C_{out}) = RN \quad (1)$$

in which *F* is the flow rate of the culture medium, C_{in} (2.2x10^8 pmol/L) and C_{out} (0 pmol/L) are the inlet and outlet oxygen concentrations in the cell culture medium, respectively, if we assume that all the oxygen is consumed in a single pass. *R* (5x10^{-3} pmol/h/cell) is the oxygen consumption rate for primary human CD4+ T cells,[20,21] while *N* (10^5 or 3x10^5 cells) is the number of seeded cells in a single-well or triplicate in our MC, respectively.

From the calculation of the above equation, the minimum flow needed to assure oxygen supply was found to be 2.27 µL/h and 6.81 µL/h for our single-well or triplicate setup, respectively. It is also worth noticing, that these values are in accordance with the volumetric flow range (0.3 to 50 µL/h) proposed in the literature for mimicking the LN flow rates.[12–18]

After establishing that the desired setting was a microfluidic system with a net unidirectional pulsatile fluid flow passing through the 3D hybrid hydrogel at the indicated volumetric flow range, the next step was to assess the possibility of obtaining these flow values in the laboratory.

To do that, a standard tube of 0.5 mm diameter was connected to the empty MC1, and 0.01 and 0.04 revolutions per minute (rpm) for 24 h were chosen to pump complete RPMI, achieving volumetric flow values of 8.0 and 42.7 µL/h respectively (**Table 5.1**). Next, one or three MC wells connected in line with bulk or IOPAL PEG-Hep hydrogels sustained by porous membranes were submitted to 0.04 rpm for 48 h, obtaining comparable volumetric flow rates of 45.4 and 47.7 µL/h, respectively (**Table 5.1**). With this experiment, we demonstrated that no significant differences were obtained in flow values when placing the components needed to mimic the artificial LNs in the MC, i.e. the hydrogels and membranes, further supporting the possibility to work with triplicates connected in line.

At last, we analysed the volumetric flow for a week to evaluate possible flow variations over a typical cell culture time. In this experiment, triplicates were submitted to a flow at 0.01 and 0.04 rpm, obtaining flow rates of 9.8 µL/h and 46.9 µL/h, respectively after 168 h (day 7). **Table 5.1** summarizes the results obtained for the different flow experiments performed, indicating that the MINIPULS® 3 Peristaltic Pump (kindly provided by the Biomedical Applications Group (GAB) from IMB-CNM-CSIC) is suitable for our requirements.

Table 5.1 Preliminary experiments to assess the stability of the flow and suitability of the MINIPULS® 3 Peristaltic Pump.

MC well components		**Revolutions per minute (rpm)**	**Time of the experiment (h)**	**Volumetric Flow (µL/h)**
Nº of wells	Presence of hydrogel and membranes			
1	No	0.01	24	8.0
1	No	0.04	24	42.7
1	Yes	0.04	48	45.4
3	Yes	0.04	48	47.7
3	Yes	0.01	168	9.8
3	Yes	0.04	168	46.9

5.3.3 Optimization of the MC materials

In the next step, we tested and optimized the composition of the different materials used in the MCs. PMMA was chosen for the MC fabrication due to its biocompatibility, good acceptance by mammalian cell cultures and its previous use in microfluidic devices.[22–24] Furthermore, to support the hydrogels while preventing the circulation of CD4+ T cells and Dynabeads outside the wells, we evaluated the use of two different porous membranes, made of polyethylene terephthalate

(PET) and polytetrafluoroethylene (PTFE, commonly known as Teflon), both with a 0.45 µm pore size.

With these objectives, we assessed cell viability and proliferation of primary human CD4+ T cells cultured on the material of the microfluidic chip (PMMA) compared to the standard polystyrene (PS) well plates, and the two different porous membranes (PET and PTFE).

5.3.3.1 Effect of the PMMA well plates

To assess the effect of PMMA as a material to build the MC on cell behavior, we used PI, a small fluorescent molecule commonly used to discriminate dead cells, as described in previous chapters. The PI viability test was performed with primary human CD4+ T cells purified from human blood donors and incubated for 6 days at 37˚C and 5% CO_2.

Thus, a primary human CD4+ T cell suspension with and without Dynabeads (positive and negative control, respectively) was seeded in regular PS 96 well plates as a commercial control material and in a home-made PMMA well plate with exactly the same sizes (**Figure 5.4**). The value of 33.4% of non-viable or apoptotic cells (PI+) was obtained for the positive control samples seeded in PMMA, which is very similar to the one obtained with the commercial PS plates (31.6%), confirming that the PMMA does not negatively affect CD4+ T cell viability.

Next, CD4+ T cell proliferation was evaluated with the CSFE staining agent. In **Figure 5.5** the proliferation capacity of T cells is represented by three usual numeric parameters, the proliferation, expansion, and replication indexes, as mentioned in previous chapters. After 6 days of culture with Dynabeads in suspension in a commercial PS well plate or in a PMMA well plate, the three indexes were measured and normalized to the PS positive control for an adequate assessment.

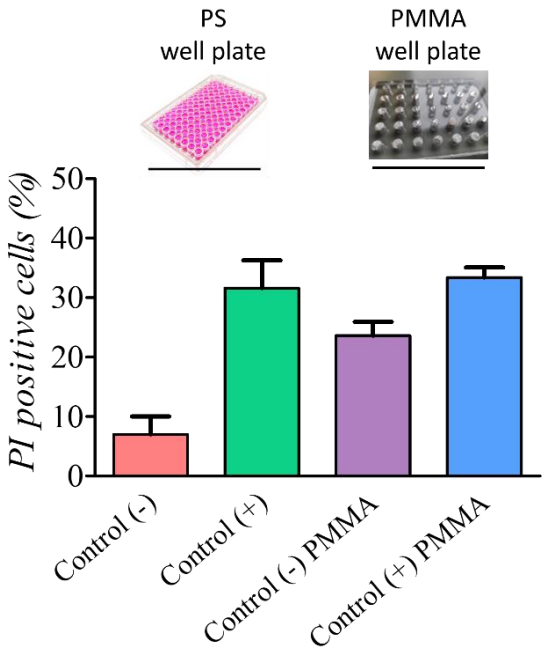

Figure 5.4 PI viability test performed on primary human CD4+ T cells. CD4+ T cells seeded for 5 days in a commercial PS or PMMA well plate in suspension with Dynabeads (control +) or without Dynabeads (control -), (N_{donors} = 1).

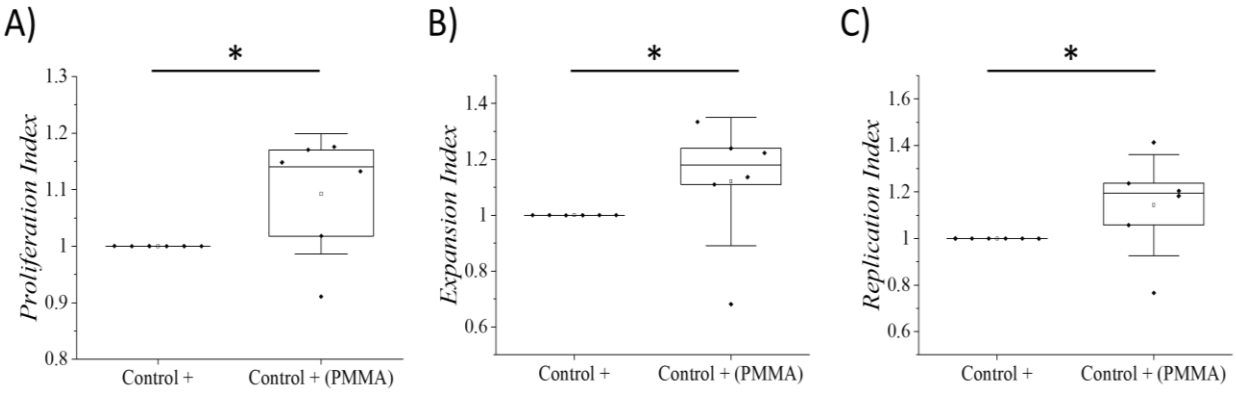

Figure 5.5 Proliferation analyses of primary human CD4+ T cells 6 days after seeding in suspension with Dynabeads in a PMMA template or in a standard 96 well plate made of PS (control +), (N_{donors} = 6). Normalized A) proliferation index, B) expansion index and C) replication index. Statistical significance was determined by the Mann−Whitney U test (*$p < 0.05$).

CD4+ T cells seeded in the fabricated PMMA well plate showed a statistically significant improvement in comparison with cells seeded in PS well plates, with median values of 1.14, 1.18 and 1.19 for proliferation, expansion and replication indexes, respectively.

In conclusion, the fabricated PMMA well plate did not negatively affect the cellular viability nor the proliferation of the CD4+ T cells. Therefore, we concluded that PMMA was a good option for the engineering of the microfluidic device.

5.3.3.2 Effect of porous membrane material: PET and PTFE

To maintain the artificial LN components (CD4+ T cells, Dynabeads and hydrogels) inside the MC wells, while allowing the circulation of cell culture medium, PET and PTFE porous membranes were studied. To evaluate the effect of the porous membrane material, primary human CD4+ T cell proliferation (**Figure 5.6**) and viability (**Figure 5.7**) experiments were performed. The porous membranes (PET or PTFE) were set on the bottom of the PMMA wells.

The median values of the proliferation (1.02), expansion (1.13) and replication (1.06) indexes for cells seeded on top of PET membranes were similar to the positive control (PMMA wells without membranes), only showing statistical significance for the expansion index. Likewise, with the PTFE membranes, the proliferation, expansion and replication indexes median values were 1.08, 1.16 and 1.15, respectively. In this case, there was statistical significance with the proliferation and expansion indexes when comparing the use of PTFE membranes to the positive control.

In conclusion, the use of membranes is not negatively affecting CD4+ T cells proliferation and it is even slightly enhancing its performance. Furthermore, since there is no statistical difference between PET and PTFE membranes, PET was selected to be used on the MC, because these membranes are transparent unlike PTFE (**Figure 5.6 D**), allowing optical control.

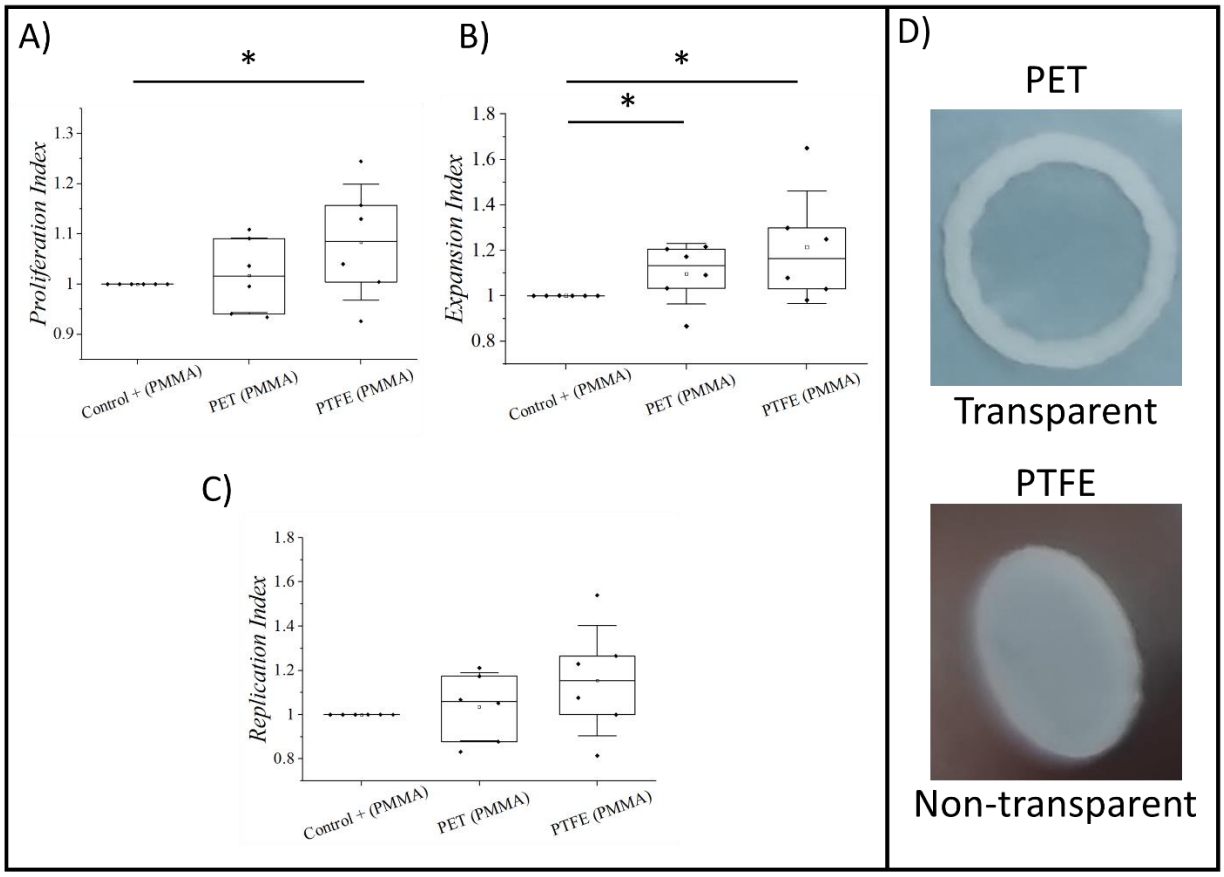

Figure 5.6 Proliferation analyses of primary human CD4+ T cells 6 days after seeding in suspension with Dynabeads in a PMMA template with PET membranes (PET (PMMA)), with PTFE membranes (PTFE (PMMA)) or without membranes (control + (PMMA)), (N_{donors} = 6). Normalized A) proliferation index, B) expansion index and C) replication index. Statistical significance was determined by the Mann−Whitney U test (*p < 0.05). D) Photographies of a transparent PET membrane (top) and a non-transparent PTFE membrane (bottom).

Once PET was chosen as a material for the membranes, a PI viability test was performed in PS well plates. PI+ mean values (non-viable cells) of 23.3% were obtained when cells were seeded in PS well plates in contact with PET membranes (**Figure 5.7**). This value is smaller than the one obtained for the positive control samples (31.6%) seeded in PS well plates without the membranes. This result confirms that the PET membranes did not negatively affect cell viability and thus, were good candidates to be used in the microfluidic device.

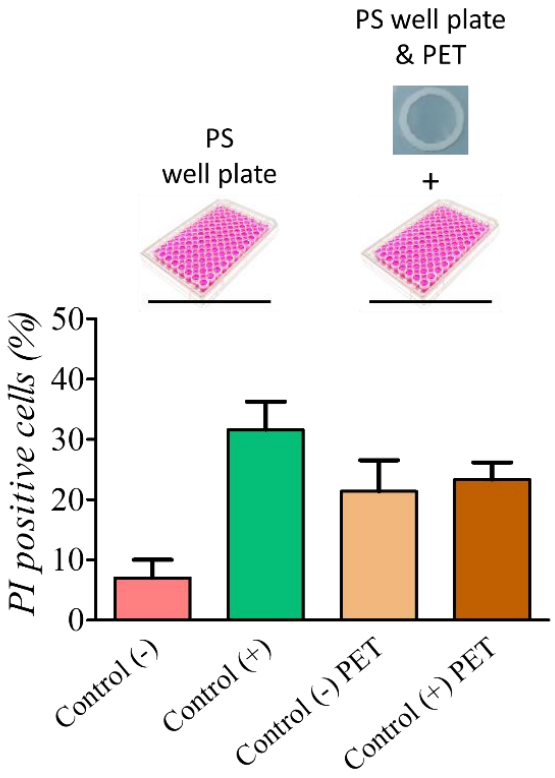

Figure 5.7 PI viability test performed on primary human CD4+ T cells. CD4+ T cells seeded for 5 days in a commercial PS with or without PET membranes. The cells were seeded in suspension with Dynabeads (control +) or without Dynabeads (control -), (N_{donors} = 1).

5.3.4 Importance of IL-2 concentration in the cell culture

Interleukin-2 (IL-2) is a 15 kDa cytokine predominantly secreted by activated T cells, and represents a key player in the cell-mediated immune response.[25] It is an early landmark in the activation program of CD4+ T cells *in vitro*,[26] and it is frequently used as a supplement in T cell culture medium. IL-2 concentrations used for T cell expansions in different ACT studies vary between 10 IU/mL and 6000 IU/mL, or 12.0 ng/ml and 7228.9 ng/mL.[27] Depending on the application, the IL-2 concentration was also found to influence the outcoming phenotype of T cells.[28]

Taking into consideration the important role of IL-2, we performed a test to evaluate its effect in our CD4+ T cell cultures. In a typical CD4+ T cell culture experiment, commonly described as a positive control in this thesis, cells are seeded in suspension in a 96 well plate made of PS, together with Dynabeads. On these typical positive control conditions, neither IL-2 is added to the complete RPMI cell culture medium during seeding, nor the IL-2 secreted by the activated CD4+ T cells is removed by replacing the cell culture medium. Indeed, in our static experiments, complete RPMI medium is added on day 2, without replacing the one in culture. Consequently, the secreted IL-2 remains in the well.

However, in a microfluidic device with constant flow in an open circuit, the IL-2 secreted by the activated CD4+ T cells would be washed out by the flow. Thus, we decided to evaluate this potential effect on cell proliferation and differentiation. For that, we cultured CD4+ T cells with Dynabeads in a common 96 well plate made of PS. On day 2, we performed different treatments to the cells, according to four testing conditions.

On the positive control samples, complete RPMI cell culture medium was directly added on top of the wells (100 µL), as usual. On sample A, cells were collected, centrifuged and re-suspended on the same vial and 100 µL of complete RPMI was added. Thus, this sample was designed to assess the effect of the experimental manipulation to the cells. On sample B, cells were collected, centrifuged and the supernatant was removed. After, 200 µL of complete RPMI was added. In this case, we could determine the influence of losing the secreted IL-2 by activated T cells. On sample C, cells were collected, centrifuged and the supernatant was removed. After, 200 µL of complete RPMI complemented with a specific concentration of IL-2 was added. Specifically, an enzyme-linked immunosorbent assay (ELISA) was performed on day 2 from the supernatant of the corresponding activated CD4+ T cells to know the concentration of the recombinant IL-2 protein to be used to substitute the natural one.

Thus, a specific concentration was obtained for the different 8 human blood donors. In particular, CD4+ T cells from 4 donors were used for proliferation studies, whereas the other 4 donors were used for differentiation studies (**Table 5.2**). Once the concentration of IL-2 on day 2 was

determined, the complete RPMI was further complemented with that concentration, before resuspending the cells on sample C.

The proliferation and differentiation results are represented in **Figure 5.8** and **Figure 5.9**, respectively. The normalized proliferation index exhibited mean values of 1.07, 1.15 and 1.04 for the samples A, B and C, respectively. For the normalized expansion index, the mean values obtained were 1.10, 1.31 and 1.09 for the samples A, B and C, respectively, whereas for the normalized replication index, the mean values were 1.05, 1.19 and 1.01. None of the normalized indexes presented statistically significant differences when using the Mann-Whitney U test ($p>0.05$).

Table 5.2 IL-2 concentration determined on day 2 from activated CD4+ T cells.

IL-2 concentration on day 2		
Donors	Concentration (ng/mL)	Used for:
1	121	**Proliferation studies**
2	63	
3	131	
4	106	
5	94	**Differentiation studies**
6	75	
7	111	
8	99	

However, while it is know that IL-2 is produced by activated T cells and promotes further growth and differentiation of activated T cells,[29] it was also discovered with *in vivo* experiments that naïve polyclonal T cells, activated with TCR and CD28-specific agonist antibodies produced IL-2 quickly (achieving its peak at 24h) but transiently. Given that IL-2 was rapidly secreted by these helper T cells, and abundant in these cultures, several studies demonstrated that IL-2 itself suppresses IL-2 production, via a classic negative feedback loop.[30]

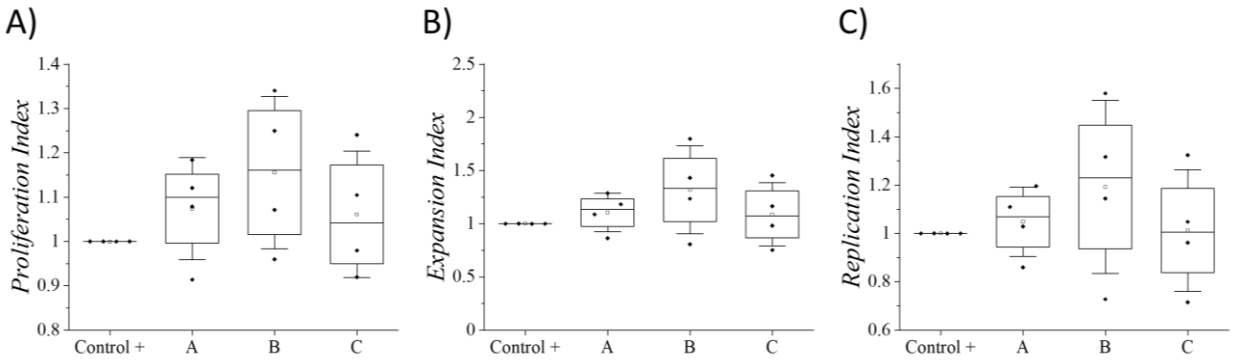

Figure 5.8 Proliferation analysis of primary human CD4+ T cells 6 days after seeding activated with Dynabeads in suspension for sample A, B and C. Normalized A) proliferation index, B) expansion index and C) replication index, (N_{donors} = 4).

This information may be the possible explanation for the fact that sample B seemed to provide slightly higher proliferation than the other samples, since the cell culture medium containing the IL-2 produced until day 2 was removed and replaced with complete RPMI without added IL-2. Thus, we could have disrupted the negative feedback loop, allowing the cells to produce again more IL-2 and continue to proliferate. Nevertheless, as mentioned before, no significant differences were detected.

Regarding the differentiation results, after 5 days of culture the resulting phenotypes were analyzed by cell staining the CD62L/CD45RO antibodies, as previously described in this thesis. The CD4+ T cell subpopulations studied were T_N (CD45RO−/CD62L+), T_{EM} (CD45RO+/CD62L−), T_{EFF} (CD45RO−/CD62L−) and T_{CM} (CD45RO+/CD62L+) (**Figure 5.9**).

For the T_N subpopulation the median percentage values obtained were 9, 9, 10 and 10% for the control +, and samples A, B and C, respectively. The T_{EM} subpopulation showed median values of 20, 21, 23 and 18%, whereas the T_{EFF} median values of 3, 4, 3 and 3% respectively. Regarding T_{CM} subpopulation the median values obtained were 64, 63, 63 and 64%, for the control +, and samples A, B and C, respectively. Similar to the proliferation results, no statistically significant differences were detected, when using the Mann-Whitney U test ($p<0.05$).

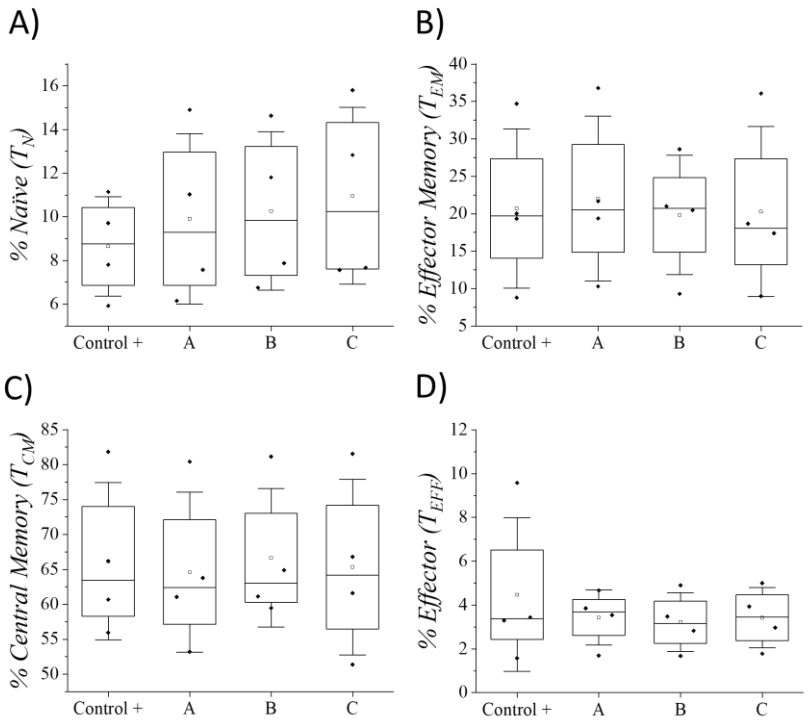

Figure 5.9 Differentiation analysis of CD4+ T cells 5 days after seeding. A) Percentage of T_N, B) T_{EM}, C) T_{CM} and D) T_{EFF} for samples A, B, C and control +, (N_{donors} = 4).

Considering the results obtained in both proliferation and differentiation analyses of this section, it can be concluded that having a flow without supplementation of IL-2 may not be detrimental. In fact, it could even be somehow beneficial for the overall expansion of CD4+ T cells, by preventing a negative feedback loop of IL-2.

5.3.5 Sterilization procedure for the MC and tubbing

After several rounds of optimization to avoid contamination in our system, and considering the characteristics of the MC material (PMMA) and its stability limitations when using ethanol, the best conditions found for the cleaning and sterilization of the MC are: 1) external cleaning of the chip with a paper soaked with small amounts of 70% ethanol and abundant MilliQ water; 2) flow

MilliQ water through the wells and the inner channels; 3) UV sterilization for at least 1 h and 4) flow sterile PBS to clean the inner connections of the MC.

To clean the polyvinyl chloride (PVC) tubes used in our microfluidic setup, they were immersed in 70% ethanol for 10 min, and then, 20 mL of 70% ethanol and MiliQ water were pump through them with a syringe. Finally, they were sterilized using UV during 1 h. The porous PET membranes were also sterilized during the same UV time (30 min on each side).

5.3.6 Microfluidic setup for cell culture experiments

In a common setup of the microfluidic system, we used the PMMA MC, PCV tubing, PET membranes, PEG-Hep hydrogels, medium, waste reservoirs and the peristaltic pump.

Preceding the sterilization, the 0.5 mm diameter PVC tubes were cut to the desired length to obtain the experimental setup shown with red lines in **Figure 5.10**. To prevent the tubes from sliding when the peristaltic pump is working, a tube with two stoppers was used on the pump head, to be further connected by using 1.6 mm tube connectors to the other PVC tubes. After sterilization, all tubes were filled with complete RPMI medium using a syringe. Further details can be found in Chapter 6.

PET membranes were glued inside the microfluidic culture wells, and then, they were cleaned and hydrated with sterile PBS. After 1 day, PBS was removed, and the MC was carefully filled with complete RPMI medium using a syringe to avoid air bubbles in the inner channels. Then, the RPMI medium was removed from the culture wells and the previously synthetized PEG-Hep hydrogels were placed inside the wells. After cell seeding (described in Chapter 6), the MC was closed, the tubes were connected and introduced inside the incubator at 37˚C and 5% CO_2, as exemplified in **Figure 5.10**. Both medium and waste RPMI reservoirs were also introduced inside the incubator. Outside the incubator, the peristaltic pump was circulating cell culture medium from the medium reservoir at 0.04 rpm for 6 days.

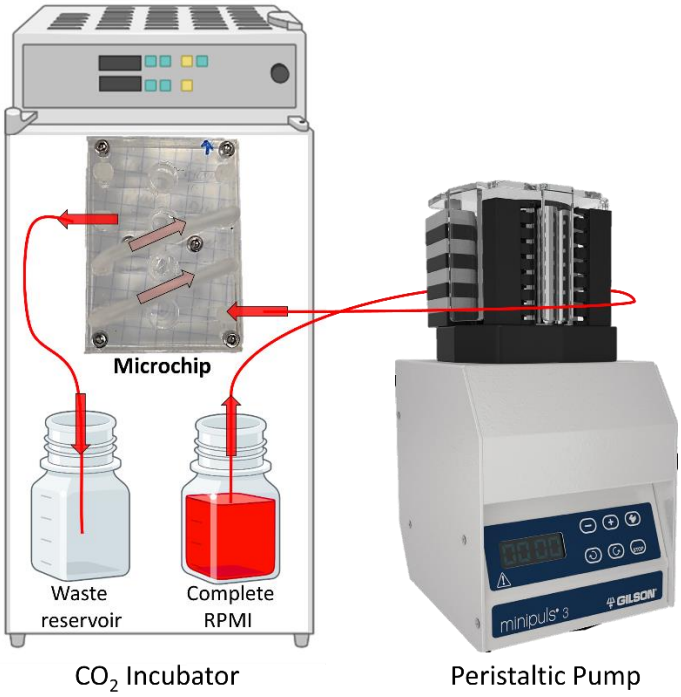

Figure 5.10 Schematic microfluidic set up for cell culture experiments, with the peristaltic pump outside the incubator. The MC containing the activated CD4+ T cells seeded in the PEG-Hep hydrogels and both medium and waste reservoirs were placed inside of the incubator. Scheme not to scale.

5.4 LN-on-a-chip optimization: MC2, MC3 and MC4

Taking into consideration the state-of-the-art organ-on-a-chip device designs, a first prototype with independent wells (MC1) was designed to perform preliminary experiments (see section 5.3.2). Anticipating our interest of working with triplicates per condition, while reducing the complexity of the microfluidic tubing setup, three wells of the MC1 were connected in line using external tubes, as shown in **Figure 5.3 B**. However, contamination was continuously observed when using this set up, probably due to the external tube connections. To overcome this issue and to decrease the manipulation steps, a chip with 3 internally interconnected wells in line, here denominated as MC2, was designed in collaboration with IMB-CNM-CSIC (**Figure 5.11 MC2**).

Despite the simplicity of the MC2, we found difficulties in generating a homogeneous pressure inside the MC, resulting in constant leakages. Thus, a new chip, the MC3, was designed with the following upgrades: 1) screws located not only on the edges of the device, but also in the middle part, 2) use of larger screws and 3) more resistant inlet and outlet ports (**Figure 5.11 MC3**).

After this round of optimization, leakage was not observed and long-time pumping experiments (up to 6 days) were possible. However, CD4+ T cell proliferation was not obtained either with the MC3, due to the presence of air inside the MC. Moreover, contamination was still difficult to be avoided. Taking these issues into consideration, a new microfluidic device (MC4) was designed, this time with a single well (**Figure 5.11 MC4**). The main purpose of this design was to minimize the complexity of the system and avoid the contamination inside, although with this design we cannot obtain data in triplicate using a single MC.

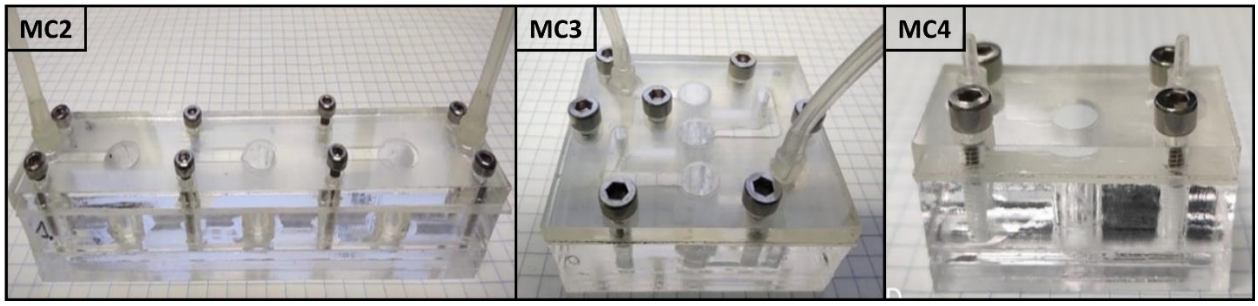

Figure 5.11 PMMA microfluidic chips fabricated, MC2, MC3 and MC4, from left to right.

5.4.1 Optimization of cell seeding conditions and microfluidic experimental setup

Once the MC3 was fabricated, and after checking that cell culture medium could flow inside for 6 days without leakage, we realised that some changes on our common seeding protocol were needed. Up to this point, the seeding step was done similarly to the one performed on the PS well plates (see Chapter 6 for details). After a typical seeding step, with a final volume of 100 µL, some air space inside the wells of the microfluidic device remained, as the wells in the MC were not filled until the top. This presence of air inside the MC resulted into unexpected volume differences once the peristaltic pump was turn on. Therefore, we decided to change our normal

amount of cell culture medium added during seeding from 100 µL to 180 µL, which consequently changed the initial cell concentration from the usual 1 M/ml to 0.56 M/mL.

To evaluate the effect of this modification, cells were seeded with 180 µL of medium and no extra one was added on day 2 of culture (as we usually do in our standard cell experiments). As shown in **Figure 5.12**, lower proliferation, expansion and replication indexes (median values of 0.9, 0.8 and 0.8, respectively) were obtained in comparison to the standard positive control.

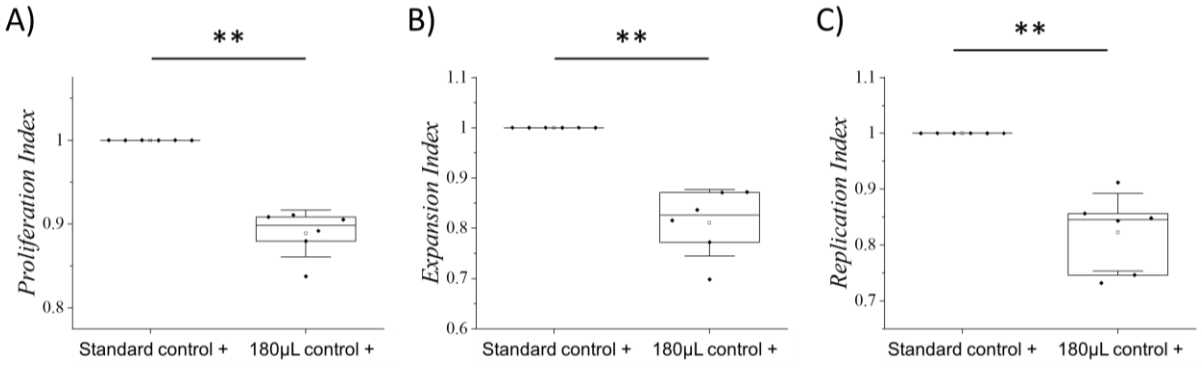

Figure 5.12 Proliferation analysis of CD4+ T cells 6 days after seeding activated with Dynabeads in suspension in a PS 96 well plate as a "standard control +" or as a "180 µL control +". A) Normalized proliferation, B) expansion and C) replication indexes for both conditions are shown, (N_{donors} = 6). Statistical significance was assessed by the Mann-Whitney U test (**p < 0.01).

This lower performance in cell proliferation was expected, since for 6 days, no addition (as we did with the positive control) or replacement (as it happens in the MC under flow) of the initial 180 µL of cell culture medium was performed. In conclusion, the modification of the cell seeding conditions did not prevent cells from proliferating in the PS 96 well plate.

Nevertheless, as a control experiment, we used these exact same conditions inside the MC3 (without a continuous flow of cell culture medium), but the cells did not proliferate. These results could be justified by the lack of oxygen inside the system, as the peristaltic pump was intentionally stopped and both PMMA and tubes suffer from poor gas permeability. Therefore,

the next cell proliferation experiments were submitted to a flow of complete RPMI with a volumetric flow of ≈ 50 µL/h, as it is supposed to ensure the constant oxygen and nutrients supply required for cell survival, as previously discussed in section 5.3.2.

Still, cells were found dead during the proliferation analysis of day 6 after pumping fresh cell culture medium during all the experimental time. So, it was hypothesized that the air available on the complete RPMI container (**Figure 5.10**) was not enough to provide the gas exchange needed to the cultured cells. To test this hypothesis but avoid contamination, we added a home-made new cap to the complete RPMI container, which incorporated an aperture covered with a 0.22 µm filter (**Figure 5.13**).

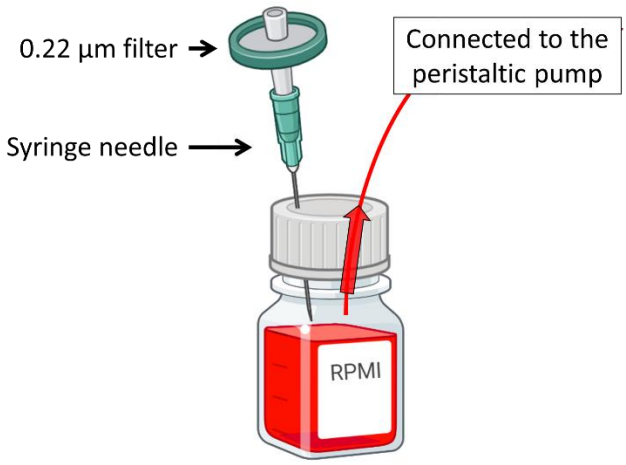

Figure 5.13 Scheme of the reservoir containing complete RPMI to be supplied to the microfluidic system. A 0.22 µm filter was attached to a syringe needle and was passed through the reservoir cap to allow constant gas exchange during the experimental time in a sterile manner.

Additionally, we decided to use IOPAL PEG-Hep hydrogels instead of bulk hydrogels, because as seen in the previous chapter, despite the extra steps for their preparation, they could significantly improve the proliferation of CD4+ T cells. Moreover, the IOPAL porosity is expected to allow a better flow within the hydrogel, granting a more homogenous distribution of nutrients to the seeded cells.

This attempt allowed to successfully observe for the first time in our experiments, alive primary human CD4+ T cells inside one of the wells of the MC3 after 6 days, with the cell culture medium being pumped with a volumetric flow of 50 µL/h (**Figure 5.14**). Worth highlighting is the fact that only the first well to receive fresh complete RPMI medium showed cell proliferation. Unfortunately, the other two wells were contaminated, and for that reason no CD4+ T cell proliferation was possible to be analysed for those wells. Despite this partial success, the normalized proliferation, expansion and replication indexes of human CD4+ T cells seeded inside the LN-on-a-chip (MC3) with IOPAL PEG-Hep hydrogels were lower than the positive control with values of 0.79, 0.44 and 0.56, respectively (**Table 5.3**).

These findings suggested that still a new MC upgraded design was needed to avoid contamination in these devices. Therefore, the design of MC4 (**Figure 5.11 MC4**) with only one well was proposed, with the objective of minimizing the complexity of the system. Further experiments are currently being performed in our research group with this optimised version, the MC4. However, due to time limitations, it was not possible to incorporate the results in this PhD thesis.

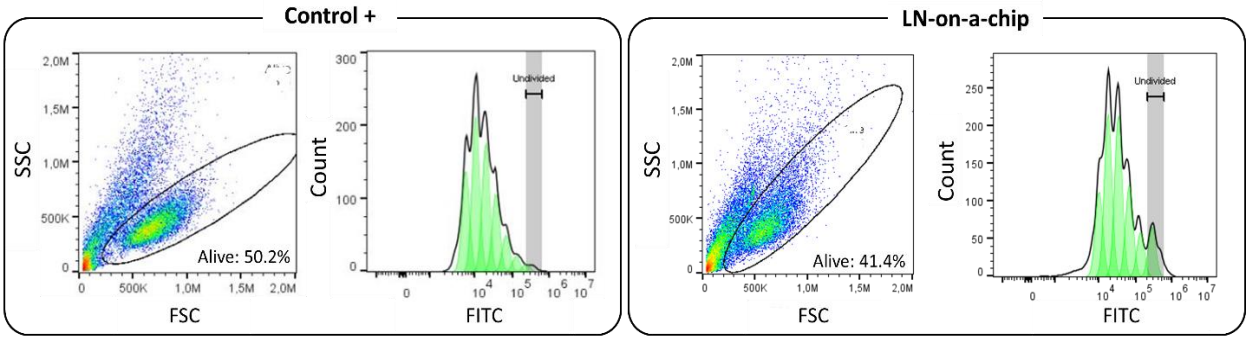

Figure 5.14 Representative alive population in an SSC Vs FSC graph and CFSE diagram of CD4+ T cells stimulated with Dynabeads 6 days after seeding in IOPAL PEG-Hep hydrogels placed in a PS 96-well plate (control +) and inside the MC3 (N_{donors} = 1; results of only one well).

Table 5.3 Normalized proliferation, expansion and replication indexes of CD4+ T cells seeded in IOPAL PEG-Hep hydrogels placed in the MC3 and inside the PS 96 well plate (control +), (N_{donors} = 1; results of only one well).

Normalized Indexes	Control +	LN-on-a-chip
Proliferation Index	1.00	0.79
Expansion Index	1.00	0.44
Replication Index	1.00	0.56

5.5 Summary and conclusions

Here we have presented the first steps toward a novel LN-on-a-chip, including a 3D scaffold to imitate the ECM of the LNs and taking into consideration the effect of flow on T cell proliferation.

Different optimization steps have been performed. The MINIPULS® 3 Peristaltic Pump connected to 0.5 mm diameter tubes could be used to obtain the desired volumetric flow values within the 0.3 to 50 µL/h range, mimicking the LN flow rates.

Neither the PMMA material of the MC, nor the PET supporting membranes, alone or in conjugation, negatively affected CD4+ T cell viability and proliferation, being both good candidates as materials for the microfluidic device construction.

The potential effect of adding IL-2 to the complete RPMI was evaluated, leading to the conclusion that not using IL-2 in the circulating cell culture medium may be beneficial for the overall expansion of CD4+ T cells, by preventing a potential negative feedback loop.

Although the initial idea was to work with simultaneous triplicates in the same device (MC2 and MC3), after several optimization steps, it was concluded that the single-well MC4 would be a better version for the LN-on-a-chip construction to avoid contamination and leakages. Moreover, a new cap has been designed to ensure proper gas exchange.

In conclusion, the optimization of the design of the microfluidic device, the volumetric flow, the sterilization process, and the cell seeding conditions has been a complex process. However, it allowed to gather key information to have the best conditions for the successful development of a LN-on-a-chip with an expected lymphocyte expansion superior to the conventional static cell cultures. Experiments are currently in progress in our laboratory with this objective.

5.6. References

1. Terrell, J. A., Jones, C. G., Kabandana, G. K. M. & Chen, C. From cells-on-a-chip to organs-on-a-chip: scaffolding materials for 3D cell culture in microfluidics. *J. Mater. Chem. B* **8**, 6667–6685 (2020).

2. Tyers, M. & Mann, M. From genomics to proteomics. *Nature* **422**, 193–197 (2003).

3. Sakolish, C. M., Esch, M. B., Hickman, J. J., Shuler, M. L. & Mahler, G. J. Modeling Barrier Tissues In Vitro: Methods, Achievements, and Challenges. *EBioMedicine* **5**, 30–39 (2016).

4. Virumbrales-Muñoz, M. *et al.* Multiwell capillarity-based microfluidic device for the study of 3D tumour tissue-2D endothelium interactions and drug screening in co-culture models. *Sci. Rep.* **7**, 1–15 (2017).

5. Adriani, G., Ma, D., Pavesi, A., Kamm, R. D. & Goh, E. L. K. A 3D neurovascular microfluidic model consisting of neurons, astrocytes and cerebral endothelial cells as a blood–brain barrier. *Lab Chip* **17**, 448–459 (2017).

6. Jeong, S.-Y., Lee, J.-H., Shin, Y., Chung, S. & Kuh, H.-J. Co-Culture of Tumor Spheroids and Fibroblasts in a Collagen Matrix-Incorporated Microfluidic Chip Mimics Reciprocal Activation in Solid Tumor Microenvironment. *PLoS One* **11**, 1–17 (2016).

7. Adriani, G. *et al.* Microfluidic models for adoptive cell-mediated cancer immunotherapies. *Drug Discov. Today* **21**, 1472–1478 (2016).

8. Coluccio, M. L. *et al.* Microfluidic platforms for cell cultures and investigations. *Microelectron. Eng.* **208**, 14–28 (2019).

9. Cinamon, G., Shinder, V. & Alon, R. Shear forces promote lymphocyte migration across vascular endothelium bearing apical chemokines. *Nat. Immunol.* **2**, 515–522 (2001).

10. O'Melia, M. J., Lund, A. W. & Thomas, S. N. The Biophysics of Lymphatic Transport: Engineering Tools and Immunological Consequences. *iScience* **22**, 28–43 (2019).

11. Gashev, A. A. Physiologic aspects of lymphatic contractile function: current perspectives. *Ann. N. Y. Acad. Sci.* **979**, 178–196 (2002).

12. Dixon, J. B. *et al.* Lymph flow, shear stress, and lymphocyte velocity in rat mesenteric prenodal lymphatics. *Microcirculation* **13**, 597–610 (2006).

13. Blatter, C. *et al.* In vivo label-free measurement of lymph flow velocity and volumetric flow rates using Doppler optical coherence tomography. *Sci. Rep.* **6**, 1–10 (2016).

14. Jafarnejad, M. *et al.* Quantification of the Whole Lymph Node Vasculature Based on Tomography of the Vessel Corrosion Casts. *Sci. Rep.* **9**, 1–11 (2019).

15. Giese, C. *et al.* A human lymph node in vitro--challenges and progress. *Artif. Organs* **30**, 803–808 (2006).

16. Giese, C. *et al.* Immunological substance testing on human lymphatic micro-organoids in vitro. *J. Biotechnol.* **148**, 38–45 (2010).

17. Ross, A. E., Belanger, M. C., Woodroof, J. F. & Pompano, R. R. Spatially resolved microfluidic stimulation of lymphoid tissue ex vivo. *Analyst* **142**, 649–659 (2017).

18. Shim, S., Belanger, M. C., Harris, A. R., Munson, J. M. & Pompano, R. R. Two-way communication between ex vivo tissues on a microfluidic chip: application to tumor-lymph node interaction. *Lab Chip* **19**, 1013–1026 (2019).

19. Hallfors, N. *et al.* Multi-compartment lymph-node-on-a-chip enables measurement of immune cell motility in response to drugs. *Bioengineering* **8**, 1–15 (2021).

20. Radisic, M., Marsano, A., Maidhof, R., Wang, Y. & Vunjak-Novakovic, G. Cardiac tissue engineering using perfusion bioreactor systems. *Nat. Protoc.* **3**, 719–738 (2008).

21. Jones, N. *et al.* Metabolic Adaptation of Human CD4(+) and CD8(+) T-Cells to T-Cell Receptor-Mediated Stimulation. *Front. Immunol.* **8**, 1–12 (2017).

22. Ni, M. *et al.* Cell culture on MEMS platforms: a review. *Int. J. Mol. Sci.* **10**, 5411–5441 (2009).

23. Lei, K. F., Chang, C.-H. & Chen, M.-J. Paper/PMMA Hybrid 3D Cell Culture Microfluidic Platform for the Study of Cellular Crosstalk. *ACS Appl. Mater. Interfaces* **9**, 13092–13101 (2017).

24. Naskar, S., Panda, A. K., Kumaran, V., Mehta, B. & Basu, B. Controlled Shear Flow Directs Osteogenesis on UHMWPE-Based Hybrid Nanobiocomposites in a Custom-Designed PMMA Microfluidic Device. *ACS Appl. Bio Mater.* **1**, 414–435 (2018).

25. Malek, T. R. The main function of IL-2 is to promote the development of T regulatory cells. *J. Leukoc. Biol.* **74**, 961–965 (2003).

26. Sojka, D. K., Bruniquel, D., Schwartz, R. H. & Singh, N. J. IL-2 secretion by CD4+ T cells in vivo is rapid, transient, and influenced by TCR-specific competition. *J. Immunol.* **172**, 6136–6143 (2004).

27. Besser, M. J. *et al.* Modifying interleukin-2 concentrations during culture improves function of T cells for adoptive immunotherapy. *Cytotherapy* **11**, 206–217 (2009).

28. Kaartinen, T. *et al.* Low interleukin-2 concentration favors generation of early memory T cells over effector phenotypes during chimeric antigen receptor T-cell expansion. *Cytotherapy* **19**, 689–702 (2017).

29. Boyman, O. & Sprent, J. The role of interleukin-2 during homeostasis and activation of the immune system. *Nat. Rev. Immunol.* **12**, 180–190 (2012).

30. Villarino, A. V *et al.* Helper T cell IL-2 production is limited by negative feedback and STAT-dependent cytokine signals. *J. Exp. Med.* **204**, 65–71 (2007).

Chapter 6

Experimental section

6.1 Materials

The Biogelx™-S and Biogelx™-GFOGER peptide powder samples were bought from Biogelx (United Kingdom). All the collagen products, i.e. the collagen masses (Col1, Col2, Col3, Col4, Col5, Col6, Col7) and sterile collagen samples (dried collagen, collagen hydrogel and sponges) were obtained from Viscofan SA (Spain). A 10% w/v aqueous suspension of poly(methyl methacrylate) (PMMA) beads (78.3 ± 1.7 µm diameter) was purchased from microParticles GmbH (Germany). The 96 well plates were obtained from Greiner Bio-One International GmbH (Germany). The PVC tubes of 0.5 mm diameter (PVC Tubing for MF1 and MF4 pump head) that connect to the standard PVC tubes with two stoppers (PVC Pump Tubes Orange/Yellow) connected to the peristaltic pump were purchased from Gilson (United States of America). Transparent PET membranes with a pore size of 0.45 µm (ipCELLCULTURE™ track-etched membrane, ion track technology) were obtained from it4ip S.A. (Belgium) and PTFE membranes with a pore size of 0.45 µm were acquired from GVS North America, Inc. (United States of America). The 0.22 µm filters (Nalgene Syringe Nylon Filter) were bought from Thermo Fisher Scientific (United States of America) and the 1.6 mm tube connectors (female and male luer lock to hosebarb adapter) were acquired from Cole-Parmer GmbH (Germany). LS columns and the CD4+ T cell isolation kit were obtained from Miltenyi Biotec GmbH (Germany). Heparin (Hep) was purchased from Fisher Scientific (Spain). Fetal bovine serum (FBS), penicillin/streptomycin (P/S), CellTrace CFSE cell proliferation kit and Dynabeads were supplied by Thermo Fisher Scientific (United States of America). The anti-human CD3 FITC, CD4 PE, CD45RO FITC antibodies and their controls used for flow cytometry were bought from Immunotools GmbH (Germany), whereas CD62L PE and its control were bought from BioLegend (United States of America). Lymphoprep (also called Ficoll) was acquired from Stemcell Technologies (Canada). pH paper was obtained from Johnson Test

Papers Ltd (United Kingdom) and the pH meter HI 5221 from Hanna Instruments (United States of America). The dentistry glue Picodent Twinsil was purchased from Picodent (Germany). Trypsin-EDTA, propidium iodine (PI), thiolated PEG (PEG-SH) (Mn 10,000 g/mol), N-(2-aminoethyl) maleimide trifluoroacetate salt (AEM), 1-hydroxybenzotriazole hydrate (HOBT), N-(3-dimethylamino-propyl)-N-ethylcarbodiimide hydrochloride (EDC-HCl), 2-(N-morpholino) ethanesulfonic acid (MES), Dulbecco's phosphate bovine serum (PBS), RPMI-1640 media, and the rest of the products not otherwise specified were obtained from Merck (Germany).

6.2 Equipment

A R1 Medium Flow Pump Head (MINIPULS® 3 Peristaltic Pump, Gilson, Spain) was used to control the flow of complete RPMI medium in the MCs experiments. Proton nuclear magnetic resonance ^{1}H-NMR spectroscopy was performed in a 400 MHz Bruker Avance-III equipment (Bruker, United States of America). The incubator employed was acquired from Galaxy® 48 R, Eppendorf (Spain). The orbital shaker used was a Heidolph Unimax 1010 DT from Heidolph Instruments (Germany). The pH meter HI 5221 employed was from Hanna Instruments (Spain). Inductively coupled plasma mass spectrometry (ICP-MS) measurements were performed with a 7900 ICP-MS, Agilent Technologies, Inc. (United States of America) and the microwave oven used was from ultraWAVE, Milestone Srl. (Italy). Continuous wave electron paramagnetic resonance (cw-EPR) measurements were done with an ELEXSYS E500 from Bruker (United States of America). Flow cytometry experiments were performed with a BD FACSCanto (BD Biosciences, United States of America). The centrifuge used was a Frontier Centrifuge FC5515 (OHAUS, Sweden). A type II biological safety cabinet (MS2020 1.8, Thermo Fisher Scientific, United States of America) was used for cell culturing experiments. The fluorescence analyses were performed with a Leica TCS SP5 confocal microscope (Leica, Germany) and a Nikon Inverted Research Microscope ECLIPSE Ts2R (Nikon, Japan). SEM measurements were performed with a FEI Quanta 650F Environmental scanning electron microscope (Thermo Fisher Scientific, United States of America). The rheology experiments were done with a Rheometer HAAKE RheoStress RS600 (Thermo Fisher Scientific,

United States of America). A Skyscan 1272 high-resolution micro computed tomography (Bruker, United States of America) was used to evaluate the porosity and connectivity of the PEG-Hep hydrogels. Epilog Laser Mini 18 (Epilog Laser, United States of America) and a thermal press (PW10H, Paul-Otto Weber GmbH, Germany) were used to cut and bond the different layers of PMMA, respectively, for the assembly of the MCs. The functionalized Hep was lyophilized in a LyoQuest, Telstar (Spain). The cell counting was performed with a Neubauer chamber (Hirschmann, Germany).

6.3 Synthesis and chemical procedures

6.3.1 Biogelx sample preparation

To prepare the Biogelx hydrogels, we followed the "Biogelx Powder – Preparation and Guidelines for Use" document, which indicates the weight values of Biogelx Powder needed to prepare hydrogels of a certain stiffness. Thus, the lyophilized powder (Biogelx Powder) was rehydrated with water (or water/complete RPMI in the ratio 85/25) following gentle pipetting steps until forming a pre-gel solution. In the occurrence of bubbles, we applied vortex and sonication (30 s). If these procedures were not enough to remove the bubbles, a centrifugation step (300 g, 6 min) was applied.

In a typical cell culture experiment, 100 µL of pre-gel solution were added to the bottom of each sample well of a 96 well plate. Then, an incubation step of 15 min at 37°C and 5% CO_2 was performed. After the incubation step, 150 µL of complete RPMI containing calcium ions (100 or 200 mg/L $CaCl_2$) were slowly added to the pre-gel solution and another incubation (for least 2 h at 37°C and 5% CO_2) was performed to obtain the hydrogels. Finally, the cell culture medium remaining on top of the hydrogels was removed and the cells were added in a 2D seeding fashion.

6.3.2 Viscofan sample preparation

From the Viscofan S.A. company, we received collagen samples in non-sterile and acidic conditions (collagen masses: Col1, Col2, Col3, Col4, Col5, Col6 and Col7), as well as sterile samples (DC, CH and "sponge").

- **Non-sterile collagen samples:** Upon reception, we performed a sterilization step under UV light for 1 h. Then the masses were divided in different 15 mL sterile "falcons" that were frozen (-20˚C) until use. The frozen samples were used only one time, in order to avoid contamination from handling and multiple freeze-thawing steps. When the collagen samples were needed to perform experiments, they were thawed and then the neutralization process was performed. This process consisted of soaking a portion of the masses with sodium hydroxide (NaOH) at 0.05 M for 30 min. This step was followed by 3 washes with PBS, followed by UV irradiation for 1 h more. Then the masses were cut and placed inside a 96 well Teflon template at pH 6-7. Then, the masses were hydrated in cell culture complete RPMI medium (200 µL) and incubated for at least one day (37˚C and 5% CO_2). Then, their pH was measured with a pH meter confirming the neutralization step.

- **Sterile collagen samples:** The DC and CH samples were sterile and provided to us in separated 96 well plates for a single use. These well plates were stored at -20˚C until cell seeding. One day before cell seeding, the well plates containing DC and CH samples were placed at 4˚C. Both samples were hydrated for at least 3 h with 200 µL of complete RPMI. After the hydration time, the samples were ready to be used after a washing step in cell culture medium.

  The "sponge" samples were provided to us in sterile bags, which were kept at 4˚C until use. When needed for cell culture experiments, the sponges were placed inside the 96 well plates and hydrated with 200 µL of complete RPMI overnight. After a washing step with the same cell culture medium, samples were used for cell culture.

6.3.3 Heparin functionalization with maleimide

A Michael-type reaction was used to functionalize the Hep with a maleimide (Mal) group yielding a Mal-Hep derivative.[1,2] Hep was dissolved in MES buffer and AEM, HOBT and EDC-HCl were added. The reaction was left overnight, and the product was purified using a dialysis membrane (MWCO 1000) with distilled and MiliQ water. After freezing the product at -80˚C, Mal-Hep was lyophilized and characterized by ^{1}H-NMR.

6.3.4 Synthesis of bulk PEG-Hep hydrogels

PEG-Hep hydrogels were formed through a maleimide-thiol reaction between the Mal-Hep derivative and a 4-arm PEG-SH (ratio of 1.5:1) in PBS. After the solutions were mixed, they were kept at 37°C in the incubator during a minimum of 1 h. This resulted in a covalent crosslink and the consequent hydrogel formation with 3% wt of PEG,[3] as demonstrated with control experiments with only one of the two reactants (Mal-Hep or 4-arm PEG-SH) at the same concentration used for the fabrication of 3% PEG-Hep hydrogels. For the characterization techniques X-ray tomography and rheology, bulk PEG-Hep hydrogels were formed by adding 100 µL of Mal-Hep with PEG-SH solution to a 1.5 mL Eppendorf cap that was used as a template. In the case of cell studies, the volume of each bulk hydrogel used was of 30 µL added to a home-made Teflon template. This template has 5 mm-diameter wells glued with Picodent Twinsil on a metallic surface. Once formed, the bulk hydrogels were removed from the templates and washed 3 times with PBS and left in the same buffer until use.

6.3.5 Synthesis of IOPAL PEG-Hep hydrogels

100 µL of PMMA bead suspension were added in the 5 mm-diameter Teflon template wells and left 24 h for solvent evaporation and OPAL formation. Then, 30 µL of PEG-Hep mixture (prepared as described previously) were added on top of the formed OPAL and left to infiltrate in order to

form the hydrogel for at least 48 h in an incubator (37˚C, 5% CO_2). Afterwards, the OPAL-PEG-Hep hybrid hydrogels were removed from the template and the PMMA beads were degraded by introducing the hybrids in glacial AcOH for 72 h with agitation in the orbital shaker (150 rpm) and heating (40˚C). Finally, IOPAL hydrogels were removed from AcOH and washed three times with PBS. After 1 h of UV sterilization, IOPAL hydrogels were washed again with complete RPMI medium and incubated until seeding at 37˚C. For the characterization techniques X-ray tomography and rheology, larger IOPAL PEG-Hep hydrogels were formed by adding 333 µL of PMMA bead suspension to a 1.5 mL Eppendorf cap. After OPAL formation, 100 µL of fresh PEG-Hep mixture was added on top. The following steps are analogous to the previously described ones for 30 µL hydrogels. In this case though, after the 3 washes with PBS, the IOPAL hydrogels were left in PBS until measurements.

6.4 Biological techniques and protocols

6.4.1 PBMC isolation and primary human CD4+ T cell purification

The buffy coats used for this research were obtained from human donors from “Banc de Sang i Teixits” (Barcelona, Spain) after the approval of the “Ethics Committee on Animal and Human Experimentation” of the Autonomous University of Barcelona (UAB; Nrs. 4951 and 5099). The buffy coats are a fraction of an anticoagulated blood containing most of the white blood cells and platelets, and for such reason PBMCs were possible to be extracted by density gradient centrifugation using a separation medium (Ficoll). In detail, the buffy coats received were diluted with PBS with 2 mM of EDTA at 37°C in a proportion of 1:4. This diluted blood was then placed carefully on top of the Ficoll in 50 mL “falcons” forming two phases as exemplified in **Figure 6.1**, in a 2:1 ration. Then a centrifugation during 20 min at 300 g at 20°C was performed, leading to a white phase just below the supernatant (plasma), consisting of PBMCs, as exemplified in **Figure 6.1**.

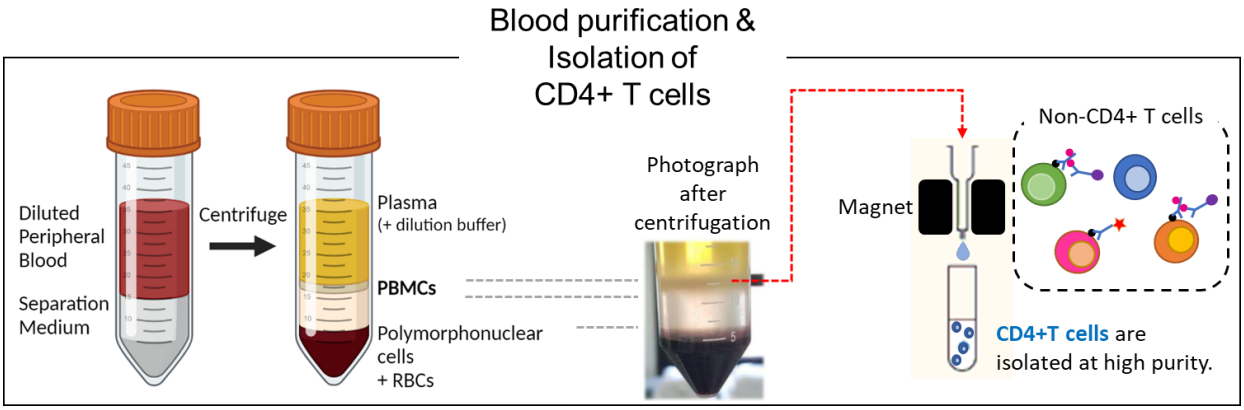

Figure 6.1 Blood purification and isolation of primary human CD4+ T cells. Scheme and photograph of the different phases resulting after the centrifugation of the blood with Ficoll, followed by the human CD4+ T cell isolation step through magnetic separation.

The PBMCs phase was then collected and washed three times with PBS with 2 mM of EDTA and further centrifuged 300 g for 10 min at 20°C. Next, the obtained PBMCs were counted with a Neubauer chamber.

To further select the CD4+ T cells population from the PBMCs, a human CD4+ T cell isolation kit was utilized. The isolation kit contains a "biotin-antibody cocktail" with antibodies against CD8, CD14, CD15, CD16, CD19, CD36, CD56, CD123, TCR γ/δ and CD235a (Glycophorin A), which are used to label non-CD4+ T cells, such as CD8+ T cells, B cells, NK cells, monocytes, neutrophils, eosinophils, dendritic cells, granulocytes, γ/δ T cells and erythroid cells. Another component of the kit is the CD4+ T cell "microbead cocktail", consisting of magnetic microbeads conjugated to the monoclonal anti-biotin which bind all the previously labeled non-CD4+ T. After incubation with "biotin-antibody cocktail" and "microbead cocktail", the cell suspension was added to a LS column attached to a strong magnet. The LS column allows the fast passage of CD4+ T cells while retaining the magnetically labelled cells.

To verify the purity of the CD4+ T cells obtained, cell suspensions were prepared in PBS + 0.1% FBS that were further stained (30 min at 0°C, in the dark) with antihuman CD3 FITC, antihuman CD4 PE and their negative controls. After washing, CD4+ T cells were analyzed by flow cytometry.

The viability of the cells analyzed after this purification protocol was usually > 90%, and their purity (CD3+CD4+ T cells) usually > 95%. It is also important to mention that we only accepted to work with purity value of at least 90%.

6.4.2 Cell seeding, culture and recovery

CD4+ T cell seeding and culture in a 2D fashion: In a typical cell culture experiment, 50 µL of a CD4+ T cell suspension at a concentration of $2x10^6$ cells/mL (10^5 cells/well) were seeded on top (2D fashion) of the Biogelx, Viscofan, bulk or IOPAL PEG-Hep hydrogels in a 96-well plate together with Dynabeads (1:1 ratio). Afterwards, 50 µL of complete RPMI medium were added and the suspension was gently mixed. Then, cells were left in an incubator (37˚C, 5% CO_2). Two days after cell seeding, 100 µL of complete RPMI medium was added to each well. The cells were finally left in the incubator until differentiation or cell viability analysis on day 5, or proliferation analysis on day 6.

Samples seeded inside the microfluidic devices were resuspended in 180 µL of complete RPMI medium the same day of the cell seeding. Moreover, they did not receive the extra 100 µL of cell media on day 2.

Negative (without Dynabeads and hydrogels) and positive controls (without hydrogels) were seeded following the same procedure. Each condition was seeded in triplicate.

CD4+ T cell seeding and culture in a 3D fashion: In Chapter 2, a 3D seeding approach was evaluated with the Biogelx samples. Specifically, the required amount of cell suspension in complete RPMI was centrifuged during 6 min at 300 g. After centrifugation, approximately 90% of the supernatant was removed, leaving about 10% to resuspend the pellet. Then it was added the required volume of pre-gel solution to obtain a final concentration of 5M cells/mL. A volume of 100 µL of the mixture pre-gel/cell suspension was used for the formation of the hydrogel at the bottom of a 96 well plate.

Then, similarly to the 2D seeding fashion used for the Biogelex hydrogels, we placed the well plate containing the pre-gel/cell solution in the incubator at 37˚C and 5% CO_2 for 15 min. After this time, 150 µL of cell culture medium was added on top dropwise, and incubated (37˚C, 5% CO_2). Two days after cell seeding, 100 µL of complete RPMI medium was added to each well, and cells were incubated (37˚C, 5% CO_2) until proliferation analyses.

Cell recovery: In a typical experiment, the cells were recovered mechanically, with several gentle resuspensions, in order to collect the maximum CD4+ T cells possible from the scaffolds used. Once collected, the cells were centrifuged (300 g, 6 min) and the supernatant was discarded. The cells were resuspended in 400 µL of FACS buffer (PBS + 0.1% FBS), being ready for flow cytometry analyses.

In Chapter 2, we also tried to collect the cells chemically with the Biogelx hydrogels by the use of trypsin (0.05% trypsin-EDTA) in addition to the gentle resuspensions. During 2 min, the Biogelx hydrogels were incubated (37˚C, 5% CO_2) in the presence of 200 µL of trypsin solution. After this time, a few more gentle resuspensions were performed. The cells were then collected and centrifuged (300 g, 6 min) and the supernatant was discarded. Finally, the cells were prepared for flow cytometry analyses as mentioned above.

6.4.3 Proliferation analyses

For proliferation studies, we used a CellTrace CFSE cell proliferation kit to stain the purified CD4+ T cells, just before their seeding. The staining solution is achieved by diluting 1 µL of CFSE stock solution in 99 µL of PBS with 5% of FBS. The CD4+ T cells to be stained were resuspended in PBS with a final volume of 900 µL. Then both, the staining solution (100 µL) and the cell suspension (900 µL) were mixed through rapid agitation in a vortex and incubated for 5 min at RT in the dark. Then, 10 mL of ice-cold PBS with 5% of FBS was incorporated with the objective of quenching the

staining. Finally, a last centrifugation (300 g, 10 min) was performed, the supernatant removed, and the CD4+ T cells resuspended in complete RPMI medium at the required concentration. Non-stained cells were also seeded as negative control. 6 days after cell seeding, the Dynabeads present on samples with activated cells, needed to be removed with a magnet prior to the CD4+ T cell proliferation analysis.

6.4.4 Differentiation analysis

The phenotypes resulting after 5 days of culture were analyzed by cell staining with the CD62L/CD45RO antibodies. The Dynabeads present on samples with activated cells, needed to be removed with a magnet prior to the staining step. The experiment was performed with the antibodies antihuman CD62L PE and antihuman CD45RO FITC, and their negative controls. Next, cells were centrifuged, resuspended in PBS with 0.1% FBS, and incubated with the antibodies (2.5 µl for the CD45RO and its control, and 1 µl for the CD62L and its control) for 30 min in ice and in the dark. Finally, the cells were washed and analyzed by flow cytometry.

6.4.5 Cell viability

The PI viability test was performed by staining the primary human CD4+ T cells with 0.5 µL of PI (1 mg/mL) during 3 min at RT before the flow cytometry measurements.

6.4.6 Confocal microscopy

The 3D images showed in Chapter 4 were obtained with a Leica confocal microscope equipped with 10X objectives, on day 5. They show CD4+ T cells inside an IOPAL PEG-Hep hydrogel in a measurement volume of 1.5 mm x 1.5 mm x 0.4 mm.

6.4.7 Fluorescence microscopy

The fluorescence analyses were carried out on the same 96 well plate where the cells were normally seeded. Furthermore, since we stained the cells with CSFE for proliferation analyses, we could directly observe them under the fluorescent microscope. For these experiments, the cells at the concentration of 10^6 cells/mL were cultured in suspension together with Dynabeads for the positive control, or without Dynabeads in the case of negative control. Similarly, cells were seeded at the same concentration on top of the hydrogels.

6.5 Physicochemical characterization

6.5.1 Environmental scanning electron microscopy (ESEM)

SEM is a technique used to examine the morphology of the surface and cross-section of various samples. It is a very common technique specially for dry samples under vacuum conditions, but to measure hydrogels, a special protocol and equipment are required. The ESEM equipment used was a versatile field emission scanning electron microscope, which provides high resolution imaging at high vacuum, low-vacuum and extended vacuum. These characteristics allow the characterization of all type of samples (conductive, non-conductive and wet samples). Therefore, the structure of the different hydrogels was possible to be analyzed with the “environmental mode”. In this mode, both pressure and temperature are slowly decreased to enable to image the structure of the hydrated samples.

6.5.2 Inductively coupled plasma mass spectrometry (ICP-MS) measurements

These measurements were performed by the “Servei d'Anàlisi Química” (SAQ) of UAB. ICP-MS is a type of mass spectrometry that uses an inductively coupled plasma to ionize the sample, creating atomic and small polyatomic ions, which are then detected.

Our collagen samples, which were all around 50 mg, were digested with a mixture of concentrated HNO_3 and HCl in a microwave oven prior the measurement.

6.5.3 Continuous wave electron paramagnetic resonance (cw-EPR) measurements

EPR is a spectroscopy method used in the study of materials with unpaired electrons, especially useful for the detection of organic radicals. The continuous wave (cw) EPR technique operates at the X-band frequency (~9 GHz frequency), and it is designed to optimize weak magnetic resonance signals. In our case, the collagen hydrogels were put into a flat cell and measured at RT with a Bruker ELEXSYS E500 setup using 2 mW of microwave power, 0.2 mT and 100 kHz modulation frequency.

6.5.4. Rheology

Small amplitude oscillation technique (SAOS) was used to characterize the mechanical properties of the IOPAL hydrogels. Strain and frequency sweeps were performed at 37˚C to obtain the G' and the G'' in the LVE. The equipment was used with a 10 mm diameter rotor. For the strain sweeps we used a constant frequency of 1.0 Hz and the shear stress was swept from 1 Pa to 50 Pa. For the frequency sweeps we used a constant shear stress of 50 Pa and the frequency was ranged from 0.01 Hz to 1.0 Hz.

6.5.5 X-ray microtomography

We used X-ray microtomography to study the 3D structure of the IOPAL PEG-Hep hydrogels and analyze the porosity, in terms of pore diameter and interconnectivity of the pores. The samples stored in PBS were frozen with liquid nitrogen and then lyophilized before the analysis. The

scanning time was 3 h with a minimum resolution of 5 µm, without any filter and with a peak voltage of 40-50kV. The connectivity density was calculated, by dividing the connectivity value by the volume of interest (VOI).

6.6 Microfluidics design and fabrication

6.6.1 Microfluidic LN-on-a-chip experimental design

Four MCs were designed and fabricated in collaboration with Dr. Mar Álvarez and Prof. Rosa Villa (Biomedical Applications Group, GAB) at the Barcelona Institute of Microelectronics - National Microelectronics Center (IMB-CNM-CSIC). The MC prototypes used were a result of several rounds of redesign, containing all of them culture wells of 8 mm in depth and 6.58 mm in diameter. The MC1 was fabricated with 4 culture wells, the MC2 and MC3 with 3 cultures wells, while MC4 had only a single well. Regarding their dimensions, MC1 was 45x35 mm, MC2 was 90x20 mm, MC3 was 40x45 mm and MC4 was 40x20 mm.

All MCs fabricated consisted in a base, built of 4 layers of PMMA with a thickness of 2 mm in the three bottom layers and 8 mm for the upper one; and a cover, with a 1 mm-thickness adhesive silicone layer and a 3 mm thickness layer of PMMA on top. More detailed information about the design of each layer is presented in **Figure 6.2**.

The PMMA and the silicone layers were cut in a laser machine. For the assembly of all the layers to form the MC, a thermal press (at 20 kN, 80˚C, 45 min) was employed with isopropanol to improve the bounding. To be able to connect the tubes responsible for the circulation of cell culture medium, inlet and outlet ports were glued on the top layer. Finally, the MCs could be properly closed by the used of screws.

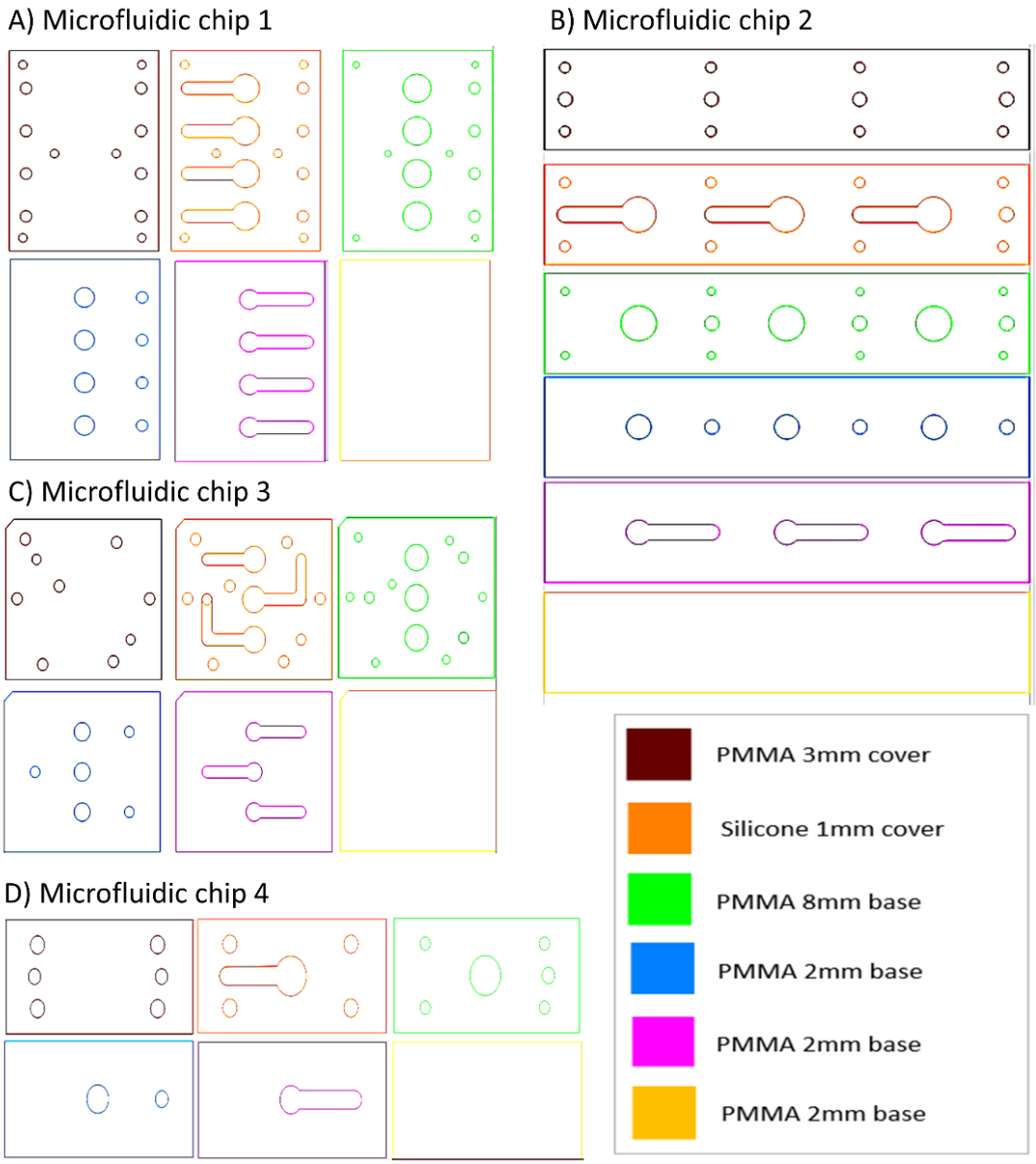

Figure 6.2 Design and composition of the different layers of the MCs. A) MC1, B) MC2, C) MC3 and D) MC4 designs. The colour indicates the material composition and thickness of the layers used for each MC.

Furthermore, to hold the hydrogels, T cells and Dynabeads inside the culture wells, while allowing the pass of cell culture medium, porous membranes cut with the same diameter as the culture wells in the same laser machine, were glued to the bottom of the well with a double tape o-ring.

6.6.2 Sterilization of microfluidic components

The cleaning and sterilization of the MCs included the external cleaning of the chip with a towel paper soaked with small amounts of 70% ethanol and abundant MilliQ water; the flow of MilliQ water through the wells and the inner channels; the UV sterilization for at least 1 h and finally the flow of sterile PBS to clean the inner connections of the MCs.

To clean the PVC tubes, they were firstly immersed in 70% ethanol for 10 min, and then 20 mL of 70% ethanol and MiliQ water were pumped through them with a syringe. Finally, they were sterilized using UV during 1 h. The porous PET membranes were also sterilized during the same UV time (30 min on each side).

6.6.3 Microfluidic setup

Preceding the sterilization, 0.5 mm diameter PVC tubes were cut to the desired length to obtain the experimental setup shown in **Figure 6.3**. To prevent the tubes from sliding during the working time of the peristaltic pump, a tube with two stoppers (the so-called standard tube (ST)) was used on the pump head. This tube was further connected by using 1.6 mm tube connectors to the other PVC tubes, the one arriving (1st tube) and the one leaving (2nd tube) the peristaltic pump as schematized in **Figure 6.3**. After sterilization, all tubes were filled with complete RPMI medium using a syringe.

PET membranes were glued inside the microfluidic culture wells, and then, they were cleaned and hydrated with sterile PBS. After 1 day, PBS was removed, and the MCs were carefully filled with complete RPMI medium using a syringe to avoid air bubbles in the inner channels. Then, the RPMI medium was removed from the culture wells and the previously synthetized PEG-Hep hydrogels were placed inside the wells.

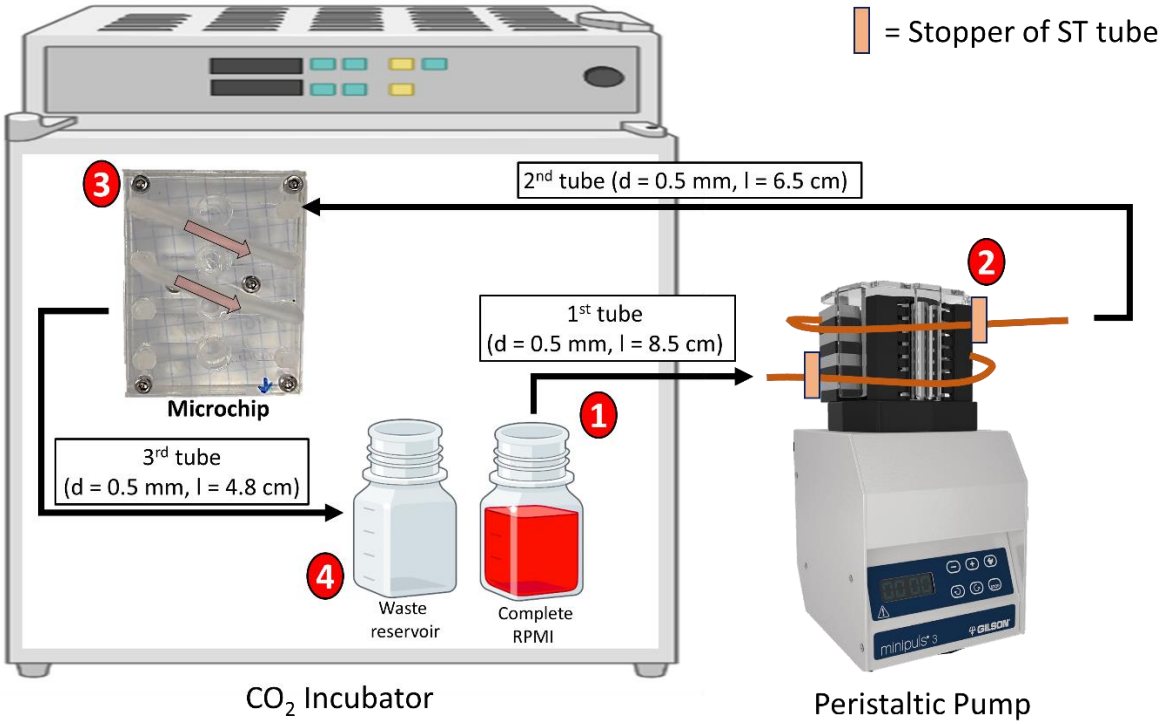

Figure 6.3 Scheme of the microfluidic LN-on-a-chip setup. The 3 different 0.5 mm diameter PVC tubes with different lengths used to connect all the components are described. Inside the CO_2 incubator are both reservoirs and the MC, while outside, is the peristaltic pump used to pump cell culture medium, following the direction 1 to 4, as exemplified. The ST tube with stoppers is also schematized with an orange line on the peristatic pump head.

After cell seeding (described in section 6.4.2), the MCs were closed, the tubes were connected and introduced inside the incubator at 37˚C and 5% CO_2, as exemplified in **Figure 6.3**. Both medium and waste reservoirs were also introduced inside the incubator. A 0.22 µm filter was added in the cap of the medium reservoir to allow gas exchange. Outside the incubator, the peristaltic pump was pumping complete RPMI medium at 0.04 rpm for 6 days.

6.7 Data treatment and statistical analyses

The PMMA layers were designed using the CorelDRAW X7 software from Corel Corporation, Canada (**Figure 6.2**). Cell viability, proliferation and differentiation data analyses were carried out with the FlowJo software (FlowJo LLC, BD, United States of America). Data processing was performed with OriginPro (OriginLab Corp. United States of America), using a non-parametric Mann Whitney U-test to evaluate the statistical significance among different conditions that included human donors. For the pore size distributions, the statistical significance was determined by a Kruskal-Wallis test. When box plots were described, the boxes correspond to the interquartile range defined by the 25th and 75th percentiles, the whiskers show 1 standard deviation, □ is the average, and the central line is the median.

6.8 References

1. Nie, T., Baldwin, A., Yamaguchi, N. & Kiick, K. L. Production of heparin-functionalized hydrogels for the development of responsive and controlled growth factor delivery systems. *J. Control. Release* **122**, 287–296 (2007).

2. Nie, T., Akins, R. E. & Kiick, K. L. Production of heparin-containing hydrogels for modulating cell responses. *Acta Biomater.* **5**, 865–875 (2009).

3. Pérez Del Río, E. *et al.* CCL21-loaded 3D hydrogels for T cell expansion and differentiation. *Biomaterials* **259**, 1–13 (2020).

Summary and outlook

This doctoral thesis has focused on the use of natural and synthetic hydrogels as scaffolds to improve the current immune cell expansion methods. This main goal was settled to improve current limitations of immunotherapies, related with the production of large amounts of specific T cells in a short period of time, while making the process more economically affordable. Different materials were studied for the development of a suitable 3D scaffold that would mimic the ECM of the LNs to sustain and expand T cells, while obtaining clinically relevant phenotypes.

Synthetic hydrogels comprising a nanofibrous network were used from the SME Biogelx company. Two different samples were studied for the culture of primary human CD4+ T cells, the Biogelx^{TM}-S and the Biogelx^{TM}-GFOGER. The first one is the standard hydrogel, which does not mimic any natural protein, whereas the second one includes a peptidic sequence that is present in collagen. Despite the in-depth optimization of the hydrogel conditions for cell culture, including the stiffness of the hydrogels, cell density, hydrogel formation step and cell recovery method, no proliferation was achieved. In fact, the synthetic peptides used to produce the hydrogels were found cytotoxic for the culture of human CD4+ T cells.

In another industrial collaboration, collagen scaffolds were provided by the publicly-traded company Viscofan S.A. Several collagen samples including the collagen masses, DC, CH, and collagen sponges, were evaluated for T cell proliferation and differentiation of adult donors. In this case, the sample CH showed a median value of replication index 2.1 times higher than the positive control. However, the reproducibility of this sample remains a challenge to be overcome. The collagen sponge has also found to promote an improvement in CD4+ T cell expansion, while not altering the phenotype obtained when compared with the positive control. These sponge samples are expected to have a higher reproducibility than the CH samples from the fabrication point of view as indicated by the Viscofan team, and thus, it is a very promising scaffold for immune cell expansion.

With the same goal of improving the current methodologies of human T cell expansion and facilitate the introduction of ACT in the clinics, we proposed to use an IOPAL strategy to achieve a controllable pore size and a well-interconnected structure in our previously reported PEG-Hep hydrogels.[1] These IOPAL hydrogels were characterized in terms of morphology and mechanical properties, but also as a culture system able to expand clinically relevant human CD4+ T cells. It was found that the IOPAL PEG-Hep hydrogels not only contributed to an improvement in cell proliferation when compared to the state-of-the-art methodologies, but also when compared to their bulk form. Moreover, we demonstrated the capacity of such IOPAL hydrogels to augment the T_{CM} phenotype percentage in comparison with the bulk hydrogel, while maintaining it in comparison with the positive control.

Finally, several efforts were focused on the design and fabrication of a LN-on-a-chip with a net unidirectional pulsatile fluid flow, that passes through a 3D hybrid hydrogel at a volumetric flow of 0.3 – 50 µL/h. After several optimizations involving the design and material of the chip, the membranes used to support the 3D hydrogels, the setup of the peristaltic pump to obtain the desired flow, the cell seeding conditions, the influence of cytokine supplementation and the sterilization procedures, we gathered valuable information for the fabrication of a LN-on-a-chip. Preliminary experiments of primary human CD4+ T cell culture in the microfluidic device using our IOPAL PEG-Hep hydrogels resulted in cell proliferation. However, contamination-related issues led to a new MC design, which is now being tested in our laboratory.

As per bellow, the best conditions found on each chapter of this thesis for the expansion of primary human CD4+ T cells are compared (**Figure S.1**). For better comparison the results shown are normalized to the positive control. As explained, no CD4+ T cells proliferation was obtained with the hydrogels from the SME Biogelx company. However, the CH samples and both bulk and IOPAL PEG-Hep hydrogels improved cell proliferation when compared to the state-of-the-art methodologies, with normalized (median) replication indexes of 2.09, 1.29 and 1.63, respectively.

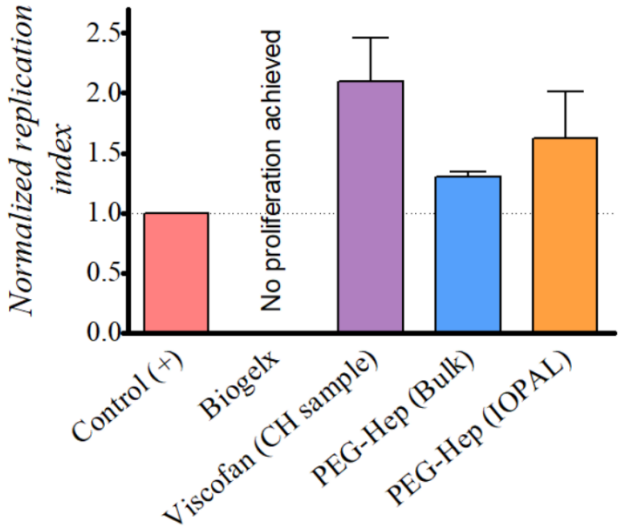

Figure S.1 Normalized replication index values from the best conditions found on each 3D hydrogel (with Dynabeads) used on this doctoral thesis for culturing and expanding primary human CD4+ T cells. Biogelx (no proliferation was achieved), Viscofan with CH sample (N_{donors} = 6), and PEG-Hep hydrogels in both, bulk and IOPAL forms (N_{donors} = 7). Control + represents CD4+ T cells cultured in suspension in the presence of Dynabeads.

Finally, it is also worth mentioning that the work presented in this doctoral thesis will be continued. Not only there are research projects to be finalized such as the LN-on-a-chip, but also there are new research paths to be explored. In the next paragraphs, there is an outlook of the work already ongoing in our lab as well as future insights divided in three main topics:

a) Immune cell migration in 2D platforms under electric fields towards clinical applications

Understanding the mechanism of cell migration and interaction with the microenvironment is not only of critical significance to the function and biology of cells, but also has extreme relevance and impact on physiological processes and diseases such as morphogenesis, wound healing, neuron guidance and cancer metastasis.[2] External guidance factors such as topography, chemical and mechanical cues of the microenvironment can result in specific changes in cell motility and

signaling mechanisms, as previously demonstrated by us in collaboration with Prof. Dr. Kemkemer's research group (Reutlingen University, Germany)[3] and others.[2,4]

In the group of Prof. Dr. Kemkemer studies have shown that cells can (actively) respond to applied electric fields (EFs) with directed migration, a phenomenon called electrotaxis. The directed cell migration is crucial for various physiological processes, and the precise manipulation of cell migration of very specific cell types would be extremely useful for the treatment of various diseases. With this in mind, targeting leukocyte migration remains a principal strategy to target enhanced or moderated immune responses towards the treatment of inflammatory disorders or cancer.[2,4] The group of Prof. Kemkemer is aiming at specifically manipulating the cell behavior of different immune cells (mainly T lymphocytes, such as CD4+ and CD8+ T cells) with small exogenous EFs in the range of physiological EF strengths (5-20 V).

I had the opportunity during my international short stay, to work in a project combining the expertise of the group of Prof. Kemkemer on modulating the migration of lymphocytes by EFs in 2D environments with my research group expertise on studying the effect of artificial ECMs on T cell viability, proliferation and differentiation. More specifically, the goal of the short stay was to study primary human CD4+ T and CD8+ T cell differentiation on 2D substrates under different EF (5-20 V) and cell-adhesive ECM protein (fibronectin and ICAM-1) coatings.

As shown in **Figure S.2 A**, the commercially available channel (Ibidi µ-Slide I, Cat.No:80106) was coated with fibronectin or ICAM-1. On the coated surfaces, previously purified and activated CD4+ T cells or CD8+ T cells were incubated at 37˚C and 5% CO_2 for 24 h. Then the electrodes were placed inside the channel as shown in **Figure S.2 B**, and the EF was applied (5V or 20V) for 1 h. The experimental setup to submit the cells to an EF is shown in **Figure S.2 C**. After the EF, the channels with the cells were further incubated for 3 days, until differentiation analyses.

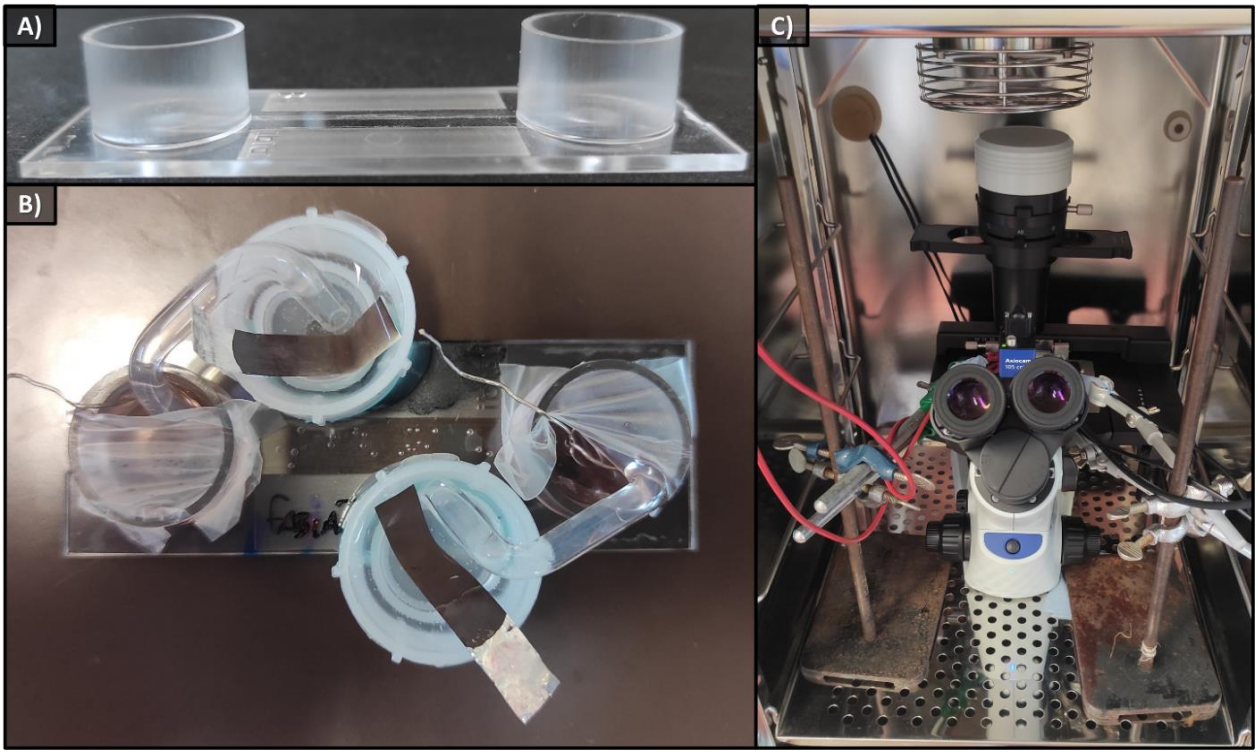

Figure S.2 A) Ibidi µ-Slide I before coating and cell seeding steps. B) Ibidi µ-Slide I just before EF stimuli, with the electrodes and the agar bridges. C) Experimental set up for the EF stimuli.

The phenotypes of the expanded primary human CD4+ T and CD8+ T cells were analyzed (**Figure S.3**) after 8 days of culture. In particular, the subpopulations of T_N (CD45RO−/CD62L+), T_{EM} (CD45RO+/CD62L−), T_{EFF} (CD45RO−/CD62L−) and T_{CM} (CD45RO+/CD62L+) were quantified by flow cytometry.

As shown in **Figure S.3 A**, we could see a tendency on the effect of the EF on the differentiation of both, CD4+ and CD8+ T cells, when seeded on fibronectin-coated substrates. Specifically, a higher percentage of T_{CM} was obtained on both cell types when using EF (5V and 20V). However, experiments with more donors are currently being performed in Prof. Kemkemer's lab, with the objective to statistically confirming the results.

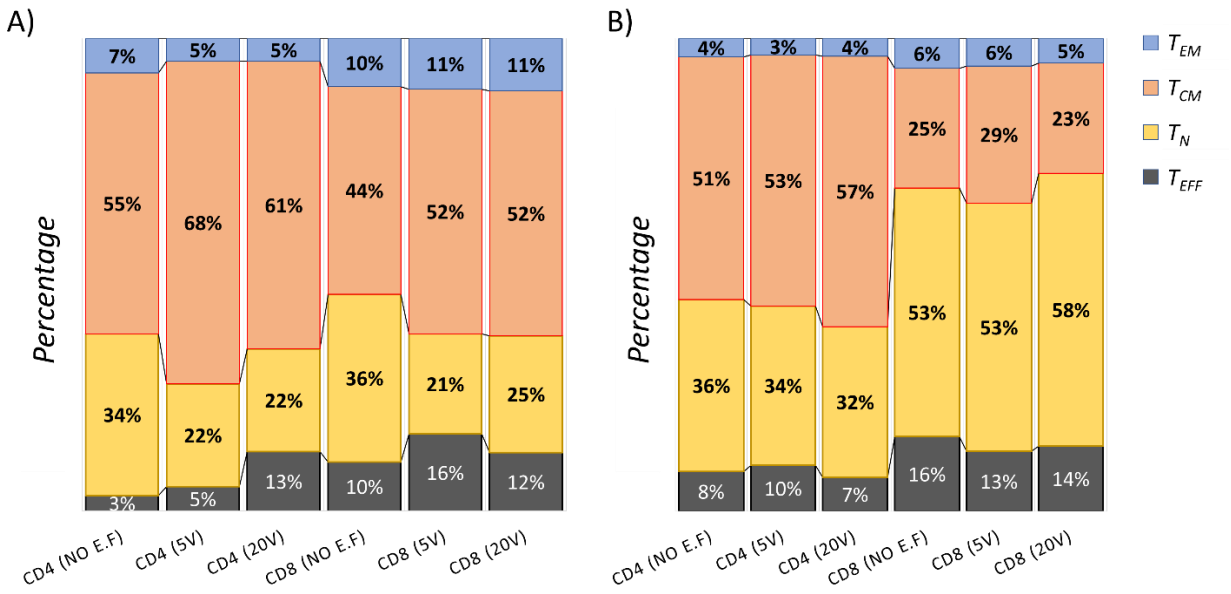

Figure S.3 T cell differentiation experiments with 2D surfaces coated with A) fibronectin (N_{donors} = 4) and B) ICAM-1 (N_{donors} = 1), showing the percentages T_N, T_{EM}, T_{EFF} and T_{CM} of CD4+ and CD8+ T cells on day 8.

Similarly, we also evaluated the effect of EF on CD4+ and CD8+ T cell differentiation, when cells were seeded on substrates coated with ICAM-1 coating (**Figure S.3 B**). Although more experiments are also being performed to have more representative data, the effect of the EF when using ICAM-1 was not so evident as in the case of fibronectin (**Figure S.3 A**). In fact, the CD8+ T cells mainly showed T_N in contrast with the T_{CM} found when using fibronectin.

So far, these promising results are in accordance with literature, since fibronectin is known to play a major role in cell adhesion, growth, migration and differentiation.[5] On the other hand, ICAM-1 is a known ligand for the integrin LFA-1, a receptor mainly found on APCs.[6]

b) PEG-Hep hydrogels (bulk and IOPAL) for CAR T cell expansion

As mentioned in the introduction, CAR T cells are achieving impressive results, especially in hematological cancers. Thus, we decided to evaluate CAR-T cell expansion using our PEG-Hep hydrogels after the positive results observed with CD4+ T cells. Initial experiments have already started in collaboration with the Institut d'Investigacions Biomèdiques August Pi i Sunyer (IDIBAPS) at the Hospital Clinic de Barcelona (Spain).

c) PEG-Hep hydrogels for the formation of clinically relevant organoids

Another potential application of our PEG-Hep hydrogels is to be used as platforms for organoid culture. Organoids are 3D multicellular in vitro systems that can mimic key structural or functional characteristics of real organs.[7] Very recently, our PEG-Hep hydrogels started to be explored by some (pre)clinical groups of IDIBAPS and collaborators. This is a very exciting application to further expand the possibilities of our hydrogels.

Scientific contributions

Patents:

Title registered industrial property: EUROPEAN PATENT: A synthetic hydrogel and its use for immunotherapy and 3D-printing.
Inventors/authors/obtainers: Eduardo Pérez del Río; Fabião Santos; Xavier Rodriguez Rodriguez; Marc Martinez Miguel; Miguel Angel Timoneda; Elisabeth Engel; Jaume Veciana; Imma Ratera; Judith Guasch.
Nº of application: 20382432.1-1118 **Date of register:** 21/05/2020

Title registered industrial property: EUROPEAN PATENT: An IOPAL hydrogel and its different uses for immunotherapy.
Inventors/authors/obtainers: Fabião Santos; Eduardo Pérez del Río; Miquel Castellote Borrell, Jaume Veciana; Imma Ratera; Judith Guasch.
(To be filed soon)

Publications:

- Peréz del Rio, E.; Santos, F.; Rodriguez, X.; Martínez, M.; Roca, R.; Arís, A.; Garcia, E.; Veciana, J.; Spatz, J.; Ratera, I; and Guasch, J. CCL21-loaded 3D hydrogels for T cell expansion and differentiation. *Biomaterials*. **259**, 1 – 13. (2020).
- Santos, F.; Valderas, J.; Perez del Río, E.; Castellote-Borrell, M.; Veciana, J.; Ratera, I; and Guasch, J. (2021) Enhanced human T cell expansion with inverse opal hydrogels. (Submitted).
- Santos, F.; Perez del Río, E.; Martínez, M.; Rodriguez, X. R.; Ávila, G.; Veciana, J.; Ratera, I., and Guasch, J. (2022) Immune cell activation and expansion in 2D and 3D systems and their applications in the clinics. (To be submitted soon).

References

1. Pérez Del Río, E. *et al.* CCL21-loaded 3D hydrogels for T cell expansion and differentiation. *Biomaterials* **259**, 1–13 (2020).

2. Thrivikraman, G., Boda, S. K. & Basu, B. Unraveling the mechanistic effects of electric field stimulation towards directing stem cell fate and function: A tissue engineering perspective. *Biomaterials* **150**, 60–86 (2018).

3. Sales, A. *et al.* Cell Type-Dependent Integrin Distribution in Adhesion and Migration Responses on Protein-Coated Microgrooved Substrates. *ACS Omega* **4**, 1791–1800 (2019).

4. Cortese, B., Palamà, I. E., D'Amone, S. & Gigli, G. Influence of electrotaxis on cell behaviour. *Integr. Biol. (Camb).* **6**, 817–830 (2014).

5. Pankov, R. & Yamada, K. M. Fibronectin at a glance. *J. Cell Sci.* **115**, 3861–3863 (2002).

6. Yang, L. *et al.* ICAM-1 regulates neutrophil adhesion and transcellular migration of TNF-alpha-activated vascular endothelium under flow. *Blood* **106**, 584–592 (2005).

7. Kim, J., Koo, B.-K. & Knoblich, J. A. Human organoids: model systems for human biology and medicine. *Nat. Rev. Mol. Cell Biol.* **21**, 571–584 (2020).